The use of 3D surface topography analysis techniques to analyse and predict the alteration of endosseous titanium dental implants generated during the surgical insertion

A Thesis submitted
in partial fulfilment of the requirements for the degree of
Doctor by Mondragon Ubibertsitatea

ALAITZ ZABALA EGUREN

Supervised by:
Dr. Wilson Tato Vega

Department of Mechanical and Industrial Production,
Mondragon Unibertsitatea

DECEMBER 2015

"We are the sum total of our experiences. Those experiences –be they positive or negative –make us the person we are, at any given point in our lives. And, like a flowing river, those same experiences, and those yet to come, continue to influence and reshape the person we are, and the person we become. None of us are the same as we were yesterday, nor will be tomorrow."

B.J. Neblett

Abstract

Dental implants have emerged as the preferred choice for tooth replacement, reaching about one million implantations per year. Among factors affecting dental implant success, surface topography has been recognised as an important parameter since it is known to affect the cellular response and, ultimately, osseointegration. Although it has generally been overlooked, the topography integrity may be jeopardised due to the stresses to which implant surfaces are subjected during surgical insertion. The study of this phenomenon is of great importance because the surface topography alteration may lead to a cellular response that differs from the ones analysed in in vitro assays, as well as to titanium particle release, which has been related to increased bone resorption, peri-implantitits and implant failure.

The main goal of the present dissertation was to analyse and predict the topographic alteration of endosseous dental implants generated during the surgical insertion.

In light of the lack of standardisation regarding dental implant topographic characterisation, the effect of the data acquisition and processing variables on the 3D topographical parameters was first evaluated. Then, based on the results obtained, a generalized topographical characterization strategy for endosseous dental implant was established.

Aimed at elucidating the effect of the insertion forces on the topography of implants, commercial dental implants were inserted into cow rib bones using standard surgical procedures. 3D topographical characterisation techniques were employed to quantify the modification and to approximate the material loss. Post-inserted implants showed wear and plastic deformation of the most prominent peaks, and released titanium particles were observed in the bone site underlying the implants. The obtained results suggest that the surface modification is a complex phenomenon conditioned by the combination of surface treatment, implant macrogeometry and surgical procedure.

Additionally, an in vitro study was conducted to investigate whether the topographic alteration generated during dental implant insertion affects the cell response. Within the limits of the study, the experimental data rejected the hypothesis that osteoblast attachment and proliferation could be significantly affected by the topographical modification generated during dental implant insertion.

Finally, the correlation between the surface modification and certain physically meaningful properties of surface topography was successfully established through the newly developed product of 3D topographical parameters named S_{i}. This novel parameter is presented as a useful tool to predict whether a surface is more prone to suffer alterations during insertion, and may therefore contribute to foster advancements in the design of better performing endosseous implants.

Laburpena

Hortz inplanteak hortzak ordezkatzeko lehen aukera bilakatu dira, eta urtean milioi bat inguru inplante ezartzera iritsi dira. Hortz inplante arrakastatsu bat lortzeko erabakigarriak diren faktoreen artean, gainazalaren topografia parametro garrantzitsutzat jotzen da, jakina baita erantzun biologikoan eta, finean, osteointegrazioan eragina duela. Orokorrean aintzat hartu ez den arren, gainazalaren topografiaren osotasuna konprometitua egon daiteke intsertzio kirurgikoan sortzen diren esfortzuak direla eta. Fenomeno horren azterketa garrantzi handikoa da, topografiaren alterazioaren ondorioz erantzun zelularra in vitro saiakuntzetan aztertutakoaren ezberdina izan eta titanio partikulak askatu daitezkeelako, zeina hezurraren erresortzio, periinplantitis eta inplantearen porrotarekin lotu den.

Tesi doktoral honen helburu nagusia, intsertzio kirurgikoan sorturiko hortz inplanteen gainazalaren topografiaren alterazioa aztertu eta aurreikusteko teknikak garatzea izan da.

Hortz inplanteen karakterizazio topografikorako estandarizaziorik ez dagoela eta, lehenik eta behin datuak eskuratzen eta prozesatzen parte hartzen duten parametroek 3Dko parametro topografikoen balioetan duten eraginaren analisi bat egin da, eta, lorturiko emaitzetan oinarrituz, hortz inplanteen topografia karakterizatzeko estrategia bat garatu da.

Intserzio kirurgikoaren esfortzuek hortz inplanteen gainazalean duten efektua aztertzeko helburuarekin, hortz inplante komertzialak behien saiheski hezurrean txertatu ziren prozedura kirurgiko estandarrak jarraituz, eta 3Dko karakterizazio teknikak erabili ziren modifikazioa kuantifikatu eta material galera kalkulatzeko. Txertatu ondoren, hortz inplanteek tontor garaienen desgastea eta deformazio plastikoa erakutsi zuten, eta titanio partikulak aurkitu ziren inplantea inguratzen duen hezurrean. Lorturiko emaitzek iradoki zuten hortz inplanteen modifikazioa fenomeno konplexua dela, gainazalaren tratamendu, inplantearen makro-geometri eta prozesu kirurgikoarekiko duen menpekotasunaren ondorioz.

Are gehiago, in vitro analisi bat burutu zen ea intsertzioan zehar sorturiko alterazio topografikoek erantzun zelularrean efekturik duen ikertzeko. Ikerketaren mugak kontuan izanik, datu esperimentalek baztertu egin zuten modifikazio topografikoak osteoblastoen ugalketan eta adhesioan efektua dutelako hipotesia.

Azkenik, gainazalaren modifikazioaren eta propietate topografikoen arteko korrelazioa arrakastarekin ezarri zen, garatutako 3Dko parametro topografikoen produktu berri baten bitartez. S_{i} izena eman zaion parametro berri horri esker, gainazal batek alterazioak jasateko duen joera aurreikusi daiteke, eta beraz, hortz inplante funtzionalagoen diseinuan aurrerapenak sustatzeko erreminta egokitzat aurkezten da.

Resumen

Los implantes dentales se han convertido en la opción preferida para la sustitución de piezas dentales, llegando a la colocación de alrededor de un millón implantes dentales por año. Entre los factores que afectan al éxito del implante dental, la topografía de la superficie ha sido reconocida como un parámetro importante ya que se sabe que afecta la respuesta biológica, y en última instancia, la osteointegración. Aunque en general se ha pasado por alto, la integridad de la topografía puede verse comprometida debido a los esfuerzos a los que las superficies de los implantes son sometidos durante la inserción quirúrgica. El estudio de este fenómeno es de gran importancia ya que la alteración de la topografía superficial puede conducir a una respuesta celular que difiere de la analizada en ensayos in vitro, así como a la liberación de partículas de titanio, que se ha relacionado con el aumento de resorción ósea, periimplantitits y fracaso del implante.

El objetivo principal de la presente tesis fue analizar y predecir la alteración topográfica de los implantes dentales endoóseos generado durante la inserción quirúrgica.

A la luz de la falta de estandarización en cuanto a la caractetrización topográfica de implantes dentales, en primer lugar se analizó el efecto de los parámetros de adquisición y procesado de datos en los parámetros topográficos 3D y se estableció una estrategia para la caracterización topográfica de implantes dentales endooseos.

Con el objetivo de dilucidar el efecto de las fuerzas de inserción en la topografía de los implantes, se insertaron implantes dentales comerciales en hueso de costilla de bovino mediante procedimientos quirúrgicos estándar, y se emplearon técnicas de caracterización topográfica 3D para cuantificar la modificación y aproximar la pérdida de material. Los implantes post-insertados mostraron desgaste y deformación plástica de los picos más prominentes, y se observaron partículas de titanio en el hueso subyacente a los implantes. Los resultados obtenidos sugieren que la modificación de la superficie es un fenómeno complejo condicionado por la combinación de tratamiento de superficie, macrogeometría del implante y procedimiento quirúrgico.

Adicionalmente se llevó a cabo un estudio in vitro para investigar si la alteración topográfica generada durante la inserción del implante dental afecta a la respuesta celular. Dentro de las limitaciones del estudio, los datos experimentales rechazaron la hipótesis de que la adhesión y proliferación de los osteoblastos podrían verse afectadas de manera significativa por la modificación topográfica generada durante la inserción.

Por último, la relación entre la modificación superficial y algunas propiedades topográficas se estableció con éxito a través del nuevo producto de parámetros topográficos 3D denominado S_{i}. Este nuevo parámetro se presenta como una herramienta útil para predecir si una superficie es más propensa a sufrir alteraciones durante la inserción, y por lo tanto, puede contribuir a fomentar avances en el diseño de implantes endoóseos de mejor rendimiento.

Acknowledgments/Eskerrak/Agradecimientos

"Not everything that counts can be counted and not everything that can be counted counts."
Albert Einstein

En primer lugar quiero a agradecer a mi director de tesis, Dr Wilson Tato, por haber confiado en mí y por toda su dedicación en la dirección de esta tesis doctoral. Muchas gracias por introducirme en el mundo de la metrología y por enseñarme la importancia de la rigurosidad.

También agradecer al grupo de tecnologías de superficie por vuestro apoyo y en especial a la Dra Andrea Aginagalde por las palabras de ánimo cuando más hacía falta. Y como no, a los estudiantes que han trabajado en la línea de superficies durante estos años: Nielka, Izaskun y Josune, por todo vuestro esfuerzo y entrega.

Eskerrik asko Mondragon Unibertsitateari, tesia bertan egiteko aukera emateagatik eta etapa berri honetan nitan apustua egin izanagatik. Ezin ahaztu Goi eskola Politeknikoa osatzen duten langile guztietaz (laborategiko teknikari, administrazioko langile...), eskerrik asko zuen lagunatza eta lan guztiagatik.

Me gustaría también agradecera BTI Biotechnology Institute y en especial al Dr Ricardo Tejero, por todas las colaboraciones llevadas a cabo durante estos años y por proporcionar los implantes dentales y discos necesarios para la consecución de los estudios.

Mila esker Cinto Gaztañaga hortz klinikari, eta bereziki Ramon Gaztañaga eta Ainhoa Azpeitiari, nire lanaren goraberak entzuteko denbora hartu eta inplante dentalen inserzioak kondizio errealetan egiteko aukera eman izanagatik.

I would like to give special thanks to Professor Liam Blunt, for giving me the opportunity to do a very enriching stay at the Centre of Precision Technologies. Thank you very much for the invaluable support, help and motivation. Words really cannot express how grateful I am. I would also like to thank the wonderful crew at CPT for making me feel like part of the group, and for being so helpful. All of you made this stay an unforgettable experience.

Gauza on eta txar asko izan dira bide honetan, baina ezergatik aldatuko ez nukeena tesi honi esker ezagutzeko aukera izan dudan jende guztia da. Bereziki, lankide baino gehiago lagun on bilakatu zaretenoi, zuei esker momenturik gogorrenak ere eramangarriak izan direlako, eta konpartitu ditugun kafe, bazkari eta juerga guztiengatik (onenak zeate!): Jokin "Langosto" (el sabio de la tribu, zure konseju on guztiengatik), Joanes "Magneto" (konpartitutako te eta mandarina guztiengatik), Javi "Trinity" (elektroiak aurkitu daitezkeela demostratzeagatik), Haritz "Sarriegi" (zure reflexio interesgarriak konpartitzeagatik), Nagore "Marraji" (sikologa lanak egin izanagatik eta rumoreak detektatzen erakusteagatik), Alain "Mr. Martan" (konbertsatzio guztitan txispa jartzeagatik), Elena (por demostrarnos que Teruel existe), Manex (bizimodu "zen"-a nolakoa den erakusteagatik) eta Ione (elkarbanatutako momentu guztiengatik). Denak ezin banan banan izendatu, baina bide honetan ezagutu zaituztedan guztiei eskerrik asko, denengatik ikasi dut zerbait.

Ezin ahaztu betiko lagunetaz, mila esker emandako animo guztiengatik, eta nire buruausteak entzuteagatik!!!

Nola ez nire eskerrik beroenak nire familiari, nitan nik baino gehiago sinisteagatik eta nire aukeratan aurrera egiteko babesa eta indarra emateagatik: ama, atta, Juantxo, Aitor, ESKERRIK ASKO!.

Eta azkenik, eskerrik asko bihotzez Fabio!. Erortzen naizen bakoitzean indar gehiagorekin altxatzen laguntzeagatik, zure pazientzia infinituagatik... Eskerrik asko laborategitik kanpo bizia dagoela gogorarazteagatik!

MODU BATERA EDO BESTERA HONAINO IRISTEN LAGUNDU DIDAZUEN GUZTIEI, ESKERRIK ASKO!

Contents

Nomenclature

List of Abbreviations

ACF	Autocorrelation Function.
AE	Acid etched.
AFM	Atomic force microscope.
ALP	Alkaline phosphatase.
APSDF	Angular Power Spectral Density Function.
AVG	Average value.
BIC	Bone-to-Implant Contact.
BM	BIOMET.
BSE	Back scattered electron.
BT	BTI.
CI	Confidence interval.
CRA	Cutting Torque Resistance Analysis.
DNA	Deoxyribonucleic acid.
DOF	Degree of freedom.
EDX	Energy Dispersive X-Ray.
FRC	Fiber Reinforced Composite.
HA	Hydroxyapatite.
ISQ	Implant Stability Quotient.
ITQ	Insertion Torque Analysis.
LF	Waviness surface.
MCN	Machined.
OC	Osteocalcin.

OPTIMA	BTI's proprietary acid etching.
PBS	Phosphate-buffered saline.
RFA	Radio Frequency Analysis.
RTT	Reverse Torque Test.
SB+AE	Sand blasted + Acid etched.
SE	Secondary electron.
SEM	Scanning electron microscope.
SF	Primary surface.
SL	Roughness surface.
SM	SensoMap.
SS	SurfStand.
TEM	Transmission electron microscope.
TPS	Titanium Plasma-Spraying.

List of Symbols

α	Rotation angle of the material probability curve.
β	Surface asperity radius.
ρ_{ti}	Density of titanium.
ΔS_{dq}	Relative peak curvature parameter (developed in the present study).
η	Surface asperity distribution.
θ	Mean profile slope.
η_{p}	The highest surface summits on the surface.
η_{v}	The lowest surface valleys on the surface.
η_{z}	The lowest and highest points of the surface.
λ_{c}	L filter size.
λ_{s}	S filter size.
ν	Poisson coefficient.
σ	Surface asperity heigh distribution.

Ψ_{GW}	Plasticity index defined by Greenwood and Williamson.
Ψ_M	Plasticity index defined by Mikik.
A_{site}	Area size of evaluation site.
C	Transition point between modified and non-modified regions.
E	Young modulus.
E'	Reduced elastic modulus.
F	F operator.
h_{tr}	Truncation heigh.
H	Hardness.
L	L filter type.
s	Standard deviation.
$step_{\mathrm{tr}}$	Truncation step size.
S	S filter type.
S_{a}	Average roughness.
S_{al}	The autocorrelation length.
S_{ci}	Core fluid retention index.
S_{dq}	The root mean square slope of the surface.
S_{dr}	The developed interfacial area ratio.
S_{ds}	Density of summits of the surface.
S_{i}	Integrated topographical parameter (developed in the present study.).
S_{ku}	Kurtosis.
S_{pc}	Arithmetic mean peak curvature of the surface.
S_{pd}	Density of peaks of the surface.
S_{p}	The highest peak of the surface.
S_{q}	Root mean square roughness.
S_{sc}	Arithmetic mean summit curvature of the surface.
S_{sk}	Skewness.

S_{td}	The texture direction of the surface.
S_{tr}	The texture aspect ratio of the surface.
S_{v}	The lowest valley of the surface.
S_{z}	Maximum height of the surface.
V_{m}	Material volume.
V_{mc}	Core material volume.
V_{mp}	Peak material volume.
V_{vc}	Core void volume.
V_{vv}	Dale void volume.

List of Figures

List of Tables

CHAPTER 1

INTRODUCTION

"There are unsolved problems, not solved,
that keep the mind active"
Erwin Guido Kolbenheyer

At this point, the motivation, scope and lay out of the thesis are defined.

1.1. Motivation and background

In the past 20 years, the number of dental implant procedures has increased steadily worldwide, reaching about one million implantations per year [LG07]. This demand increase is due to different factors, including: ageing population, tooth loss related to age, anatomic consequences of edentulism, poor performance of removable prostheses, psychologic aspects of tooth loss, predictable long-term results of implant-supported prostheses and advantages of implant-supported prostheses [Mis09]. The goal of modern dentistry is to restore the patient to normal function, speech, health and aesthetics.

Despite of the high success percentage of dental implants (more than 95 %), which are in fact between the most successful treatments used in medicine [Abu10], implant failures do occur, and what causes them is not always clear. Clinical success of dental implants is obtained when osseointegration, *i.e.* structural and functional bounding between implant surface and bone, is achieved. The achievement of the osseointegration depends on several factors. Among them, surface topography is one of the most important, since it is known to modify cell–tissue interactions ([Git11], [Van08]).

Understanding factors that influences osseointegration and applying them appropriately in the science of dental implants can lead to achieve predictable osseointegration, thus minimizing potential implant failures. As implant dentistry continues to evolve, there is increasing interest in providing patients with immediate functional and aesthetic replacement for a missing tooth or teeth. Therefore, one of the challenges is to improve tissue response, decreasing the conventional waiting time for traditional implant systems. On the other hand, with this knowledge, implant therapy could be easily applied even in the less favourable situations (*e.g.* early immediate loading, smokers, diabetics or unfavourable bone quality).

This being so, an intense field in dental implant research is focused in studying the interactions between topography and cell response. Nevertheless, due to the lack of standardization regarding dental implant topographical characterization as well as the numerous variables involved in the osseointegration assessment, the ideal surface texture has not been established yet.

Another important aspect to consider and often overlooked is the impact of the stresses generated during implant surgical insertion on the surface characteristics. It has been reported that release of titanium to the adjacent bone tissue may occur due to the friction and abrasion forces to which implant surfaces are subjected during insertion [Fra04]. Detachment of titanium particles has been related to an increased bone resorption activity [Men13a], potential cause for periimplantitis ([TS14], [Olm13]), increased early bone loss [OH15] and implant failure ([Böl13], [Fri02]). Furthermore, the migration of titanium particles to distanct inner organs has also been reported ([Wei94], [Sch92]).

In spite of these evidences, very little research has been carried out regarding the numerical characterization of the implant topography after insertion, and non at all analysing different parts of post-inserted implants. There is therefore a lack of knowledge regarding the interactions between the insertion forces and the topographic alteration and particle release.

Besides the potential contamination of the peri-implant area, the possibility of a different cellular response of the post-inserted surfaces compared to the pre-inserted ones should be considered, however, to the authors' knowledge there are currently no studies dealing with the effect of surface modification on the cell response.

1.2. Scope of the thesis

The main goal of the present dissertation is to analyse and predict the topographic alteration of endosseous dental implants generated during the surgical insertion. In order to meet this main goal, the study comprise the following specific objectives:

- Using the 3D techniques available, to define a topographical characterization strategy to effectively and robustly characterize the topography of endosseous dental implants.
- To evaluate the modification of dental implants surface topography generated during standard surgical insertion.
- To characterize the influence of surface modification generated during surgical insertion on cell response.
- To establish a correlation between the surface modification generated during surgical insertion and 3D topographical parameters.

1.3. Thesis layout

The current thesis comprises seven chapters including the introduction. For a better understanding of the work, the overall scheme is sketched in Figure 1.1, where the different chapters and associated objectives (defined in previous section) are depicted. A general description of each chapter is given below.

Chapter 2

Chapter two is dedicated to the review of the state of the art about the main areas related to the problematic studied in this research work. Additionally, some general concepts are reviewed in order to aid in the understanding of the present study.

From this analysis the different research opportunities addressed in the present study were identified.

Chapter 3

Chapter three summarizes the studies carried out in order to set a generalized topographical characterization strategy for endosseous dental implants. The first part of the chapter deals with the development of tools for setting bases for the accurate and repeated handling and positioning of dental implants. The effect of the data acquisition and processing variables on the 3D topographical parameters are subsequently analysed and

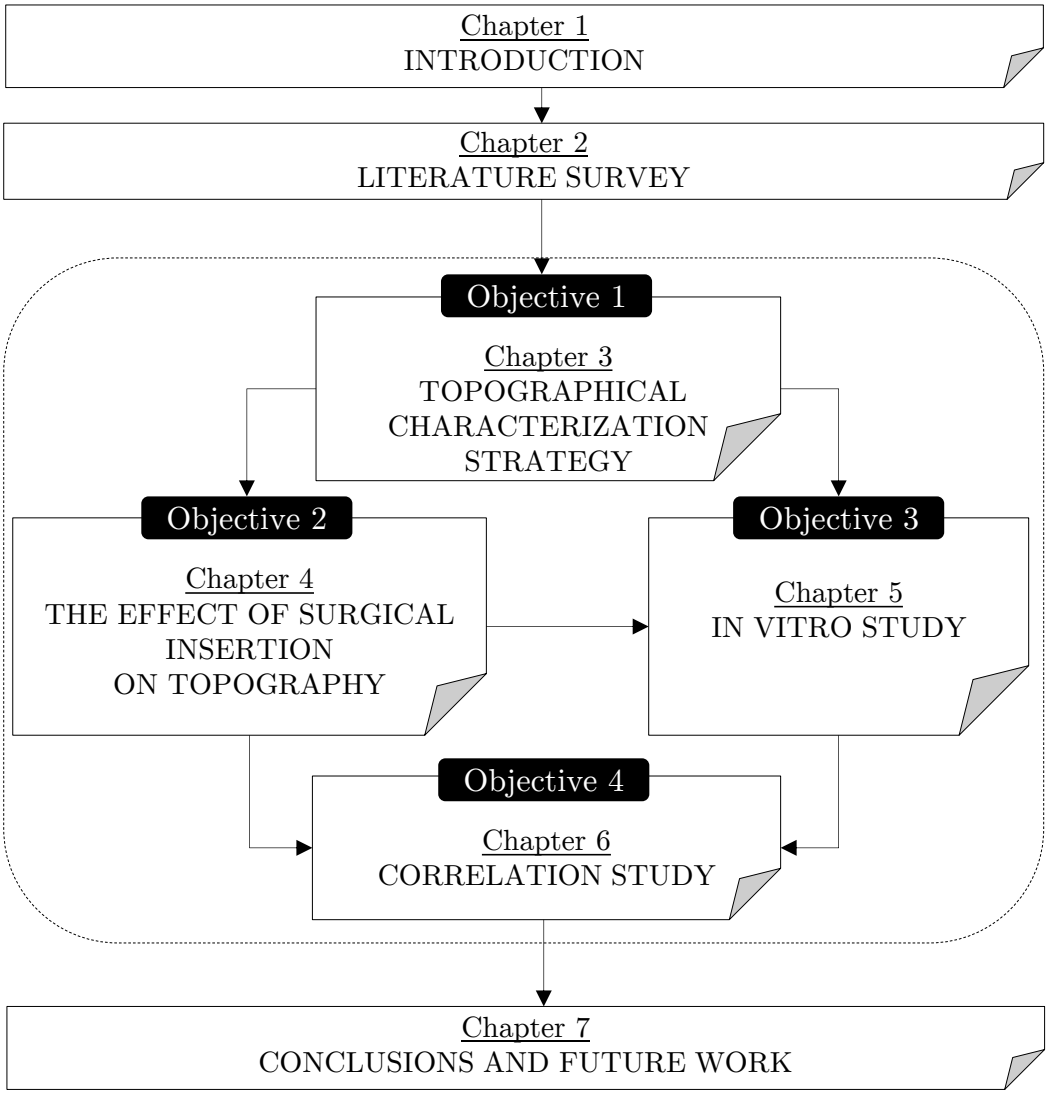

Figure 1.1: Outline of the whole work, depicting the different chapters and associated objectives.

evaluated. Finally, based on the results obtained, a generalized topographical characterization strategy for dental implants is established and applied to two commercially available dental implant systems as examples.

Chapter 4

This chapter presents the study of the topographic modification of dental implants generated during the surgical insertion. Two commercially available dental implant systems were introduced in cow rib bone following standard surgical insertion procedures, and different parts of the implants were characterized both before and after insertion in order to elucidate the effects of the insertion on surface topography. Additionally the bone site underlying the implants was analysed in order to evaluate the released particles and the material loss was approximated though functional material volume parameter (V_{m})

variation analysis.

Chapter 5

Chapter 5 summarises the in vitro study carried out in order to determine whether the topographical alterations generated during dental implant insertion affects the cell response.

The first part of the chapter deals with the development of a device to reproduce the surface alterations generated during the surgical insertion on disc samples (format required for in vitro tests). Subsequently, disc format titanium samples treated with typical dental implant surface treatments were modified by means of the developed device. Finally, both modified and unmodified samples were assayed in vitro using human MG-63 osteosarcoma cells to test the impact of surface topography and its modification on cell attachment and proliferation.

Chapter 6

This chapter presents the correlation study carried out between the modification of dental implant surfaces and 3D topographical parameters. The first part of the chapter presents the method developed to separate the tested surfaces into modified and non-modified regions, which allowed the quantification of modified area percentages. In the second part, different wear predictive models and plasticity indexes were analysed in order to detect the most relevant topographical characteristics to predict wear and plastic deformation behaviour. Following this the suitability of 3D topographical parameters to describe these characteristics was analysed. Due to the key role of some feature parameters a deeper analysis was carried out, which included the comparison between two commercial metrological software (SensoMap and SurfStand). Owing to the discrepancies and the lack of representativeness observed, a new parameter to characterize the relative surface mean peak curvature was developed. Finally a correlation study between 3D topographical parameters and surface modification was carried out, and a new topographical parameter was developed and successfully correlated with surface modification.

Chapter 7

In Chapter 7 a summary with the global conclusions is drawn, the perceived contributions to knowledge are identified and some ideas opened for future research are given.

CHAPTER 2

LITERATURE SURVEY

"I believe in evidence. I believe in observation, measurement, and reasoning, confirmed by independent observers. I'll believe anything, no matter how wild and ridiculous, if there is evidence for it. The wilder and more ridiculous something is, however, the firmer and more solid the evidence will have to be."
Isaac Asimov

This chapter presents a general background and the state of the art of the research field under study. First of all, dental implants and their classification will be revised. Osseointegration, which is the clue factor for implant success will be addressed subsequently. Some basic notions will be given for understanding purpose and factors affecting osseointegration and methods to assess it will be described and discussed. Afterwards, biomaterials and their requirements will be reviewed, centring the study on titanium and titanium alloys. Surface treatments applied to dental implants and different aspects concerning surgical placement and loading conditions will be presented later on. Finally, particular emphasis will be put on the surface topography characterization process, evaluation methods and reported results in implant research. To conclude, a critical review of the state of the art is presented.

2.1. Dental implants

Dental implants are biocompatible metal anchors surgically positioned in the jaw bone to support an artificial crown where natural teeth are missing [Osh10].

Dental implants can be classified into three broad categories: endosseous implants (Figure 2.1 (a)), subperiosteal implants (Figure 2.1 (b)), and transosteal implants (Figure 2.1 (c)).

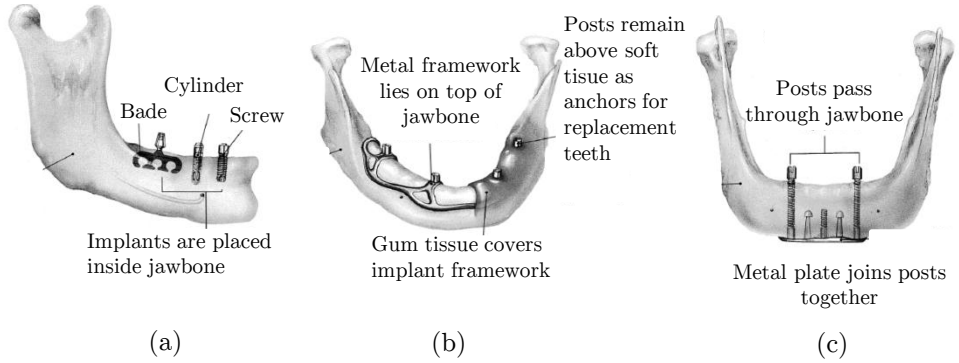

Figure 2.1: Dental implant types. (a) endosseous implants; (b) subperiosteal implants; (c) transosteal implants ([O'B97a]).

Endosseous implants are embedded in mandible or maxilla, subperiosteal implants rest on the surface of the bone beneath the periosteum, and transosteal implants penetrate the inferior mandibular border. Dental implant types and indications for each are extensively reviewed in [O'B97a].

2.1.1. Endosseous dental implants

Endosseous implants are the most used implant type and can be placed in both jaws to replace only one missing tooth or in cases of partial and total edentulism. Endosseous implants can be classified according to their designs as pins needles, blades, discs and root-formed analogues. Nowadays it is accepted that threaded designs are preferable for implant fixation [Bru01a]. The main advantages of the thread design are the improved primary stability (which is a condition to obtain a osseointegrated implant) and better load transmission [Sch98]. Figure 2.2 shows the comparison between natural tooth and endosseous threaded dental implant system, as well as the denomination of the different parts of the implant.

Implant design can be divided into two categories: macrodesign (overviewed in this section) and microdesign (analysed in section 2.4). Macrodesign includes body shape and thread form (see Figure 2.3), while microdesign constitutes surface morphology and surface coatings ([Gen04a], [Gen04b]). As stated by Shin *et al.* [Shi06] the macro and micro design of the implant is the key factor for the successful achievement and maintenance of osseointegration.

As far as macro geometry is concerned, parameters that may affect the primary stability are the implant diameter, length, thread pitch, shape and depth [MB06]. In the review

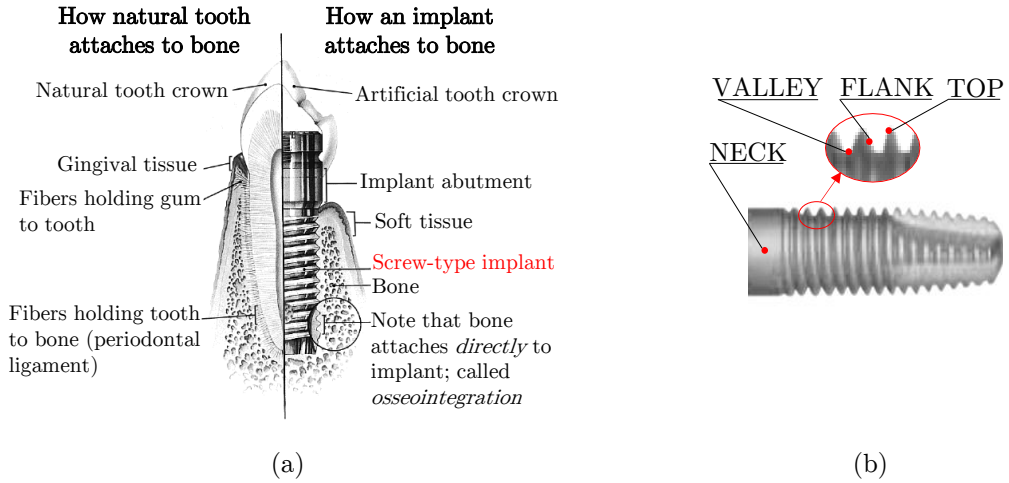

Figure 2.2: Endosseous dental implant. (a) schematic of natural tooth vs endosseous dental implant. In red, the subject matter of the present study (adapted from [Tay90]); (b) denomination of the different parts of the implant.

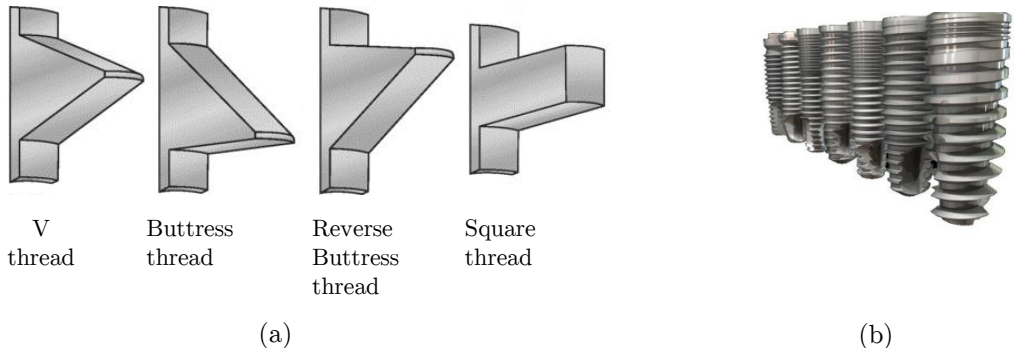

Figure 2.3: Different macro geometry designs of dental implants. (a) examples of different thread designs [CAR15]; (b) examples of different commercially available dental implants [Eli11].

carried out by Abuhussein *et al.* [Abu10] they conclude that when primary stability is a concern (poor bone quality, high occlusion stresses...), implants with smaller pitch, more and deeper threads, decreased thread helix angle, and a longer implant and/or a wider diameter may be beneficial. The large number of commercially available implant types are reviewed in [Bin00].

2.1.2. Dental implant failure

Despite of the high success percentage of dental implants (more than 95 %), which are in fact between the most successful treatments used in medicine [Abu10], implant failures do occur, and what causes them is not always clear.

Implant failures could be classified into pre-osseointegration failure (or early failure) and post-osseointegration failure (or late failure). Inside this classification, failures can be classified into biologic (related to biologic process), mechanical (related to fractures

of implants, coatings, components, prostheses etc.), iatrogenic (violation of anatomical structures such as the alveolar inferior nerve, malpositioned implants etc.) and functional (phonetic, aesthetic, psychological problems etc.), ([Esp99], [Esp98]).

Even if success rates for dental implants are high, there are many factors that favour implant failures (Table 2.1).

Table 2.1: Factors contributing to early and late implant failure [Abu10].

Early failure	Late failure
Micromovement (lack of primary stability)	Bacterial infection
Short implants	History of Periodontitis
Narrow implants	Smoking
Early/immediate loading	Neck of the implant
Low-density bone (osteoporosis)	One-piece vs. two-piece
Surgical trauma	Excessive load
Overheating	Inadequate restoration
Compression osteonecrosis	Short/narrow implants
Infection	Trauma
Impaired healing	
Smoking	
Diabetes	
Age	

Some of them (surgical trauma, excessive load...) can be modified by clinicians to enhance outcome, whereas some of them are patient dependant (smoking, diabetes, age...). Patients with chronic diseases like diabetes or smokers constitute groups with increased risk of dental implant failures.

2.2. Osseointegration

Brånemark[1] coined the term 'osseointegration', which is defined as follows:"*clinical osseointegration implies histologic osseointegration, it is necessary [there is] a contiguous contact between the alveolar bone and the implant surface*" [Brå83].

Different stages could be defined in the osseointegration process: the stability during healing (primary stability) and stability after healing (secondary stability). The primary stability is the mechanical interlocking between the implant and the surrounding bone, which will evolve during the bone healing process (explained in the following section). After the bone healing process will result in secondary (biological) stability [Cho11].

Albrektsson *et al.* [Alb81] stated that osseointegration process is affected by six parameters, which will be analysed in the following sections:

[1]Professor emeritus Per-Ingvar Brånemark received the European Inventor Award for his development of osseointegration [BRA12].

- (i): Implant design (analysed in section 3.4.1)
- (ii): Status of the bone (section 2.2.1)
- (iii): Implant material (section 2.3)
- (iv): Implant finish (section 2.4)
- (v): Surgical technique (section 2.5.1)
- (vi): Implant loading conditions (section 2.5.2).

2.2.1. Bone

Bone is distinguished into the cortical (or compact) and cancellous (or trabecular or spongy) types at macroscopic level, which are distinguished by their degree of porosity or density (hierarchical structural organization of bone is extensively reviewed in [Rho98]).

Mandibles generally are more densely corticated (mean thickness 2.22 mm ± 0.47 mm) than maxillae (mean thickness 1.49 mm± 0.34 mm) [Miy05]. Furthermore, Norton and Gamble [Nor01] found out that both jaws tend to decrease in their cortical thickness and increase in their trabecular porosity as they move posteriorly (Figure 2.4 (a)). Lekholm *et al.* [Lek85] classified the jawbones of the maxilla and the mandible into four qualities based on the relative proportion and density of cortical to trabecular bone, defining four bone types (see Figure 2.4 (b)).

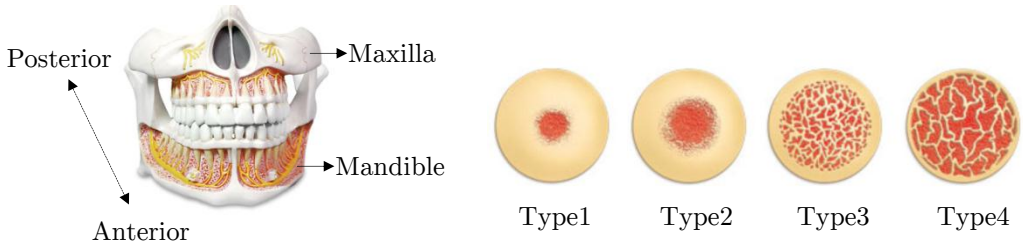

Figure 2.4: Bone types. (a) illustration of human jawbone (adapted from [too12]); (b) bone quality classification based on the relative proportion and density of cortical to trabecular bone (adapted from [Lab12]).

The quantity and density of the bone available at the implant site influences the outcome of the procedure. Thus, implants inserted into the anterior mandible have higher survival rates than implants placed in the posterior maxilla [Tab10a].

Regarding the bone healing process, bone (re)modelation is carried out by continuous bone resorption (by means of osteoclasts, bone-resorbing cells) and bone formation (by means of osteoblasts, bone forming cells) [Rui05] as illustrated in Figure 2.5. This is the reason why the mechanical locking obtained right after the insertion evolves during the bone healing process.

In normal conditions resorption and formation are balanced, which is called bone remodeling process. In that case old bone is continuously replaced by new tissue. However, if these processes occur at different locations, the bone morphology is altered, which is called bone modeling process ([Cla08], [Fro90a], [Fro90b]).

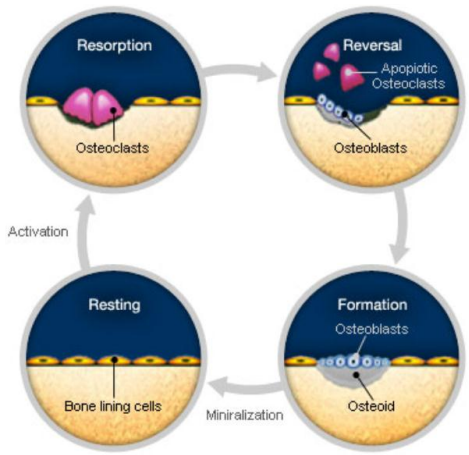

Figure 2.5: Illustration of the bone (re)modeling process [BS12].

However, adequate cells for bone repair are not only differentiated bone cells (osteoblasts, osteoclasts), but also undifferentiated immature cells. Osteoinduction is a basic biological mechanism that occurs regularly (in fracture healing and implant incorporation for example) where immature cells are recruited and stimulated to develop into osteoblasts [Alb01].

2.2.2. Osseointegration assessment

As mentioned previously, implant stability or primary stability has been identified as a prerequisite to achieve osseointegration. Furthermore, several authors suggested that primary stability may be a useful predictor of osseointegration [Ned04]. Table 2.2 shows the currently available methods to evaluate implant stability (which are extensively reviewed in [Ats07]), where the time of use (pre-, intra- or post-surgical) and the invasiveness of each method is specified.

To determine when the implant may be exposed to functional load, clinical settings require non-invasive techniques to assess stability. Among non-invasive methods resonance frequency analysis (RFA) is such a method designed to determine the implant stability over the healing period [Abr09]. With this method, implant stability is measured either by determining the resonance frequency of the implant-bone complex or by reading an implant stability quotient (ISQ) value given by the Osstell apparatus (Integration Diagnostics AB, Gothenburg, Sweden) [Ned04].

Another common technique for evaluating primary stability is to monitor insertion torque on the drill unit. This is referred to as insertion torque analysis (ITQ) or cutting torque resistance analysis (CRA). This method estimates the energy (J/mm^3) required for cutting off a unit volume of bone during implant surgery, which is indirectly represented

by the implant insertion torque in Ncm [Ats07]. A higher insertion torque represents better primary stability. Nevertheless, an excessive torque is not desirable. It has been proposed that the desirable interval relies between 30-50 Ncm [SM10].

Table 2.2: Currently available methods to evaluate implant stability: time of use and invasiveness. "✓"= applicable. "-"= non-applicable (modified from [Ats07]).

Method	Pre	Intra	Post	Non-invasiveness
Histologic analysis	✓	✓	✓	-
Percussion test	-	✓	✓	✓
Radiographs	✓	✓	✓	✓
Reverse torque (RTT)	-	-	✓	-
Cutting resistance (CRA)	-	✓	-	✓
Vibration analysis				
Periotest	-	✓	✓	✓
RFA	-	✓	✓	✓

Regarding the invasive methods, the reverse torque test (RTT) or removal torque test indirectly provides information on the degree of bone to implant contact (BIC). This method, applied in the in vivo tests after specimen scarification, applies a slowly increasing torque gradually to implant until loosening ([Tab10b], [Sul09]). Table 2.3 shows the relation between the roughness and removal torque of different implants removed from rabbit's tibia as reference data.

Table 2.3: Dental implant roughness and torque required to remove from rabbit's tibia [Eli10].

Surface	R_q (μm)	Torque (Ncm)
Machined	0.81±0.17 (μm)	57±18.6
Acid etched	0.71±0.07 (μm)	75.4±10.5
Sandblasted	0.98±0.04 (μm)	72.1±14.9
Anodized	1.12±0.18 (μm)	83.1±12.7

Nevertheless, in vivo tests limit the number of surfaces under study due to the price and legal and ethic issues involved in this kind of studies ([Rec98] taken form [Apa05]). That is why the first approach to evaluate the response of a surface is an in vitro study.

Bone/biomaterial interactions take place at the material surface, therefore, osteoblasts covering the implant surface are the crucial cells determining the tissue response at the biomaterial surface. Cell material interaction process has different subsequent stages, divided in: protein adsorption, cell attachment, cell adhesion and finally cell spread.

Protein adsorption is believed to be the first event that takes place after contact of body fluids and is influenced by physico-chemical characteristics of the material. Proteins involved in osteoblast cell adhesion are extensively reviewed in [Ans00a]. Protein adsorption is followed by the cell attachment phase which occurs rapidly and is governed by physico-chemical interactions between cells and materials (*e.g.* ionic forces and van der Waals forces among others). The cell adhesion phase occurs over longer periods and in-

volves various biological molecules which interact together to induce the subsequent cell response in terms of migration and differentiation. Basic reactions between osteoblasts and surfaces are extensively reviewed in [Mey05]. Results obtained in cell cultures will depend on the used cell lines, selected differentiation markers, experimental conditions etc. ([Apa05], [Mey05]), which will be discussed subsequently.

Different cell models are used to study bone-like cell behaviour (see Table 2.4). The cell response to Ti implants in vitro has been mostly analysed using human osteosarctoma cells (MG-63) as an osteoblast-like cell or fetal rat calvarial cells (MC-3T3-E1) as a model of immature osteoprogenitor cells ([Git11], [Yao05], [Boy01], [Ans00b]).

Table 2.4: Common cell culture models to examine the response of cells to surface morphology [Boy01].

Cell model	Source	Phenotype
MG-63	Human osteosarcoma	Immature osteoblast
FRC	Fetal rat calvaria	Multi-potent-osteoprogenitor cells and osteoblasts
MC-3T3-E1	Mouse non-transformed cell line	Osteoblast-like
OCT-1	Transgenic mouse Large T-antigen Osteocalcin promoter	Mature osteoblast-like cells
MLO-Y4	Transgenic mouse Large T-antigen Osteocalcin promoter	Osteocyte-like
NHOst	Commercial preparations of human bone	Osteoblast-like
ROS 17/2.8	Rat osteosarcoma	Osteoblast-like
2T9	Transgenic mouse Large T-antigen BMP-2 promoter	Osteoprogenitor cells

Most frequently used markers of osteoblast differentiation process are the alkaline phosphatase (ALP) specific activity as an early differentiation marker, and osteocalcin (OC) content in the conditioned media as a late differentiation marker ([Git11], [Mic05], [Eri04]). Cell proliferation is usually characterized throw DNA content. Regarding the quantitative evaluation of cell adhesion, it generally implies the detachment of cells. Diffe-

rent methods can be used to detach cells (paramagnetic beads, spinning disk...) which are extensively reviewed in [Ans00b].

Currently, there is enough evidence about the influence of topography in the cell response [Git11]. However, despite much research activity, the relationship between cell behaviour and surface texture is still not fully understood [For10].

The differences found in osteoblast behaviour towards different surface topographies may partly be based on the different cell lines used [Mey05]. On the other hand, there is no consensus concerning the proper representation of implant surface topography (this topic will be discussed further in following sections). Due to the existing ambiguity around topographical characterization it is difficult to compare the in vitro findings on osteoblast behaviour on different surface types.

On the other hand, it must be taken into a count that in vitro study doesn't represent the complex reality involved in the integration of a dental implant. This complexity resides in numerous factors like the presence of blood vessels, the fact that the cells used in the cultures are previously isolated cells, and all reactions that may be in the real insertion process which are not considered in the culture models.

2.3. Biomaterials

In general, there are three terms in which a biomaterial may be classified into representing the tissues responses: bioinert, bioactive and bioresorbable materials [Hen05].

Biologically inert, or bioinert materials, are ones which once placed in the human body have a minimal interaction with its surrounding tissue (*e.g.*: stainless steel, titanium, cobalt-chromium alloy, zirconium, alumina and high molecular weight polyethylene) [Blo00]. Bioactive materials have an effect on or cause a reaction in living tissue, encouraging bonding to surrounding tissues. Bioactive materials can be classified into osteoconductive (*e.g.*: synthetic hydroxyapatite and tri-calcium phosphate ceramics), and osteoproductive materials (*e.g.*: bioactive glasses), ([Hen05], [Alb01]). Bioresorbable materials starts to being resorbed partially or completely upon placement within the human body and thereby disappear partially or completely over a period of time (*e.g.*: tri-calcium phosphate ($Ca_3(PO_4)_2$) and polylactic-polyglycolic acid co-polymers) [Hen04].

2.3.1. Biomaterial requirements for successful dental implant

A successful and biofunctional implant requires three compatibilities: biological compatibility, biomechanical compatibility and morphological compatibility [Osh07a] (see Figure 2.6).

The biological compatibility is the so called biocompatibility. The definition of this term is under discussion currently [Wil08], but in general, is the quality of not having toxic or injurious effects on biological systems. In the case of dental implants, corrosive conditions are hostile, therefore, biological compatibility of metallic materials essentially equates to corrosion resistance. It's important to point out that the corrosion resistance is influenced by surface topography, since many authors show that an augmented roughness increases

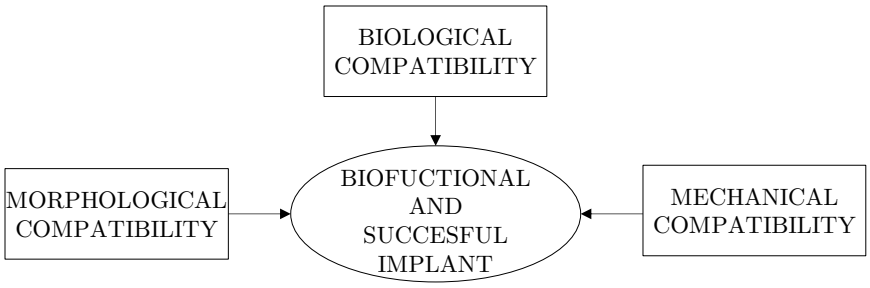

Figure 2.6: Required compatibilities for a biofunctional and successful implant.

the ion release to biological medium ([Bar11], [Apa03], [Tan03]).

Implantable materials must function under biomechanical environments so that the mechanical compatibility is necessary to accomplish intended biofuctionality. Remarkable differences in modulus of elasticity between the implanted material and bone tissue will generate interfacial stress leading to a failure in the implant (a phenomenon known as "stress shielding effect"). On the other hand, the biomaterial must be able to support the biting forces, and it is essential that neither implant nor bone must be stressed beyond the long-term fatigue capacity [Osh10]. Therefore, important mechanical properties in designing implant materials are: stiffness (or modulus of elasticity, related to the ability to transmit stresses to the adjacent tissue), yield and ultimate strengths (to minimize material failures), fracture toughness (a gauge of the energy needed to cause failure in the presence of damage) and fatigue strength (to minimize material failures) [O'B97a].

The surface plays a crucial role in biological interactions since the surface of a biomaterial is the only part in contact with the bioenvironment. For biomaterials that neither release nor leak biologically active or toxic substances, the characteristics of the surface govern the biological response. It is widely accepted that surface characteristics affects the protein adsorption and modulates the cell proliferation and differentiation ([Git11], [Sul09], [Van08]). This is the third compatibility, morphological compatibility [Osh10], which will be extensively reviewed in further sections.

2.3.2. Biomaterials for dental implant application

Biomaterials used in long term implant field can be broadly classified into metallic, ceramic, polymeric and composite materials. The high tensile and fatigue strength of metals compared with ceramics and polymers, make them the material of choice for implants that carry mechanical loads, like dental implants.

Commercially pure titanium or titanium alloys are the commonly used biomaterials for dental implants (which will be reviewed in the following section). Table 2.5 shows the alternative materials that has been used or studied for dental implant applications and their mechanical properties.

Ceramics are fully oxidized materials and therefore chemically stable. Thus they are less likely to elicit an adverse biological response compared to metals. Ceramic materials has already been utilized as dental implant material like aluminium oxide ([Sch84] taken from [Bal08]). This material showed good osseointegration but the biomechanical properties we-

Table 2.5: Biomaterials for dental implant application and their mechanical properties [Bal08]. FRC*=Fiber reinforced composite.

Materials /Property	Titanium	Alumina	Zirconia	Hydroxyapatite	FRC*
Strength(MPa)	800-1000	400-600	900-1200	115-150	700-1000
Young´s modulus (GPa)	110-120	380	210	85	20-40
Hardness (HV)	100-140	2200	1200-1500	300-400	70-80

re not sufficient. Recently, zirconia has been introduced as a new ceramic dental implant material, which compared to other ceramics exhibits higher fracture toughness and bending strength [Den10]. Zirconia implants are made currently either of yttria-stabilized tetragonal, zirconia polycrystals or yttria-partially stabilized zirconia [Wen08]. The advantage of this material compared to titanium is the tooth-like colour. This property overcomes the aesthetic problems that may appear in cases that implant become visible over time [Pri11]. However, these ceramic materials have very high elastic moduli (210 GPa) compared to that of human bone (17-24 GPa).

Regarding the bioactive ceramics, important examples are bioactive glasses, glass ceramics and calcium phosphate ceramics [Hen98]. Hydroxyapatite (HA) ceramics have been investigated extensively and used for dental implant application for the past 30 years as bioactive ceramic coating. This material is going to be analysed in section 2.4 more extensively.

Recently, fibre reinforced dental implants has been analysed, which enable to tailor properties close to that of natural bone [Bal08].

2.3.3. Titanium and titanium alloys for dental implant application

Nowadays there is a natural selection of titanium-based materials due to the combination of its outstanding characteristics such as high strength, low density (high specific strength), high immunity to corrosion, complete inertness to body environment, enhanced biocompatibility, low modulus and high capacity to join with bone and other tissues [Gee09]. There are four grades of commercially pure titanium (CpTi) under the category of “unalloyed grades”of ASTM specification (Grade 1 to 4) [ASTb]. Only oxygen is intentionally alloyed, while elements like C and Fe are considered impurities. Four CpTi grades are differentiated by their impurity contents [Pet03], with the most pure being Grade 1. Despite the popularity of grade 2 in industry, grades 3 and 4 are equally selected in most of the 20 major dental systems [Osh07b].

Ti-6Al-4V alloy presents greater yield strength and fatigue properties comparing with pure titanium [LG07]. However, there are some concerns due to the release of aluminium and vanadium since it has been associated with long-term health problems. Furthermore, the cytotoxicity of V has been demonstrated [Rao96]. That is the reason of the current tendency to exclude Vanadium and Aluminium from new biomaterials.

The second generation biomedical titanium alloys (β titanium alloys), namely Ti-Nb-Ta-Zr, are based on the reduction of the strength modulus (close to bone) and the elimination of toxic Al and V alloying materials. Ti-Nb-Zr ([CA10], [Maj08], [Sam08], [Rao96]), Ti-Nb-Ta-Zr ([Eli06], [Li04]) and Ti-Nb-Zr-Sn-Fe [Guo10] are some of the alloys under development.

The development of β-titanium alloys has drawn considerable attention in biomedical area for their much lower elastic modulus comparing to α or (α+β) dual phase titanium alloys, thus exhibiting better biomechanical compatibility. These alloys are being analysed for dental implant application ([Gol15], [Bai11], [Kum10]).

2.4. Surface treatments of titanium dental implants

Surface topography is considered one of the most important surface properties regarding the biological responses [Bru01b]. It is a key factor since it influences the bone healing process, encouraging a favourable cellular response by means of protein-surface and cell-surface interactions. Different surface modification methods has been developed for increasing surface roughness or applying osteoconductive coatings to titanium dental implants in order to improve osseointegration.

The classification and description of these techniques could be done from different points of view. If physiochemical character is considered, the classification could be done in five groups: mechanical methods (*e.g.*: machining, polishing and sand blasting), chemical methods (*e.g.*: acid attacks, alkaline attacks and electrochemical methods), vacuum methods (*e.g.*: ion implantation and glow discharge treatment), coating methods (*e.g.*: sol-gel, plasma spraying, magnetron sputtering and laser ablation), and treatments using biomimetic agents (*e.g.*: bioceramics, bioactive proteins, ions and polymers).

Commonly used techniques to modify dental implant surfaces can be classified into techniques adding material on the bulk metal (convex profile), and techniques that remove particles from the surface creating pits or pores on the surface (concave profile), see Table 2.6.

Table 2.6: Commonly used techniques to alter titanium dental implant surface topography [Wen09]. * treatments that will be analysed in the following sections.

Subtractive processes	Additive processes
Electropolishing	Calcium phosphate coatings*
Mechanical polishing	Titanium plasma-sprayed (TPS) surfaces*
Blasting*	Ion deposition
Etching*	
Oxidation	

Complete descriptions of surface modifications applied in titanium for biomedical applications can be found in bibliography ([Osh10], [Ram07], [Apa05], [Bag04], [Bru01b]). The references ([Avi09], [Kok04]) are focused in biomimetic treatments whereas the re-

ferences ([Liu10], [Jay07], [Men08]) review the treatments for nano-functionalization of biomaterials.

Next sections will review the most used surface treatments of currently available commercial dental implants, such as titanium plasma-spraying, calcium phosphate coatings, acid etching and sand blasting followed by acid etching. Their corresponding surface morphologies are shown in Figure 2.7 and properties and outcomes will be described and discussed is subsequent sections.

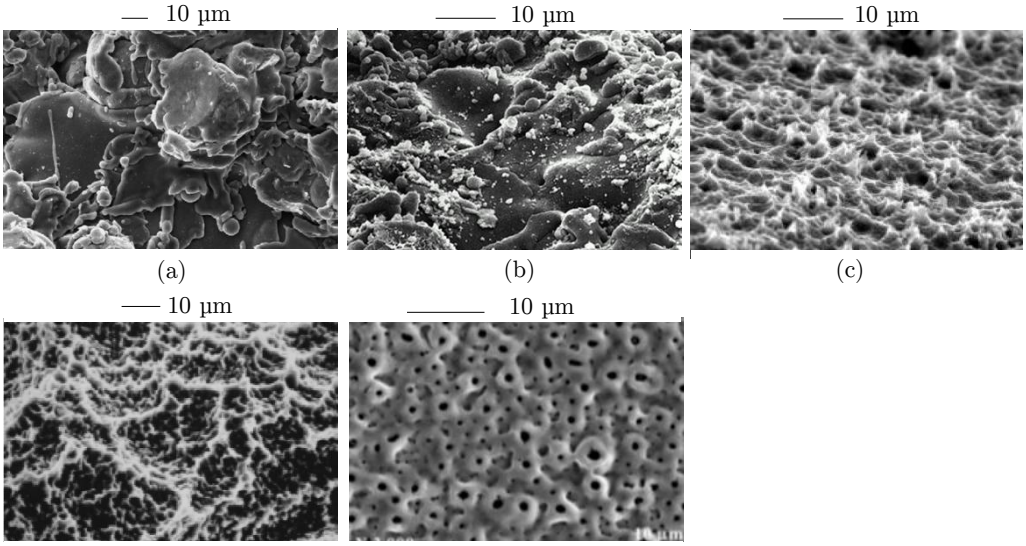

Figure 2.7: Surface morphologies of titanium dental implants. (a) titanium plasma sprayed [LG07]; (b) air-plasma-sprayed hydroxyapatite coating on a grit-blasted titanium substrate [Wil96]; (c) acid etched [Juo03]; (d) sand blasted and acid etched [Li02]; (e) anodized [Cho14].

2.4.1. Additive processes

Titanium Plasma Spraying (TPS)

This method consists in projecting titanium powder particles at a high temperature (by means of a plasma torch) onto the surface of the implants. This particles condense and fuse together, forming a film about 30 µm thick, increasing the surface area of the implant [LG07]. An example of a titanium plasma-sprayed surface is shown in Figure 2.7 (a).

TPS shows higher roughness than sand blasted, acid etched or hydroxyapatite-coated titanium dental implants. However, the bonding between the coating and the titanium substrate is considered to be weak [Ong04]. Furthermore, granules of titanium have been found to leak into the bone pocket adjacent to the TPS implants [Mar03]. Metal ions released from implants are a source of concern due to their potentially harmful local and systemic carcinogenic effects [Bro00]. Nowadays, there is a consensus on the clinical advantages of implanting moderately rough surfaced implants rather than using rough TPS implant surfaces [Ong04].

Hydroxyapatite Coating (HA)

Hydroxyapatite is a naturally occurring mineral ($Ca_{10}(PO_4)_6(OH)_2$). It is a bioactive ceramic, which forms part of the crystallographic family of apatites. This is the calcium phosphate compound most commonly used for biomaterials, since 70 % of human bone is made up of this inorganic mineral [Sub10]. This bioactive material (which stimulates new bone tissue growth around implant) is brittle and susceptible to crack growth, therefore it is only used as a coating material (see Figure 2.7 (b)).

The requirements of the coating are chemical stability (not be dissolvable in body fluid and don't react with the substrate) and mechanical stability (good adhesion to the substrate). Therefore the key issues are the control of coating composition and microstructure during deposition, and the control of adhesion of the coating to the metallic substrate ([FM08], [Ram07]).

The effect of the HA coating of dental implants is controversial. While the potential in short-term advantages are well documented, the long term fate has been subject of some criticism [Sim05]. The instability of HA in a biological environment is the most frequently discussed disadvantage ([Eli10], [Sub10]). However this disadvantage has not been proven conclusively, and there are works showing a good long-term success rate for HA coated implants ([Lee00] taken from [Avi09]). Recent developments have concentrated on improving coating stability and adhesion [Ram07].

2.4.2. Subtractive processes

Sand Blasting

Sand blasting treatment consists in blasting the implants with hard ceramic particles, which are projected through a nozzle at high velocity by means of compressed air.

The degree of roughness of the sandblasted surface depends on several controllable parameters, such as type and size of the grits, duration of blasting, air pressure and distance between the source of the particles and the implant surface [Gup09]. When implant surface is blasted, compressive residual stress is generated in the surface (which depend on both hardness and granulometry of the particles used), increasing the material surface energy [Eli10]. Different ceramic materials are used for blasting like alumina (Al_2O_3), titanium oxide (TiO_2) and calcium phosphate (*e.g.* hydroxiapatite $Ca_{10}(PO_4)_6(OH_2)$) particles ([LG07], [Müe03]).

Alumina is the more effective grit in terms of increasing surface roughness, since it is a harder material than titanium oxide. However, alumina is often embedded into the implant surface even after cleaning and sterilization, since it is insoluble in acid and hard to remove [LG07]. Despite of the poor biocompatibility of alumina [Apa03], Wennerberg *et al.* [Wen95b] concluded that implants blasted with TiO_2 or Al_2O_3 show similar bone-implant contact but much more fixation of the implant when compared to smooth titanium.

Animal experiments results showed that for samples blasted with 25 and 75 µm sized Al_2O_3 particles the removal torque and bone-to-implant contact (defined as the percentage of dental implant surface covered by newly formed bone) was higher comparing to a

implants blasted with 250 μm particles ([Wen96b], [Wen95a]). This finding suggested that a moderately rough surface is more adequate than high roughness surface.

Acid etching

Acid etching is often performed using hydrofluoric (HF), nitric ($HN0_3$), sulfuric (H_2SO_4) or hydrochloric (HCl) acid and combinations thereof ([Ehr10], [LG07]). Concentration of acidic solution, time and temperature are factors determining the result of chemical attack and microstructure of the surface [Gup09]. This treatment provides homogeneous roughness (micro pits with sizes ranging from 0.5 to few micrometers in diameter [Mas02]), increased active surface area, low surface energy and improved bioadhesion, reducing the possibility of contamination (no particles are encrusted) [Eli10]. An example of a titanium acid etched surface is shown in Figure 2.7 (c).

When treating dental implants in fluoride solutions, soluble TiF_4 is formed, generating micro-rough topography [LG07]. This chemical treatment of the titanium creates both a surface roughness and fluoride incorporation, and it is demonstrated that is favourable to the osseointegration of dental implants ([Eli10], [Coo06]).

It must be taken into a count that chemical treatments might reduce mechanical properties of titanium. For example, acid-etching can lead to hydrogen embrittlement of titanium, which creates micro cracks on its surface and could promote the reduction of fatigue resistance of the implant [Yok02].

Acid etching is often used in combination with sandblasting (explained in the following section).

Sand blasting followed by acid etching

The titanium dental implant surface is first sandblasted with large grits making the surface grossly rough. Then, the implant is acid etched to form micro-pits on its surface. Hence, a multi-scale roughness is generated, achieving an implant macro-topographically wavy and rough at the micro-level (see Figure 2.7 (d)).

Anodizing

Anodizing is an electrochemical process where the implant is immersed in an electrolyte while a current is applied, which will make the implant the anode in an electrochemical cell. The morphology and the crystal structure of the titanium oxide of the implant surfaces is modified and a porous surface structure is created (see Figure 2.7 (e)).

Rutile and anatase are the most important oxide structures for osseointegration of implants. Blasted and acid etched surfaces exhibit predominately rutile forms (despite of having different morphologies), while anodized surfaces have a predominance of anatase forms.

This technique has attracted a great deal of attention in the recent years due to controllable and reproducible results and the simplicity of the technique. Titanium dioxide (TiO_2) self-ordered nanotubes can be generated in the surface by means of optimized anodizing

parameters ([Sub10], [Mac07]). These nanotube like pores, have been shown to possess higher surface energy and wettability compared to unanodized Ti [Yao05].

2.5. Surgical placement and loading of dental implant

2.5.1. Surgical techniques

There are two surgery techniques depending on the implant type: two stage technique (submerged implants, Brånemark type) and one-stage technique (non-submerged implants). In the two stage traditional approach, placed implants are left submerged beneath the gum tissues, protected from the bacteria in the environment of the mouth. After a period of three or six months a second small surgical procedure is performed (step or stage two), to re-expose the implant into the mouth. Regarding the one stage approach, the implant is inserted leaving its head protruding out of the mucosa, which leads to place a temporary crown on an implant so that patients can leave their dentist's office with a tooth. Finally, if the implants are inserted after tooth removal (without healing period time), this is referred to as immediate implant placement [Gap03].

Concerning the insertion procedure, first of all a small incision is done into the gingival soft tissue, making the bone visible (Figure 2.8 (a), (b)). Afterwards, a pilot hole is drilled using a round bur, which is successively augmented with different drills up to the final cavity [Neo09] (Figure 2.8 (c)). The implant is finally inserted into the bone cavity manually (by means of a torque ratchet) or mechanically (using a surgical micro-motor), (see Figure 2.8 (d)).

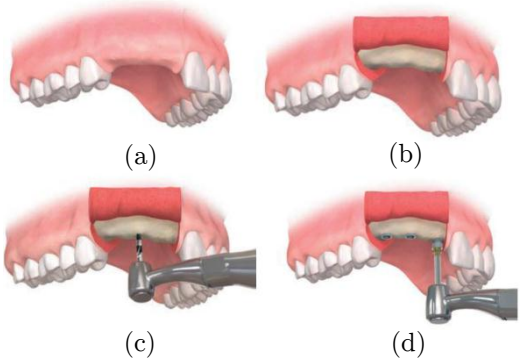

Figure 2.8: Dental implant insertion process [Neo09]. (a) implant site preparation; (b) incision into the gingival soft tissue; (c) cavity drilling; (d) implant insertion.

As general rule, implants must be inserted into bone with minimum trauma to surrounding tissues. Bone is heat sensitive, and a temperature of more than 47 °C combined with exposure time of more than a minute has been shown to result in a reduced bone formation [Eri84b]. To avoid increased temperature in the bone during the drilling process, intense cooling with saline solution, a graded series of drills and well sharpened instruments have been recommended [Eri84a]. Depending on the bone quality, different insertion strategies are followed.

The main surgical procedures for dental implant insertion can be classified in three groups: (i) osteotome technique, (ii) press-fit technique and (iii) undersized technique. The osteotome technique was conceived for soft maxillary bone and its based on placing implants without drilling. The objective of this technique is to maintain all existing maxillary bone aside with minimal trauma while developing an accurately shaped osteotomy [Sum94]. On the other hand, the press-fit technique theoretically creates an implant bed reproducing exactly the implant diameter, but often involves a small percentage of undersized drill in practice [Tab10b]. Finally, the undersized technique uses smaller drill diameter than implant diameter and is extensively used [Tab10a]. Although the exact reduction diameter seems to be a critical parameter, no consistent term or definition is used in literature. Tabassum *et al.* [Tab10b] gathered information on the published works using undersized technique with respect to discrepancy between implant diameter and final drill diameter. They concluded that in many works the percentage of diameter reduction was not possible to estimate due to the lack of information, and the percentages ranged form 14 to 40 % of diameter reduction.

2.5.2. Load condition

The loading condition is relevant for primary and secondary stability [Cho11], being necessary to control it to obtain osseointegration as soon as possible and maintain it as long as possible. Time estimated to bone healing is from three to six months [Alb81]. Due to the fact that micromotions may lead to fibrous tissue in growth or encapsulation, implants are conventionally kept load-free during this healing period. Nevertheless, it has been suggested that a range of tolerable micromotion exists of the order of 50-150 μm that may be favourable of osseointegration ([Van08], [SM98]).

Nowadays, there are immediately loaded, early loaded (after 6-8 weeks healing period) and the mentioned classically loaded implants (after 3-6 months healing period) [Ned04]. These immediate and early load protocols expose the implant to potential mechanical stresses prior to biologic integration, increasing the possibility to micromovements that may lead to implant failure [Mel09], therefore, they are applied only under favourable circumstances.

2.5.3. Surface alteration during insertion

Shear forces arises when an implant is placed into a predrilled hole of smaller-diameter in bone [Ska00]. Guan *et al.* [Gua11] carried out a dynamic modelling and simulation of dental implant insertion process through finite element method. It was observed that dynamic localized stress concentration spots were randomly created during insertion of the implants, which suggests that the contact between implant surface and bone was not uniform during insertion. Due to this stress concentrations generated between bone and implant, it is possible that the endosseous implant surface could be damaged or modified during insertion procedure.

It has been reported that release of titanium to the adjacent bone tissue may occur due to the friction and abrasion forces to which implant surfaces are subjected during

insertion [Fra04]. Released particles have been identified as one of multiple factors involved in the loss of balance between bone formation and bone resorption, given the increased osteoclast differentiation and resorption activity found in presence of titanium particles [Men13a]. Furthermore, recent studies suggest that the detachment of titanium from the implant surface may be a potential cause for periimplantitis ([TS14], [Olm13]), increased early bone loss [OH15], and implant failure ([Böl13], [Fri02]).

As well as the release of particles to the bone site overlying the implant, several reports describe the presence of titanium particles in distant inner organs. Shliephake *et al.* [Sch92] encountered titanium particles in the peri-implant area immediately after the installation of two screw implants. Five months later, particles were no longer observed on the bone surface next to the implants but were in the lungs, kidneys and liver, proving that transfer of microparticles can occur. Titanium migration to lymph nodes was also reported by other authors [Wei94]. However, the effect of those particles remains a biological concern ([Wan03], [Zaf03]).

It is clear from the foregoing that the possibility of surface alteration during dental implant insertion may have several implications in the implant performance and survival, and also as potential health hazard. This makes it important to develop a better evaluation and understanding of the interplay between insertion forces and surface modification.

In spite of these evidences, little has been published concerning the numerical analysis of topography alteration generated during insertion. Two recent studies analysed the topography alteration of different dental implant tops after insertion, reporting morphological variation and particle release ([Min14], [Sen13]). However, the characterization of these studies was restricted to implant tops, and therefore, the possible alterations on other parts of the implant remains unknown.

2.6. Surface topography characterization

Surface metrology is the science of measuring small-scale geometrical features of surfaces: the topography of the surface. Surface topography is significant for surface performance and the importance of its measurement as a means of functional analysis and prediction is indisputable. Surface metrology is therefore a link between manufacturing and function, as shown in Figure 2.9.

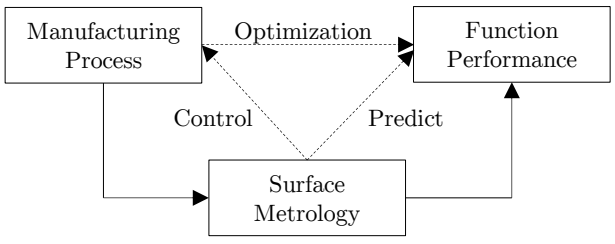

Figure 2.9: The role of surface metrology ([Dag80] taken from [Liu99]).

In the last decades this discipline is undergoing major changes, as stated by X. Jiang *et al.* [Jia07a]: *"Surface metrology as a discipline is currently undergoing a huge paradigm*

shift: from profile to areal characterization, form stochastic to structured surfaces, and from simple geometries to complex free–form geometries, all spanning the millimeter to sub–nanometre scales".

Quantification of surfaces using 2D profiles has been extensively used in engineering, however, it is now accepted that the characteristics of a surface cannot be completely interpreted without three dimensional information. Stout *et al.* [Sto00a] listed 6 reasons why 3D topographic analysis is better to 2D :

1. Surface topography is three-dimensional in nature, therefore 2D profile analysis is not able to represent natural characteristics of a surface.

2. Three-dimensional parameters are more realistic than those obtained from a 2D profile.

3. Three-dimensional surface measurement allows calculating functional extra parameters, such as oil volume, debris volume and the calculation of contact area.

4. The statistical analysis of 3D surface topography is more reliable and more representative, since the larger volume of data increases the independence of the data.

5. By means of different visualization techniques, 3D images provide significant information comparing to 2D images.

6. Almost all quantitative 3D measurement systems are digital system, while 2D systems normally use analog measures. Digitally based systems are more flexible in processing and storing data.

Consequently, this state of the art will be focused in three dimensional characterization of surfaces. The procedures for characterizing surface features are analysed in the following sections and include surface texture measurement (section 2.6.1), pre-processing (section 2.6.2) and numerical evaluation (section 2.6.3).

2.6.1. Measuring instruments

There are many measuring instruments and measuring methods to characterize surfaces. The most common classification of instrument types is into three groups: contact (stylus instruments), non-contact (optical instruments) and scanning probe microscopy (electron microscopy and atomic force microscopy), as shown in Figure 2.10.

Detailed descriptions of these instruments and fidelity issues have been extensively discussed in literature ([Wen00], [Sto93a]). The following section deals with the comparison between different measuring instruments. Subsequently the theoretical basis and advantages and disadvantages of the characterization techniques used in this study (SEM, confocal profilometry and focus variation) are presented. Finally, the suitability of each instrument for dental implant characterization is analysed.

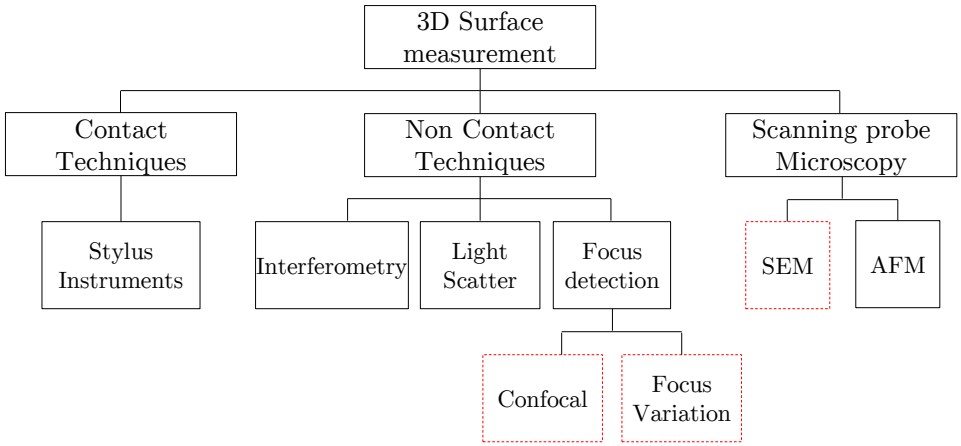

Figure 2.10: Classification of surface topography instruments based on the physical principles of measurement. Note: Dashed red outline indicates the methods used in current project.

Comparison between instruments

It is difficult to compare between instruments, since each one has its own working principle, measuring ranges and pros and cons. On this matter, Stedman [Ste87] developed a method for delineating the effective working range of instruments, by means of the ability to measure sinusoidal perturbations of varying amplitude or wavelength. The limiting factors considered are: vertical range and resolution, horizontal range and resolution, and horizontal datum and probe size/geometry. This way the working amplitude wavelength space (AW space) is obtained for a given instrument, where each block indicates the working area of an instrument and the two axes represent the resolution towards the axes (Figure 2.11)

In general terms, the STM/AFM measuring system has the highest resolution in both directions, but the measurement range is small. The stylus instrument has a large vertical range, however it must be taken into account that is a contact method, so the surface may be damaged during measurement. Among optical methods, the interferometer has the highest resolution in the vertical direction (but the horizontal one is less comparing to focus system). It must be pointed out that non contacting methods have the advantage that the surface under test is seldom physically damaged or chemically changed. Regarding the resolution of the quantitative SEM, is the reverse of that of the interferometer (high horizontal resolution, and lower vertical resolution).

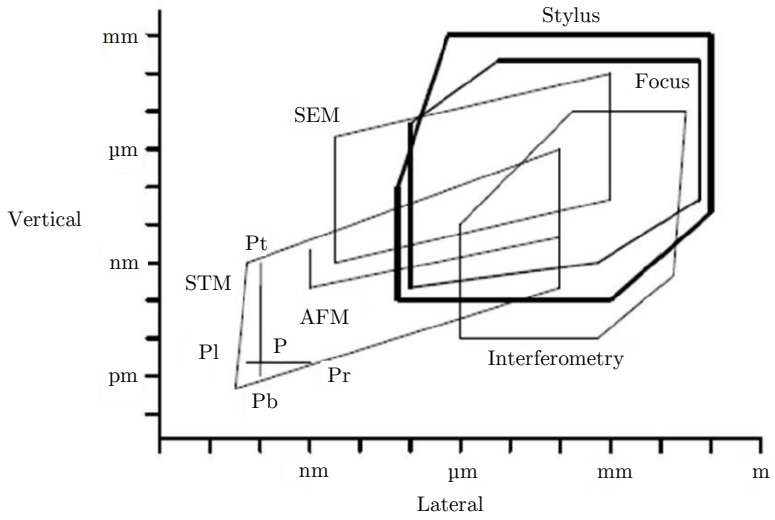

Figure 2.11: Amplitude-wavelength plot of the working range of 3D surface measurement instruments [Sto00a].

Scanning Electron Microscope (SEM)

The transmission electron microscope (TEM) was the first type of electron microscope developed in 1931 by Knoll and Ruska. Subsequent research resulted in the first SEM.

A scanning electron microscope (SEM) is a type of electron microscope that images a sample by scanning it with a high-energy beam of electrons in a raster scan pattern, point by point. Figure 2.12 (a) shows an schematic diagram of the SEM as used in its most common mode, the emissive mode. As can be seen, a stream of monochromatic electrons is produced in an electron gun (usually composed of the tungsten hairpin filament) and is condensed by magnetic lens. The electron beam then passes through scan coils that deflect horizontally so that the beam scans the surface of the sample. The whole column and sample chamber must always be at a vacuum when in use, in order to produce a stable electron beam and avoid the presence of other molecules. Several phenomena are produced when the incident electron beam (*i.e.* the primary beam) bombards the specimen surface (see Figure 2.12 (b)). There are two broad categories of electron scattering: elastic and inelastic.

Elastic scattering happens when the electron trajectory is altered but the kinetic energy doesn't vary. This phenomena results in elastic backscattered electrons, which are primary electrons (*i.e.* electrons belonging to incident electron beam). This iteration gives chemical information of the analysed sample since the higher the atomic number the more backscattered electrons. Thus, looking at the contrast of the backscattered electrons, different chemical compositions can be detected (where brighter zones indicate more backscattered electrons, and therefore bigger atomic number), but the chemical element cannot be identified.

When inelastic scattering occurs part of the energy of the electron is transferred to the

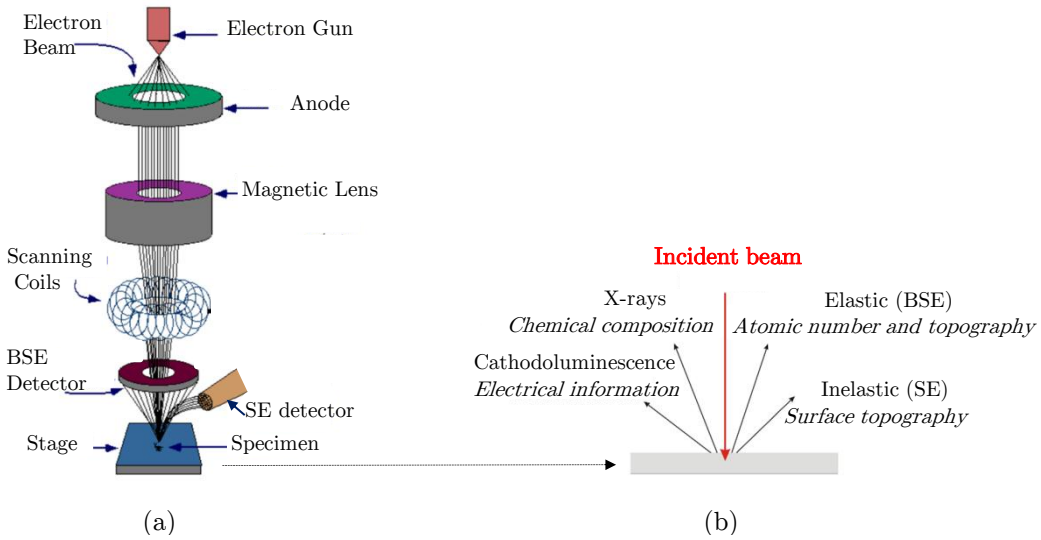

Figure 2.12: Scanning electron microscope. (a) schematic diagram of basic Scanning Electron Microscope equipment [Uni15]; (b) interactions between electrons and sample in a scanning electron microscope [SEM].

atom in the sample (excitation), generating different types of signal. The inelastic backscattered electrons (so-called secondary electrons), which are electrons belonging to the sample, give surface topography information. The cathodoluminescence gives electrical information, and X-rays give information about chemical composition of the surface. Further information on these and other interactions can be found in the bibliography [Gol03].

All of these phenomena can be detected by using a proper detector. The detectors basically count the number of interactions that occur and display them as a pixel on a screen (CRT), where the intensity of the pixel is proportional to the number of interactions counted. The detection process is repeated throughout the scan, point by point. The principle images produced in SEM are of three types: secondary electron images (SE), backscattered electron images (BSE), and elemental X-ray maps.

The advantages of the SEM over light microscopes are mainly two: they have very much larger depth of field, which allows a large amount of the sample to be in focus at one time, and far greater resolution is possible overcoming the theoretical limit of magnification of light microscopes (approximately 1000 times). On the other hand, the main disadvantage is related to the sample size, which is limited, and to the fact that samples must be conductive (if not, they must be covered by a conductive layer).

From the point of view of topographical characterization, the major disadvantage is the inability of the conventional SEM to measure in the third dimension, or depth of topographical features. Despite the fact that in the past two decades some stereology techniques have been developed to obtain quantitative 3D information [Sto00a], it is usually used qualitatively and as a lateral quantifier only, rather than as a primary surface measurement instrument.

Confocal Microscopy

Confocal microscopy was pioneered by Marvin Minsky [Sem05] in 1955. Minsky's approach is based in illuminating a single point at a time through a pinhole in order to avoid the unwanted scattered light that obscures an image when the entire specimen is illuminated at the same time. Furthermore, the light returning from the specimen pass through a second pinhole aperture that reject rays that are not directly from the focal point. In this way the scattered and reflected light from out of-focus planes is eliminated keeping the light in focus as strong as possible. The term confocal here relates to the fact that the image of the illuminating pinhole and the back-projection of the detection pinhole have a common focus in the specimen [Sto93a].

Advances in optics and electronics have been incorporated in modern confocal microscopes, however, the key elements of Minsky's design has been kept. The majority of confocal microscopes image either by reflecting light off the specimen or by stimulating fluorescence from dyes applied to the specimen. The former is more used for topographical characterization and will be further described subsequently, while the later is most commonly used in biological applications.

A confocal profilometer is a noncontact technique based on confocal microscopy which provides an areal quantitative data of the surface. The schematic diagram of conventional confocal profilometer is shown in Figure 2.13 (a). By software treatment of the intensity patterns (Airy intensity distributions) captured by the detector (CCD camera), the particular plane where the system was focused may be determined, yielding the measurement of the height of the surface from the reference plane at that particular point. During the measurement, the sample is scanned vertically (z_{scan}) at different steps so that every point on the surface passes through the focus (see Figure 2.13 (b)). The focused points of the consecutive sections are converted computationally obtaining areal numerical surface data.

The 3D surface topography measurement is obtained by scanning each illuminated point in the vertical direction and moving the point in horizontal plane subsequently. This process is repeated to map the surface until completing the selected acquisition area. In order to improve the speed at which measurements are taken, quite often an array of pinholes ("pattern"), is imaged simultaneously onto the surface. This way numerous points can be measured simultaneously, decreasing the measuring time.

Confocal profiling provides the highest lateral resolution that can be achieved by an optical profiler, thus, spatial sampling can be reduced to 0.10 μm [NEO15]. Regarding the limitations of the technique, focus detection systems requires a minimum reflectivity of the sample, and the measurable maximum surface slope is limited by the numerical aperture of the objective. Furthermore, when steep slopes are encountered, the scanning focus spot loses focus and the instrument rapidly searches for focus in the z plane before going to the next scan position. This leads to spurious spikes and sharp pits in the data, so caution should be taken [Sto93a]. Further information can be found in ([Web99], [Kin94], [Sto93a]).

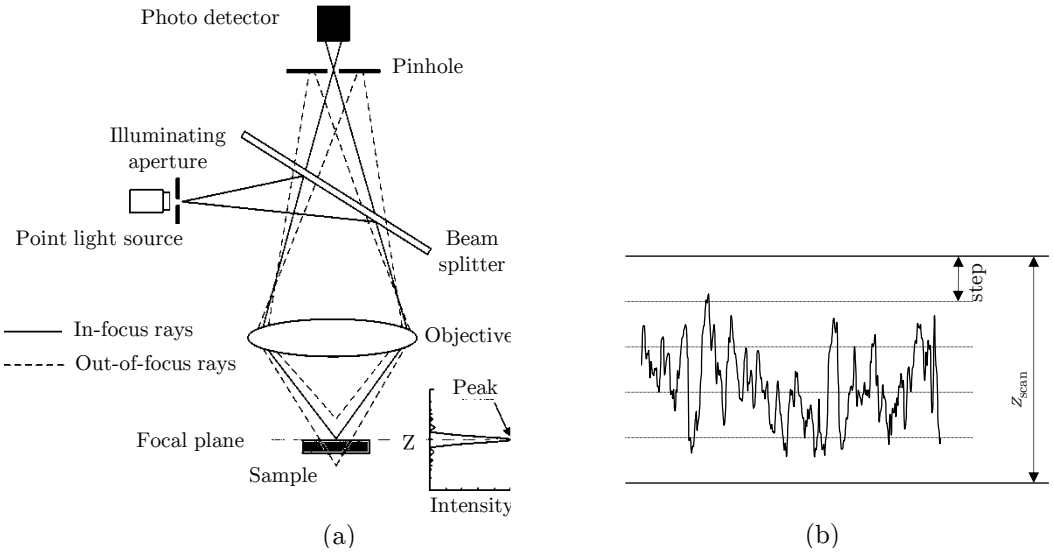

Figure 2.13: Confocal profilometer. (a) schematic of a basic confocal profilometer set-up (adapted from [Che12]); (b) scheme of the vertical scan carried out during measurement.

Focus variation

Focus variation is a rather new technique that provides topographical and colour information by differentiating between images of a surface that are in and out of focus. The nominal operating characteristics of this instrument group are detailed in [ISO15] and an schematic representation is shown in Figure 2.14.

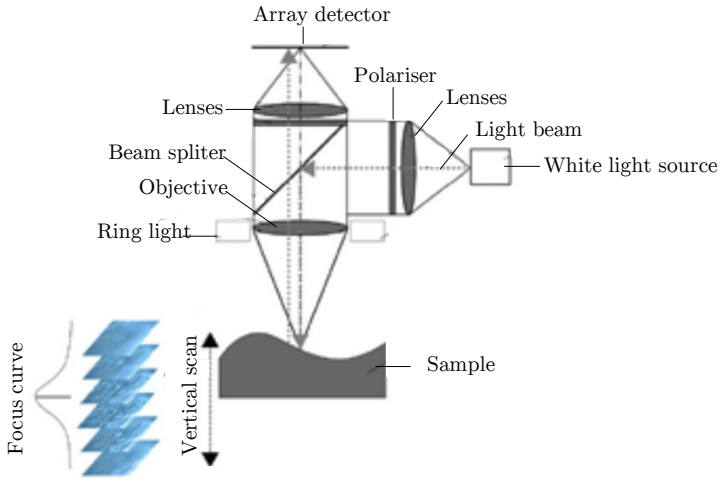

Figure 2.14: Schematic representation of a focus variation instrument [Wan15].

The sample is scanned vertically acquiring a series of images across the vertical scanning range. The image of a surface can be considered in terms of pixel intensities, and the relative intensity changes (focus variations) of these pixels across images allows to estimate

the focus position of each spot through robust algorithms.

A number of different focus measure operators have been employed but the Sum-modified-Laplacian method developed by Nayar is favoured [Nay92]. This method achieves high sensitivity by high pass filtering the image frequency data thus accentuating this crucial band of frequencies.

In contrast to other optical techniques, two issues should be especially addressed. First, the method is not limited to coaxial illumination, which allows to introduce ring light and to measure slope angles exceeding 80°. On the other hand, in addition to the scanned height data, focus variation delivers a real colour image of the surface. However, this technique relies on analysing the variation of focus, and therefore it is only applicable to surfaces where the focus varies sufficiently during vertical scanning process (R_a >10 nm) [Dan11]. This limits its use for relatively smooth surfaces.

Suitability for dental implant characterization

From the point of view of the suitability of an instrument to measure the implant surface topography, some considerations must be taken. Dental implant surfaces use to be rough surfaces, so the maximum height range of the system is an important factor to consider. Obviously, depending on the surface morphology, different vertical and lateral resolutions may be needed to characterize properly the topography. Finally, due to the threaded geometry of implants, and taking into account that different zones must be measured (as will be explained later), the working distance must be considered.

Most of these aspects has been analysed by Wennerberg [Wen00], who gathered typical properties of representative systems of the three major types of measuring instruments, as shown in Table 2.7.

Table 2.7: Instrument properties and suitability for dental implant characterization [Wen00]. Note: This data is just for guidance, since instruments are rapidly being improved. *TPS= Titanium Plasma Spray.

	Contact stylus instrument	**Focus detection**	**Confocal laser scanning profilometer**	**Interferometry**	**Scanning probe microscope**
Maximal area	100x100 mm	300x300 mm	2x2 mm	200x200 µm	100x100 µm
Maximal height range	8 mm	500 µm	108 µm	2 mm	6 µm
Horizontal resolution	1 µm	1 µm	0.5 µm	0.4 µm	100 pm
Vertical resolution	10 nm	5 nm	6 nm	0.1 nm	10 pm
Method suitable for screws?	No	No	Yes	Yes	No
Method suitable for cylinders?	Yes	Yes	Yes	Yes	Yes
Method suitable for polished surfaces?	Yes	Yes	Yes	Yes	Yes
Method suitable for turned or milled surfaces?	Yes	Yes	Yes	Yes	May exceed measuring range
Method suitable for blasted surfaces?	Yes	Yes	Yes	Yes	May exceed measuring range
Method suitable for TPS* surfaces?	Yes	Yes	Yes	Yes	No

The interferometry, confocal profilometry, and stereo SEM has been pointed out as the only acceptable instruments for threaded dental implant measurement ([Ehr13], [Wen00]).

Based on the present review, the focus variation system should be added to the list.

2.6.2. Data processing

Reason ([Rea44] taken from [Tuk11]) suggested a classification system for surface topography in 1944, which was subsequently widely accepted. The classification considers a surface as a range of spatial frequencies, which are decomposed into three components: form (low frequency components), waviness (medium frequencies) and roughness (high frequencies), see Figure 2.15.

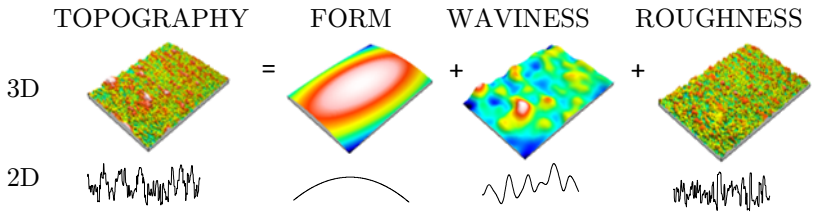

Figure 2.15: 2D and 3D representations of topography components: form, waviness and roughness.

Therefore, data processing is required to extract the desired spatial information, which is usually accomplished through the application of filters. Figure 2.16 shows this filtering sequence, which is based on the filtering process specified for 2D texture characterization ([ISO97], [ISO96a]), and also fits the conventional filtering sequence established for 3D characterization [Sto93f].

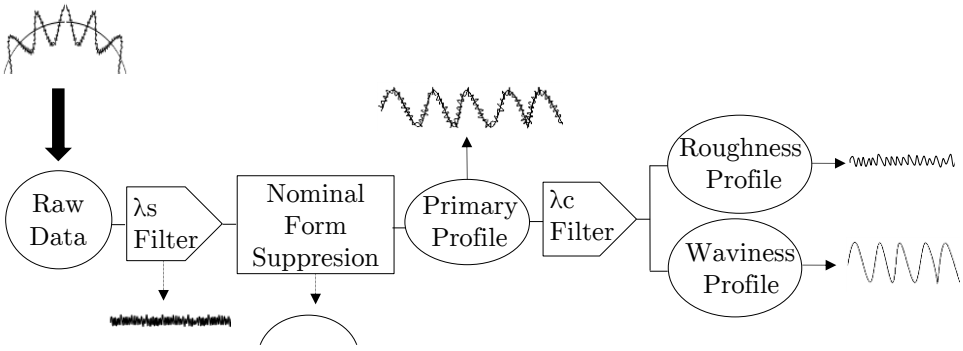

Figure 2.16: Scheme showing the stages of data processing before numerical characterization.

λ_s is usually applied first as part of the extraction process, which removes short wavelength features such as noise. Following this process the surface form is removed leaving the primary surface. By applying the high pass or low pass filter with a cut-off λ_c, the roughness and waviness surfaces are obtained. It is from these set of data that topographical parameters are usually calculated.

Traditional concepts (conceived for 2D characterization) do not always accommodate the needs of 3D surface characterization. Several new filtering methods have now been specified which do not rely on the concept of wavelength ([ISO12], [Bla06], [ISO06]). Consequently new concepts have emerged, which have been recently standardized ([ISO12],

[ISO06]). In 3D characterization, a filtered surface is referred to as scale limited surface rather than surface with limited bandwidth. Figure 2.17 shows the equivalences between the 2D terminology and the recent 3D/areal terminology (based in the descriptions given in [Jia07a]).

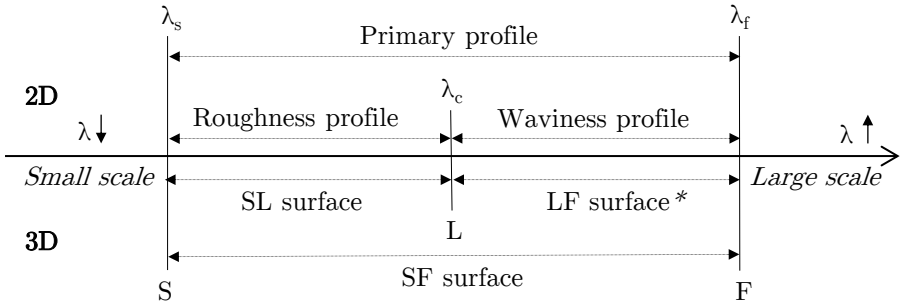

Figure 2.17: Equivalences between 2D and 3D terminology. *LF surface is not envisaged in the standard ISO 25178-2 [ISO12].

The S filter eliminates information at the smallest scale, which can be compared with the λ_s used to remove high frequencies. The roughness filter has been replaced by an L filter, which can be compared with λ_c. The F operator eliminates the nominal form. Two scale limited surfaces has been defined in ISO 25178-2 [ISO12], namely the SL surface and the SF surface. It must be highlighted that the scale limited LF surface defined in Figure 2.17 is not envisaged in the standard where the SF surface can refer to the primary or waviness surface depending on areal S filter nesting index. The terminology described in Figure 2.17 (where SF=Primary surface, SL=Roughness surface, and LF=Waviness surface) will be used in this work, in order to allow to different scale limited surfaces to be extracted from the same measurement unambiguously.

Filters

Fundamentally, filters brake down the signal in the frequency or scalar domain in order to isolate specific frequency bands with relevant surface features [Sto00b].

Filtering technology has been in use for more than 70 years in surface characterization, and its progression has been very closely related to the development of modern mathematics and signal-processing techniques. ISO/TS 16610-1 [ISO06] have recommended a toolbox of new and novel filter tools classified into four categories: linear filters, robust filters, morphological filters and segmentation filters.

There are different types of linear filters [Jia11], but the most used filter in metrology as well as in dental implant surface characterization is the Gaussian filter([Raj02], [Wen00]). The gaussian filter replaces every point on a profile or surface by a weighted average of points in its neighbourhood, obtaining the mean line (2D) or mean surface (3D), which serves as reference for topographical parameter calculation. The name of this filter comes from the bell-shaped Gaussian function which was chosen as a weighting function. An important property of Gaussian filter is its linear phase which is a major advantage over 2RC filter, and is designed to have 50 % transmission at the cutoff (see Figure 2.18).

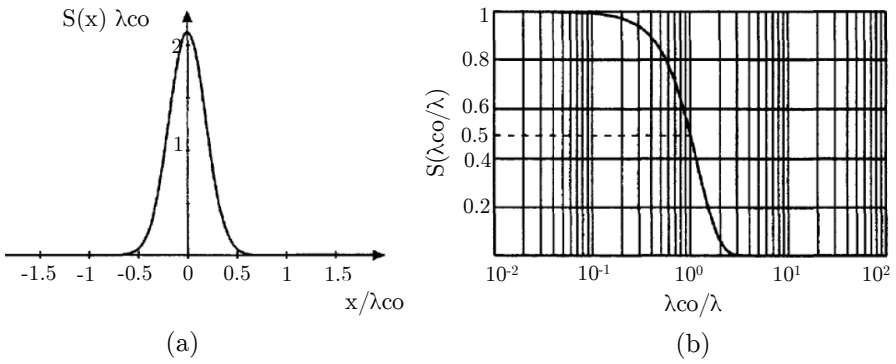

Figure 2.18: Weighting (a) and transfer function (b) of the Gaussian filter [Bri03].

This filter presents certain drawbacks: the edge effects (due to the boundary distortion because of the local weighed average), the sensitivity to outliers and form, and the arbitrary implementation (since it is a continuous filter, there is not a unique algorithm), see Figure 2.19. Due to this drawbacks, it is suggested to remove form from the acquired data before filtering, and the ends of the surface are cut to remove distortions.

Robust filters emanated form the Time Series Modelling Theory. A filter is called robust if the freak values don´t lead to the distortion of the filter mean line (waviness profile), therefore, robust filters has been introduced to suppress the influence of outliers (see Figure 2.20).

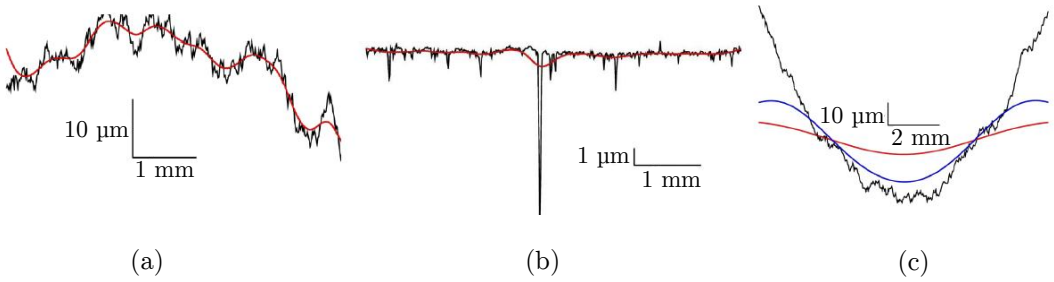

Figure 2.19: Principal drawbacks of Gaussian filter, where the red line is the mean line. (a) end effects; (b) distortion when outliers are present; (c) distortion with large form components. The effect increases with increasing curvature and increasing cut-off (red: large cut-off, blue: smaller cut-of) [Kry08].

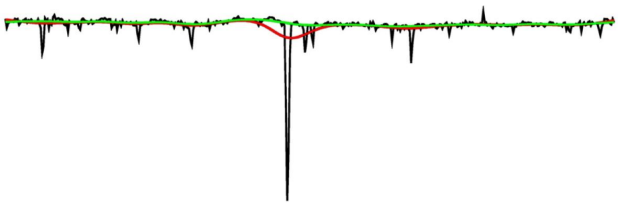

Figure 2.20: Gaussian filter (red mean line) Vs Robust Gaussian filter (green mean line) [Kry08].

Morphological and segmentation filters are included in the non linear filter group. Morphological filters, the so-called envelope system filters, operate by sweeping the input geometrical object using a second geometric (structuring) element, simulating contact phenomena in dilation or erosion mode (see Figure 2.21 (a)). There are three categories of morphological filters: closing & opening filters, alternating symmetrical filters and space-scale techniques [Jia11].

Finally, the segmentation technique, is a filter that partition a profile into portions according to specific rules [Jia07a]. Further information can be found in [Sco04] and [Sco03]. This filter has been used for different purposes, including the identification of active grains of grinding wheel or the identification of extrusion marks and grain boundaries of anodised extruded aluminium [Sco03]. This filter is also used to calculate the feature parameter set, explained in the subsequent section (see Figure 2.21 (b)).

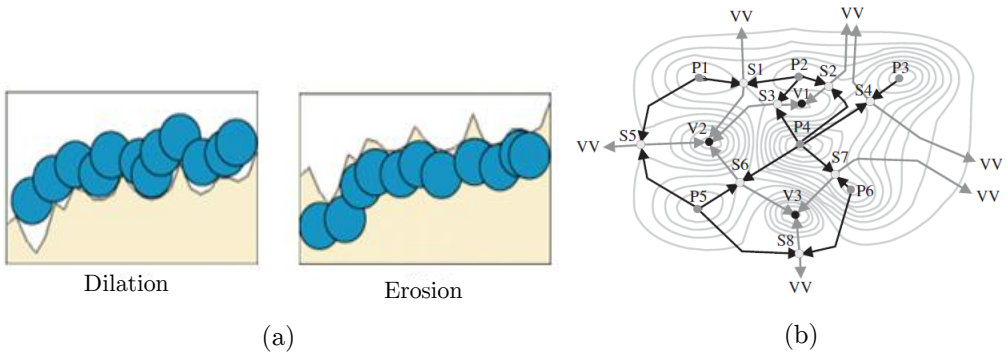

Figure 2.21: Representative images of morphological and segmentation filters. (a) 2D representation of morphological operations [Dig08]; (b) features detected by segmentation technique: P, peaks; V, pits; S, saddles; VV,virtual valley [Sco04].

2.6.3. 3D Topographic parameters

Following measurement of a surface and data treatment it is necessary to quantitatively characterize the surface to be able to make direct comparison between different surfaces. As mentioned previously, 2D quantification has been historically used. A large number of parameters (more than 150) were developed, some of them with overlap in definition and characterization. Whitehouse used the term "parameter rash" to define it [Whi82]. However, it is now accepted that the characteristics of a surface cannot be completely interpreted without three dimensional information.

During the 90's, the European Community supported important programmes for the development of methods for the characterization of roughness in three dimensions under the leadership of Birmingham University (UK). As a result of this work a parameter set called the "Birmingham 14 parameters" (described in [L.B03c]) was proposed, intended to characterize some major aspects of topographic features. Subsequently, from 1998 to 2001, two important programs took place: the AUTOSURF project led by the Rover/Brunel University (UK) and the SURFSTAND protect led by the Huddersfield University (UK). In

2003 the so called "Green book" was published [L.B03c] containing the detailed results from the SURFSAND project, which proposed further parameters in addition to the original Birmingham 14 parameters.

Following this feat the areal parameter study progressed rapidly and the parameter list has grown to encompass over 30 parameters in the recently published ISO 25178:2 standard [ISO12]. The parameters for areal surface texture are currently partitioned into two main classes called "field" and "feature" parameters. The field parameters are based on statistics of the whole surface whereas the feature parameters are defined using subsets of pre-defined features using segmentation based on pattern recognition. Figure 2.22 shows the parameter sets described in ISO 25178-2 [ISO12].

The field parameter set is divided into S-parameters and V-parameters. The former depend on the height amplitude and spacing frequency and the later give fundamental volumetric information based on the area material ratio curve (Abbott-Firestone curve).

It should be remarked that unlike 2D parameters, which are evaluated along several sampling length, the 3D parameters are determined within one sampling area, and there is not any distinction in nomenclature as to whether they derive form primary, roughness or waviness information. Detailed descriptions and formulations can be found in appendix A and further information in ([Lea13], [ISO12]).

The most commonly used 3D parameters for dental implant characterization are analysed in the following section.

2.6.4. Topographical characterization of dental implants

Wennerberg *et al.* [Wen00] took the first steps in measurements' standardization suggesting some guidelines for dental implant characterization: three samples in a batch must be evaluated, three dimensional measurements must be made at three evaluation areas (tops, flanks and valleys), the filter size must be specified, and at least one of each height, spatial, and hybrid parameters should be presented. More recently, Ehrenfest *et al.* ([Ehr13], [DE11]) presented some guidelines for the publication of articles related to implant surfaces, suggesting classification and codification systems with a view to making progress in the standardization process. However, there is presently no standard that defines how to characterize a dental implant surface topography, but it should be remarked that an open debate about the necessity of such standard has been started very recently [Dav14].

In order to asses the homogeneity of published characterizations, Table 2.8 gathers information collected from recent publications that reports dental implant topographical characterization. It can be observed that some the works follow the guideline suggested by Wennerberg [Wen00], but almost all omit key information about characterization process. On the other hand, it is clear that there is not any consensus about the topographical parameters that must be published. Regarding the data processing parameters, the most used filter is a Gaussian filter with a cutt–off of 50 μm, which is based on previous works made by Wennerberg *et al.* [Wen96a].

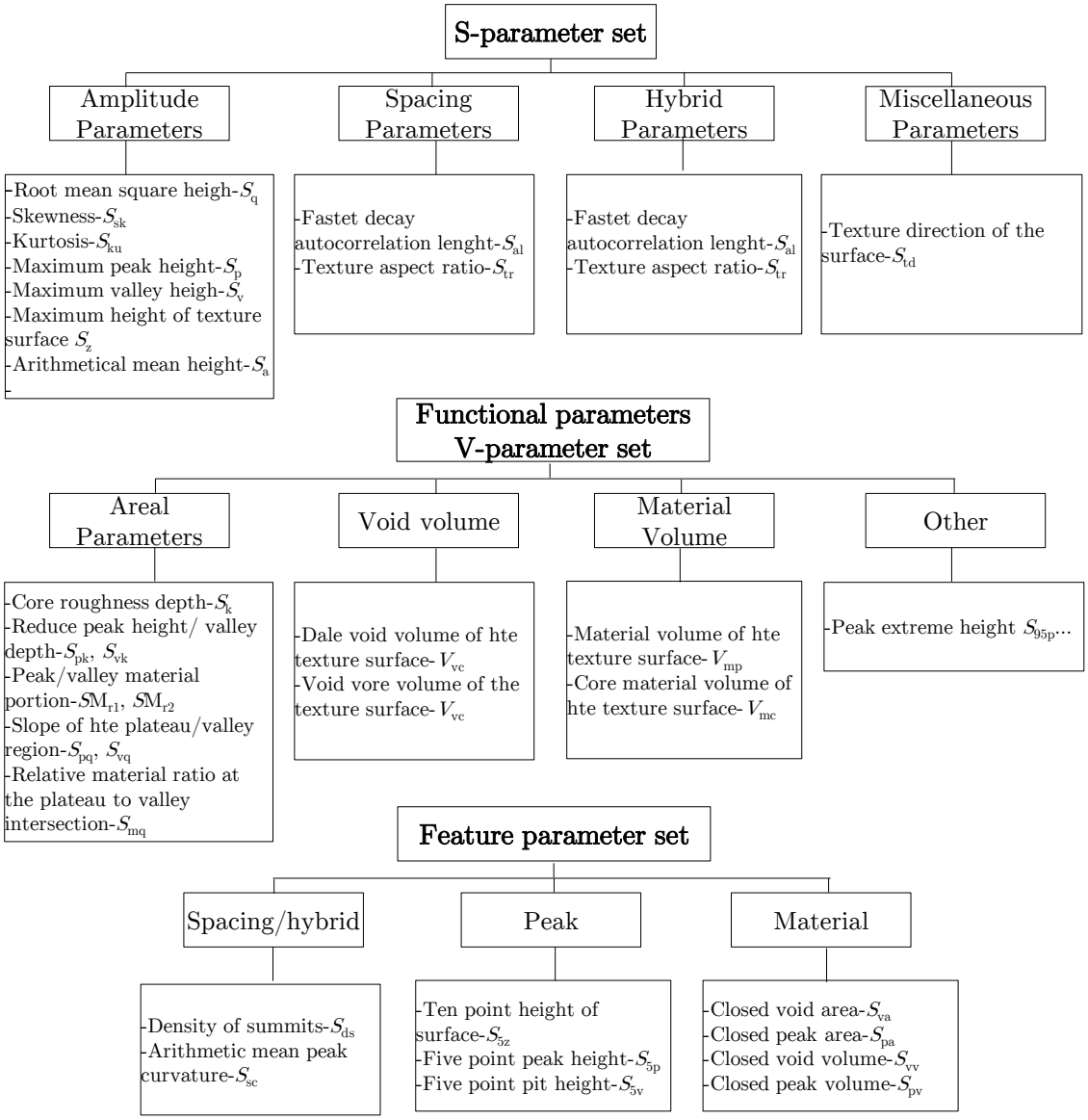

Figure 2.22: Parameter sets included in the ISO 25178-2. Field parameters (S parameters and V parameters) and Feature parameters [Jia07b].

Table 2.8: Parameters published in bibliography for implant surface characterization. n*= implants per group.

Ref.	**Geometry / n***	**Quantity/ Sites**	**Instrument/ Configuration**	**Area** (μm^2) **/length** (mm)	**L filter type**	**L filter size** (µm)	**Roughness Parameters**
[Sen13]	Screw-shaped n=6	All tops	Optical Interferometry/ 50x	—	Gaussian	—	Height (S_a, S_{sk}) Hybrid (S_{dr}) Functional (S_k, S_{vk}, S_{pk})
[Cho11]	Screw-shaped n=3	3/ Top 3/ Valley 3/ Flank	Optical Interferometry/ —	—	Gaussian	50x50	Height (S_a) Hybrid (S_{dr}, S_{ds}) Functional (S_{ci})
[Coe11]	Screw-shaped Cylindrical n=3	3/ outer diameter	Optical Interferometry/ —	—	—	100x100	Height (S_a, S_q) Hybrid (S_{ds})
[Tab10a]	Screw-shaped n=2	-/Thread area	—	—	—	—	Height (R_a, R_q, R_{sk})
[Sva09]	Screw-shaped n=3	3/ Top 3/ Valley 3/ Flank	Optical Interferometry/ Objective=50x Zoom=0.62	264x200	Gaussian	50X50	Height (S_a) Hybrid (S_{dr}, S_{ds}) Functional (S_{ci})
[Sul09]	Screw-shaped n=3	3/ Top 3/ Valley 3/ Flank	Optical Interferometry/ —	260x200	Gaussian	50X50	Height (S_a) Hybrid (S_{dr}, S_{ds})
[Tab09]	Screw-shaped n=3	3/ Threads	Stylus Instrument/ Load=1 mN V=0.1 mm/s	Threadh length	—	—	Height (R_a)
[Bus04]	Cylindrical n=—	10/ Areas	Confocal Microscope/ —	—	—	—	Height (S_a,S_q S_t) Functional (S_k)
[RR05]	Screw-shaped n=1	3/ Areas of thread 1/ apical area	Confocal Profilometry/ Objective=20x	—	—	—	Height (S_a, S_q S_p, S_t) Functional (S_v)
[Müe03]	Cylindrical n=3	3/ Profiles	Stylus Instrument/ —	5	—	—	Height (R_z, R_{max} R_a)

2.6.5. Correlation between topographic parameters and functional response

The parameter S_a or its analogous in 2D $R_\mathbf{a}$ is the most used parameter to define roughness, thus the discussion is usually focused in the mean roughness (S_a or R_a).

In the review carried out by Dohan *et al.* [Ehr10] is determined that the averaged roughness around 1–2 µm elicit better cell responses. Similarly, Wennerbgerg *et al.* stated that optimum roughness based in the averaged value (S_a) is 1–1.5 µm ([Wen98], [Wen95b], taken from [Wen00]). Other study suggests that the range of average roughness that probably affect the bone response may be of a broader range of 0.5–8.5 µm ([Sha06] taken from [Tab09]).

Based on the previous, it could be said that in general terms the optimum averaged roughness value (S_a) is around 1– 2 µm. Accordingly, Svanborg *et al.* [Sva09] reported that the commercial dental implant roughness is around 1–2 µm. However, it should be pointed out that the S_a parameter is insensitive in differentiating peaks, valleys and spacing of the various texture features, and therefore the same value may represent a very different surface topographies.

The pertinence of surface roughness parameters to describe dental implant surfaces has been questioned since surfaces with very different appearance have similar parameter values [Han99]. Hansson *et al.* [Han00] described the surface shown in Figure 2.23 by means of the following parameters: R_a, R_q, R_t, R_z, R_{ku}, Δ_q, R_{dr} (which are the 2D analogous of S_a, S_q, S_t, S_z, S_{ku}, S_{dq}, S_{dr} respectively), and λ_q (see Equation (2.1)).

$$\lambda_q = \frac{2 \cdot \pi \cdot R_q}{\Delta_q} \tag{2.1}$$

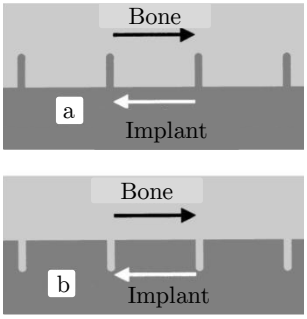

Figure 2.23: Different profiles with the same R_a, R_q, R_t, R_z, R_{ku}, Δ_Q, R_{dr} and λ_q values [Han00].

They showed that the parameters described above are not able to discriminate between mirror surfaces. Therefore, even if the bone plugs interlocking with the implant surface are much bigger for implant *a* than for implant *b*, the topographical parameter values are the same.

Nonetheless, some authors have found the relevance of certain parameters for describing dental implant surfaces. Sosale *et al.* [Sos08] characterized two titanium alloy implants which elicit different bone responses by means of a set of topographical parameters. After

analysing the differences between all parameters, they concluded that the root-mean square slope (S_{dq}) and summit curvature (S_{sc}) are particularly sensitive parameters, and therefore necessary for dental implant description. The theoretical study carried out by Hansson *et al.* [Han10] supported this finding, since they observed that the interfacial shear strength (important for osseoingration) increases linearly with the root-mean-square slope (S_{dq}) as well as with the average roughness (S_a). In accordance with these results, Löberg *et al.* [Löb10] suggested that besides the most used parameter (S_a), the root-mean square of the surface slope (S_{dq}) and the void volume parameter (V_{vc}) must be included to be used for correlation with in vivo performance. Similarly, and based on in vivo tests, Arvidsson *et al.* [Arv06] concluded that low core fluid retention index (S_{ci}), which is related to the V_{vc} parameter as shown in Equation (2.2), seems favourable for bone-anchored implants. Therefore, S_{dq}, S_a and V_{vc} had been highlighted as important parameters for dental implant surface description.

$$S_{ci} = V_{vc}/S_q \tag{2.2}$$

On the other hand, the distances between peaks have been detected as important factor. However, there seems to be no consensus on the optimum value.

Boyan *et al.* [Boy00] cultured cells of the osteoblastic linage on Ti surfaces with varying topographies in order to analyse the effect of surface topography on osteoblast morphology. According to their findings, the micrometry of the surface must be close to the dimensions of the cell (approximately 10 µm) to obtain cell sensing. They concluded that when osteoblasts are cultured on a smooth surface (R_a<0.2), they assume a flattened fibroblastic morphology. In case of surfaces with R_a< 2 being the distances between peaks (referred to as R_m) greater than the length of the cell, the surface is perceived as smooth. If the distance between peaks is inferior to the cell size while the R_a is bigger than 2, cells are unable to flatten and spread, assuming more osteoblastic morphology. Finally on surfaces with mixed topography, the behaviour of the culture will reflect the average of the two morphologies (see Figure 2.24).

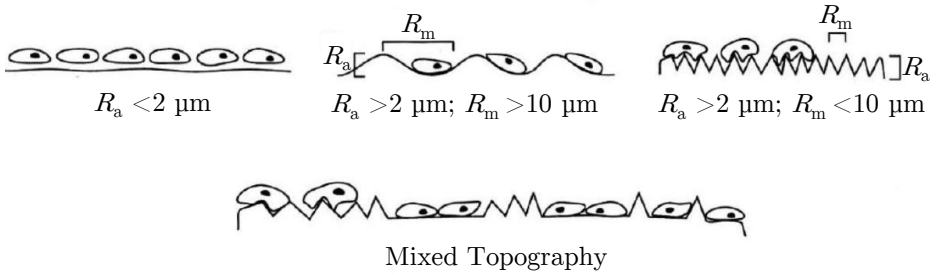

Figure 2.24: Effect of surface topography on osteoblast morphology according to Boyan *et al.*. R_a<0.2: flattened fibroblastic morphology. R_a>0.2-R_m>10 µm: surface perceived as smooth. R_a<2 µm-R_m<10 µm: cells unable to flatten and spread, assuming more osteoblastic morphology. On surfaces with mixed topography: average behaviour [Boy00].

However, these authors give confusing parameter definitions. The value of the R_a pa-

rameter is interpreted as peak height, therefore, the statement is not correct. On the other hand, the distances between peaks are referred to as R_{m}. According to ISO 4287:1997, this parameter refers to the maximum valley heigh in the edition made in 1984. Posteriorly, in the edition made in 1997, the same parameter was referred to as R_{v}. According to the mentioned norm, the distance between peaks is named S_{m}. It seems that in this case, the nomenclature has been misinterpreted.

Conversely, Aparicio *et al.* [Apa05] found out that peak distances higher than 10 µm (upper limit stated by Boyan *et al.*) could sense cells. Furthermore they found out that human osteoblast size is higher than 10 µm emphasizing that in order to stablish relations between roughness and cell adhesion, it is essential to define adequately the roughness and cell size.

In short, despite a very active research activity, the optimum surface has not been established yet. In addition to the lack of understanding about the interplay between surface topography and cell response, the absence of standardisation regarding topographic characterization makes it difficult to sort and interpret the published findings. Wennerberg *et al.* [Wen09] concluded that most of the works reporting surface characterization are not adequate, due to the omission of these parameters.

A work made by Macdonald *et al.* [Mac04] highlights the ambiguity around dental implant topographycal characterization. Different dental implants were submitted to three internationally renowned laboratories for surface texture characterization. The area of measurement was specified but specific measurement parameters were not requested. Techniques used included contact profilometry, two- and three-dimensional laser profilometry and atomic force microscopy. Four to thirteen parameters were reported, 2D or 3D, including R_{a} or S_{a}; only three were common to all centres and the results varied by as much as ± 300–1000 %, depending on technique and surface type. For example, one dental implant surface was reported with R_{a} of 0.17, 0.85, 1.9 and 4.4 µm. This results show the ambiguity situation around topographical characterization of dental implants, and highlights the necessity of an standard process due to the influence of the arbitrary selected parameters used in topography characterization.

2.7. Critical Review

From the reviewed bibliography it can be concluded that there is enough evidence about the influence of surface topography in the cell response, and therefore in the performance of dental implants ([Pas10], [Lim07], [Apa05], [Sam05], [Hua04], [Mar04], [Ros03], [Boy00]). However, despite of much research, the relationship between cell behaviour and surface texture is still not fully understood and the preferred surface has not been stabilised. This is reflected in the wide range of topographies encountered on currently commercially available dental implants ([Chr12], [Sva09], [Wen93]).

One difficulty is that the different factors that affect cell response like topography, chemistry and energy are difficult to segregate because their interdependence. On the other

hand, the lack of standardization in surface characterization techniques and the multiple variables involved in the in vitro and in vivo studies that have an influence in the results, make it difficult to extract general conclusions from different works.

Concerning surface topography, it was demonstrated that the topography characterization process involves a numerous variables that impact on results. In spite of the existence of some guidelines ([Ehr13], [DE11], [Wen00]), they don't address all the involved variables and presently there is a huge inhomogeneity (due to the use of different variables and techniques) and ambiguity (due to the omission of key information) in the published results ([Wen09], [Mac04]). This lack of consensus regarding the topographic characterization of dental implants makes it difficult to sort and interpret the published data, and makes it impossible to carry out meta-analysis, obstructing the development of the knowledge in this area. Additionally, there is a generalized use of an L filter of 50x50 μm in order to separate waviness and form, based on the work carried out by Wennerberg *et al.* [Wen96a]. The inclusion of an L filter is a critical point in the characterization, insofar as the surface texture information is fully separated once filtering applied. Hence, filtering should be used to clearly define texture bandwidths where the spatial bandwidth are related to the surface function. However, the functional bandwidth is actually unknown and the inclusion of this filtering may eliminate important information from the surface. Based on this literature review, it must be highlighted the necessity to establish a specific surface analysis protocol for dental implants providing detailed guidelines for future development. The future of dental implantology should aim at developing surfaces with controlled topography and chemistry, and therefore it is indispensable to develop traceable and standardized topographical characterization methods from the stand point of being able to correlate with functional performance.

On the other hand, there are evidences of surface alterations during dental implant insertion. Release of particles to the bone site overlying the implant has been reported ([Sen13], [Fra04]), as well as the migration of this particles to the distant organs ([Wei94], [Sch92]). It is clear from the review that the possibility of surface alteration during dental implant insertion may have several implications in the implant performance and survival and also as potential health hazard ([OH15], [TS14], [Böl13], [Men13a], [Olm13], [Fri02]). Despite this fact, little has been published concerning the numerical analysis of topography alteration generated during dental implant insertion, and there is a lack of information about the critical aspects of this phenomena. This makes it important to develop a better evaluation and understanding of the interplay between insertion forces and surface modification. Additionally, it must be taken into account that the novel surfaces are tested in vitro, however, these surfaces may not represent the surfaces facing the real biological environment after implantation due to the suffered alteration. The effect of topographical alterations on the cell response has not been studied yet. This knowledge may contribute to foster advancements in the design of better performing endosseous implants.

CHAPTER 3

TOPOGRAPHICAL CHARACTERIZATION STRATEGY

"What we measure affects what we do."
Joseph Stiglitz

The importance of the correct topographical characterization of dental implants is indisputable due to its effect on biological response. However, owing to the lack of standards and of a general consensus regarding dental implant surface characterization, ambiguous topographical analyses are reported. The aim therefore of the present study is to determine and evaluate the factors affecting 3D topographical parameters and to establish a topographical characterization strategy for dental implants. The first part of the chapter deals with the development of tools for the accurate and repeated handling and positioning of dental implants. The effect of the acquisition and data processing variables on the 3D topographical parameters are subsequently analysed and evaluated. Finally, based on the results obtained, a generalized topographical strategy for endosseous dental implants is established and applied to two commercial dental implant systems as examples.

3.1. Introduction

Surface topography is currently considered one of the most important surface properties regarding the biological response ([Men13a], [Eli10], [Vör01]). Accordingly, an intense amount of implant research has been focused on the development of new surface treatments ([Men08], [LG07], [Bag04], [Juo03]), and the study of the effects of varying implant surface topographies on the biological response ([Nik12], [Git11], [Dav10], [Eli08]). The correct topographical characterization of dental implants has thus great importance as a means of surface topography control and osseointegration prediction. Topography characterization is a process divided into three steps[1]: i) data acquisition, ii) data processing and iii) numerical characterization. Each stage contains variables that may strongly influence the results of the characterization.

Due to the lack of standards and of a consensus regarding dental implant surface characterization, ambiguous topographical analyses are reported ([Wen09], [Mac04], [Coo00]). The aim therefore of the present study is to determine and evaluate the factors affecting 3D topographical parameters and to establish a generalized topographical characterization strategy for endosseous dental implants.

To begin with, dental implant handling and positioning devices were developed in order to manipulate the samples without damaging or contaminating the surface, and also to obtain accurate measurements. The second part of the chapter deals with the effect of data acquisition variables on 3D topographical parameters. Acquisition parameters of a confocal profilometer regarding the microscope objectives, z-scan value, step size and area size were analysed in order to determine the optimum configuration. The third part concerns the effect of data processing parameters. The analysis was carried out using a full experimental design where variables considered included: i) S filter size (λ_s), ii) F operator (F), iii) L filter type (L) and iv) L filter size (λ_c). Two surface treatments, acid etching and sand blasting followed by acid etching were analysed in this study.

Finally, based on the results obtained, a generalized topographical characterization strategy for endosseous dental implants is proposed, and the characterization of two commercial dental implant systems (those used for the insertion tests, analysed in Chapter 4) is presented as an example.

3.2. Objectives and hypotheses

The overall aim of this chapter is to establish a generalised strategy for dental implant topography characterization. The specific aims are as follows:

- To develop sample holders and positioning devices for quantitative as well as qualitative evaluation.
- To analyse and evaluate the effect of data acquisition and data treatment variables on 3D topographical parameters.

[1]For a detailed description the reader is referred to section 2.6 “Surface topography characterization”.

- To establish a generalized topographical characterization strategy for endosseous dental implant characterization.

These are the hypotheses under consideration:

- Measurement and data treatment variables affect the value of 3D topographical parameters.
- A robust topographical characterization strategy for endosseous dental implants can be established.

3.3. Development of handling and positioning devices

In order to obtain an appropriate characterization it is essential to position each evaluation area perpendicular to the light or electron beam, and to accurately select the measurement location. Furthermore, the surface of the samples must not be damaged or contaminated during surface characterization. To aid in the quality, repeatability and time optimization of the characterization process, dental implant handling and positioning devices were developed.

First, a support for implant handle was designed and fabricated in order to facilitate dental implant manipulation, minimizing the risk of damage or contamination during the characterization process. The support was made of aluminium in order to fulfill the conductivity requirement for the scanning electron microscope, and the fixing system used the internal implant thread, making it flexible for all types of dental implants (Figure 3.1 (a)).

As already mentioned, different parts of the implant (neck, top, valley and flank) should be characterized, and therefore an adequate location system is of great importance. For qualitative analysis, aluminium positioning devices were developed, in order to locate the handling support in the required position inside the scanning electron microscope in a fast and repeatable way (Figure 3.1 (b)-(c)). Concerning the quantitative analysis, a positioning device for the confocal profilometer consisting of three degrees of freedom (DOF) was made of resin, due to the superior machinability and lightness of this material. The support was designed to integrate with the handling support (Figure 3.1 (d)) and also to fit into the confocal profilometer base (Figure 3.1 (e)). This enabled an accurate positioning of measurements through the three DOF.

The tools developed consisted of the base for accurate and repeatable handling and positioning of dental implants.

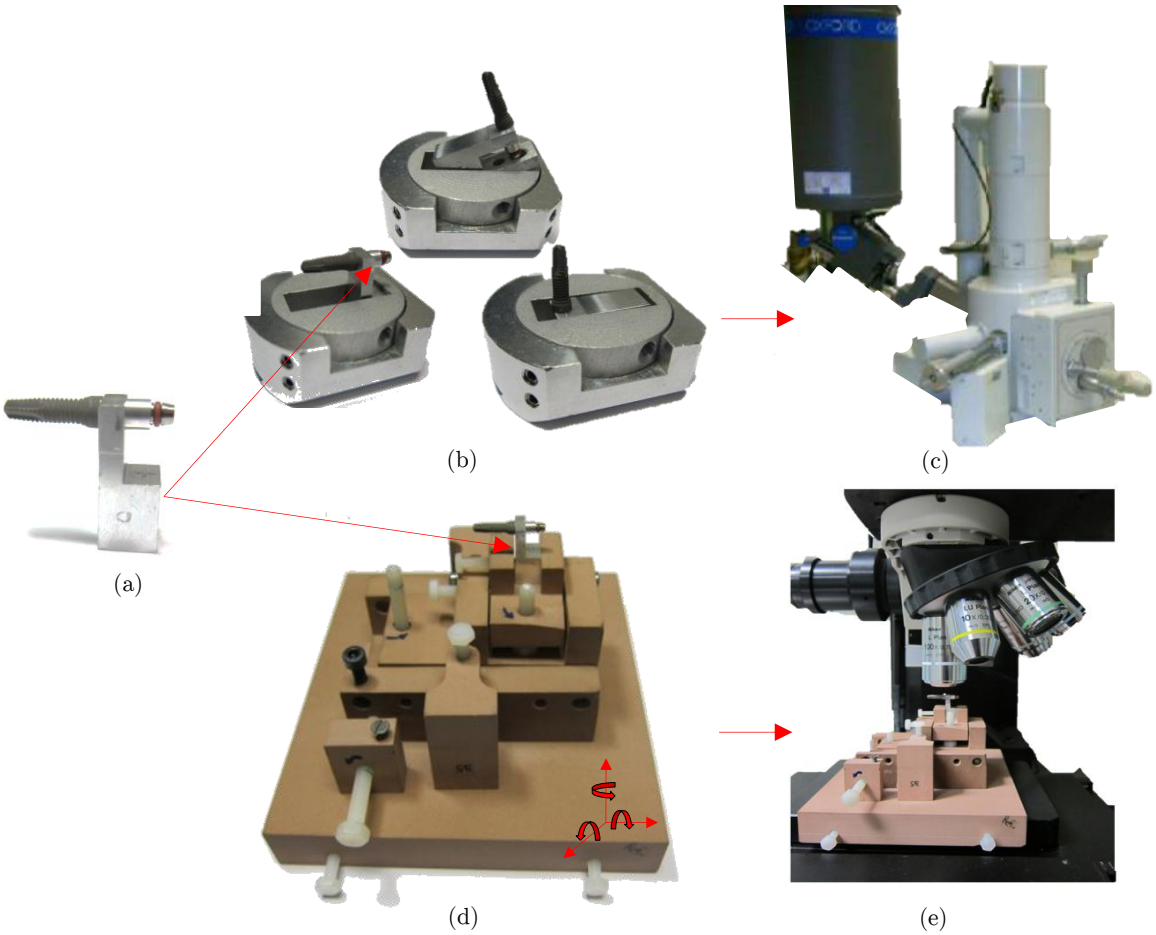

Figure 3.1: Dental implant handling and positioning devices: (a) dental implant handling support; (b) positioning devices for the qualitative analysis; (c) scanning electron microscope JEOL JSM 5600 LV used for the qualitative characterization; (d) positioning device with three degrees of freedom for the quantitative analysis; (e) confocal profilometer Sensofar Plμ used for the quantitative characterization.

3.4. Effect of acquisition variables

3.4.1. Materials and Methods

Dental implants

A total of 10 screw-shaped commercially pure titanium INTERNA® dental implants from BTI (Biotechnology Institute, Vitoria, Spain) were used for the study (see Figure 3.2). BTI's proprietary acid etching (commercially known as OPTIMA) and standard sand blasting followed by acid etching (referred to as SB+AE) treatments were selected to cover the wide range of surface roughness present in current dental implantology. Five implants (1-5) had the OPTIMA, and the rest (6-10) the SB+AE.

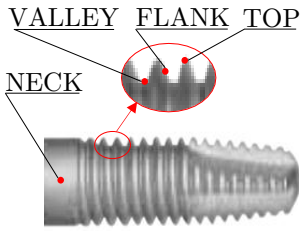

Figure 3.2: BTI INTERNA® dental implant. Denomination of the different evaluation sites.

Equipment and acquisition variables

A confocal imaging profiler (Plμ-SENSOFAR) was used for the study[2]. With this equipment the pinhole is replaced by a structured pattern consisting of a set of parallel slits, and the photodetector measuring the light intensity is a CCD camera (768 by 576 pixels), which works simultaneously as a pinhole and photodiode. This equipment includes a motorized XY stage and PZT device and allows measurements of extended topographies.

The effect of the acquisition variables on 3D topographical parameter values was evaluated in terms of the microscope objective (see Table 3.1), z-scan, step size and area size. All measurements were treated using the same data processing variables (see Table 3.2) through the metrological software SensoMap Turbo 5.1.

Table 3.1: Specifications of the microscope objectives used in the study.

Characteristic	10xEPI	20xSLWD	50xSLWD	100xSLWD
Working Distance (mm)	17.3	24	17	6.5
Numerical Aperture	0.3	0.35	0.45	0.7
Field of view (μm^2)	1400x1050	700x525	280x210	140x105
Spatial Sampling (μm)	1.82	0.91	0.36	0.18
Maximum Slope	14°	16°	21°	35°

Table 3.2: Variables used for data processing in the study of the influence of data acquisition variables.

S filter	F operator	L filter
Gaussian (λ_s = 0.36x0.36 μm)	Second order polynomial fitting	Gaussian (λ_c = 50x50 μm)

Measurement details are shown in Table 3.3. To study the effect of the microscope objective, z-scan value, and step size, all other acquisition variables were kept constant (Measure. No 1-12). The influence of the area size was analysed by taking into account three aspects: i) the influence of the area size when no high form components are present (Measure. No 13-22), ii) the interaction between area size and evaluation site (Measure.

[2]For a general description of the technique, the reader is referred to section 2.6.1 "Confocal Microscopy".

No 23-25) and iii) the relation between the area size and the reliability of topographical parameters (Measure. No 26-85).

Table 3.3: Details of the measurements carried out to evaluate the effect of acquisition variables on 3D topographical parameter values.

Variable under study		Meas.No	Implant No	Treatment	Site	Objct.	Area (μm^2)	Zscan (μm)	Step (μm)
	Object.	1	1	OPTIMA	Neck	10x	138x104	90	0.2
		2				20x			
		3				50x			
		4				100x			
	zscan	5	1	OPTIMA	Neck	100x	138x104	14	0.2
		6						50	
		7						100	
	Step	8	1	OPTIMA	Neck	100x	138x104	90	0.2
		9							0.4
		10							0.8
		11							1.6
		12							2.4
	Area size	13-17	1-5	OPTIMA	Neck	100x	470X353	20	0.2
		18-22	6-10	SB+AE	Neck		470X353	48	
		23	1	OPTIMA	Top	100x	250X187	24	0.2
		24			Top		138X104	12	
		25			Flank		250X187	12	
		26-55	1	OPTIMA	Neck	100x	250X187	10	0.2
		56-85	6	SB+AE			250X187	20	

Topographical parameters

A set of field parameters defined in ISO 25178 [ISO12] were selected for the study, belonging to height (S_q, S_{sk}, S_{ku}), spatial (S_{al}), hybrid (S_{dr}, S_{dq}) and functional (V_{mp}, V_{mc}, V_{vc}, V_{vv}) families[3].

In this part of the study, a Gaussian L filter of 50x50 µm was used following the suggestions given in [Wen00], and parameters were calculated on the roughness (SL) surface (data treatment details are shown in Table 3.2).

Statistical analysis

A statistical *t*-test was conducted to calculate confidence intervals in the analysis of area size and reliability (95 % confidence level). All statistical calculations were carried out through Matlab® R2013a.

[3]Detailed descriptions can be found in Appendix A "3D Topographic parameters".

3.4.2. Results

Influence of the microscope objective

The influence of the microscope objective was evaluated by acquiring the same area using objectives of 10x, 20x, 50x and 100x magnifications. The acquired data was cropped to obtain the same evaluation area for all acquisitions.

As shown in Figure 3.3 (a), a smoothing of the surfaces was observed as the microscope magnification decreased.

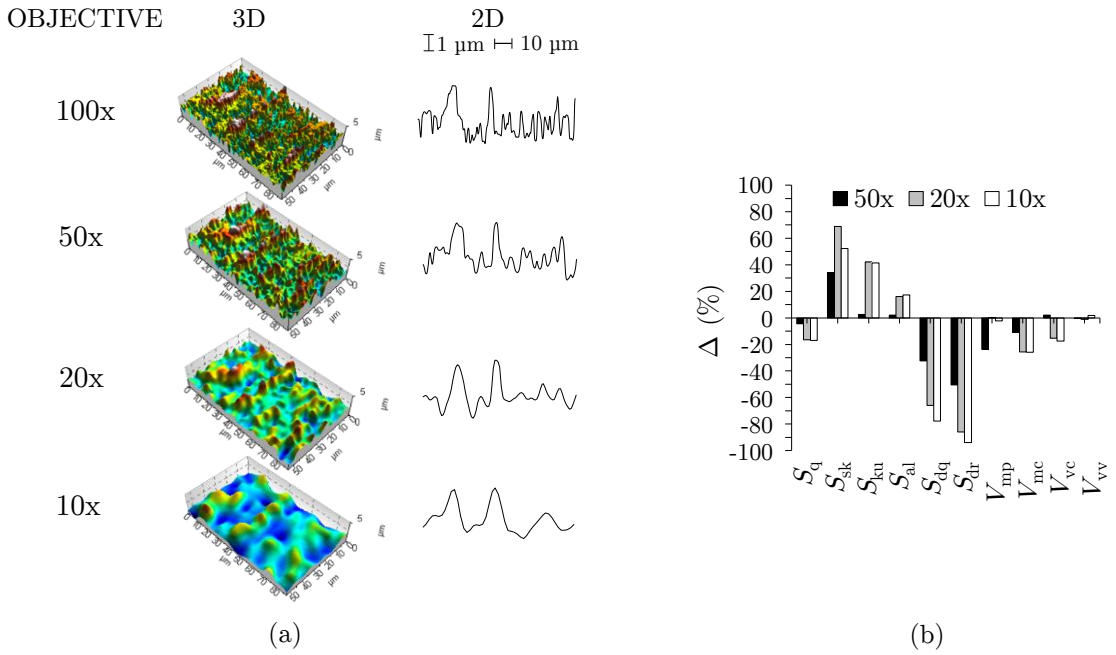

Figure 3.3: The influence of the microscope objective: (a) axonometric projections and corresponding representative 2D profiles of the same surface area acquired with 100x, 50x, 20x and 10x microscope objectives; (b) Topographical parameters presented as a percentage change from the more precise measurement (objective: 100x, spatial sampling: 0.18 µm).

This is attributed to the fact that the diminution in lateral resolution acts as a kind of averaging filter due to the aliasing effect. This smoothing was reflected in the topographic parameter values, which are presented in terms of percentage change from the more precise measurement in Figure 3.3 (b), (topographic parameter values can be found in Appendix B). The root mean square roughness (S_q), the developed area (S_{dr}) and the root mean square slope (S_{dq}) decreased as the objective magnification decreased. Conversely, the autocorrelation length (S_{al}) increased, due to the increased width of the acquired features when using lower magnifications. The skewness (S_{sk}) and kurtosis (S_{ku}) also increased, which indicated that the surfaces acquired with lower magnification objectives presented a less Gaussian height distribution (S_{ku} >3)[4] and more predominance of peaks (S_{sk} >0)[5]

[4] A Gaussian surface has a kurtosis value of 3.

[5] A negative S_{sk} indicates a predominance of valleys, whereas a positive S_{sk} indicates a predominance of peaks.

comparing to the more precise measurement acquired with 100x objective (S_{sk} ~0, S_{ku} ~3). The functional parameters showed that in general the peak material volume (V_{mp}) and void volume (V_{vv}) were not significantly affected, while the core material volume (V_{mc}) and core void volume (V_{vc}) parameters decreased when decreasing the objective magnification. Hybrid parameters (S_{dr}, S_{dq}) containing both amplitude and lateral information were the most sensitive parameters, followed by the height parameters S_{sk} and S_{ku}.

Five of the ten parameters under study were considerably influenced (>10 %) by the objective change already for the 50x objective (spatial sampling= 0.36 µm).

Influence of the z-scan value and step size

The influence of the z-scan value (z_{scan}) was investigated, with measurements acquired on the same surface area using three z_{scan} values. The smallest value (14 µm) corresponded to the minimum z_{scan} required to span the whole height rank of the surface, and the highest value (100 µm) corresponded to a typical z_{scan} value used to measure very rough surfaces in dental implantology. An intermediate value (50 µm) was selected with the ultimate goal of detecting possible tendencies. As shown in Figure 3.4, the z_{scan} variable showed negligible effect (<2.5 %) when analysing percentage changes calculated from the more precise measurement carried out with the minimum z_{scan}[6], (the topographical parameter values can be found in Appendix B).

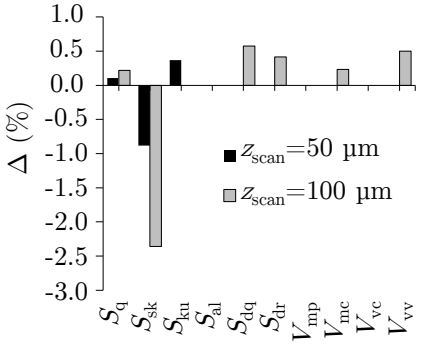

Figure 3.4: Influence of the z_{scan} on the 3D roughness parameters presented as a percentage change from the minimum z_{scan} (14µm).

The influence of the step size was analysed by acquiring the same area at varying step sizes (0.2 µm, 0.4 µm, 0.8 µm, 1.6 µm and 2.4 µm). As shown in Figure 3.5 (a) less peaks were acquired as the step size increased, which was reflected in the changes of topographical parameters (see Figure 3.5 (b)), (the topographical parameter values can be found in Appendix B). This smoothing of the surface resulted in the decrease of the root mean square slope (S_{dq}) and the developed interfacial area (S_{dr}) values. However, the general height of the surface was not affected (no significant variation in S_q parameter) and the shape of the remaining features did not change significantly (small variations in the autocorrelation length S_{al}). The presence of less peaks resulted in an increase of the

[6]The vertical resolution of the equipmnent is a % of the z_{scan}.

skewness parameter (S_{sk}), indicating that the surfaces acquired with greater step size presented a bigger predominance of peaks. Although to a lesser extent the kurtosis value also increased (S_{ku}), which indicates a slight change in the height distribution shape. Regarding the functional parameters, the void volume parameters (V_{vc}, V_{vv}) indicated no substantial difference (<10 %), the core material volume (V_{mc}) decreased and the the peak material volume (V_{mp}) presented varying tendencies. Regarding the sensitivity of parameters, the height parameter S_{sk} was the most affected, followed by the hybrid parameters S_{dr} and S_{dq}.

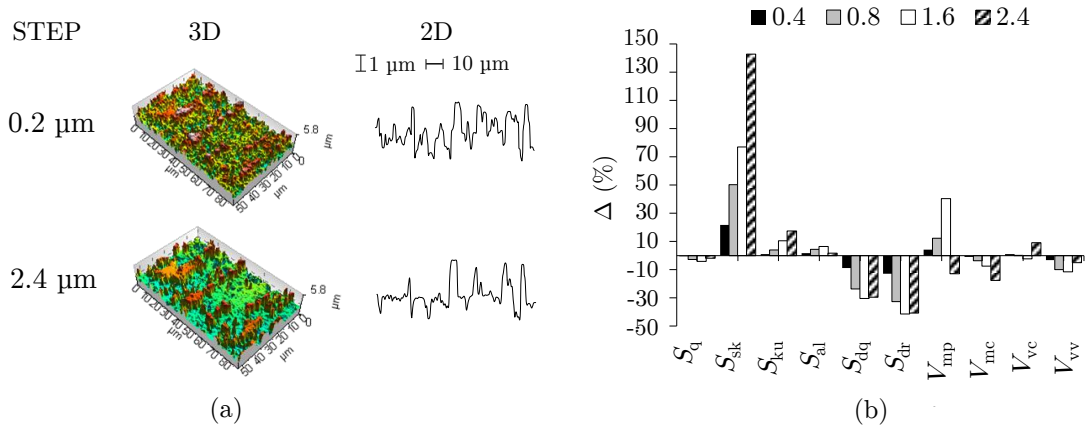

Figure 3.5: Analysis of the step size effect. (a) axonometric projections and corresponding representative 2D profiles of the same surface acquired with steps of 0.2 and 2.4 µm; (b) influence on the 3D roughness parameters presented as percentage change from the minimum step size (0.2 µm).

Influence of the area size

Effect of the area size

The influence of the area size was analysed, taking into account the wide range of roughness levels and typical dispersions in dental implants. To that end an extended topography of 4x4 (470x353 µm^2) was performed on five implants in the neck for each treatment, see Table 3.3. From these data files smaller extended areas were cropped, corresponding to 2x2 (250x187 µm^2), and 1x1 (138x103 µm^2) topographies, in order to evaluate the effect of the area size on the topographical parameter values. For a convenient display of the results, Figure 3.6 shows all of the S_q values corresponding to one implant (spots), and the extreme values obtained from all measurements of the five implants (crosses) for the two treatments under study.

As the area size decreased the dispersion of the values increased considerably. Figure 3.7 shows the maximum percentage error that may be made by calculating parameters from one unique measurement, taking as a reference the mean value obtained in the larger area (4x4) for all topographical parameters.

The chances of large errors in the results were greatly increased when decreasing the area size, especially for the SB+AE treatment, which presented higher dispersion in the

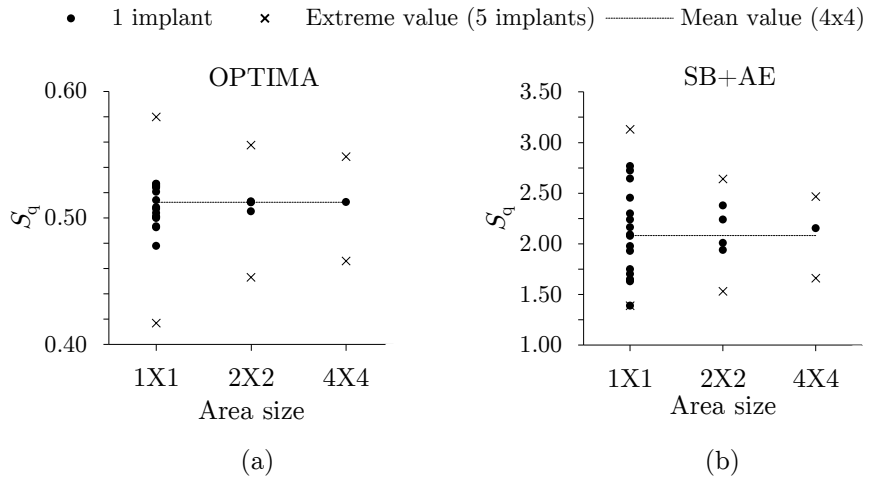

Figure 3.6: The roughness height parameter S_q in function of area size. All the area sizes were cropped from a 4x4 extended topography measurement performed in the neck of the implants; (a) OPTIMA; (b) SB+AE.

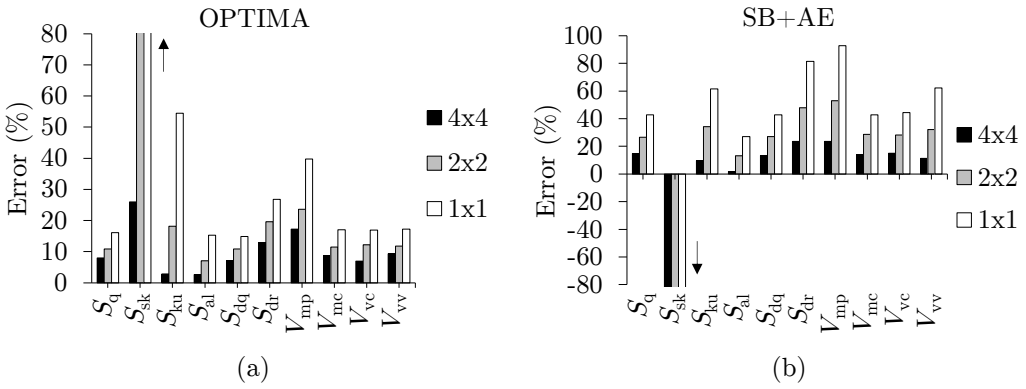

Figure 3.7: The percentage error that can be made with one unique measurement for different evaluation area sizes, taking as a reference the mean value (5 measurements) obtained with the largest area 4x4 (470x353 μm^2); (a) OPTIMA, $\uparrow$ 2x2=187 %, 1x1=498 %; (b) SB+AE,$\uparrow$ 4X4=143 %, 2x2=338 %, 1x1=672 %.

results. Regarding the sensitivity of parameters, S_{sk}, S_{ku}, S_{dr} and V_{mp} were the most affected parameters for both surface treatments.

Based on these results, it is concluded that the maximum area size should be evaluated in order to obtain a representative value of the surface topography. However, due to the complex macro geometry of dental implants, the area size may be limited by the evaluation region. This issue is addressed in the following section.

Area size and evaluation site

In order to analyze the interplay between the area size and evaluation site, the thread top of one implant was measured using two area sizes, corresponding to 2x2 (250x187 μm^2) and 1x1 (138x103 μm^2) extended topographies. The adjacent flank was also measured using

a 1x1(138x103 µm^2) area. Figure 3.8 (a) shows the S_q values of these measurements.

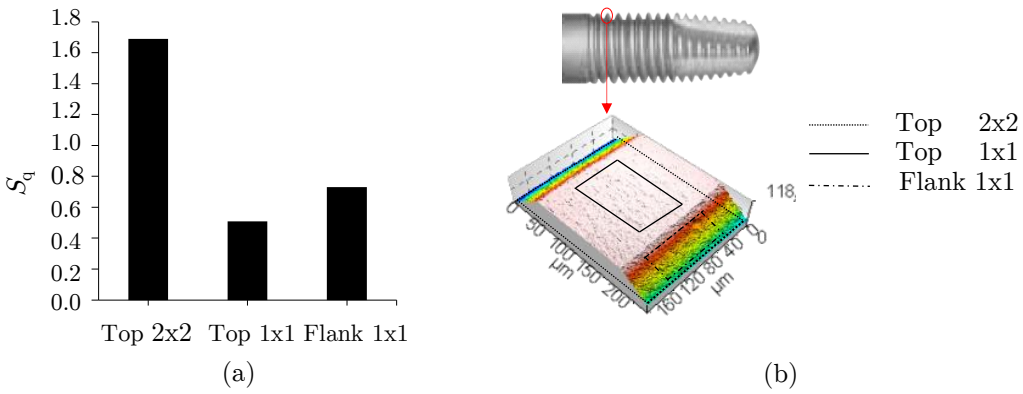

Figure 3.8: Analysis of the influence of the evaluation site and area size: (a) S_q values of implant thread top measurements using two areas (2x2= 250x187 µm^2, 1x1= 138x104 µm^2), and implant thread flank measurement (1x1= 138x104 µm^2); (b) diagram showing the three analysed areas.

As can be seen in 3.8 (b), the 2x2 (250x187 µm^2) measurement of the thread top included the top and the flank sites. However, the S_q value obtained when using large area (2x2) was 230 % and 130 % higher than the top and flank measurements (acquired with 1x1 area) respectively (see Figure 3.8 (a)). With the aim of identifying the source of this difference, each step in the data processing corresponding to the thread top measurement with the large area was analysed in more detail. In order to analyse the influence of the form extraction, two different form operators were analysed: the second order polynomial fitting (used for the rest of the study), and the least square plane fitting or levelling (which is the most commonly used operator), see Figure 3.9.

It could be seen that the thread form had not been properly removed through the form operators, neither through the Gaussian L filter, resulting in a distorted roughness surface, and therefore misrepresenting the topographical parameters. The same effect was observed for the valley evaluation site when using the large area (250x187 µm^2).

Due to these interactions, it was concluded that the most appropriated area size should be selected for each evaluation site in order to avoid the inclusion of high form components or mixing different evaluation sites. However, as demonstrated in the previous section, the variability of the topographical parameters depends on the area size. Next section analyses the relation between the area size and the reliability.

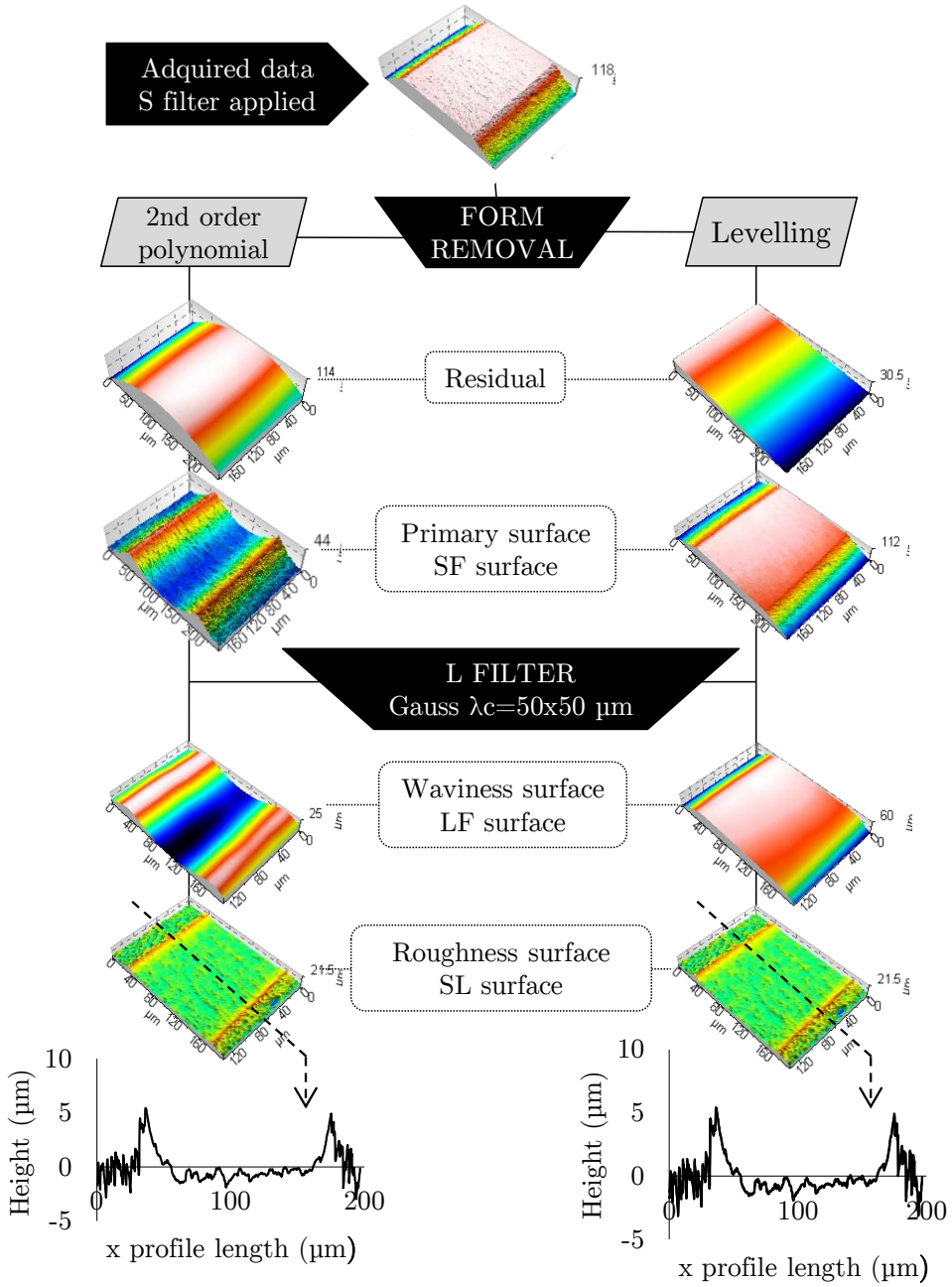

Figure 3.9: Flux diagram of the treatment steps for the implant thread top measurement using 2x2 area (250x187 µm^2), for two different F operators.

Area size and reliability

The confidence interval of each topographic parameter in function of the measurement quantity and area size was calculated through a statistical t-test. To that end, one implant of each surface treatment (OPTIMA, SB+AE) was measured thirty times in the neck at different locations (through implant rotation) using an acquisition area of 2x2 (250x187 μm^2). The mean and the standard deviation of each roughness parameter were calculated from an increasing number of measurements, both for 2x2 and 1x1 area sizes (obtained by cropping). The results corresponding to the height parameter S_q calculated on the OPTIMA surface are shown in Figure 3.10, where the x-axis represents the number of measurements performed and the Y-axis depicts the confidence interval (with 95 % confidence level) as a percentage for each case.

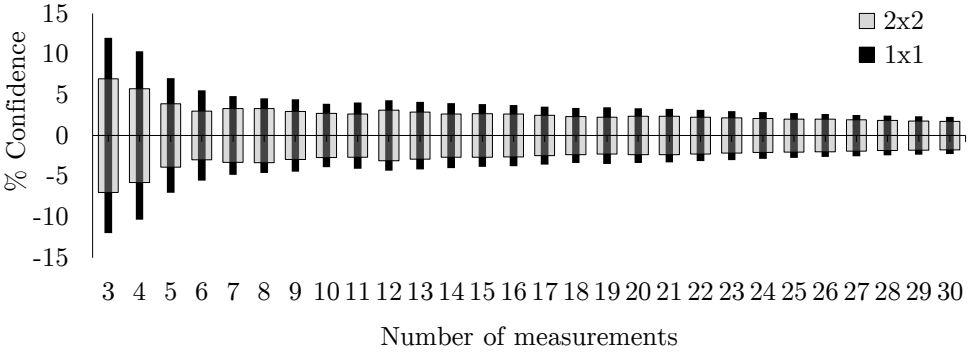

Figure 3.10: Graph showing confidence interval using t-distribution (confidence level=95 %) against the number of measurements for the parameter S_q corresponding to the OPTIMA treatment for two evaluation area sizes 2x2 (250x187 μm^2) and 1x1 (138x104 μm^2).

By means of this method, the number of measurements needed to keep each roughness parameter value within ±10 % (a value considered acceptably low for topography [Ohl03] at the 95 % confidence interval) were determined for each surface treatment, and for two area sizes (2x2 and 1x1), see Figure 3.11.

The use of increasing evaluation area size resulted in a decrease in the number of measurements required for the same confidence interval. For the OPTIMA treatment, at the given measurement and data treatment conditions, it was found to be generally sufficient to take a mean value of three measurements (in the case of 2x2 area) and five measurements (in the case of 1x1 area) to meet the established confidence interval, except for the S_{sk} parameter. As far as the SB+AE treatment is concerned, there were several parameters requiring more than 30 measurements in order to create a stable mean value according to the 10 % criteria. When using a 20 % limit (see Figure 3.12) 14 measures were required for the 2x2 area and 18 for the 1x1 area. Once again, the height parameter S_{sk} did not meet the established confidence interval after 30 measures.

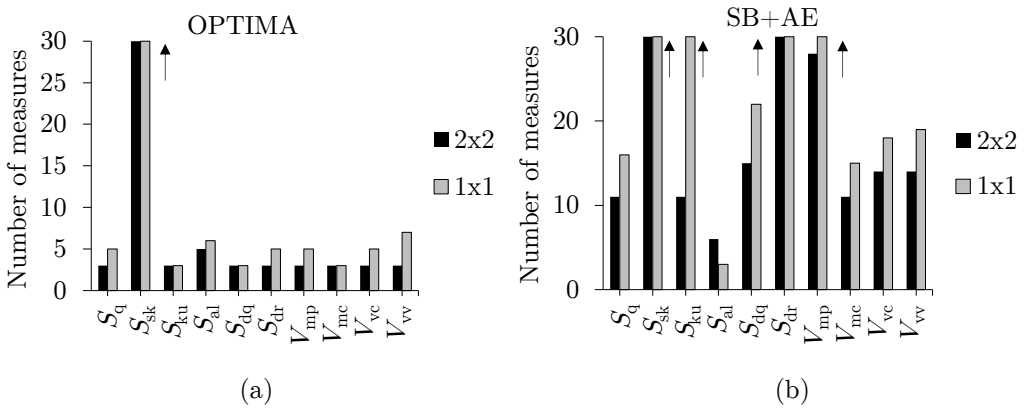

Figure 3.11: The number of measurements required to keep parameter values within 10 % using the t-distribution with 95 % confidence level for two area sizes (2x2=250x187 µm^2, 1x1=138x104 µm^2); (a) OPTIMA; (b) SB+AE.↑ Requires more than 30 measures.

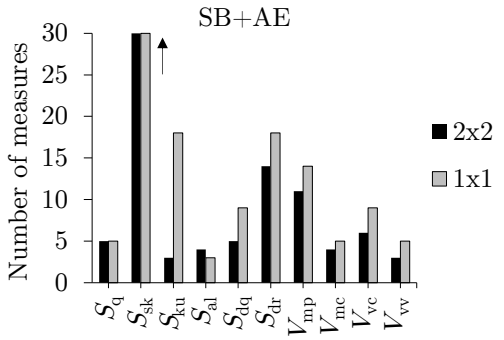

Figure 3.12: The number of measurements needed to keep parameter values within 20 % using the t-distribution with 95 % confidence level for SB+AE treatment for two area sizes (1x1=138x104 µm^2 2, 2x2=250x187 µm^2). ↑ Requires more than 30 measures.

3.4.3. Discussion and conclusion

The effect of data acquisition parameters on 3D topographical parameters was analysed in order to select the optimum acquisition variables. It was shown that the use of a low magnification objective results in an important loss of information due to an aliasing effect. It is therefore suggested to use a 100x objective for maximum resolution.

The z_{scan} and the step size settings are directly related to the acquisition time, since they determine the quantity of measured planes in the vertical direction. The z_{scan} showed a negligible effect on the topographical parameters; conversely, for the step size of 0.8 µm five parameters were significantly affected ($> 10\,\%$). It is suggested therefore to use the required minimum z_{scan} to span all the vertical range of the surface and the minimum step size in order to optimize the acquisition time and to maximize the resolution of the acquisition.

Topographical parameter dispersion increased as the area size decreased. Therefore a compromise must be obtained between statistical reliability and data acquisition time.

In the case of dental implants the screw geometry limits the size of the measuring area. The most commonly used evaluation area in the bibliography for evaluation of the three recommended areas (top, flank and valley) is about 250x250 μm^2 ([Ros13], [Sul09], [Sva09]). For the implant geometry under study, an area size of 250x187 μm^2 was too large to evaluate both top and valley sites in isolation, mixing different sites and introducing large form components. It was shown that neither form operators (least square plane fitting and polynomial fitting) nor Gaussian filtering were able to remove the large form component, resulting in distorted topographical parameters. Therefore the assertion by many authors that the waviness and the form are removed through the Gaussian filter may be incorrect in cases where high form components are included in the measurement.

Due to the wide range of dental implant geometries on the market, it is difficult to establish a generic optimum area size. It should be stressed, however, that the evaluation area must be as large as possible but should avoid the mixture of zones and the inclusion of high form components. For the implant geometry under study, suggested evaluation areas are 2x2 (250x187 μm^2) for the evaluation of the neck and flank and a reduced area of 1x1 (138x104 μm^2) for the evaluation of the top and valley.

It has been proven that reliability depends both on surface treatment and area size, and varies depending on the topographical parameter. For both surface treatments, the number of measurements increased when decreasing the area size to meet a certain confidence interval. For all parameters measured, the rougher SB+AE surface required significantly more measurements than the OPTIMA surface to obtain the same confidence interval, indicating that the SB+AE surface finish is more variable than the OPTIMA.

Overall, the most sensitive parameters to the analysed acquisition variables were those that required more measurements in order to obtain reliable values, in descending order: S_{sk}, S_{ku}, S_{dr}, S_{dq} and V_{mp}. It must be emphasized that the skewness parameter (S_{sk}) required an unworkable measurements (>30) in order to obtain a stable value, and therefore must be treated with care. The peak material volume parameter V_{mp} (calculated at 5 %), showed no clear tendencies when acquisition conditions varied (although the resulting acquired surfaces were different). It therefore seems convenient to augment the percentage at which it is calculated, although studies correlating parameters with functional response are required to establish an optimum value. The widely used S_q parameter, which is an average of the heights of a surface, was in general not sensitive to changes in the acquired surfaces. This parameter did not allow for discernment between different surfaces and thus should not be reported alone.

It has been proven that acquisition parameters strongly influence the topographical parameters. However, many investigators omit key acquisition data such as microscopic objective and area size ([Min14], [Sen13], [Cho11], [Coe11], [RR05], [Sam05], [Bus04]). This implies that different studies could be using identical surfaces but reporting them with different topographical parameters, or reporting identical parameters for surfaces that are actually different. As a result, it is almost impossible to carry out comprehensive systematic reviews and meta-analyses, which are fundamental to advance in the knowledge of the impact on living tissues of different implant topographies.

Even though the results presented depend upon the implant geometry used and sur-

face treatment to a greater or lesser degree, general tendencies have been presented and useful information for the formulation of a generalized strategy (defined in section 3.6) was obtained.

3.5. Effect of data processing variables

3.5.1. Materials and methods

Dental implants

Two of the implants used in the previous study (defined in section 3.4.1) were selected for the present analysis: the implant number 1 treated with acid etching (OPTIMA), and the implant number 6 treated with sand blasting followed by acid etching (SB+AE).

Topography measurements

A confocal imaging profiler (Plμ-SENSOFAR) was used for data acquisition. Three measurements were carried out on each implant at the neck (through implant rotation), using the acquisition variables defined in Table 3.4 for maximum resolution (based on the results presented in the previous section 3.4).

Table 3.4: Details of the measurements carried out to evaluate the effect of data processing variables on 3D topographic parameters.

Meas. No	Implant No	Treatment	Site	Objective	Area (μm^2)	z_{scan} (μm)	Step (μm)
1-3	1	OPTIMA	Neck	100x	250x187	14	0.2
4-6	6	SLA	Neck			42	

Design of experiments

A statistical method, *i.e.* the two level full factorial design of experiments [Dow11], was adopted in order to investigate the effects of data processing variables on 3D topographical parameters. The analysed data processing variables[7] included: i) S filter size (λ_s), ii) F operator (F), iii) L filter type (L), iv) L filter size (λ_c), and two surface treatments: acid etching (OPTIMA) and sand blasting followed by acid etching (SB+AE). A reduced set of topographic parameters belonging to height (S_q), hybrid (S_{dq}), and functional (V_{vc}) families were selected[8] (based on the suggestions given in ([Han10], [Löb10], [Sos08]) in order to limit the output of the study. The parameters were calculated both in the roughness (SL) and waviness (LF) surfaces. The metrological software SensoMap Turbo 5.1 was used for data processing, and the design of experiments was carried out using the statistical software

[7]Detailed information about data processing can be found in section 2.6.2 "Data processing".
[8]Detailed information about 3D parameters can be found in Appendix A "3D Topographic parameters".

Minitab 16. All factors (variables), levels, and codes used in the experimental design are shown in Table 3.5.

Table 3.5: Factors, abbreviations, level codes, and levels for the design of experiments.

Factor	Abbreviation	Level code	Level
S filter size	λ_s	-	0.36x0.36 μm
		+	2.5x2.5 μm
F operator	F	-	Least squares plane fitting
		+	Second order polynomial fitting
L filter type	L	-	Gaussian
		+	Robust Gaussian
L filter size	λ_c	-	20x20 μm
		+	50x50 μm
Surface treatment	S	-	OPTIMA
		+	SB+AE

The design matrix of the full factorial design is presented in Appendix C (Table C.1), which was performed with three measurements (at three different locations) for each experiment (a total of 96 runs). In general, one of the levels corresponded to the values selected in compliance with 2D criteria, while the other was selected according to 3D criteria and according to its suitability for dental implant characterization (discussed below).

Regarding the S filter, 2D characterization uses a standardized Gaussian filter with a typical value of λ_s =2.5 μm. This value is suitable for contact instruments, and is chosen according to tip radius and spacing distance [ISO96a]. For areal measurements carried out by optical instruments, Stout [Sto93b] suggested using a λ_s value of twice the lateral resolution (using 100x objective, λ_s =0.36x0.36 μm).

Concerning the F operator, the least square fitting of a plane is the simplest and most widely used operator in the literature. Due to the complex geometry of threaded dental implants, the second order polynomial surface fitting was selected as the most appropriate algorithm for extracting the nominal form of the surface, due to the small size of the assessed area [Blu03].

With respect to filter type (L), there are different techniques, which are extensively reviewed in the literature ([Dob11], [Mat10], [Raj02]). Discussion here is limited to the Gaussian and Robust Gaussian filters. The most widely used filter in metrology is the Gaussian filter [ISO11]. Nevertheless, this filter presents two main drawbacks: i) the edge effects (due to the boundary distortion because of the local weighed average), and ii) the sensitivity to outliers and form [Kry08]. The boundary distortion is usually overcome by removing one cut-off length of the boundaries, which results in significant data loss, especially in 3D characterization. Robust filters have been introduced to suppress the influence of outliers and boundary distortions, allowing for the numerical evaluation of all acquired data without running-in and running-out effects [ISO10]. In this study the boundaries were removed prior to using the robust filter in order to obtain the same evaluation area size when comparing both filter types.

With respect to the L filter size or the cut-off value (λ_c), 2D standards state that the profile must be assessed over a length equal to five times the cut-off length [ISO96b]. Therefore, since one cut-off is removed after filtering, the measured length must be six times the cut-off length. Following these criteria, the selected area of 250x187 μm^2 requires a cut-off value of 30x30 µm. On the other hand, regarding dental implant 3D characterization, there is a generalized use of a cut-off value of 50x50 µm in the bibliography (due to the suggestion given in [Wen00]). Thus in order to magnify the effect of this factor in the study, a cut-off value of 20x20 µm was selected as the low value and 50x50 µm as the high value.

3.5.2. Results

All the experimental results can be found in Appendix C (Table C.2). The Pareto Charts shown in Figure 3.13 depict the main effects and interactions of each topographical parameter calculated using a risk factor of 0.05.

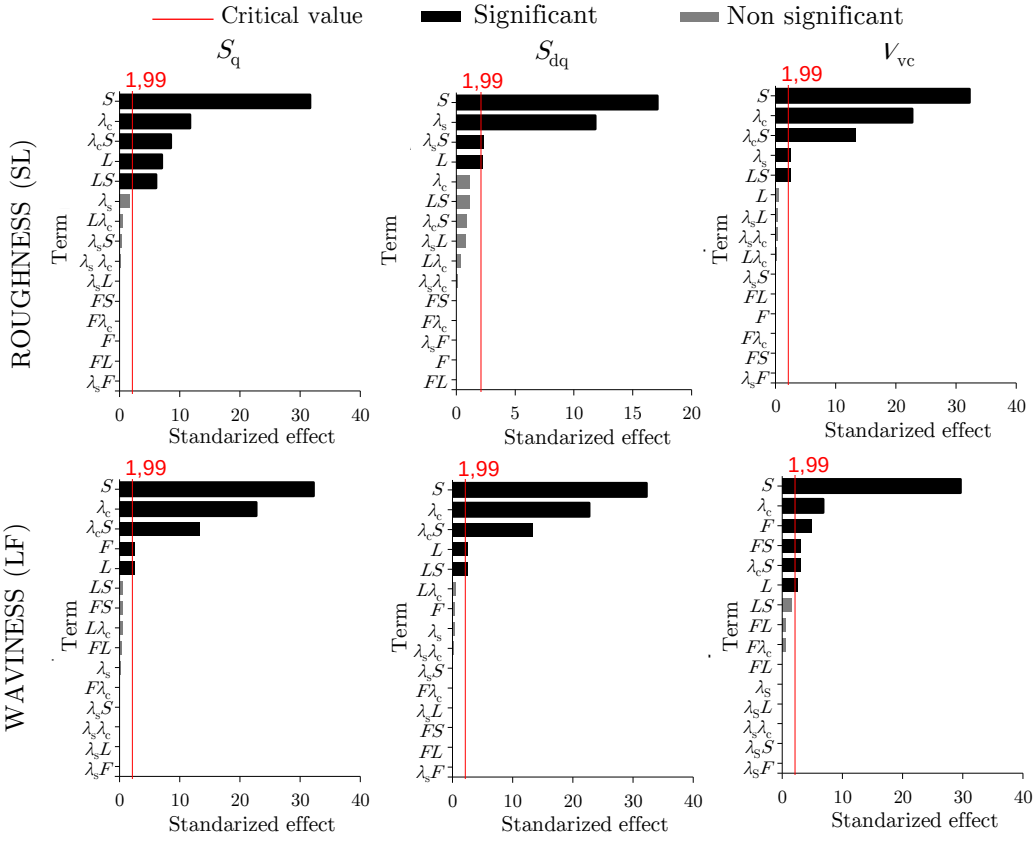

Figure 3.13: Pareto Charts of the S_q, S_{dq} and V_{vc} parameters calculated at the roughness (SL) and waviness (LF) surfaces: their main effects and their interactions.

The surface treatment (S) was the dominant factor for all parameters. The λ_s factor was statistically significant only for the S_{dq} and V_{vc} parameters calculated on the roughness (SL) surface, while the F factor was affected significantly for the S_q and V_{vc} parameters calculated on the waviness (LF) surface. Regarding the rest of the factors (L, λ_c), they were significant for nearly all parameters, although in different proportions. In general,

the cut-off value (λ_c) was the most influential parameter among data processing variables followed by the filter type (L). As an exception, the λ_s factor was the most influential one for the spatial S_{dq} roughness parameter. All of these factors presented interactions with the surface finish (S), but there were no significant interactions between data processing variables.

The effect of a factor on a response variable is the change in the response (negative if it has decreased, positive if it has increased) when the factor shifts from its lowest level (-1) to its highest level (+1). Figure 3.14 shows the main effects of each topographical parameter, where statistically significant effects ($p<0.05$), already commented in Pareto Charts, are marked with an $*$.

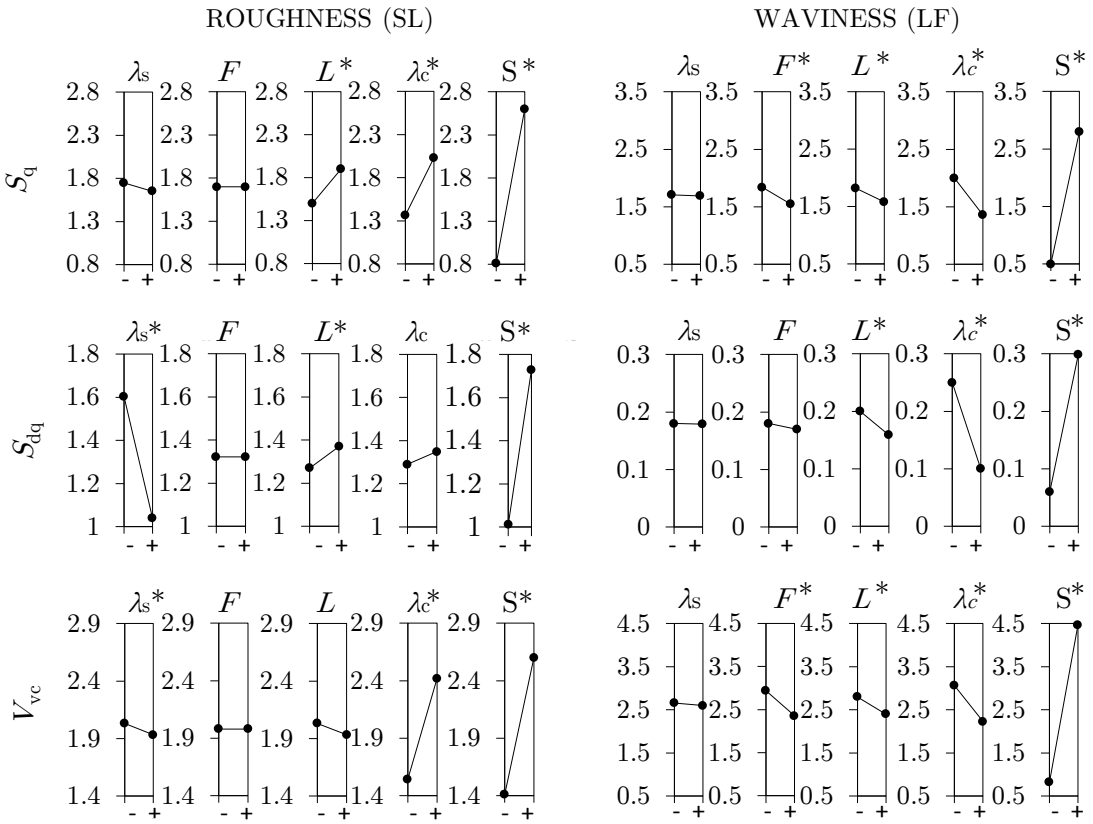

Figure 3.14: The main effects of the topographical parameters with $p<0.05$ being considered statistically significant ($*$).

Both the λ_s and F factors (which affect roughness and waviness parameters respectively) presented a negative effect. The L and λ_c factors presented a positive effect for roughness parameters and a negative effect for waviness parameters. Regarding the influence of the filter type (L), Figure 3.15 shows representative images of waviness profile variations (extracted from the corresponding surfaces for better representation) when varying the L factor level, for the two surface treatments. It can be seen that the waviness profile calculated through the Robust Gaussian filter (+1 level) is not distorted by sudden peaks or valleys, unlike that calculated through the Gaussian filter (-1 level).

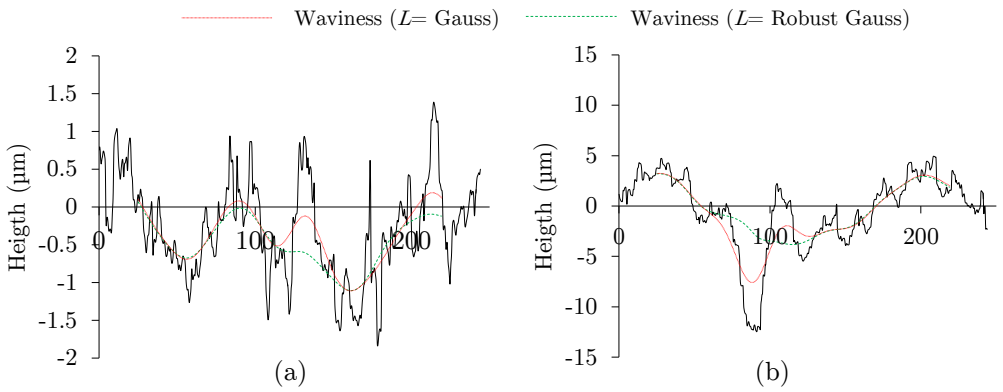

Figure 3.15: Effect of filter type L (Gaussian filter: -1 level, Robust Gaussian filter: +1level) in the mean line (waviness profile). (a) acid etching treatment (OPTIMA). (b) sand blasting followed by acid etching treatment (SB+AE).

Concerning the cut-off value (λ_c) effect, Figure 3.16 depicts representative images of the primary (SF), roughness (SL), and waviness (LF) surfaces when varying this factor (λ_c). It can be observed that the roughness and waviness surface varies considerably when varying the cut-off value. The use of a cut-off value of 20x20 µm (-1 level) introduced more information into the waviness surface and it therefore presented a smooth roughness surface. By contrast, the use of a cut-off value of 50x50 µm (+1 level), resulted in a smoother waviness surface and a rougher roughness surface.

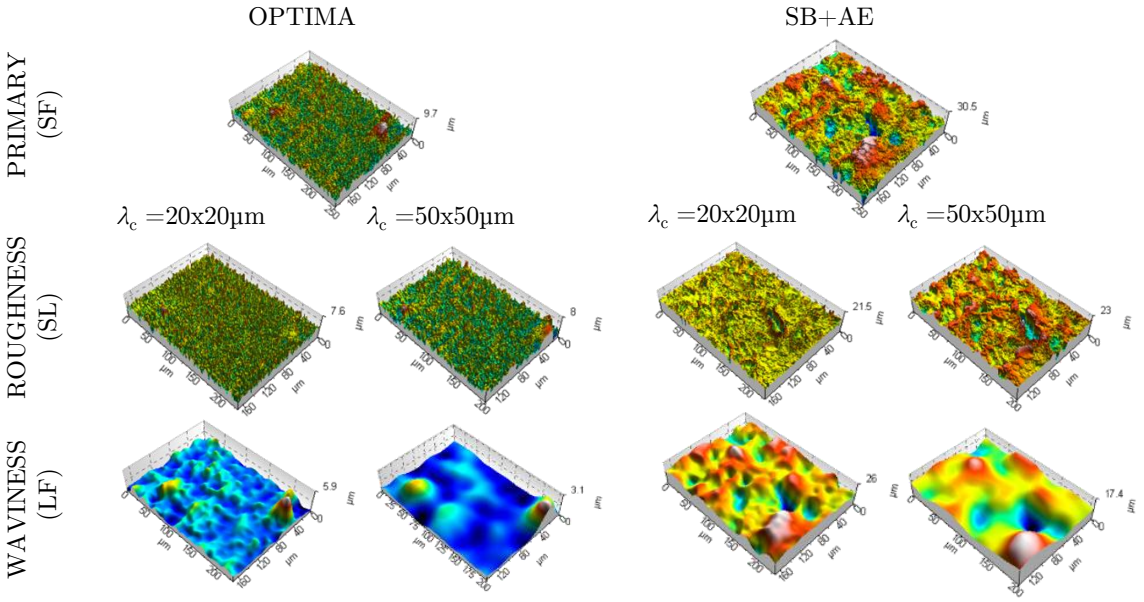

Figure 3.16: Representative 3D images of the primary (SF), roughness (SL), and waviness (LF) surfaces of OPTIMA and SB+AE treatments calculated with λ_c =20x20 µm (-1 level) and λ_c =50x50 µm (+1 level). Note that each surface has its own scale in the z axis.

Due to the strong influence of the cut-off, it was found convenient to analyse this variable over a wider range of values. Figure 3.17 depicts the evolution of the S_q parameter calculated on the roughness and waviness surface when applying a Gaussian filter of diffe-

rent cut-off wavelengths for the two treatments under study (parameters calculated on the primary surface are marked as references). It could be seen how the S_q parameter calculated on the roughness surface increased with an increasing cut-off value. By contrast, the waviness S_q parameter decreased with an increasing cut-off value. The changes were more pronounced for the rougher surface (SB+AE).

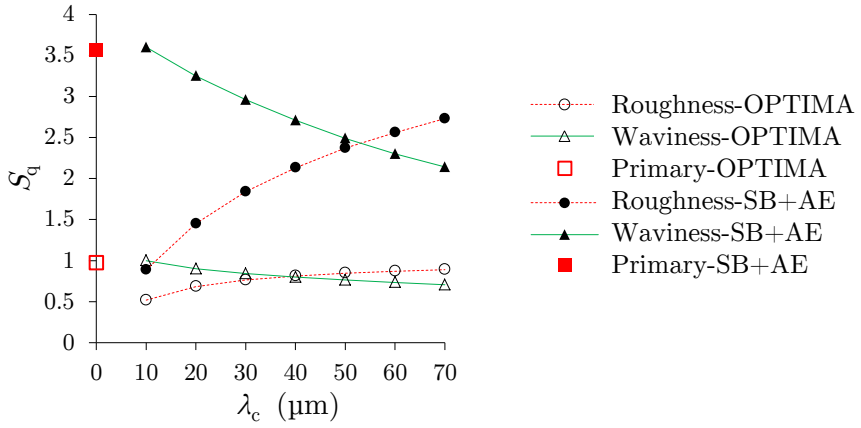

Figure 3.17: The effect of the cut-off value (λ_c) in the height deviation parameter S_q calculated both on roughness and waviness surfaces, for OPTIMA and SB+AE treatments. Values calculated on primary surface are marked as references. The lines are presented as a visual guide.

3.5.3. Discussion and conclusion

As expected, the dominant factor was the surface treatment. The λ_s factor, which is aimed to eliminate measurement noise and delimits the lower limit of the SL bandwidth, was significant only for parameters calculated on the roughness surface. The use of the λ_s =2.5x2.5 µm extracted more information from the roughness surface, and considerably affected the S_{dq} parameter. Therefore it is considered more adequate to use a lower λ_s value (twice the lateral resolution [Sto93b], λ_s =0.36x0.36 µm) in order to avoid the elimination of roughness features from the analysis.

The most influential factor among data processing variables was the cut-off value (λ_c) followed by the L filter type (L). In both cases, the change of level from lower value to higher resulted in a diminution of waviness parameter values and an increase of the roughness parameter values. When the cut-off value is increased, more frequency content is considered as roughness, and therefore less information is introduced into the waviness surface. Here lies the relative nature of the terms roughness and waviness, which depends on the cut-off value. The mean surface was also dependent on the filter type. It was shown that the Robust Gaussian filter is a promising filter for dental implant characterization. Besides generating a more realistic mean surface, the Robust Gaussian filter allows for evaluation of the whole of the acquired data, which is especially relevant for dental implant characterization due to the reduced evaluation areas.

Regarding the interactions found in the study, it was shown that the effect of data processing parameters varies depending on the surface treatment. Due to the added effect

of coarse particles on the etched topography, the sand blasting followed by acid etching treatment was more sensitive to changes in the frequency range (λ_c) or outlier suppression (L). Conversely, the inclusion (or extraction) of form components (F) affected more greatly the purely acid etched surface because of its smaller frequency spectrum.

Even though results depend on the implant geometry used, surface treatments, and to a greater or lesser degree the selected parameter levels, general tendencies were presented and useful information for the formulation of a generalized strategy (defined in section 3.6) was obtained. It was proven that the processing variables have a strong influence on topographical parameters, although to differing extents. This shows the relative nature of topographical parameters, which strongly depend on the data processing and are not inherent features of surface treatments. However, to date most reported topographical characterizations omit specifying key processing variables such as filter type and cut-off size ([Koh13], [Chr12], [Coe11]), which makes it difficult to sort and interpret the published findings.

The guidelines suggested by Wenneberg *et al.* [Wen00] have become a reference point in dental implant topographical characterization ([Ale13], [Ito13], [Ros13], [Mon12]). Nevertheless, not all data processing variables are addressed. This guideline recommends the use of a Gaussian filter with a cut-off value of 50x50 μm but there is no allusion to the S filter or F operator, which as shown in this work, affects roughness and waviness parameters respectively. Regarding the suggested cut-off value (50x50 μm), the selection was based on numerous measurements on turned and blasted implants [Wen96a]. However, when using the mentioned cut-off value of 50x50 μm, it was shown that there is a non-negligible transfer of topographical information from the waviness to the roughness surface (especially for the SB+AE treatment, see Figure 3.16). As far as optimum values are concerned, it should be noted that the specification of filtering (L and λ_c) is an application-specific issue that must be selected according to the desired objective, and implies an understanding of the function. The ultimate goal of the topographical characterization of dental implants is to link the biological response to the physical features of the implant. However, a full understanding about the interactions between topography and cell response is lacking. The use therefore of topographical parameters calculated on the primary surface is suggested to avoid removal of potentially important information from the surface.

It is indisputable that all data processing variables must be clearly specified in order to publish a meaningful topographical characterization.

3.6. Generalized topographical characterization strategy for endosseous dental implants

Based on the results obtained in previous sections, a generalized topographical characterization strategy for endosseous dental implants is proposed.

3.6.1. Data acquisition

Acquisition variables

The literature review revealed that the confocal profilometry, interferometry, stereo SEM and focus variation are the only acceptable instruments for threaded dental implant measurement[9].

In this work, a confocal profilometer (SensoFar Plμ) was used for dental implant characterization. Table 3.6 gathers the acquisition variables set for an optimum measurement based on the results presented in section 3.4.

Table 3.6: Data acquisition variables for an optimum measurement using a confocal profilometer SensoFar Plμ. *Default value. A smaller area size may be required depending on the evaluation site (discussed in the following sections).

VARIABLE	SELECTION GUIDE	VALUE
Objective	Maximum resolution	100x (0.18 µm)
z_{scan}	Required minimum z_{scan}	Normally between 10-100 µm
Step size	Minimum step available	0.2 µm
Area size	Maximum area available	250x187µm *

Evaluation sites

A preliminary study revealed that the surface topography of a dental implant depends on the surface treatment and the evaluation site [Zab12]. Accordingly, four evaluation sites are suggested for a proper description of surface topography of an endosseous dental implant: neck, top, valley and flank (see Figure 3.18).

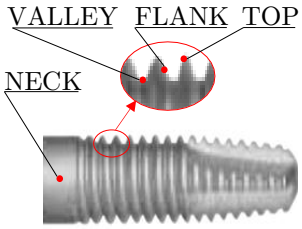

Figure 3.18: Evaluation sites.

[9]For detailed descriptions, the reader is referred to section 2.6.1 “Measuring instruments”.

Area size and number of measurements per evaluation site

Based on the results obtained in section 3.4, the following guideline for the selection of the area size and the measurement quantity for each evaluation site (neck, top, valley and flank) was established:

- Select the maximum area size avoiding the inclusion of high form components and the mixture between sites (default area size=250x187 μm^2).

  - If default area size is measurable: acquire a minimum of three measurements of 250x187 μm^2 at different locations of the evaluation site.
  - If smaller area size is necessary: acquire the required measurements at different locations of the evaluation site in order to obtain a minimum of total measured area of 140250 μm^2 (equivalent to three measurements of 250x187 μm^2).

This way, the same representativeness of the surface topography for all evaluation sites will be obtained. Based on the studies carried out by Wennerberg [Wen96a], it is suggested to evaluate three implants per batch.

3.6.2. Data treatment

Based on the study presented in section 3.5, topographical parameters should be calculated on the primary (SF) surface in order to avoid extracting information that could be of interest from the surface. However, as discussed in the previous section, distinct area sizes may be required for the different evaluation sites. In this case, comparison between regions could not be performed using primary parameters, since the frequency spectra would be different. It is therefore suggested to calculate parameters both on the primary surface (SF, to obtain the entire information) and the roughness surface (SL, to set a common range of spectra for comparison purposes). Based in the results obtained in section 3.5, the following data treatment variables are suggested (see Table 3.7).

Table 3.7: Suggested data treatment variables for dental implant characterization.

VARIABLE	VALUE
S Filter	Gaussian filter λ_s =0.36x0.36 μm
F operator	Second order polynomial fitting
L filter	Robust Gaussian filter λ_c =50x50 μm

Depending on the goal of the study different topographical parameters should be calculated, but at least one hight, one hybrid and one functional parameter should be reported.

3.7. Topographical characterization of two commercial dental implants

3.7.1. Introduction

This section presents the topographical characterization of two commercial dental implant systems as an example of the application of the generalized strategy presented in the previous section. Analysed implants correspond to those used in the study of the effect of the insertion on the surface topography (Chapter 4).

3.7.2. Materials

Tapered self-tapping endosseous dental implants with different surface topographies were analysed (n= 3): BTI Tiny implant 3.5x11.5 (Ref: IRT3511, referred to as BT) and BIOMET 3iT3TM 3.25x8.5 (Ref: BOST3285, referred to as BM). The BT surface is produced by acid etching while the BM surface is produced by the combination of sand blasting followed by acid etching processes in the implant body and solely acid etching in the neck.

3.7.3. Qualitative analysis

The implants were mounted on the specially designed supports (see section 3.3) which allowed for accurate and repeatable positioning without damaging the implant surface. Morphological analysis of the implants was carried out at the four evaluation sites (neck, top, valley and flank) through scanning electron microscopy (JEOL JSM 5600 LV) at a voltage of 15KV.

3.7.4. Data acquisition

BTI Tiny implant characterization

Following the generalized strategy set out in previous section, BTI Tiny implant surface topography was characterized.

Figure 3.19 shows the characterized locations, and details of all measurements are summarized in Table 3.8. The axes of the implants were either oriented perpendicular to the optical axes (see Figure 3.19 (b)), to examine the neck, top and valley areas, or were tilted at an angle of approximately 40° in order to measure the flanks (see Figure 3.19 (c)), through the specifically designed position device (described in section 3.3).

The neck of the implant was measured in the central part and three measurements were acquired of 250x187 μm^2 by rotating the implant. In the case of the valley site the maximum area available was smaller than the set initial value (250x187 μm^2), and therefore ten measurements of 138x104 μm^2 distributed along the whole implant were carried out in order to acquire the same representative surface. Concerning the tops of the thread, Figure 3.19 (a) clearly shows how the top width varies from greater to smaller in the implant body and from smaller to greater in the apex. The measurement locations were therefore selected in order to obtain the maximum acquisition area, which resulted in two

tops in the body and two tops belonging to the apex (area size=138x104 μm^2). A total of 16 measurements were distributed on these selected tops by rotating the implant. Finally, the working distance limited the accessible flanks without the risk of collision due to the required tilting of the implant (see Figure 3.19 (c)). Therefore three flanks located in the threshold between the body and the apex areas were evaluated using an area size of 250x187 μm^2.

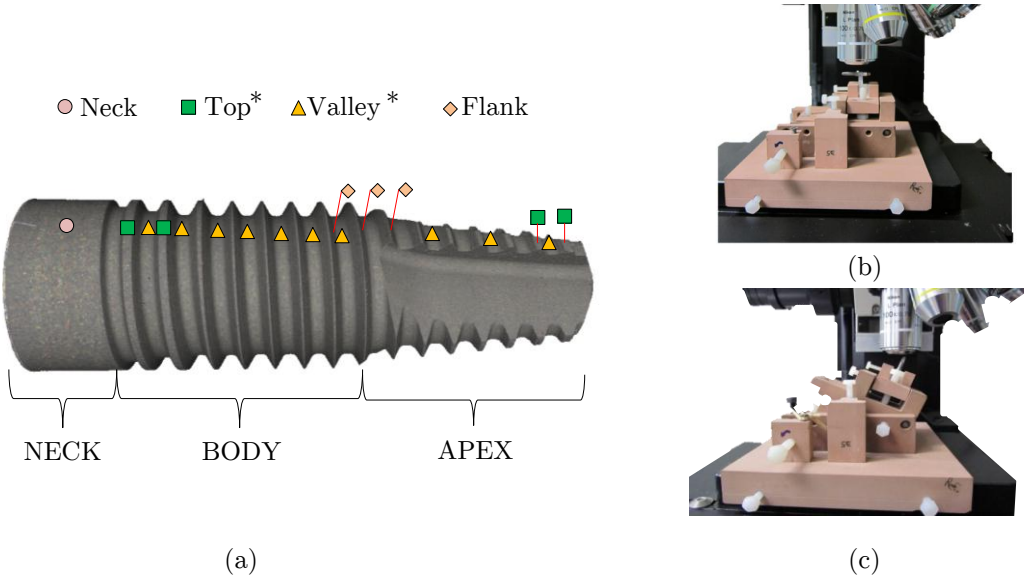

Figure 3.19: BT implant topographic characterization. (a) details of the evaluated regions; (b)-(c) dental implant positioning through the specifically designed device. $*$: area size<default value (250x187 μm^2).

Table 3.8: BT implant measurements details.

SITE	AREA (μm^2)	No. MEASURES
Neck	250x187	3
Top	138x104	10
Valley	138x104	10
Flank	250x187	3

BIOMET 3iT3TM implant characterization

Figure 3.20 depicts the characterized locations for the BM implant, and the measurements details are summarized in Table 3.9. The implant positioning was the same as that for the BT implant (shown in Figure 3.19 (b), (c)).

The neck was measured in the centre, with three measurements acquired of 250x187 μm^2 by implant rotation. Due to the small width of the thread tops a total of 16 measurements were taken on the selected threads by rotating the implant (area size=95x95 μm^2). Regarding the valley region, three measurements of 250x187 μm^2 distributed along the implant were taken. Concerning the flank site, it can be clearly seen in Figure 3.20 that

the flanks are very small in the implant body and become much deeper in the apex. Due to this, and also to the working distance limitation, three apex flanks were characterized (250x187 μm^2).

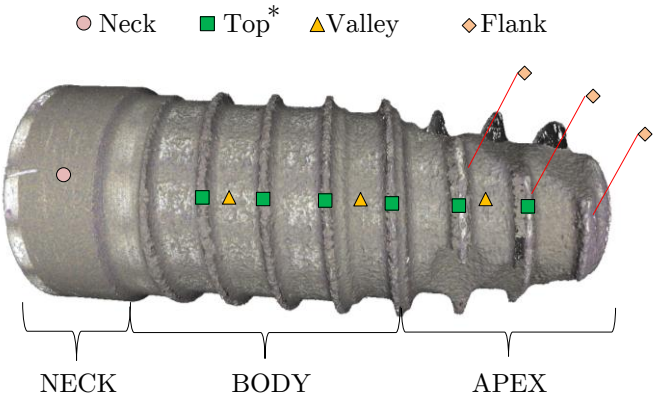

(a)

Figure 3.20: Details of the evaluation regions for BM implant. $*$: area size<default value (250x187 μm^2).

Table 3.9: BM implant measurements details.

SITE	AREA (μm^2)	No. MEASURES
Neck	250x187	3
Top	95x95	16
Valley	250x187	3
Flank	250x187	3

3.7.5. Data treatment

Following the data treatment protocol described in section 3.6.2, height (S_q), hybrid (S_{dq}, S_{dr}) and functional (V_{vc}) parameters[10] were calculated both on the primary (SF) and roughness (SL) surfaces.

3.7.6. Results and discussion

The SEM images of the BT and BM implants are depicted in Figure 3.21. It could be seen that the acid etching of the BT implant was directional, since it generated different topographies in the longitudinal (parallel to the implant axes) and transversal directions (perpendicular to the implant axes). The longitudinal regions (neck, top and valley) presented a homogeneous distribution of fine 2–4 µm micropits with sharp edges, corresponding to a typical acid etched morphology. Conversely, the flank site (transversal region) presented a combination of typical acid etched morphology and homogeneously distributed

[10]For detailed descriptions the reader is referred to Appendix A "3D Topographic parameters".

holes of 10-20 µm diameter. Regarding the BM implant, it should be reminded that its surface is produced by the combination of sand blasting followed by acid etching process in the implant body and solely acid etching in the neck. Accordingly, the BM implant micrographs also presented a differing morphologies along the implant (see Figure 3.21). The neck site presented a typical etched morphology, similar of that explained for the BT implant. On the other hand, top, valley and flank regions presented a rougher two scale micro-topography, since the etching procedure was superimposed on the coarse topography generated by the sand blasting. It could be observed that the blasting was more severe at the tops of the implant compared to the valley and flank, which suggests that the sand blasting treatment was also directional, since affected different regions differently.

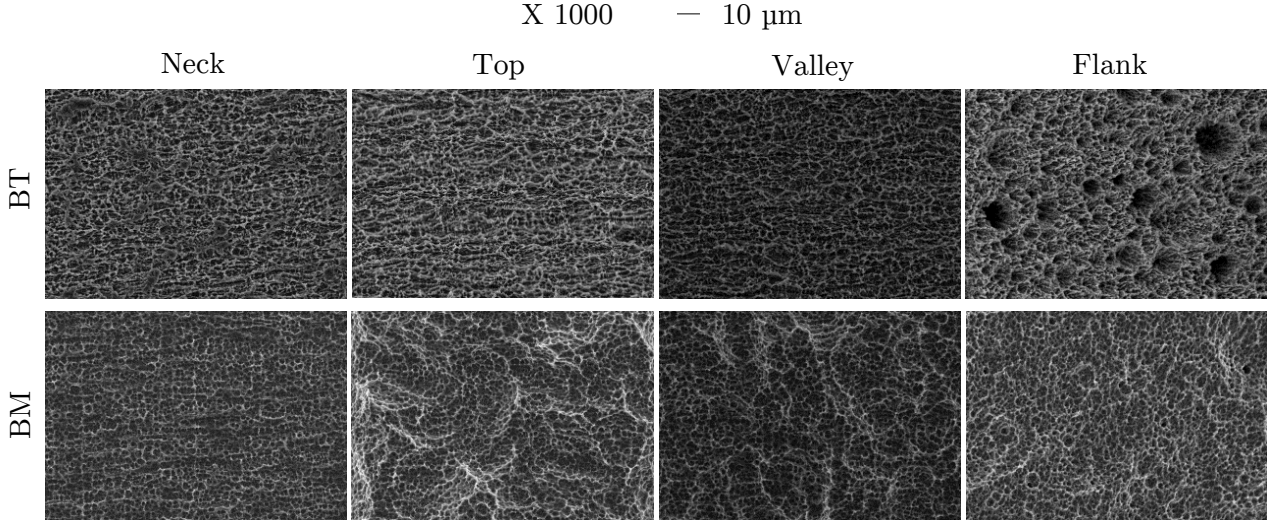

Figure 3.21: SEM images of the four evaluation sites for the BT and BM implants.

The results of the quantitative evaluation of the BT and BM implants are shown in Table 3.10 and Table 3.11 respectively. As expected after the qualitative analysis, the topographical parameter values varied between different parts of the screw shaped implants. In order to evaluate the differences between regions, the topographical parameters calculated on the roughness (SL) surface were normalized with respect to the neck value for each implant system (see Figure 3.22). The roughness rankings differed from one implant to another, but all parameters presented the same trends between regions for each implant.

Table 3.10: Results of the topographical characterization of the BT implant.

		NECK	TOP	VALLEY	FLANK
S_q	SF	0.92±0.04(4 %)	1.07±0.15(14 %)	1.11±0.07(7 %)	1.95±0.23(12 %)
(µm)	SL	0.857±0.03(3 %)	1.02±0.15(14 %)	1.00±0.07(7 %)	1.82±0.24(13 %)
S_{dq}	SF	1.3±0.09(7 %)	1.79±0.24(14 %)	1.74±0.15(9 %)	2.14±0.12(6 %)
	SL	1.29±0.07(5 %)	1.78±0.25(4 %)	1.73±0.14(8 %)	2.12±0.12(6 %)
S_{dr}	SF	65.59±8.21(12 %)	112.16±23.21(21 %)	106.72±14.94(14 %)	165.94±16.61(10 %)
(%)	SL	64.06±5.98(9 %)	111.55±24.01(22 %)	105.45±12.85(12 %)	165.74±16.65(10 %)
V_{vc}	SF	1.40±0.11(8 %)	1.77±0.27(15 %)	1.80±0.15(8 %)	2.39±0.09(4 %)
($\mu m^3/\mu m^2$)	SL	1.31±0.09(7 %)	1.66±0.26(15 %)	1.68±0.15(9 %)	2.12±0.05(2 %)

Table 3.11: Results of the topographical characterization of the BM.

		NECK	TOP	VALLEY	FLANK
S_q	SF	0.51±0.03 (6 %)	4.52±1.19(4 %)	3.66±0.57(16 %)	2.39±0.84(35 %)
(µm)	SL	0.47±0.03(1 %)	3.16±0.82(3 %)	2.26±0.44(2 %)	1.38±0.36(26 %)
S_{dq}	SF	0.82±0.06(7 %)	2.33±0.45(2 %)	1.48±0.11(8 %)	1.18±0.10(8 %)
	SL	0.81±0.06(1 %)	2.30±0.44(2 %)	1.46±0.11(1 %)	1.14±0.08(8 %)
S_{dr}	SF	28.61±3.41(12 %)	187.25±70.67(175 %)	81.15±11.07(14 %)	54.23±7.73(14 %)
(%)	SL	28.32±3.65(77 %)	183.27±69.38(171 %)	79.19±10.56(82 %)	51.54±6.97(13 %)
V_{vc}	SF	0.77±0.05(7 %)	7.02±1.76(7 %)	5.33±0.97(18 %)	3.2±1.20(37 %)
($\mu m^3/\mu m^2$)	SL	0.69±0.06(2 %)	4.89±1.16(5 %)	3.19±0.70(3 %)	1.85±0.55(30 %)

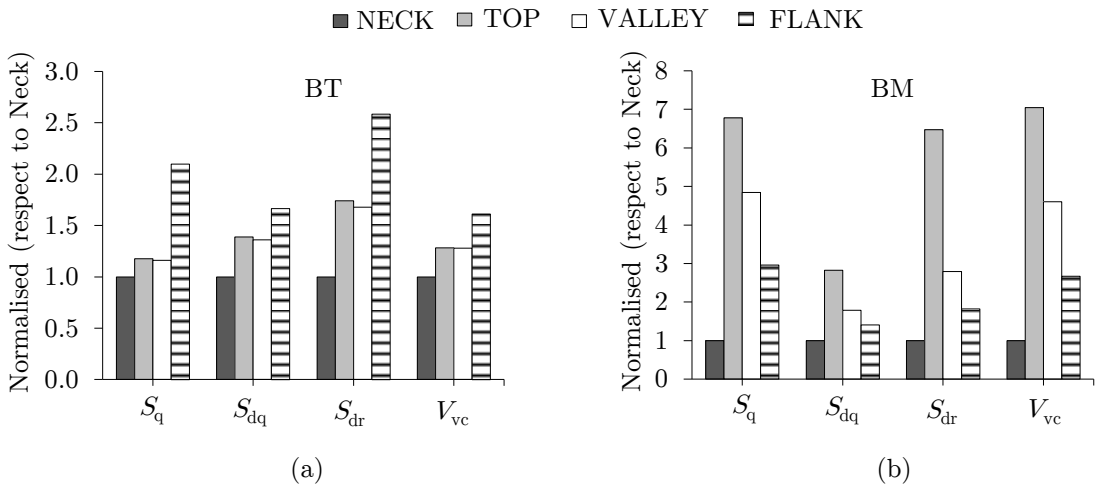

Figure 3.22: Analysis of the differences between regions for the BT (a) and BM (b) implants. Topographic parameters calculated on the roughness (SL) surface are normalised with respect to the neck.

In the case of the BT implant (see Figure 3.22 (a)), the flank was the roughest and the neck was the smoothest region, while the top and valley presented similar topographical values. The qualitative analysis demonstrated that the acid etching treatment of the BT implant was directional, since the morphology of the longitudinal (neck, top and valley) and transversal (flank) regions differed significantly. The numerical characterization corroborated these observations and also showed that although presenting the same morphology, the neck site was smoother than the top and valley areas.

For the BM implant (see Figure 3.22 (b)), the roughest region was the top site followed by the valley, flank and the neck. The smoother surface of the neck site was due to the different treatment applied to this region (acid etching) compared to the rest of the implant (sand blasting followed by acid etching). As expected after the qualitative evaluation, the top, valley and flank regions presented different topographical values. This suggests that the blasting did not reach the different regions with the same power or frequency, generating different topographies. The most exposed top region presented the rougher topography followed by the valley and flank.

Concerning the differences between the roughness parameters of the two implant sys-

tems, the S_q and V_{vc} parameters were higher for the BM implant apart from the neck and flank sites. In case of the hybrid parameters (S_{dq} and S_{dr}) this trend was reversed and the BT implant presented greater values in general apart from the top. This emphasizes the necessity to report at least one height, one hybrid and one functional parameter for a complete characterization of the surface.

As far as primary parameters are concerned, only measurements carried out using the same measuring area could be compared. In this regard it should be emphasized that in the case of the flank sites of the BT and BM implants, the comparison between topographical parameters calculated on the roughness and primary surfaces led to different conclusions. The S_q (see Figure 3.23 (a)) and V_{vc} (see Figure 3.23 (b)) parameters calculated on the primary surface were larger for the BM implant, while the opposite trend was found when comparing the same parameters calculated on the roughness surface. This reinforces the importance of characterizing both primary and roughness surfaces.

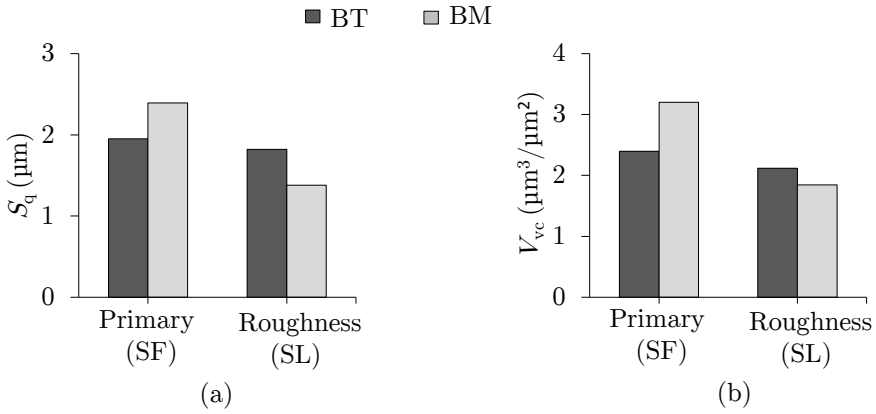

Figure 3.23: Comparison of the S_q (a) and V_{vc} (b) parameters calculated on the primary (SF) and roughness (SL) surfaces for the two implants under study (BT, BM).

3.8. Conclusions

This chapter has analysed the effect of data acquisition and treatment on 3D topographical parameters and presented a generalised topographical characterization strategy for endosseous dental implants. The strategy was then demonstrated using two commercial dental implant systems. The main conclusions are listed below:

Data acquisition and processing influence

- The microscopic objective variation affected very significantly the topographical parameters due to the aliasing effect observed when changing the objective to a lower magnification.

- The z_{scan} variable showed a negligible effect on 3D topographical parameters.

- The topographical parameters were significantly affected when increasing the step size, due to the smoothing of the acquired surface.
- As the area size decreased, the dispersion of the topographical values increased considerably.
- In cases where large form components were included (due to the mixing of evaluation regions, *e.g.* top and flank), distorted topographical parameters were obtained due to the impossibility of removing the form component through the F operator and L filtering.
- The topographical parameter reliability depended on both measurement area size and surface treatment, and varied depending on the topographical parameter.
- Among the data processing variables, the most influential was the L filter size (λ_c) followed by L filter type (L), affecting significantly both roughness and waviness parameters. The S filter size (λ_s) and form operator (F) resulted in significant for roughness and waviness parameters respectively.

Topographical characterization of two commercial dental implants

- Surface roughness of the analysed commercial dental implant systems varied between different parts of the screw shaped implants (neck, top, valley and flank), but followed a different patterns for each implant system.
- For BT implant the flank was the roughest and the neck was the smoothest region, while the top and valley presented intermediate but similar values.
- For the BM implant, the roughest region was the top, followed by the valley, flank and the neck.
- Different conclusions were obtained when comparing topographical parameters calculated on the primary (SF) and roughness (SL) surfaces. Accordingly, topographical parameters should be calculated both on the primary surface (SF, to obtain the whole information) and the roughness surface (SL, for comparison purposes, in the case of using different acquisition areas) for a full description of surface topography.

The initial aim of this chapter was to establish a robust protocol for dental implant topographical characterization. This has been achieved through the development of implant handling and positioning devices and the analysis of data acquisition and processing variables on 3D topographical parameters. The tools developed consisted of the base for accurate and repeatable characterization, and the information gained in the studies allowed for the establishment of a generalized topographical characterization strategy for an optimum dental implant topographical characterization (summarized in section 3.6). This topographical characterization strategy was followed in the subsequent analysis of the present project.

CHAPTER 4

THE EFFECT OF SURGICAL INSERTION ON TOPOGRAPHY

"The real voyage of discovery consists not in seeking new landscapes, but in having new eyes."
Marcel Proust

Dental implant surface integrity may be compromised during surgical insertion, due to the stresses generated by the mismatch between the implant diameter and the osteotomy.

However, to date very little research has been carried out on the numerical characterization of implant topography after insertion, and none at all on the analysis of different parts of post-inserted implants.

This chapter therefore deals with the quantitative and qualitative study of the modification of two commercial dental implant systems under standard surgical insertion procedures. Different parts of the implants were characterized both before and after insertion in pieces of fresh cow rib bone. Furthermore, the bone site underlying the implants was analysed in order to evaluate the released particles, and the mass loss was approximated through the functional volume parameter (V_{m}) variation analysis.

4.1. Introduction

An important aspect to consider, and one often overlooked, is the impact of the stresses generated during surgical implant insertion on the surface characteristics. The standard method of preparing a bone site to receive an endosseous implant includes preparing the osteotomy with a series of drills of increasing sizes [Sum94]. The use of a final undersized drill is common practice attempting to increase primary stability by generating a discrepancy between implant diameter and the implant bed ([Tab10a], [O'S00]). However, shear forces arises when an implant is placed into a predrilled hole of smaller-diameter in bone ([Gua11], [Ska00]).

It has been reported that the release of titanium to the adjacent bone tissue may occur because of the friction and abrasion forces to which implant surfaces are subjected during insertion [Fra04]. The detachment of titanium particles has been linked to an increased bone resorption activity [Men13a], a potential cause of peri-implantitis ([TS14], [Olm13]), increased early bone loss [OH15] and implant failure ([Böl13], [Fri02]). Furthermore, the migration of titanium particles to distant inner organs has also been reported ([Wei94], [Sch92]).

It is clear from this that the possibility of surface alteration during dental implant insertion may have several implications in implant performance and survival, as well as being a potential health hazard. These factors make it imperative to develop a better evaluation and understanding of the interplay between insertion forces and surface modification.

In spite of this evidence, very little research has been carried out regarding the numerical characterization of the implant topography alteration after insertion. Only two works are known that analyse the alteration of implant tops ([Min14], [Sen13]), and none at all that analyse different parts of post-inserted implants.

This study therefore aims to characterize the modification generated through standard dental implant insertion procedures along the different parts of the implant. Comparisons between topographies both before and after insertion were carried out qualitative and quantitatively, and the implantation site was inspected through a scanning electron microscope in order to evaluate the presence of loose titanium particles. Additionally, the mass of the released particles was approximated through the functional volume parameter (V_{m}) variation analysis.

4.2. Objectives and hypotheses

In view of the sparse literature on the quantitative analysis of the surface modification generated during dental implant insertion, the purpose of this chapter is to study the modification of two commercial dental implant systems under standard insertion procedures. Below are the specific objectives of the chapter:

- To analyse both qualitatively and quantitatively the surface modifications generated during dental implant surgical insertion at different implant sites.
- To analyse the morphology of detached titanium particles.

- To approximate the material loss.
- To compare the behaviour of different surface treatments under insertion stress.

These are the hypotheses under consideration:

- That the surface topography of dental implants is modified during the insertion process.
- That modification generated during insertion differs among different parts of the implant.

4.3. Materials and methods

4.3.1. Dental implants and surgical procedure

Tapered self-tapping endosseous dental implants with different surface topographies were selected (n=3): BTI Tiny implant 3.5x11.5 (Ref: IRT3511, referred to as BT) and BIOMET 3iT3TM 3.25x8.5 (Ref: BOST3285, referred to as BM), see Figure 4.1. The BT surface is produced by acid etching while the BM surface is produced by the combination of sand blasting and acid etching processes in the implant body and solely acid etching in the neck. Both implant systems are made out of commercially pure titanium.

(a) (b)

Figure 4.1: Images of the analyzed dental implants acquired by the ALICONA system with the 3D rotation unit. (a) BTI Tiny (BT) and (b) BIOMET 3iT3TM (BM).

Fresh cow rib bone was selected for the study, since it is thought to mimic human type II due to the thick compact bone and dense trabecular bone [AG09]. This bone has been extensively used for dental implant insertion analysis ([Sen13], [Tri09], [AL08], [Edm96]). In order to ensure that the evaluated surface damage was due exclusively to the insertion procedure, bone blocks had been previously cut transversely to allow a non-traumatic extraction of the implants after insertion, avoiding any extra damage due to the extraction process. Blocks measuring approximately 20x15x15 mm with a transversal section in the middle were prepared through a horizontal mill with a sawblade (Metba MB-1) and used immediately (Figure 4.2). All blocks had a cortical thickness of 1.5±0.5 mm to resemble human maxilla and mandible bones ([Kat07], [Miy05], [Zar85]).

The two bone halves were bound tightly back together by a mechanical clamp and implants were inserted in the upper part of the transversal section (Figure 4.3 (a)) through the drilling unit Implantmed DU 9000, following the manufacturers' instructions (Figure 4.4). Dental implants insertions were carried out by a professional dental surgeon in order to resemble the clinical scenario as accurately as possible.

After the implants were fully inserted, the clamp was removed, and the implants were easily retrieved by separating the two previously generated bone block halves (Figure 4.3 (b)-(c)).

(a) (b) (c)

Figure 4.2: Cow rib bone blocks preparation: (a) fresh cow ribs; (b) bone cutting in the horizontal mill with a sawblade; (c) cow rib bone block with transversal section in the middle (to allow non-traumatic implant extraction) used for the insertion test.

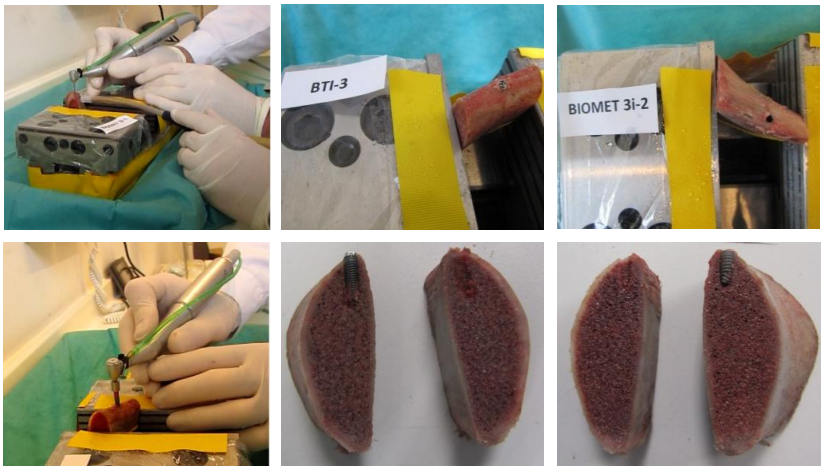

(a) (b) (c)

Figure 4.3: Representative images of the insertion test: (a) implant bed preparation and insertion; non-traumatic extraction of the BT (b) and BM (c) dental implants by separating the previously generated two bone block halves.

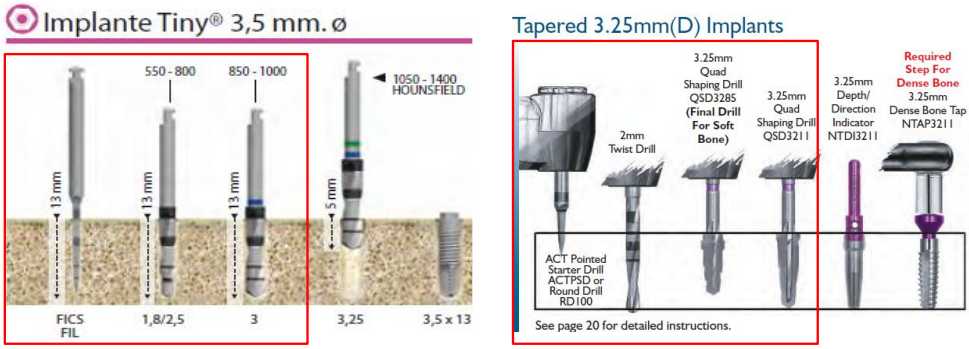

(a) (b)

Figure 4.4: Drilling protocol established by manufacturers for the BT [Bio14] (a) and BM [BIO13] (b) dental implants for different bone qualities (red squares delimit the steps followed in this study, which corresponds to a bone type II).

4.4. Surface characterization

4.4.1. Sample preparation and cleaning

Prior to the insertion test, implants were marked in the neck (for relocating purposes) and characterized immediately after removal from the packaging. Following the insertion, implants were sonicated in sodium hypochlorite (3 %, 4 minutes), purified water (40 minutes) and acetone (10 minutes) to remove all residual bone debris from the surface before characterization. Bone blocks were dried at 37°C for 78 hours after implant removal and existing bone debris were removed with a stream of air.

4.4.2. Qualitative analysis

Implants were mounted in the specifically designed supports (described in Chapter 3, section 3.3) which allowed the accurate and repeatable positioning without damaging the implant surface. Morphological and chemical analysis of implants was carried out at the same locations both prior and after the modification test through scanning electron microscopy (JEOL JSM 5600 LV) fitted with secondary electron (SE) and back scattered electron (BSE) probes, and also with X-ray dispersive spectroscopy (EDX), at voltages of (15-20KV). The bone sites overlying the implants were analysed after insertion in order to detect the presence of loose titanium particles by BES/EDX at low vacuum (1 Pa), using 20 KV voltage.

4.4.3. Quantitative analysis

Topographical characterization

The quantitative analysis was carried out following the measurement strategy defined in Chapter 3. For data acquisition and treatment details the reader is referred to section 3.7, where the characterization of the commercial implants under analysis prior to insertion is dealt with. Implants were characterized exactly at the same areas, following the same procedure after insertion.

Height (S_q, S_{sk}), hybrid (S_{dq}, S_{dr}), spatial (S_{al}), feature (S_{pd}) and functional parameters (explained below) were calculated on the primary surface both prior and after the insertion test.

Analogous functional parameters from both the European report 15178N [Sto93e] and ISO25178 standard [ISO12] were calculated for comparison purposes. These parameters describe the surface characteristics at different levels (peak, core, and valley) in terms of height and volume respectively:

- Functional parameters described in the European Report EUR 15178N are an extrapolation of 2D R_k parameters described in ISO 13565-2 (Figure 4.5 (b)). S_{pk}: peak height above the core roughness. S_k: core roughness (peak-to-valley) of the surface with the predominant peaks and valleys removed. S_{vk}: valley depth below the core roughness.

- Functional parameters described in the new ISO standard 25178 (Figure 4.5 (c)). V_{mp}: volume of material comprising the surface from the height corresponding to a 5 %[1] material ratio level to the highest peak. V_{mc}: volume of material comprising the texture between heights corresponding to the material ratio values of 5 %[1]-80 %. V_{vv}: volume of space bounded by the surface texture from a plane at a height corresponding to 80 % material ratio level to the lowest valley.

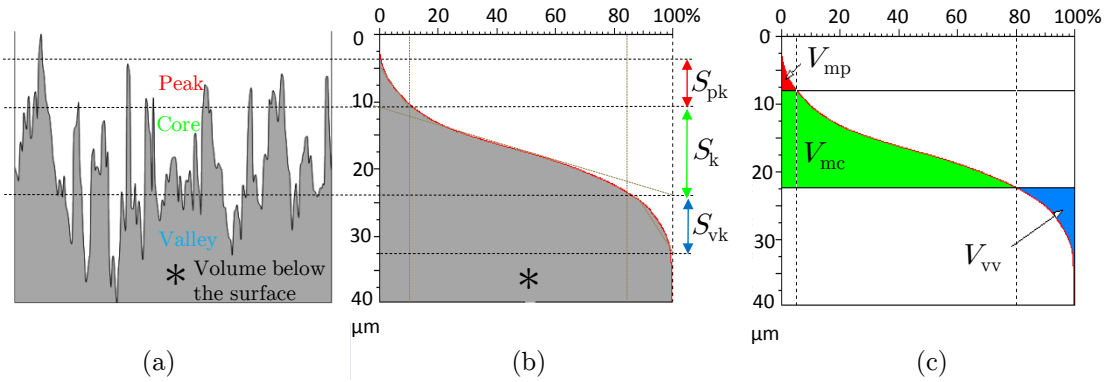

Figure 4.5: Scheme of the functional parameter calculation on the Abott Firestone curve (areal material ratio curve): (a) 2D profile; (b) functional parameters described in the European Report EUR 15178N (peak-S_{pk}, core-S_k and valley-S_{vk} as a function of height); (c) functional parameters described in the new ISO 25178 standard (peak-V_{mp}, core-V_{mc} and valley-V_{vv} as a function of volume). ∗volume below the surface calculated through the V_m parameter (described in ISO 25178) calculated at 100 % material ratio (corresponds to the area below the Abbott Firestone curve).

Additionally, the V_m parameter defined in ISO 25178 was calculated at 100 % material ratio in order to approximate the mass loss (procedure explained in the following section). This parameter represents the total material volume per area unit ($\mu m^3/\ \mu m^2$) and corresponds to the whole area below the Abbott Firestone curve (see "*" in Figure 4.5).

Mass loss approximation

There is not any instrumentation available to provide surface measurements of the entire implant at a high enough resolution to gain an accurate measurement of the material volume of the entire implant[2]. Therefore, the followed approach (explained below) is based on local measurements, and can only be termed as a mass loss approximation rather than a quantitative mass loss characterization.

The V_m parameter was calculated both before and after insertion at the same evaluation sites as the rest of the topographical parameters (explained in the previous section). In this way the mean volume variation of each evaluation site (neck, top, valley and flank) was computed:

$$\Delta V_m = V_{m(before)} - V_{m(after)} \tag{4.1}$$

and a good indication of the volumetric wear in localized areas of the implant was obtained.

[1]Default value in ISO 25178-2 standard is 10 %.
[2]The reader is referred to Chapter 2 where the measurement instrument limitations are explained.

These mean volumetric variations were then used to approximate the total mass of particles detached from each evaluation site. For this, the total surface area of one implant of each group was measured in ALICONA Infinite Focus with the real 3D rotation unit (which allows for the measurement of the entire sample at 360°) using a 10x objective (see Figure 4.1). From these measurements the area size of each evaluation site (A_{site}) was determined through Siemens NX 8.5 software using the surface fitting tool. Finally, the mass loss (m) at each site that presented a statistically significant material volume variation (see Equation 4.1) was determined according the following formula, considering the titanium density (ρ_{ti}) as 4.506 g/cm^3:

$$m = \Delta V_{\text{m}} \cdot \rho_{\text{ti}} \cdot A_{\text{site}} \tag{4.2}$$

4.5. Statistical analysis

A statistical paired t-test was conducted through Matlab® R2013a to determine whether the topographical parameter variations following the insertion test were statistically significant using a confidence interval (CI) of 95 %.

4.6. Results

4.6.1. Insertion

The implant insertion torque never exceeded the maximum value recommended by the manufacturer, and was in all cases lower than 30 Ncm.

4.6.2. Qualitative analysis

General SEM inspection after insertion exhibited clear topographical modifications in the apical region threads for the two implant systems (see Figure 4.6). The BT implant presented small widespread flattened areas of around 5 µm, while the BM implant showed greater and more isolated modified regions of approximately 20 µm.

A detailed SEM inspection of the evaluation sites (neck, top, valley and flank) both prior and after insertion revealed subtle topographical modifications, appreciable only at high magnification inspection (3000x). In the case of BT implants, no changes were identified in the neck after insertion (Figure 4.7). On the contrary, top (Figure 4.8) and valley (Figure 4.9) analysis disclosed material removal (particles approximately 1 to 5 µm in size) and morphology variation due to the insertion forces. The flank area presented, in addition to particle removal, severe plastic deformation of some prominent peaks that blinded the surrounding pores (Figure 4.10). On the other hand, the BM implant showed no changes in the neck (Figure 4.11), valley (Figure 4.13) and flank (Figure 4.14) sites after the insertion test. Only the top site of the BM implant (Figure 4.12) showed alterations.

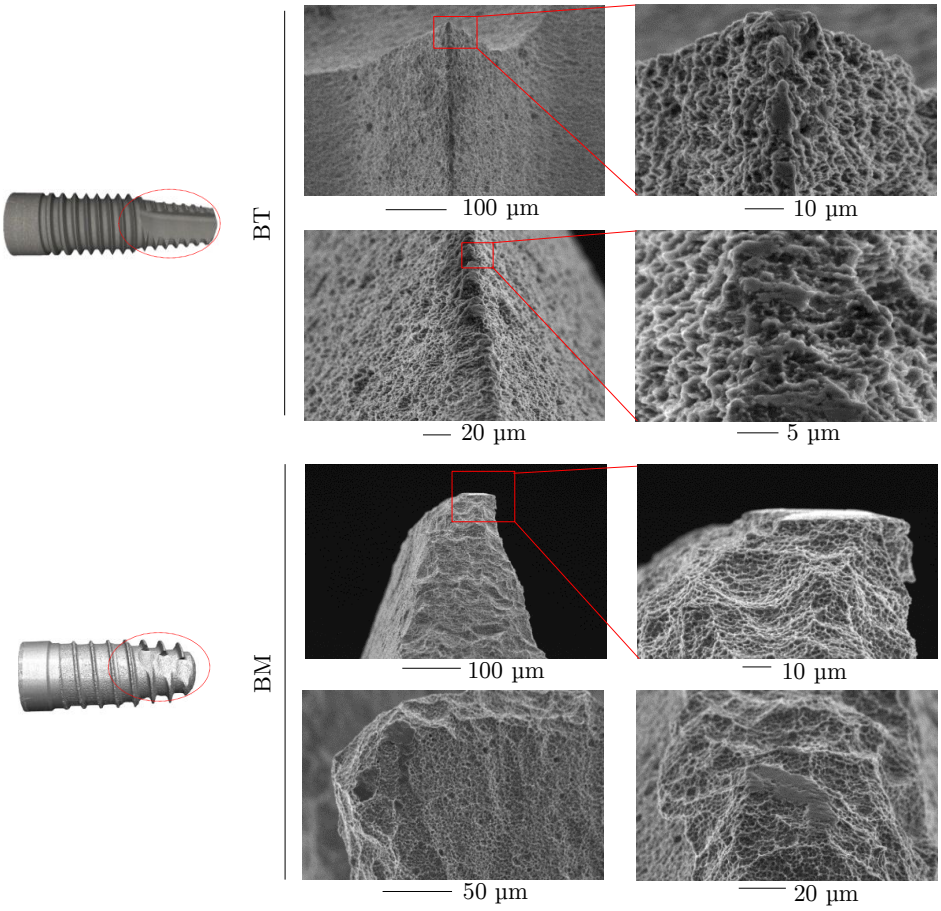

Figure 4.6: SEM images of the apical region threads of the BT and BM implants after insertion.

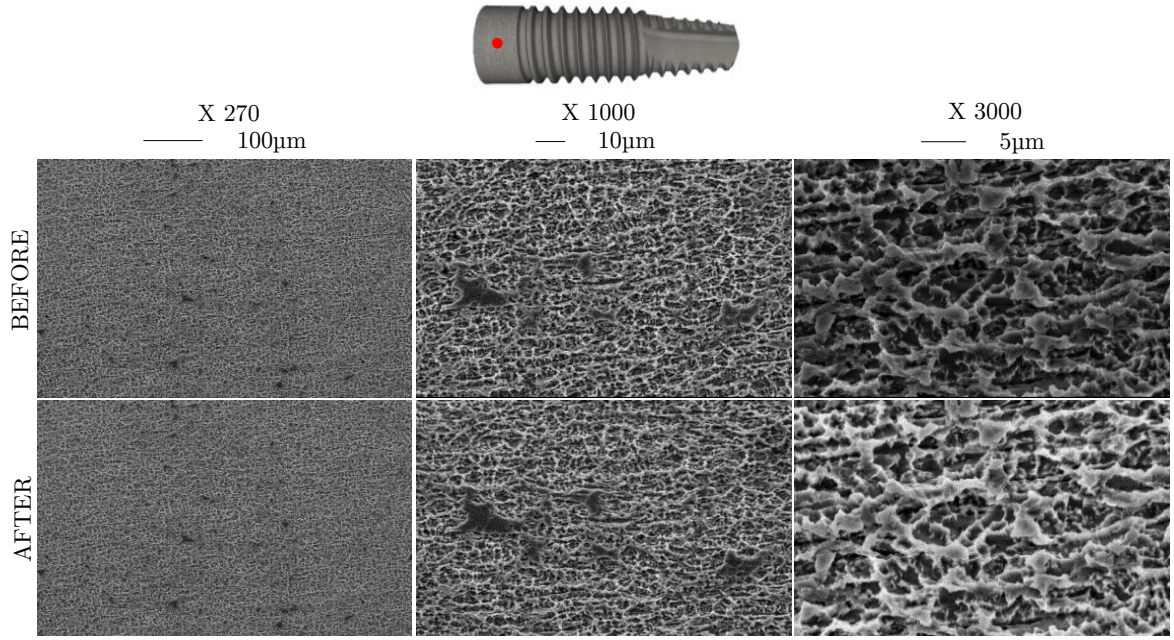

Figure 4.7: SEM images of the BT neck at different magnifications taken at the same area both before and after insertion.

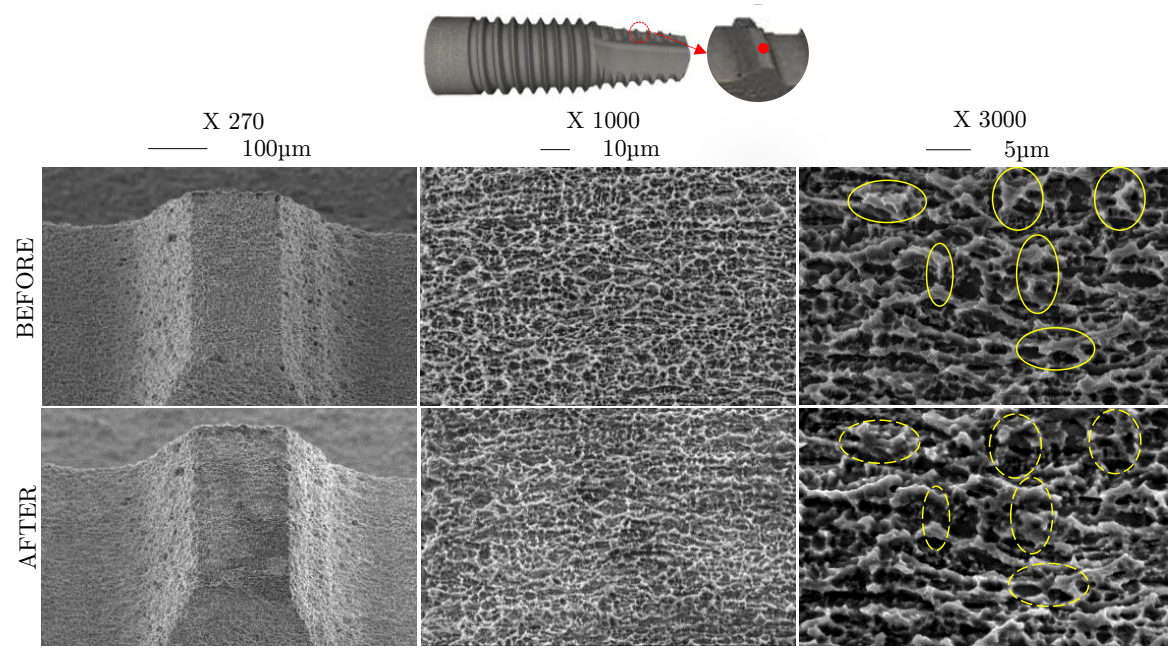

Figure 4.8: SEM images of the BT top at different magnifications taken at the same area both before and after insertion. Detected damaged areas are marked with circles for easy identification.

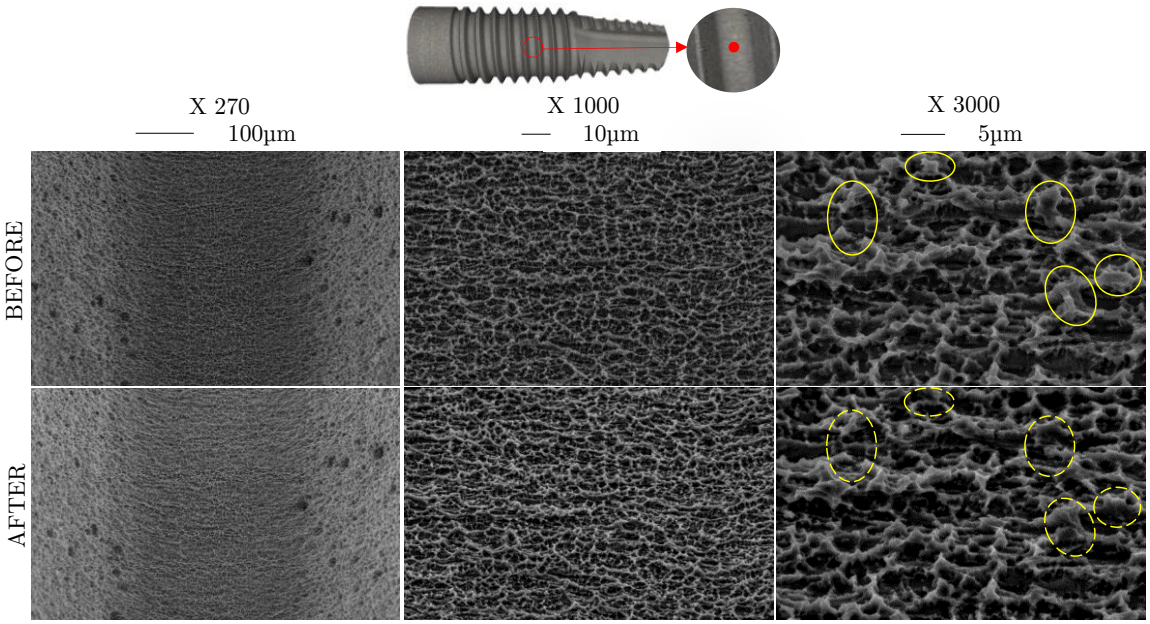

Figure 4.9: SEM images of the BT valley at different magnifications taken at the same area both before and after insertion. Detected damaged areas are marked with circles for easy identification.

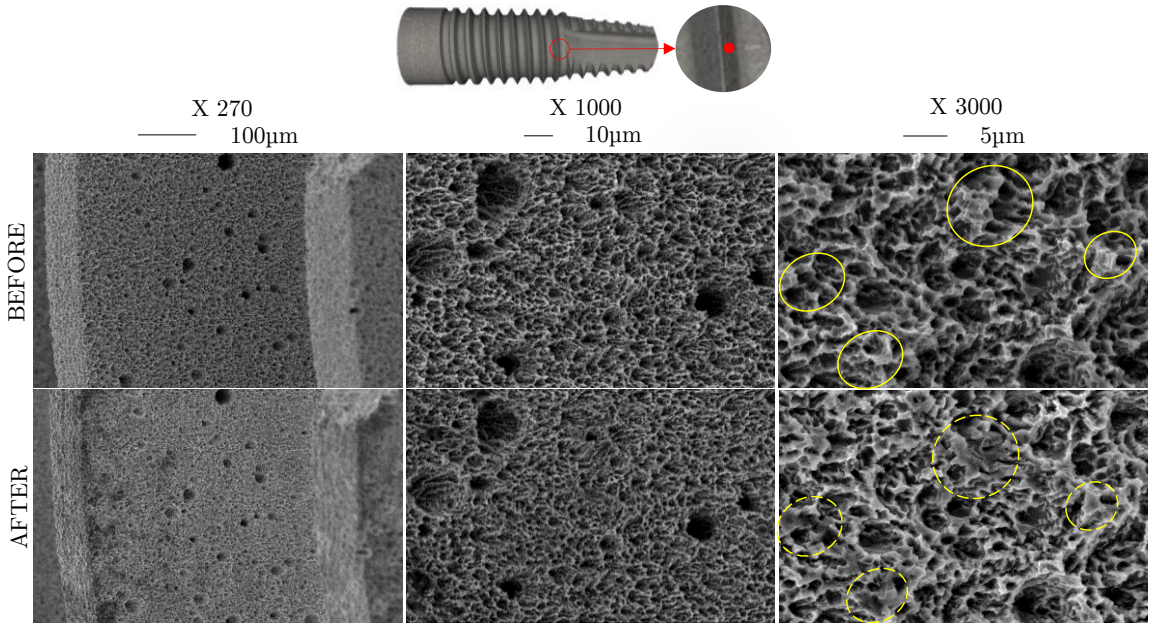

Figure 4.10: SEM images of the BT flank at different magnifications taken at the same area both before and after insertion. Detected damaged areas are marked with circles for easy identification.

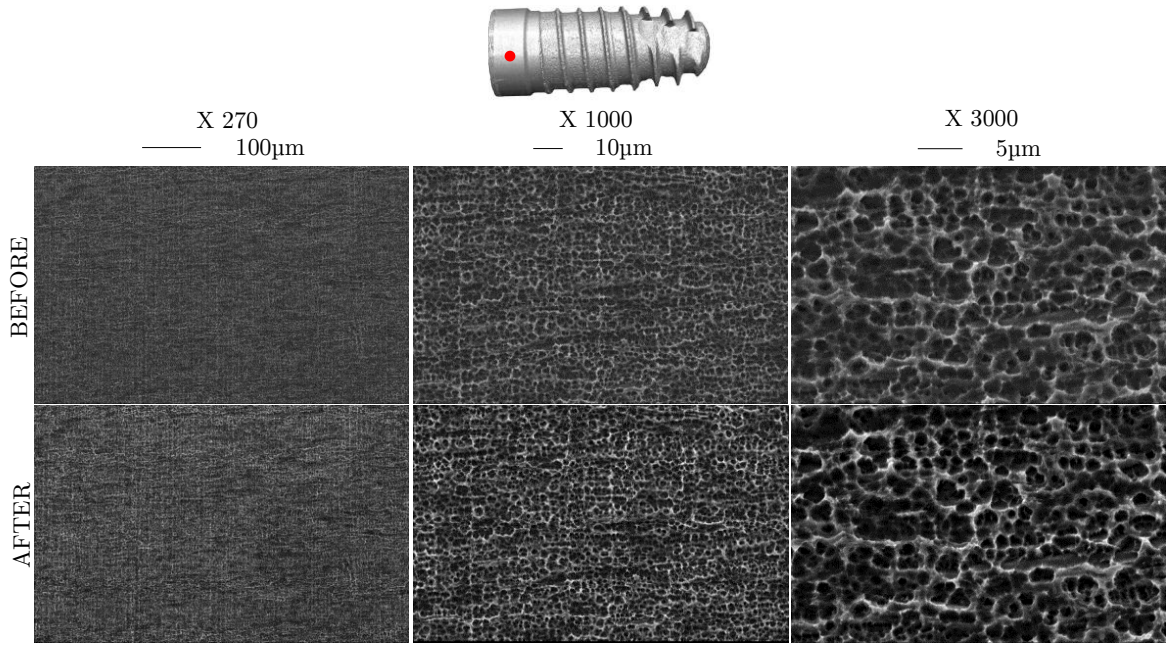

Figure 4.11: SEM images of the BM neck at different magnifications taken at the same area both before and after insertion.

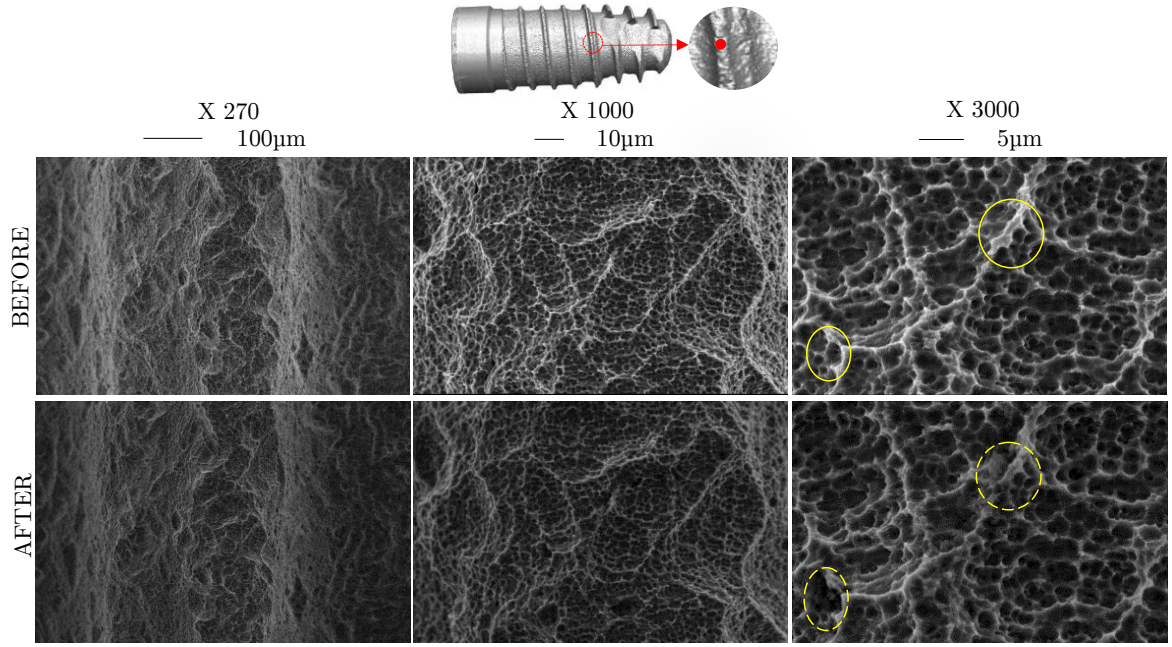

Figure 4.12: SEM images of the BM top at different magnifications taken at the same area both before and after insertion. Detected damaged areas are marked with circles for easy identification.

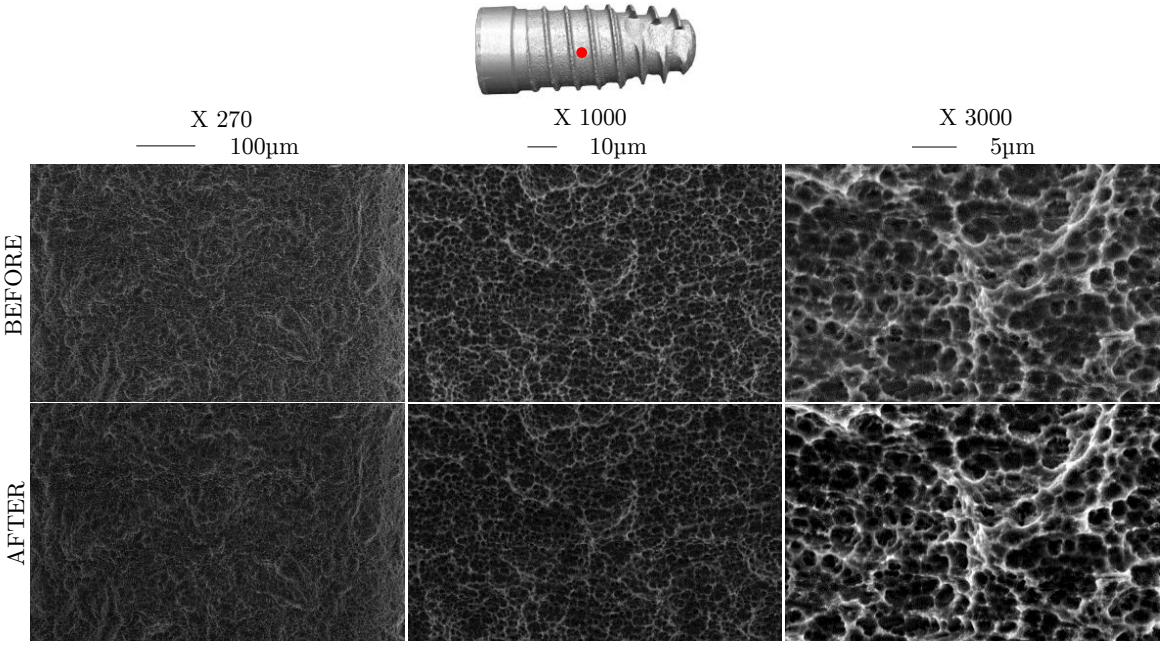

Figure 4.13: SEM images of the BM valley at different magnifications taken at the same area both before and after insertion.

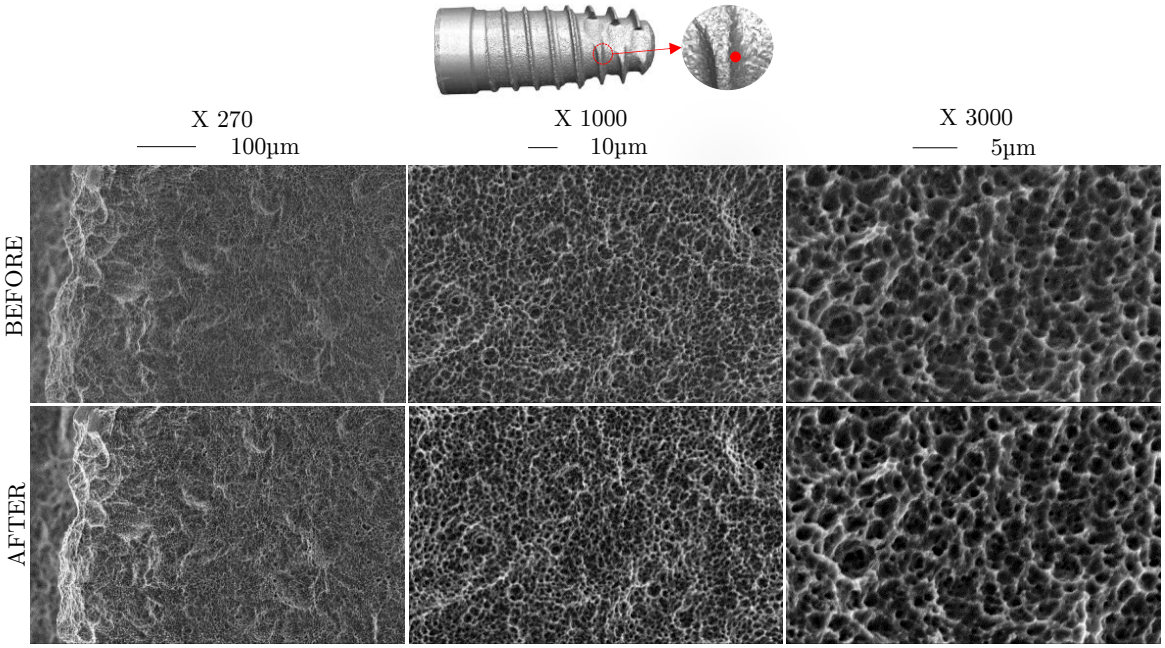

Figure 4.14: SEM images of the BM flank at different magnifications taken at the same area both before and after insertion.

A summary of the modified regions for both the BT and BM implants is shown in Table 4.1.

Table 4.1: Summary of the modified regions detected in the qualitative analysis for the BT and BM dental implants: "-": Non modified."+": Modified.

	NECK	TOP	VALLEY	FLANK
BT	-	+	+	+
BM	-	+	-	-

Back scattered electron (BSE) and electro dispersive X-Ray (EDX) analysis of the bone blocks at implantation sites revealed presence of titanium debris (visualized as bright particles) for both implants, mainly around the cortical bone layer (see Figure 4.15). The quantity and size of these particles differed from one implant to another. The BT implantation site showed a large quantity of small particles of 1 to 5 µm (see Figure 4.15 (a)), while a few isolated particles of 10 to 20 µm were found at the BM implantation sites (see see Figure 4.15 (b)).

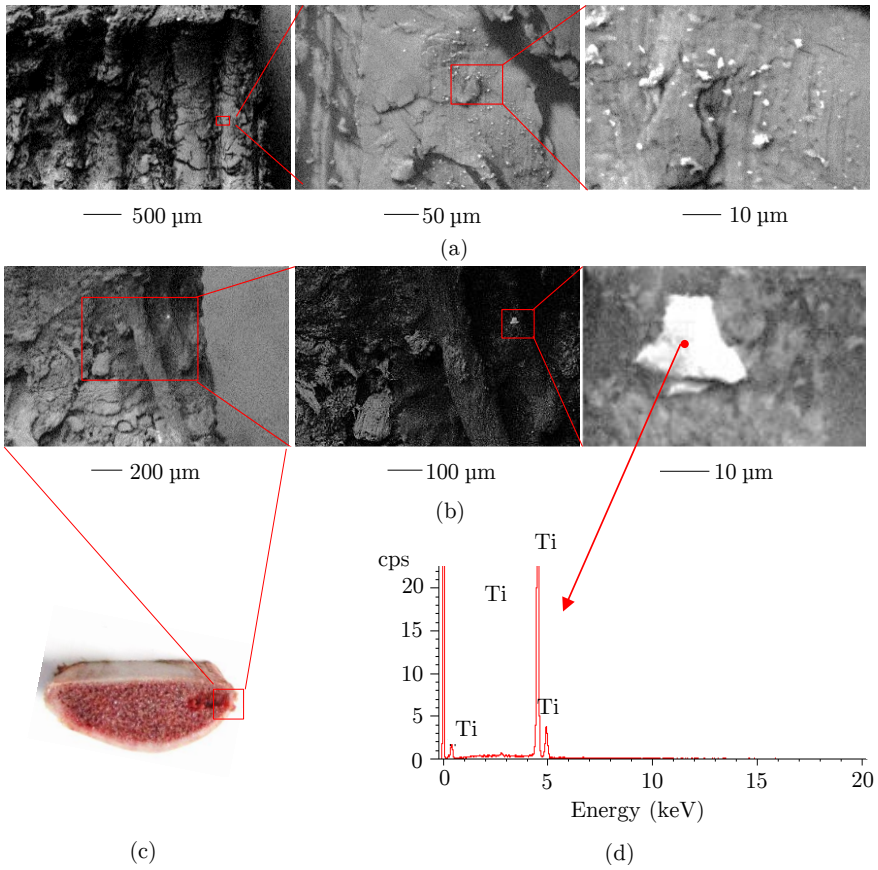

Figure 4.15: Analysis of the cow rib bone after insertion. Back scattered electron images of the BT (a) and BM (b) implantation sites (titanium debris appearing as bright particles); (c) Location of the SEM images on the bone blocks; (d) the elemental content of the bright particles encountered.

4.6.3. Quantitative analysis

Topographical characterization

The results of the quantitative analysis of the BT and BM implants are summarized in Table 4.2 and Table 4.3 respectively. The topographical characterization of the implants prior to the insertion test was previously analysed and discussed in Chapter 3 (section 3.7). This section will therefore focus on the topographical variations generated during dental implant insertion.

Figure 4.16 shows axonometric representative projections of the measurements taken at the same regions before and after insertion for both implant systems. The sites that showed statistically significant topographical parameter variations ($p<0.05$) are marked with *. It can be noted that the sharp peaks initially present became less prominent or had completely gone after insertion in the top, valley and flank of the BT implants and only on the top of BM implants, which is consistent with the qualitative evaluation (see Table 4.1). The results of those significantly modified areas are analysed in more detail below.

The pre-inserted BT implants showed a predominance of peaks in the top and valley sites ($S_{sk} >0$), while at the flank site, valleys were more predominant ($S_{sk} <0$). All areas maintained the initial predominance but showed a lower skewness value after insertion, which means that the height distribution shifted towards a more negatively skewed shape due to the removal or crashing of peaks. The top region of the BM implants indicated similar values before and after insertion, thus the height distribution was not significantly changed after the insertion test, indicating that the modification was not severe.

The material volume calculated at 100 % (V_m) decreased significantly in the modified sites mentioned (except the BT implants flank), which represents the material loss due to the particle removal already detected in the qualitative analysis. This was further corroborated by the peak density (S_{pd}) decrease after insertion, which suggests that peaks were removed or modified during insertion. The change of the material volume (V_m) followed the same pattern as that observed for the height (S_q), and hybrid (S_{dq}, S_{dr}) parameters, and was inversely related to the autocorrelation length variation (S_{al}), (see Figure 4.17).

As far as functional parameters are concerned, analogous functional parameters from both the European report 15178N and ISO 25178 standard were calculated for comparison purposes. Only the BT implant demonstrated significant variations of functional parameters and they were therefore further analysed (see Figure 4.18). The parameters from both families exhibited the same change patterns of change and similar variation degrees. However, for the functional parameters related to the valley (S_{vk}, V_{vv}) the variations were statistically significant only for the ISO 25178 void volume parameter (V_{vv}) as shown in Figure 4.18 (c).

All functional parameters reduced their value after insertion excluding the void volume of the BT flank site, whose value increased. The functional parameters describing peaks (S_{pk}, V_{mp}) underwent the biggest change after insertion, but they did not follow the material volume loss pattern: the BT flank area exhibited the largest V_{mp} variation and the lowest (and non-significant) V_m variation.

Table 4.2: Topographical parameters of the BT implant both before and after insertion expressed as mean value ± standard deviation. Parameter variation after insertion is expressed as a percentage change with respect to the unmodified surface (%Δ).∗ Statistically significant change (paired t-test, CI 95 %).

		NECK		TOP		VALLEY		FLANK	
		Value	Δ	Value	Δ	Value	Δ	Value	Δ
S_q (µm)	Before	0.93±0.04 (4 %)	-1 %	1.08±0.15 (14 %)	-11 %*	1.11±0.08 (7 %)	-7 %*	1.95±0.23 (12 %)	1 %
	After	0.91±0.04 (4 %)		0.96±0.15 (16 %)		0.96±0.08 (7 %)		1.96±0.31 (16 %)	
S_{sk}	Before	-0.05±0.18 (348 %)	-27 %	0.34±0.39 (115 %)	-72 %*	0.21±0.12 (56 %)	-71 %*	-1.41±0.65 (46 %)	26 %
	After	-0.04±0.13 (336 %)		0.09±0.30 (322 %)		0.06±0.12 (196 %)		-1.77±0.63 (35 %)	
S_{dq}	Before	1.30±0.09 (7 %)	-4 %	1.79±0.24 (14 %)	-26 %*	1.74±0.15 (9 %)	-16 %*	2.14±0.12 (6 %)	-13 %*
	After	1.25±0.11 (9 %)		1.33±0.14 (10 %)		1.47±0.15 (10 %)		1.86±0.11 (6 %)	
S_{dr} (%)	Before	65.59±8.21 (12.52)	-7 %	112.16±23.21 (21 %)	-41 %*	106.72±14.94 (14 %)	-26 %*	165.94±16.61 (10 %)	-23 %*
	After	61.18±9.49 (15 %)		66.44±12.09 (18 %)		79.04±14.94 (19 %)		127.83±13.39 (10 %)	
S_{al} (µm)	Before	4.09±0.46 (11 %)	3 %	4.09±0.98 (24 %)	19 %*	6.31±0.70 (11 %)	8 %*	7.69±1.14 (15 %)	9 %*
	After	4.21±0.53 (123 %)		4.88±0.85 (17 %)		6.82±0.70 (10 %)		8.39±1.00 (12 %)	
S_{pd} ($1/mm^2$)	Before	34756±5498 (16 %)	7 %	44324±10411 (23 %)	-19 %*	43987±3222 (7 %)	-10 %*	16491±4891 (30 %)	-25 %*
	After	37361±6604 (18 %)		36021±8912 (25 %)		39610±3168 (8 %)		12291±4235(34 %)	
V_m ($µm^3/µm^2$)	Before	4.44±0.46 (10 %)	-1 %	5.19±1.30 (25 %)	-11 %*	4.73±0.37 (8 %)	-6 %*	15.54±2.76 (18 %)	-1 %
	After	4.39±0.31 (7 %)		4.62±0.70 (15 %)		4.45±0.37 (8 %)		15.31±2.85 (19 %)	
V_{mp} ($µm^3/µm^2$)	Before	0.011±0.002 (18 %)	6 %	0.031±0.014 (45 %)	-21 %*	0.028±0.002 (8 %)	-14 %*	0.033±0.004 (13 %)	-24 %*
	After	0.011±0.002 (18 %)		0.025±0.010 (40 %)		0.024±0.002 (10 %)		0.025±0.002 (7 %)	
V_{mc} ($µm^3/µm^2$)	Before	0.883±0.045 (5 %)	-1 %	0.944±0.102 (11 %)	-9 %*	0.994±0.064 (6 %)	-6 %*	1.513±0.086 (6 %)	-1 %
	After	0.877±0.039 (4 %)		0.857±0.123 (14 %)		0.936±0.064 (7 %)		1.494±0.136 (9 %)	
V_{vv} ($µm^3/µm^2$)	Before	0.098±0.009 (9 %)	-2 %	0.108±0.011 (10 %)	-2 %	0.121±0.011 (9 %)	-2 %*	0.308±0.070 (23 %)	6 %*
	After	0.096±0.004 (4 %)		0.106±0.012 (11 %)		0.118±0.011 (9 %)		0.328±0.080 (24 %)	
S_{pk} (µm)	Before	0.55±0.17 (32 %)	8 %	1.30±0.39 (28 %)	-21 %*	1.25±0.12 (10 %)	-15 %*	1.38±0.16 (12 %)	-22 %*
	After	0.59±0.14 (23 %)		1.03±0.32 (31 %)		1.07±0.12 (11 %)		1.07±0.08 (7 %)	
S_k (µm)	Before	2.56±0.18 (7 %)	-2 %	2.60±0.26 (10 %)	-9 %*	2.72±0.18 (7 %)	-6 %*	4.11±0.14 (3 %)	-2 %
	After	2.52±0.14 (5 %)		2.38±0.34 (14 %)		2.56±0.18 (7 %)		4.04±0.32 (8 %)	
S_{vk} (µm)	Before	0.84±0.09 (11 %)	-3 %	0.98±0.16 (16 %)	-2 %	1.05±0.13 (12 %)	-2 %	3.40±0.85 (25 %)	6 %
	After	0.82±0.04 (5 %)		0.96±0.14 (15 %)		1.03±0.13 (12 %)		3.61±1.00 (28 %)	

Table 4.3: Topographical parameters of the BM implant both before and after insertion expressed as mean value ± standard deviation. Parameter variation after insertion is expressed as a percentage change with respect to the unmodified surface (%Δ).∗Statistically significant change (paired t-test, CI 95 %).

		NECK		TOP		VALLEY		FLANK	
		Value	Δ	Value	Δ	Value	Δ	Value	Δ
S_q (µm)	Before	0.51±0.03 (6 %)	-2 %	4.52±1.19 (4 %)	2 %	3.66±0.57 (16 %)	0.30 %	2.39±0.84 (35 %)	2 %
	After	0.50±0.03 (5 %)		4.60±1.01 (22 %)		3.67±0.57 (15 %)		2.43±0.85 (35 %)	
S_{sk}	Before	-0.11±0.14 (128 %)	9 %	0.04±0.34 (1 %)	-25 %	-0.22±0.27 (118 %)	14.90 %	-0.56±0.19 (33 %)	-2 %
	After	-0.12±0.15 (122 %)		0.03±0.34 (1050 %)		-0.26±0.26 (101 %)		-0.55±0.16 (29 %)	
S_{dq}	Before	0.82±0.06 (7 %)	-3 %	2.33±0.45 (2 %)	-6 %	1.48±0.11 (8 %)	-2 %	1.18±0.10 (8 %)	-4 %
	After	0.80±0.04 (5 %)		2.19±0.33 (15 %)		1.44±0.12 (8 %)		1.13±0.09 (7 %)	
S_{dr} (%)	Before	28.61±3.41 (12 %)	-5 %	187.25±70.67 (175 %)	-12 %*	81.15±11.07 (14 %)	-4 %	54.23±7.73 (14 %)	-7 %
	After	27.05±2.42 (9 %)		165.26±47.44 (29 %)		77.66±11.75 (15 %)		50.56±6.84 (13 %)	
S_{al} (µm)	Before	4.50±1.00 (22 %)	0.20 %	12.03±1.63 (13 %)	2 %*	19.29±2.20 (11 %)	0.20 %	17.88±1.51 (8 %)	0.30 %
	After	4.52±0.93 (20 %)		12.24±1.40 (11 %)		19.34±2.35 (12 %)		17.93±1.90 (11 %)	
S_{pd} ($1/mm^2$)	Before	45885±7897 (17 %)	-7 %	6821±3282 (1 %)	-23 %	3917±1231(31 %)	-13 %	8321±6373 (76 %)	-11 %
	After	42667±4980 (12 %)		5185±2472 (48 %)		3417±1219(36 %)		7418±6134(83 %)	
V_m ($\mu m^3/\mu m^2$)	Before	3.08±0.59 (19 %)	0.6 %	15.62±5.64 (15 %)	-0.3 %*	12.76±2.18 (17 %)	0.6 %	11.31±4.28 (38 %)	0.80 %
	After	3.10±0.48 (15 %)		15.57±4.92 (32 %)		12.84±2.18 (17 %)		11.40±4.47 (39 %)	
V_{mp} ($\mu m^3/\mu m^2$)	Before	0.010±0.002 (18 %)	-6 %	0.098±0.056 (0.1 %)	-2 %	0.073±0.019 (26 %)	0.09 %	0.035±0.013 (38 %)	1 %
	After	0.009±0.002 (17 %)		0.096±0.047 (49 %)		0.073±0.018 (25 %)		0.035±0.014 (39 %)	
V_{mc} ($\mu m^3/\mu m^2$)	Before	0.476±0.028 (6 %)	-1 %	4.226±1.222 (4 %)	2 %	3.407±0.538 (16 %)	-0.20 %	2.185±0.739 (34 %)	2 %
	After	0.469±0.019 (4 %)		4.335±1.053 (24 %)		3.400±0.501 (15 %)		2.224±0.761 (34 %)	
V_{vv} ($\mu m^3/\mu m^2$)	Before	0.059±0.004 (7 %)	-2 %	0.480±0.160 (1 %)	1 %	0.453±0.091 (20 %)	2 %	0.334±0.113 (34 %)	0.50 %
	After	0.058±0.004 (7 %)		0.485±0.156 (32 %)		0.463±0.097 (21 %)		0.336±0.111 (33 %)	
S_{pk} (µm)	Before	0.43±0.06 (13 %)	-6 %	4.49±2.18 (4 %)	0.08 %	3.11±0.76 (24 %)	-1 %	1.52±0.64 (42 %)	1 %
	After	0.40±0.05 (12 %)		4.49±1.90 (42 %)		3.07±0.77 (25 %)		1.54±0.65 (42 %)	
S_k (µm)	Before	1.35±0.08 (6 %)	-1 %	11.66±3.69 (11 %)	2 %	9.16±1.58 (17 %)	-0.10 %	5.82±2.38 (41 %)	3 %
	After	1.34±0.06 (4 %)		11.85±3.30 (27.83 %)		9.15±1.48 (16 %)		5.98±2.45 (41 %)	
S_{vk} (µm)	Before	0.54±0.06 (12 %)	-3 %	4.30±2.38 (4 %)	-1 %	4.06±1.15 (28 %)	4 %	3.35±1.28 (38 %)	0.30 %
	After	0.52±0.06 (12 %)		4.26±1.94 (46 %)		4.22±1.24 (29 %)		3.36±1.25 (37 %)	

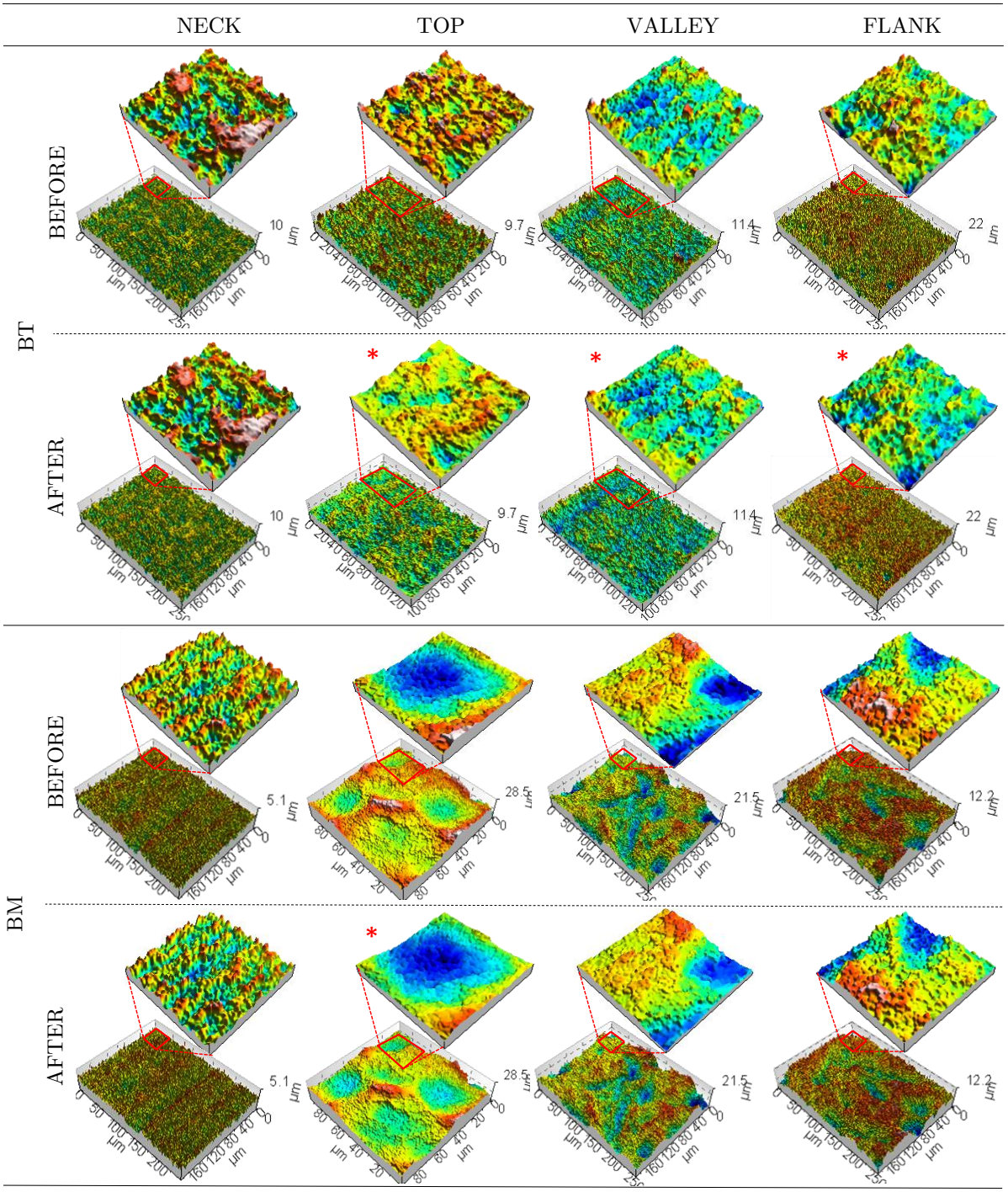

Figure 4.16: Representative axonometric projections of the measurements of the BT and BM implants at the four evaluation sites both before and after insertion. Those sites presenting statistically significant topographical parameter variations (t–paired test, CI 95 %) are marked with $*$ (zoomed area= 40x40 μm^2).

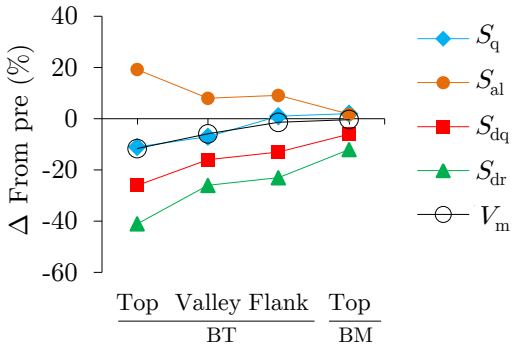

Figure 4.17: Topographic parameter analysis of the significantly modified sites after insertion. The average percentage variation of the height (S_q), spatial (S_{al}), hybrid (S_{dq}, S_{dr}), and material volume (V_m at 100 %) parameters.

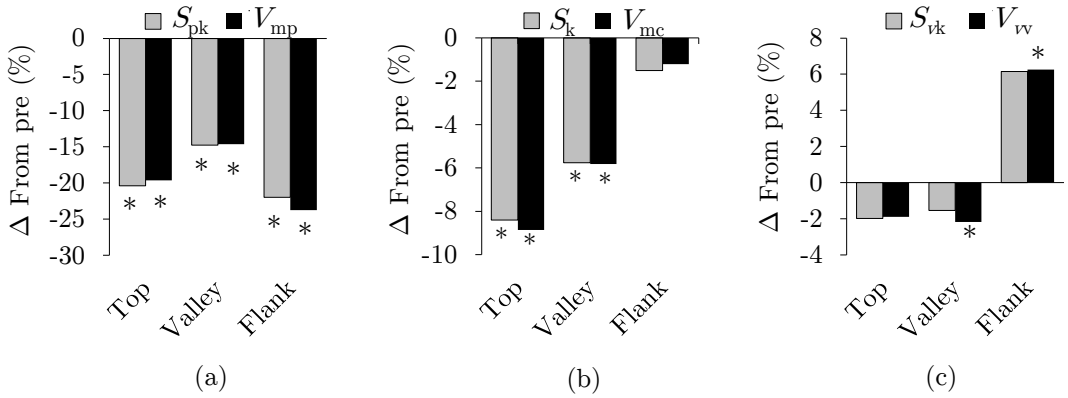

Figure 4.18: Comparison between percentage variation after insertion of the BT implant functional parameters from the European report 15178N (S_{pk}, S_k, S_{vk}) and ISO 25178 standard (V_{mp}, V_{mc}, V_{vv}). Parameters that describe the surface at different levels: peak (a), core (b), and valley (c). $*$ Statistically significant variation (paired t-test, CI 95 %).

Mass loss approximation

As already mentioned, the material volume decreased significantly in the top and valley regions of the BT implants and only at the top of BM implants (see Table 4.2 and Table 4.3 respectively). In order to analyse the distribution of the material volume loss along the implant, the mean material volume reduction of each significantly modified site was split between the apical region and the implant body (see Figure 4.19 (a)). It was observed that for the tops of BT implants, those located in the apex region were more damaged, while this trend was reversed for the valleys. Similarly, the BM tops of the apex region were more affected than those located in the implant body.

Table 4.4 summarizes the total surface area of each evaluation site for the two implant systems. Once the areas were determined, the mass loss of significantly affected sites was approximated applying the Equation 4.2. Figure 4.19 (b) shows a cumulative bar graph of the mass loss values split between implant body and apex areas. It was observed that in all cases more particles were released from the implant body compared to the apex. The average significant volume reduction of the tops and valleys of the BT implants correspon-

ded to an average mass loss of 9.8 µg and 26.7 µg respectively, resulting in a total of 36.5 µg of titanium released on average by the BT implants. In the case of the BM implants, only the tops exhibited significant volume reductions, which corresponded to a total of 1 µg of released particles on average by the BM implants. Although the top site of the BT implants showed the greater mean volume reduction (Figure 4.19(a)), more titanium was released from the valley region (Figure 4.19(b)).

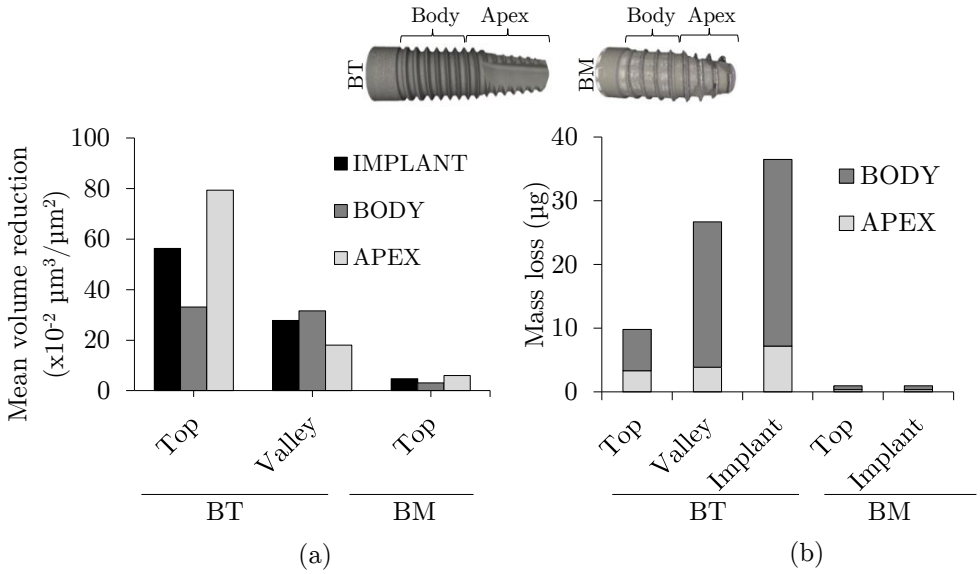

Figure 4.19: Analysis of the volume reduction and material loss along each implant system. (a) mean volume reduction at each site considering the whole implant, and the results split between implant body and apex; (b) cumulative bar graph of the mass loss split between implant body and apex for each evaluation site, and the corresponding total material loss for each implant system.

Table 4.4: The total area of each evaluation site (neck, top, valley and flank) for the two implant systems and area values split into body and apex regions.

		Area (mm^2)		
		BODY	APEX	TOTAL
NECK	BT	-	-	17.9
	BM	-	-	12.5
TOP	BT	4.65	0.98	5.63
	BM	4.81	1.36	6.17
VALLEY	BT	17.02	5.08	22.1
	BM	23.46	6.11	29.57
FLANK	BT	48.55	6.66	55.21
	BM	14.44	8.15	22.59

4.7. Discussion

This investigation has demonstrated that changes in the surface topography of commercial endosseous implants occurred during standard insertion procedures.

4.7.1. Qualitative analysis

Two degradation mechanisms (wear and plastic deformation) were detected after the insertion test. Although some modified areas were observed at relatively low magnifications, a detailed analysis comparing images taken both prior and after insertion at the same sites was necessary in order to detect surface modifications. This thorough inspection revealed peak removal and morphology alterations (sizes ranging from 1 to 20 μm), only perceptible at x3000 magnification, that would have been overlooked if no prior characterization at the same site had been carried out. This calls into question whether the absence of topographical modification reported by some authors ([CV14], [Bat12]) was real or if the modification was overlooked due to the observation being carried out at low magnifications (35x and 137x respectively).

The qualitatively observed peak removal was further corroborated in the bone block analysis, where titanium debris appearing as bright spots in the BSE overview mode were detected for both implant systems. Previous works ([Men13b], [Sch91] taken from [Kra94]) reported metallic particle release of 5-20 μm and 1-10 μm in non-specified screw implants respectively. The present results agree with these size ranges, and it was also shown that the particle size depends on the surface treatment, since the particles released by the sand blasted and acid etched BM implants (∼20 μm) were four times greater than those released by the acid etched BT implants (∼5 μm).

4.7.2. Quantitative analysis

Topographical characterization

The modified surfaces presented a more negatively skewed height distribution after the insertion, due to the removal and deformation of some peaks, which was also corroborated with the peak density diminution (S_{pd}). The S_{sk} parameter was valuable in evaluating the shift in the height distribution curve but this parameter should be used carefully, due to its high variability. The height (S_{q}) and hybrid (S_{dq}, S_{dr}) parameter variations were positively correlated with the material volume reduction (ΔV_{m}). Among them, the developed area ratio (S_{dr}) underwent the major changes and is therefore considered the best damage indicator. On the other hand, the autocorrelation length (S_{al}) was inversely correlated to the material volume reduction (ΔV_{m}). The increase of the S_{al} value after the insertion is likely to be related to the generation of wider features due to the removal and flattening of some peaks during the insertion process.

The use of functional parameters from the European report 15178N has been suggested for the analysis of modified surfaces [Sen13]. In the present work, the analogous functional parameters defined in ISO 25178 standard were also calculated for comparison purposes.

The comparison analysis showed that parameters from both families underwent similar variations following the same trends. However, the functional volume parameters of ISO 25178 standard reported more sensitivity, since more statistically significant changes were found. Therefore, based on these results, it is suggested that the functional volume parameters of ISO 25178 standard be used rather than the R_k family parameters to evaluate dental implant surface modifications. The functional volume parameter variations will be discussed below.

As expected the material peak volume (V_{mp}) was the most affected parameter. It should be noted however that this parameter did not correlate with the material loss, since the BT flank showed the largest V_{mp} variation and the lowest volume reduction. The SEM inspection of the BT flank site showed that some peaks underwent severe plastic deformation and blinded the surrounding pores. This could have caused the larger variation in the peak material volume parameter (V_{mp}). The material core volume (V_{mc}) also decreased for all areas after the test and was positively correlated with the material loss. Regarding the void volume parameter (V_{vv}), it decreased for all regions except for the BT flank site, which could be again related to the prevalence of plastic deformation observed in the qualitative analysis.

The results obtained agree with previous studies carried out by Senna *et al.* [Sen13], where the topographical evaluation of dental implants top region before and after insertion demonstrated an overall decrease of roughness parameters. However, this study did not find any correlation between parameter variations and material volume reduction. The study mentioned analysed roughness parameters by applying a non-specified filter size, while the present study has analysed primary topographical parameters. It is unclear whether this is the reason for the lack of correlation between parameter variation and material loss in the study mentioned. Nevertheless, the use of primary topographical parameters rather than roughness parameters is recommended in order to avoid removal of potentially important information from the surface.

Mass loss approximation

There is not a consensus on the relationship between the surface treatment and material loss. Sridhar *et al.* [Sri15] reported no surface damage of sand blasted large grit acid etched implants, and suggested that the topography damaging likelihood of this surface treatment may be low. Conversely, increased roughness has been related to the increased probability of particle release [Fra04]. The mass loss approximation carried out in the present study revealed that the etched BT implants released in average more particles (36.5 µg) compared to the rougher sand blasted and acid etched BM implants (1 µg). However, no direct comparison between different surface treatment behaviours could be undertaken, since the implants were not subjected to the same load regime during insertion. The mismatch between osteotomy and dental implant diameter varied from one implant type to another. The surgical procedure of the BM implants had a specific final drill that replicated the minor diameter of the implants [Mel09] while the cylindrical final drill of the osteotomy for the BT implants [Bio14] did not follow the tapered shape of the implant body. Furthermore,

the thread shape and height of both implant systems differed significantly, the threads of BT implants being more prominent and sharp (see Figure 4.1). It can be concluded from this that the stress ranges suffered by the BM implants during insertion were probably lower than those experimented by BT implants. This is a possible reason for the lower modification encountered.

It was observed that the material loss at each evaluation site varied along the implant when the results were split between the apical region and the implant body. As expected, the tops located at the apex region were more seriously damaged compared to those located at the implant body, since they were the first threads cutting their way into the adjacent host bone. Concerning the greater damage on the valleys of the BT implants located in the body region, this was probably due to the macrogeometric relationship between tapered implant and cylindrical osteotomy, which generated stronger stresses in the valleys located at the implant body. Interestingly, the study revealed that even if the most mean volume reduction took place at the tops of BT implants, the major material loss occurred at the BT valleys, since they cover a greater area of the implants. This emphasizes the importance of the evaluation of different implant sites.

As previously mentioned, the statistically significant average volume variations corresponded to a total material loss of 36.5 µg for the acid etched BT implants and 1 µg for the sand blasted and acid etched BM implants. Similar values have been previously reported. Krafft *et al.* [Kra94] described a material loss up to 31.8 µg and 11.65 µg for titanium plasma sprayed and sandblasted and etched implants respectively, where the detached material was quantified by dissolving the bone and quantifying the titanium concentration by means of induction-coupled plasma. Conversely, Senna *et al.* [Sen13] reported a material loss up to 0.5 mg for sand blasted and acid etched implants, based on the material volume variation of the tops extrapolated to the entire implant. However, this value was probably overestimated, since as demonstrated in the present study, the material loss is not homogeneous along the whole implant but varies depending on the region. The wide range of reported material loss values is probably due to the differing implant geometries, surface treatments and surgical procedures (leading to varying stress ranges), and also to the use of distinct methods to assess the mass loss.

Regarding the accuracy of the selected method to assess the mass loss, it should be reminded that the followed approach is an approximation since it is based in local measurements of each evaluation site and therefore does not consider the whole surface of the implant. Within its limitations, it resulted useful to analyse the differences in mass loss between different implant sites and its distributions along the implant. However, it should be highlighted that although the flank site of the BT implant presented a non-significant material volume variation (ΔV_{m}), the remaining parameters varied significantly, indicating that the surface was modified. This fact could be ascribed to the absence of wear and prevalence of plastic deformation. However, it should be considered that the severe plastic deformation observed in the BT flank site (with blinded pores by dragged material) may have distorted the material volume calculus. As shown in Figure 4.20, in case air gets trapped below the dragged material, this empty volume would be computed as material volume, and the mass loss calculus would therefore not be correct. It is not clear whether

this was the reason of the non-statistically significant volume variation of the BT flank site. Nevertheless, the V_m parameter variation analysis may not be an adequate method for mass loss approximation when severe plastic deformation occurs, and therefore, further studies should be carried out in order to assess the accuracy of the method and to look for alternative methods.

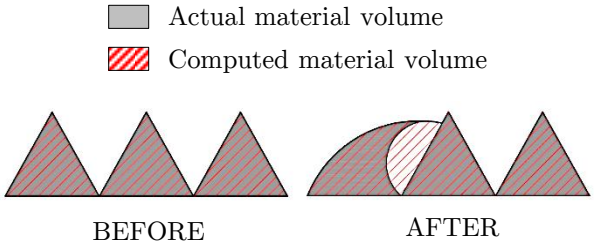

Figure 4.20: Schematic illustration of the V_m parameter variation analysis when plastic deformation with pore blinding is present.

The evaluation and quantification of the released particles is of big importance since the presence of titanium particels on the peri-implant area has been associated with a larger osteoclastic activity [Men13a], increased early bone loss [OH15], greater risk of periimplantitis ([WJ15], [TS14], [Olm13]) and implant failure ([Böl13], [Fri02]). Furthermore, the migration of titanium to inner distant organs has also been reported ([Wei94], [Sch92]). Although the BM implants released a smaller quantity of titanium, it should be remembered that the released particles were of a larger size (20 μm) compared to those detached from the BT implants (5 μm). This fact is notable since it has been pointed out that the quantity and size of particles themselves may be more significant in developing lesions than the bulk accumulated titanium metal [Swa91]. Although the threshold limit of detached particle size and quantity for successful implants has not been yet established, it is clear that surface degradation should be avoided or at least minimized.

4.8. Conclusions

This study set out to characterize the topographical modifications generated upon standard dental implant insertion procedures. To that end two commercial dental implant systems of different surface treatments (acid etched BT implants and sand blasted and acid etched BM implants) were introduced in fresh cow rib bone pieces reproducing an actual clinical scenario and fully characterized both before and after insertion. The following points can be concluded from the various components of this study:

- Two degradation mechanisms were detected: wear phenomena (with the resulting particle removal), and plastic deformation (with the corresponding morphological variation).
- A detailed qualitative analysis comparing images taken both prior and after insertion at the same sites using a minimum of x3000 magnification was required to detect surface alterations.

- Surface damage varied at different evaluation sites for each implant system (neck, top, valley and flank) and also along the implant within each site.
- The BT implants presented significant alterations at the top, valley and flank sites while the BM implants presented significant modifications only at the top site.
- The developed interfacial ratio (S_{dr}) variation correlated positively with the material volume variation (V_{m}) and is considered to be the best damage indicator.
- The use of functional volume parameters of ISO 25178 standard is sugested rather than the R_{k} family parameters defined in the European report EUR 15178N due to the higher sensitivity encountered.
- The use of primary topographical parameters is suggested rather than roughness parameters in order to avoid removal of potentially important information from the surface.
- BT implants were more seriously damaged than the etched BM implants, resulting in an average of 36.5 and 1 μg of released particles respectively. However, it was not possible to compare between different surface treatment behaviours, since the implants were not subjected to the same load regime during insertion.
- Particles released by the sand blasted and acid etched BM implants (∼20 μm) were four times greater than those released by the acid etched BT implants (∼5μm).
- The tops located at the apex region were more seriously damaged compared to those located at the implant body, while the trend was opposite for the valleys due to the different macrogeometric relationship between each evaluation area and the osteotomy.
- Even if the tops were the most seriously damaged parts, the major material loss occurred at the BT valleys, since they covered a greater area of the implants. This emphasizes the importance of analysing different sites of the implants.

The initial aims of this study were to:

(I) To analyse both qualitatively and quantitatively the surface modifications generated during dental implant surgical insertion at different implant sites.

(II) To analyse the morphology of detached titanium particles.

(III) To approximate the material loss.

(IV) To compare the behaviour of different surface treatments under insertion stress.

The first two aims (I-II) were fully achieved. The surfaces of commercial dental implants demonstrated wear and plastic deformation as a result of standard dental implant insertion

procedure, and the morphological analysis of detached titanium particles revealed that the size and quantity depends on the surface treatment. The third aim was also achieved (III) through the analysis of the variation of the functional parameter V_{m}, which allowed the approximation of the material loss at different implant sites. However, it was seen that under severe plastic deformation the V_{m} parameter variation analysis may led to erroneous results. It would therefore be interesting to assess the accuracy of the method through alternative methods.

It was not possible to achieve the final aim (IV), since the analysed implants were subjected to different load regimes. This objective will be addressed in the following chapters.

To the author's knowledge, this is the first study dealing with the qualitative and quantitative study of the surface modification generated during surgical insertion analysing different regions of the implant. Due to the complexity of the observed multivariable interactions, including implant macro geometry, surgical procedure and surface treatment, future studies should continue examining the effect of insertion on the surfaces of dental implants. It is to be hoped that greater understanding of the mechanisms of surface integrity loss during surgical implant insertion, as well as the interplay between topography and modification, will bring significant advance in the design of endosseous implants, resulting in enhanced performance.

CHAPTER 5

IN VITRO STUDY

"Ever tried. Ever failed.
No matter.
Try again. Fail again.
Fail better"
Samuel Beckett

The previous chapter clearly demonstrated that dental implant surface topography is altered during surgical insertion. Namely, both wear and deformation were observed on the surface of post-inserted dental implants. However, the influence of these topographical alterations on the cell response is unknown. This chapter aims therefore to analyse the effect of varying surface roughness and topography modification on cellular response. To that end a device to reproduce the observed alterations on disc samples (format required for the in vitro test) was first developed. Subsequently, disc-shaped samples were treated with typical dental implant surface treatments and modified by means of the developed device, reproducing the topographical alterations generated during dental implant insertion. Finally, both modified and unmodified samples were assayed in vitro using human MG-63 osteosarcoma cells to test the impact of roughness and its modification on cell attachment and proliferation.

5.1. Introduction

The previous chapter dealt with the characterization of dental implant topography after insertion. Flattened smooth areas arising from the deformation of asperities and released particles due to wear were encountered, demonstrating that the surface of dental implants is modified during the insertion process. In addition to the potential contamination of the peri-implant area (which has been addressed in section 2.5.3 "Surface alteration during insertion") the possibility of a different cellular response of the post-inserted surfaces compared to the pre-inserted ones should be considered. Indeed, the surfaces analysed in vitro may not represent the surfaces facing the actual biological environment after implantation, which could lead to unpredicted results.

However, there are currently no studies dealing with the effect of surface modification on cell response. Therefore the effect of topographical alteration generated during dental implant insertion on cell response will be dealt with in the present chapter.

In vitro studies are carried out using disc format samples, in which the cells interact with the flat surface. The first step therefore was to develop an experimental set-up to reproduce the modifications encountered on dental implant surfaces in the flat surface of a disc. Following this titanium discs treated with typical dental implant surface treatments were modified using the designed device, reproducing the alterations generated during dental implant insertion. By performing topographical measurements on the same area both prior and after modification, detailed information about the topographical alteration was obtained. Finally, both modified and unmodified discs were subjected to in vitro tests using human MG-63 osteosarcoma cells in order to test the impact of roughness and its modification on cell attachment and proliferation.

5.2. Objectives and hypothesis

The aim of this chapter is to study the effect of the topographical alteration generated during dental implant insertion on the cell response. The specific aims of the chapter are listed below:

- To reproduce the modification generated during dental implant insertion homogeneously on the flat surface of a disc.
- To evaluate the in vitro response of modified and unmodified surfaces.

These are the hypotheses under consideration:

- Topographical modification of dental implant surface generated during surgical insertion can be reproduced on the flat surface of a disc.
- Dental implant surface alteration generated during insertion process affects cell response.

5.3. Materials and methods

5.3.1. Samples

A total of 72 titanium Cp4 discs (⌀6x1mm) were used for the study. Ti discs were prepared with three different surface treatments (n=24 per treatment): as-machined (MCN), acid-etched (AE) and sand blasted and acid etched (SB+AE). Half of the samples for each treatment were subjected to the modification assay as described in the following section, obtaining 6 groups of surfaces (see Table 5.1).

Table 5.1: Samples used for the in vitro study. "-": non modified, "+": modified.

GROUP	TREATMENT	STATE	N° SAMPLES
1	MCN	-	12
2	MCN	+	12
3	AE	-	12
4	AE	+	12
5	SB+AE	-	12
6	SB+AE	+	12

5.3.2. Experimental set-up for the modification test

Objectives of the experiment

The aim of this experiment was to reproduce the modification generated on dental implant surface topography during insertion process on a flat disc surface. Given that the in vitro assays reveal the dominant phenotype based on the average response [Boy01], the goal was to generate a homogeneous modification over the entire surface without any contamination (to prevent non-desired variables in the in vitro assay).

Experimental set-up: first approach

The dental implant surface is subjected to compressive and shear stresses during surgical insertion due to the mismatch between the hole and the dental implant diameter. In order to reproduce this stress state on a flat surface, a device was designed and fabricated, and was integrated into the Universal Mechanical Testing System INSTRON 4206.

Figure 5.1 shows the general scheme of the modifying device. The vertical load (compressive stress) was provided by the Instron machine, while the horizontal force (shear stress) was supplied by a commercial linear actuator. Vertical and horizontal movements were guided by a commercial die and linear guide respectively. A specifically designed disc holder (in which titanium disc shaped samples were placed) was assembled on the linear guide and joined to the actuator's piston rod. In this way a relative movement between the disc surface and the counterpart (assembled in the upper die) was obtained.

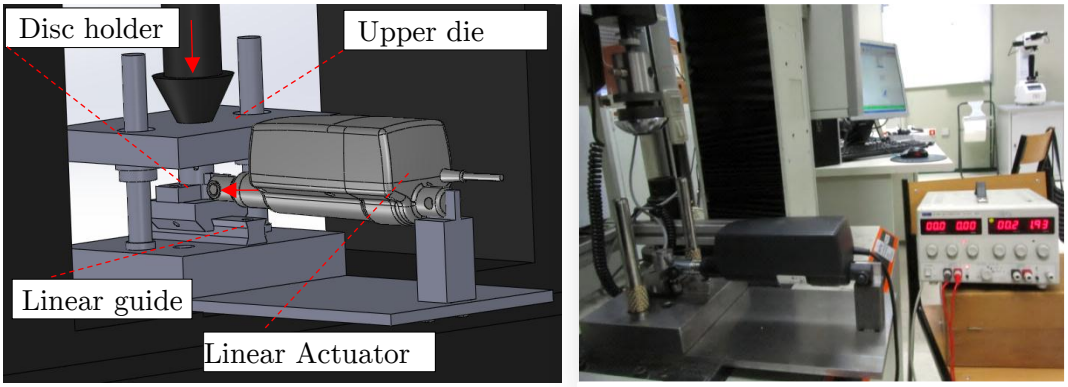

(a) (b)

Figure 5.1: General scheme of the modification device. Surface modification device CAD design (a) and final assembly (b).

Two materials were tested for use as a counterpart: stainless steel as a rigid counterpart and solid rigid polyurethane foam from Sawbones® (40pcf, 0.64 gr/cm^3) as a flexible counterpart. The latter is widely used as an equivalent for jaw bone and meets ASTM F-1839-08 [ASTa]. 30x12x3 mm parts of both materials were cut and fixed in the upper die (see Figure 5.2 (a)-(b)). The designed disc holder (where a circular pocket was machined to locate the titanium sample) had a pivoting system to auto-align the disc and to obtain a parallelism between the counterpart and the disc surface for each assay (Figure 5.2 (c)).

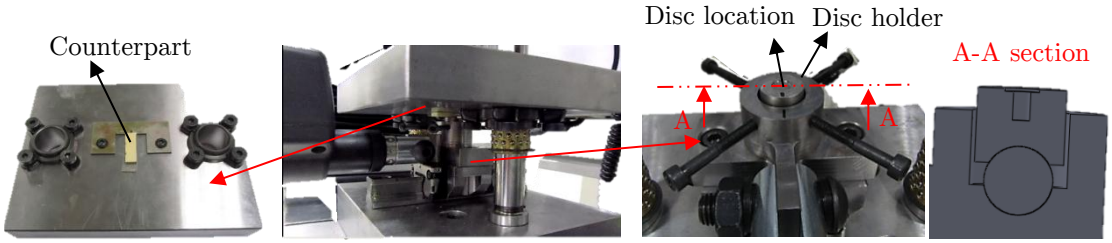

(a) (b) (c)

Figure 5.2: Modification device details. (a)-(b) polyurethane foam counterpart stick in the upper die (the stainless steel counterpart was also tested); (c) self-aligning system with pivoting disc holder.

Tune-up tests were carried out using the 5 KN load cell following the next stages. Each test commenced by bringing the counterface into contact with the titanium sample. First a compression load was applied and the pivoting system was blocked by four locking screws (see Figure 5.2 (c)). Following this (while the device was subjected to compression) the linear actuator was activated to push the disc holder until a 6 mm route was completed (introducing the shear stress), and finally the system was unloaded. After conducting tune-up experiments at different compression loads, several problems were observed.

To begin with, regardless of the load and counterpart material, it was observed that all contact was generated in the periphery of the discs (although this effect was more pronounced when using the rigid stainless steel counterpart). The titanium discs were analysed in more detail in order to discover the source of this problem, acquiring profile

measurements of disc diameter lengths. As shown in Figure 5.3 (a), a slight curvature was observed in the discs, which was attributed to the machining process (similar to that used for dental implant production). Although the height difference was only six micrometres, it was enough to prevent the homogeneous contact along the whole surface.

Additionally, in case of the polyurethane counterpart, it was not possible to completely remove the simile debris from the titanium disc surfaces. Different washing procedures were analysed (sonicated in acetone for 15, 20, 30 and 40 min followed by alcohol 10 min) but simile traces remained in all cases (see Figure 5.3 (b)). This contamination would have compromised the posterior in vitro assay so direct contact between simile and titanium surface was avoided.

These issues led to discarding this first approximation. In order to overcome these detected problems, the system was redesigned as presented in the following section.

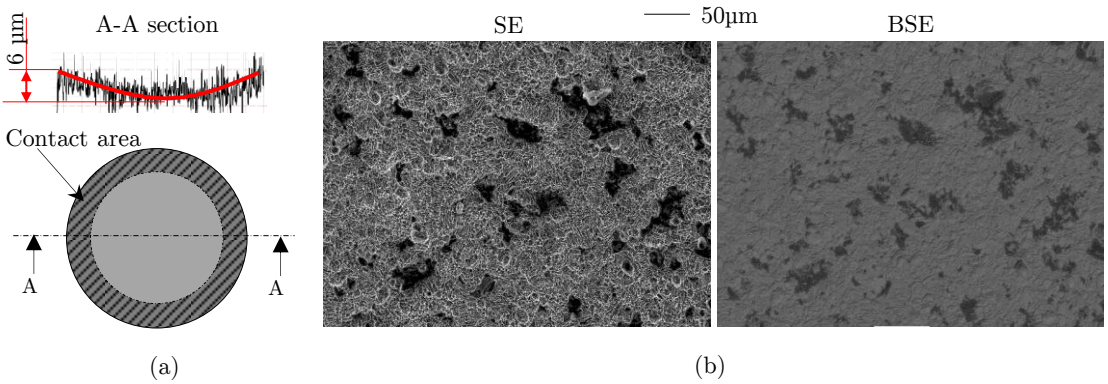

Figure 5.3: Problems detected in the tuning-up experiments. (a) curvature on the titanium discs preventing homogeneous contact along the whole surface; (b) secondary electron (SE) and back scattered electron (BSE) images of the tested sample after cleaning process; simile traces can be detected (dark areas).

Experimental set-up: final design and validation

Owing to the problems explained in the previous section, the modification device was redesigned in order to obtain the target modified surface. Due to the curvature detected on the titanium disc surfaces, it was not possible to obtain a homogeneous contact along the whole surface, since all the load was supported in the periphery of the discs, the centre being intact. Due to this problem, the second approach discarded the lateral movement and considered only the compressive forces. In order to avoid the periphery of the discs (higher than the centre part) a stainless steel punch with a diameter 0.5 mm smaller than the titanium disc was designed to apply the compressive force (see Figure 5.4 (a)). It was observed that the homogeneous contact was still difficult to obtain when using the rigid punch as a direct counterpart, since it generated few local contact areas. Therefore, the bone simile was cut in a cylindrical shape (the same diameter as the punch) and stick to the steel punch to provide a flexible support in order to facilitate the homogenisation of the contact.

Finally, in order to avoid the previously mentioned sample contamination when using the bone simile, a calibrated 20 µm thick stainless steel foil (VOGEL) was introduced between the simile and the titanium sample (see Figure 5.4 (b)). The horizontal movement was blocked by means of magnetic bases (see Figure 5.4 (c)).

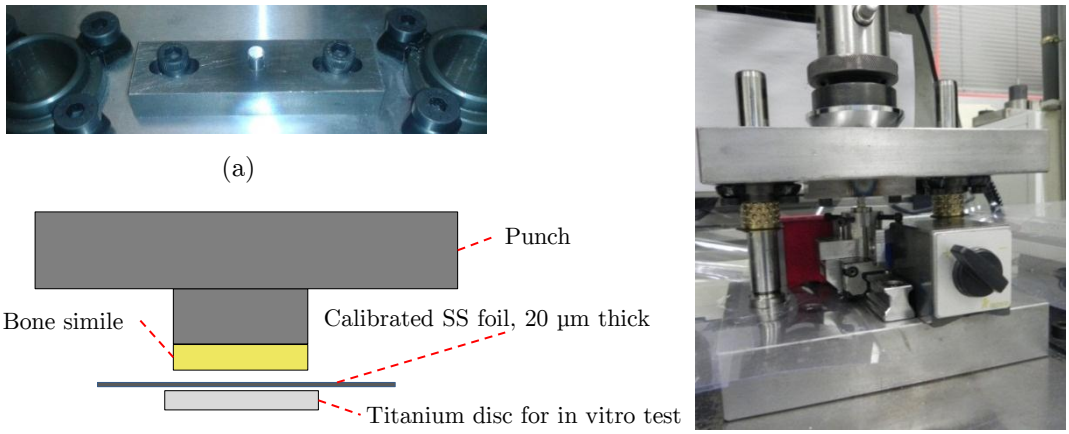

Figure 5.4: Modification device, the final design: (a) stainless steel punch; (b) configuration for the test. A bone simile was attached to the stainless steel punch and a calibrated stainless steel foil was introduced between the bone simile and the titanium disc; (c) the horizontal movement was blocked with two magnetic bases.

This experiment configuration allowed the set goals to be obtained. The modification was homogeneous along the whole surface (with homogeneously distributed contact points, see Figure 5.5 (a)), and the back scattered electron analysis showed a lack of compositional variation (lack of contrast, see Figure 5.5 (b)) revealing that the assayed titanium discs were free of contaminants.

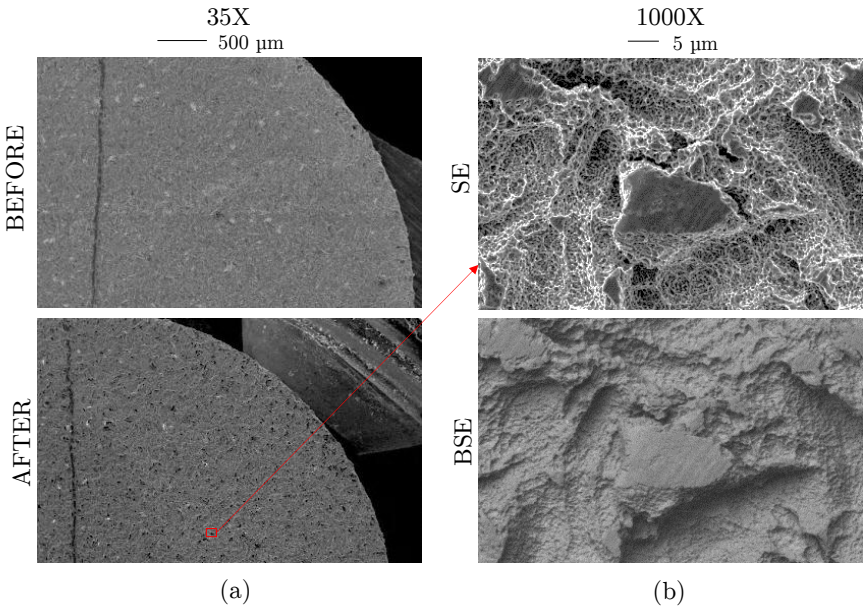

Figure 5.5: Preliminary test carried out using 1500 N compressive load on SB+AE surface. (a) SEM image of the surface before and after modification test (vertical line generated as reference); (b) secondary electron (SE) and back scattered electron (BSE) images of a modified area.

Tests at varying loads were conducted in order to select a modification level for the in vitro test. SB+AE treated samples were used for the tune-up, and loads of 500, 750, 1000, and 1500 N (corresponding theoretical pressures: 18, 26, 35, and 53 MPa) were tested. Four measurements were taken both before and after the tests on the same area for each sample (one for each load condition). The results of the topographical parameters normalized in reference to the origin surface (before) are shown in Figure 5.6.

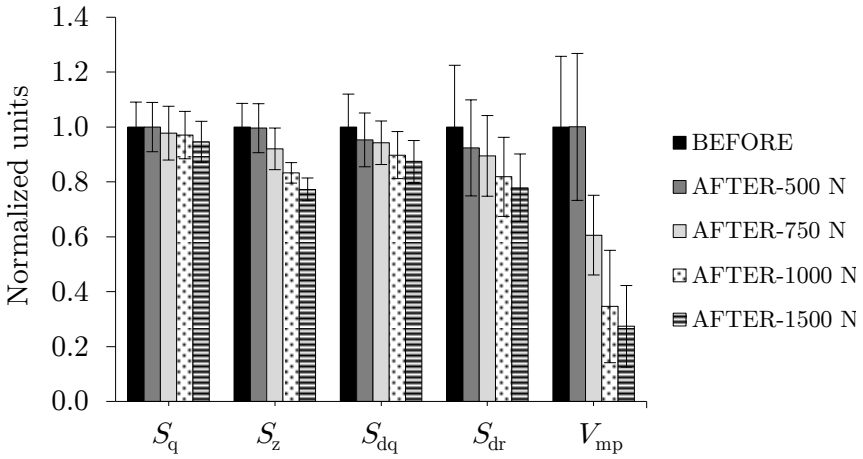

Figure 5.6: Results of the tune-up tests at 500 N, 750 N 1000 N and 1500 N compression loads. Normalised values in reference to the origin surface (before).

Height (S_q, S_z) and hybrid (S_{dq}, S_{dr}) parameters decreased uniformly as the load increased while the material peak volume parameter (V_{mp}) presented abrupt changes. The 500 N load generated slight modification, and the 1000 N load presented similar changes compared to the maximum load (1500 N).

Figure 5.7 (a)-(b) shows SEM images of the surfaces tested ad 750 N and 1500 N respectively. The surfaces tested at 1500 N presented a stronger modification observed as considerably more and larger flattened areas. The comparison between the modified areas obtained in the modification test (5.7 (c)) and the modified areas observed in commercially available implants after insertion test (Figure 5.7 (d)-(e)-(f)) demonstrated that although being a simplified simulation, the morphology of the plastic deformation generated during dental implant insertion was successfully reproduced.

.

Therefore, a load of 1500 N was selected for the in vitro samples modification. Final tests were carried out using a 5 KN load cell and applying 1500 N load at 1 mm/s rate. Bone simile and calibrated foil were substituted for each assay.

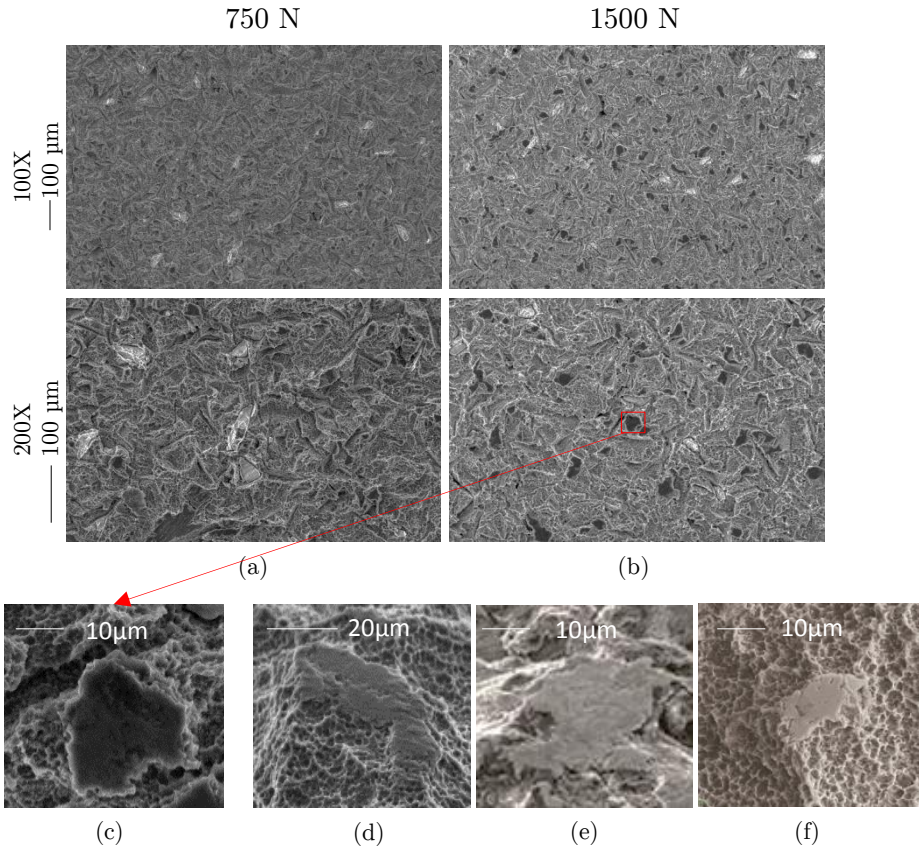

Figure 5.7: Analysis and validation of tested surfaces. SEM images of the SB+AE surfaces tested at 750 N (a) and 1500 N (b). Comparison of the morphology of the modified areas obtained in the test carried out at 1500 N (c) with the ones observed on post-inserted commercial sand blasted and acid etched dental implants: (d) BIOMET 3i (analysed in the previous chapter); (e) OsseoSpeed [Sen13]; (f) SLActive Bone Level [Sen13].

5.3.3. Surface analysis

Morphological and chemical analysis was carried out both prior and after the modification test through scanning electron microscopy (JEOL JSM 5600 LV) fitted with secondary electron (SE) and back scattered electron (BSE) probes, and with X-ray dispersive spectroscopy (EDX), at voltages of (15-20KV).

Five discs per group (see Table 5.1) were randomly selected for numerical characterization. All the discs were marked on one side for relocating purposes and the same area was acquired both prior and after the modification test at four different locations (see Figure 5.8). Topographical characterization was carried out following the configuration set in Chapter 3 (data acquisition and processing variables can be found in Tables 3.6 and 3.7 respectively). A total of 10 topographical parameters (the same as selected for the insertion test analysis, see section 4.4.3) were calculated on the primary surface.

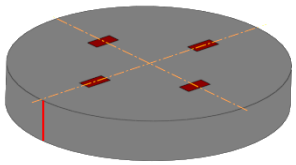

Figure 5.8: Schematic drawing illustrating the four evaluation areas and lateral mark for relocating purposes.

5.3.4. In Vitro test

Cell cultures

Osteosarcoma cells from the MG-63 cell line were used to assess the influence of different surfaces on cellular behaviour. MG-63 cells were maintained for routine cell culture in Dulbecco's modified Eagle's medium (DMEM)/F12 (Gibco-Invitrogen, Grand Island, NY, US) supplemented with 2 mM glutamine, 50 µg/ml gentamicin (Sigma-Aldrich, St Louis, MO, USA) and 5 % fetal bovine serum (FBS) (Biochrom AG, Leonorenstr, Berlin, Germany). Cultures were maintained in an incubator at 37°C in a humidified 5 % CO2 atmosphere.

Cell attachment

Cell attachment was evaluated on the six surface groups using six replicates per group (see Table 5.1). Discs were placed on a tissue culture of 96-well optical bottom black plates. MG-63 cells were seeded at a density of 20000 cells/cm^2 with complete medium. Polystyrene surfaces of the 96-well plates were used as a control. Cells were allowed to adhere for 4 hours. After this time, culture medium was discarded and wells were rinsed with phosphate-buffered saline (PBS). Then, the microplates with the adhered cells were frozen at -80°C until assayed. Attached cells were quantified using CYQUANT cell proliferation assay (Molecular Probes, Invitrogen, Grand Island, NY) following the manufacturer's instructions.

Cell proliferation

Discs with the same characteristics as used in the adhesion assay were included to study the effect of surface modification on cell proliferation (6 groups in six replicates). Cells cultured on tissue-culture polystyrene were also used as control. Osteosarcoma cells were seeded at a density of 5000 cells/cm^2 with complete medium for 72 h. Following this, culture medium was discarded, the wells were rinsed with PBS and the microplates with the cells were frozen at -80°C until assayed. CYQUANT assay was used following the manufacturer's instructions.

5.3.5. Statistical analysis

A statistical paired t-test was conducted to determine whether the topographical parameter variations between the unmodified and modified surfaces for each treatment were

statistically significant using a confidence interval (CI) of 95 %. In vitro test results were analysed through a statistical t-test (CI 95 %).

5.4. Results

5.4.1. Surface analysis

The SEM morphological characterization of the modified samples revealed flattened smooth areas in both the AE and SB+AE surfaces, while no perceptible changes were detected in the MCN surface (see Figure 5.9).

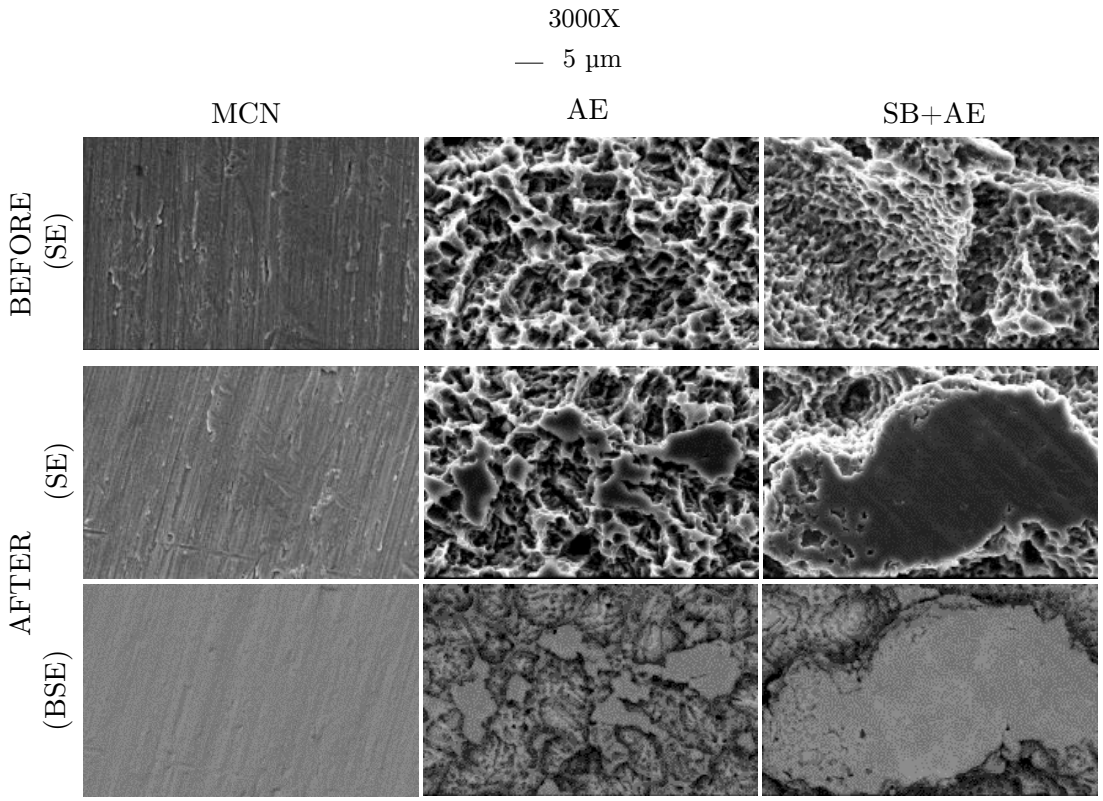

Figure 5.9: SEM secondary electron (SE) and back scattered electron (BSE) images of the (MCN), acid-etched (AE) and sand blasted and acid etched (SB+AE) surfaces prior (before) and after modification (after).

The distribution and area size of the flattened regions differed significantly between the two surfaces. AE treatment presented homogeneously dispersed small islands (∼5 µm), while the rougher SB+AE surface contained larger and more dispersed flattened areas (∼30 µm).

No compositional variation was detected at BSE images of the flattened areas. X-ray dispersive spectroscopy revealed Ti content on all surfaces. Aluminium content was found in the SB+AE surface due to the grit debris inserted during the gritting process that were not completely removed during the etching process. Nevertheless, no chemical variation between the surfaces prior and after modification was observed.

Confocal profilometry images of the same surface area both prior and after modification test are shown in Figure 5.10. As on SEM inspection, no changes could be discerned visually for the MCN surface and AE and SB+AE surfaces presented differently distributed flattened areas.

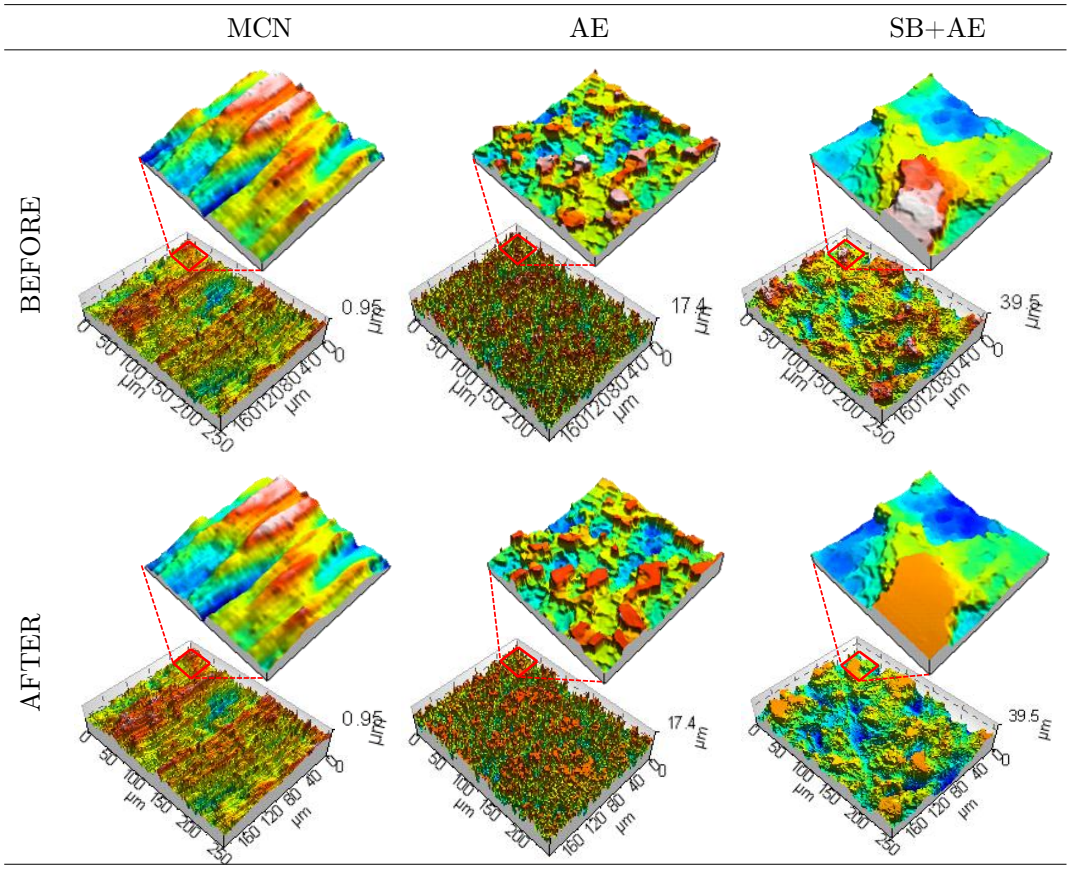

Figure 5.10: Confocal profilometry images of the machined (MCN), acid-etched (AE) and sand blasted and acid etched (SB+AE) surfaces prior (before) and after modification (after) acquired at the same location (zoom view of 40x40 μm^2).

The topographical parameters are summarized in Table 5.2 as a mean value $\pm$ standard deviation; covariance is shown in brackets and the variation after the modification is expressed as a percentage change with respect to the unmodified surface. Statistically significant values (paired t-test, $p<0.05$) are marked with an asterisk: $*$.

Table 5.2: Summary of the numerical characterization expressed as mean value ± standard deviation. Differences between measurements before and after modification are shown as percentage change with respect to the unmodified surface (% △). ∗ Statistically significant change (paired t-test, CI 95 %).

		MCN		AE		SB+AE	
		Value	Δ	Value	Δ	Value	Δ
S_q	Before	0.12±0.014(11 %)	-3 %	1.76±0.12(7 %)	-9 %*	5.82±0.64(11 %)	-2 %*
(µm)	After	0.12±0.016(14 %)		1.60±0.25(16 %)		5.69±0.57(10 %)	
S_{sk}	Before	0.26±0.45(173 %)	-11 %	-0.24±0.16(-67 %)	94 %*	-0.09±0.27(-306 %)	203 %*
	After	0.023±0.11(460 %)		-0.45±0.14(-31 %)		-0.27±0.18(68 %)	
S_{dq}	Before	0.06±0.006(10 %)	-8 %*	1.85±0.14(8 %)	-15 %*	2.63±0.32(12 %)	-8 %*
	After	0.056±0.006(11 %)		1.57±0.22(14 %)		2.41±0.24(10 %)	
S_{dr}	Before	0.18±0.03(20 %)	-14 %*	124±17.55(14 %)	-25 %*	232±55(23 %)	-15 %*
(%)	After	0.15±0.03(22 %)		92.7±19.45(21 %)		197.64±39(20 %)	
S_{al}	Before	19.12±7.91(41 %)	2 %	6.75±1.13(17 %)	3 %	16.29±2.85(18 %)	3 %*
(µm)	After	19.57±7.65(39 %)		6.95±1.00(15 %)		16.78±2.82(17 %)	
S_{pd}	Before	3693±424(12 %)	0.4 %	20748±3011(15 %)	-8 %	2369±307(13 %)	7 %
($1/mm^2$)	After	3678±735(20 %)		19088±2863(15 %)		2203±352(16 %)	
V_m	Before	0.548±0.096(18 %)	0.1 %	8.99±1.13(12 %)	-2 %	19.30±2.57(13 %)	-0.5 %
($\mu m^3/\mu m^2$)	After	0.549±0.14(25 %)		8.82±1.24(14 %)		19.19±2.42(13 %)	
V_{mp}	Before	0.0036±0.0014(40 %)	-5 %	0.033±0.004(12 %)	-76 %*	0.115±0.054(47 %)	-73 %*
($\mu m^3/\mu m^2$)	After	0.0034±0.0012(41 %)		0.008±0.002(19 %)		0.039±0.026(67 %)	
V_{mc}	Before	0.104±0.014(14 %)	-1 %	1.590±0.111(7 %)	-4 %	5.369±0.585(11 %)	2 %*
($\mu m^3/\mu m^2$)	After	0.103±0.015(15 %)		1.524±0.253(17 %)		5.487±0.594(11 %)	
V_{vv}	Before	0.014±0.001(11 %)	-1 %	0.215±0.017(8 %)	-7 %*	0.684±0.111(16 %)	-1 %
($\mu m^3/\mu m^2$)	After	0.013±0.001(12 %)		0.199±0.034(17 %)		0.677±0.102(15 %)	

In general (with the exception of S_{sk}, S_{al} and S_{pd}), unmodified surfaces showed increasing topographic parameter values following this order: MCN, AE, SB+AE.

The V_m and S_{pd} parameters presented non statistically significant variations after the test, which means that neither the material volume nor the peak density varied during the modification. Despite the MCN surface underwent no perceivable morphological change under qualitative examination, the quantitative data showed statistically significant decreases for the hybrid (S_{dq}, S_{dr}) parameters. This suggests that the MCN had undergone a smoothing process without considerably affecting the height. On the other hand, the modified AE and SB+AE surfaces showed more pronounced changes after the modification, most of them reaching statistical significance. Height (S_q, S_{sk}) and hybrid (S_{dq}, S_{dr}) parameters decreased significantly after the test. Conversely, the spatial parameter S_{al} increased, although the percentage change was significant only for the SB+AE treatment. Concerning functional parameters, the peak material volume underwent the largest variations, presenting a considerable decrease after the modification. The material core (V_{mc}) and void volume (V_{vv}) parameters presented small variations, which were significant only for SB+AE and AE respectively. The most affected parameters in decreasing order were height S_{sk}, volume V_{mp} and hybrid (S_{dr}, S_{dq}) parameters, although the large dispersion of the first one should be emphasised.

5.4.2. In Vitro test

As shown in Figure 5.11 (a), cell proliferation at 72 hours on unmodified surfaces-decreased as roughness increased. The differences between the rougher (AE, SB+AE) and the machined (MCN) surfaces were statistically significant, however no differences were encountered between the AE and SB+AE treatments. Concerning the effect of the surface modification on cell proliferation, no significant differences were observed between the modified and non-modified surfaces, except for the machined surface, in which a statistically significant decrease was found.

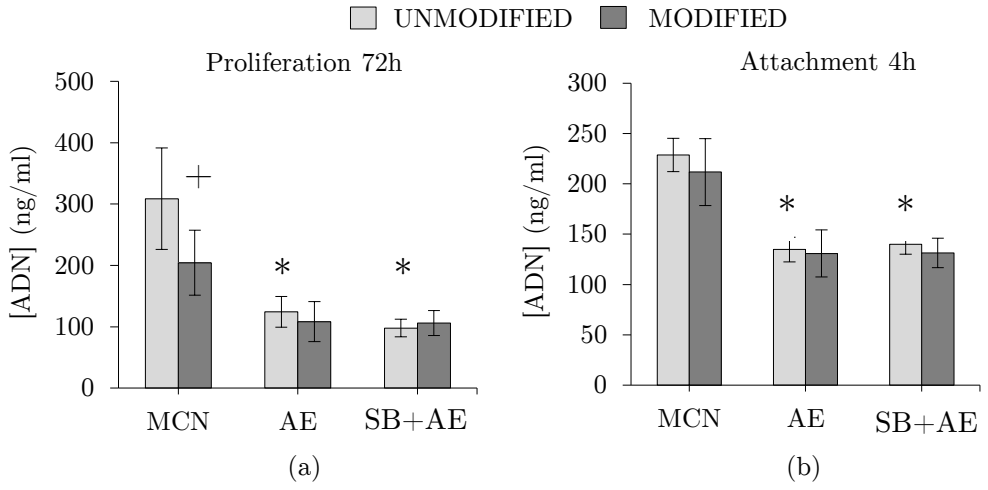

Figure 5.11: In Vitro test results for the unmodified and modified samples of machined (MCN), acid etched (AE) and sand blasted and acid etched (SB+AE) treatments. (a) proliferation assay, at 72 h; (b) attachment assay, at 4 h. $*$ Statistically different from MCN unmodified (t-test, $p < 0.05$). +Statistically different from the respective unmodified surface (t-test, $p < 0.05$).

Similarly, osteoblast attachment at 4 hours on unmodified surfaces varied significantly between the rougher (AE, SB+AE) surfaces and the machined (MCN) surface (Figure 5.11 (b)). The number of cells attached decreased with the increasing roughness. After comparison of the unmodified and the modified surfaces no statistical difference was found.

5.5. Discussion

The previous chapter demonstrated that the surface topography of dental implants is altered during surgical insertion. Plastic deformation and wear of surface was observed in the post-inserted dental implants.

Multitudinous variables are involved in the insertion process. Each implant manufacturer has its own implant design (macro-geometry), surface treatment and surgical procedure. Hence, each dental implant is subjected to different stress state during the insertion process. This makes it difficult to draw any general conclusions concerning the behaviour of different surface treatments when subjected to insertion forces. In this work a simple and scalable surface modification process has been developed in order to analyse the effects of insertion forces in different surface treatments, and to analyse the effect of these alterations in the cellular response. Although the first attempt was to reproduce both plastic deformation and wear phenomena observed on dental implants on disk-shaped samples, the final approach considered only the plastic deformation (compressive loads) due to the different difficulties encountered (discussed in section 5.3.2). However, although being a simplified simulation, the morphology of the plastic deformation generated during dental implant insertion was successfully reproduced.

The topographical alteration generated applying the same load varied from one treatment to another. SEM inspection revealed widespread small flattened areas for AE surface, while for AE+SB surface the flattened areas were larger and more dispersed. The modified areas could be ascribed to the plastic deformation of the most prominent peaks. These results agreed with the observations of post inserted acid etched (BT) and sand blasted and acid etched (BM) dental implants, discussed in Chapter 4. However, no differences were detected visually on the MCN surface after modification. It should be noted that although non alteration of the surface was perceptible in the SEM inspection for the MCN treatment, the S_{dr} and S_{dq} parameters presented statistically significant decrease after the test, which indicates that the surface had undergone a smoothing process without considerably affecting the height.

Due to the simplified simulated modification that considered only the compressive forces, no wear was encountered on the surfaces, as demonstrated by the absence of significant variation in the total material volume (V_{m}) after the test. Similarly, the peak density did not vary after the test, which means that the peak morphology was varied (as observed in the visual inspection) but not removed from the surface. The remaining topographical parameter variation trends were generally in accordance with those observed in post-inserted dental implants (analysed in Chapter 4).

Height parameters (S_{q}, S_{sk}) decreased after the insertion test. Although the large dispersion of the skewness parameter should be emphasised, it was observed that the height

distribution shifted towards a more negatively skewed shape after the modification, due to the breakdown of the most prominent peaks. The spatial parameter S_{al} increased in all cases, but the change was significant only for the SB+AE parameter, probably due to the wider morphology of the modified areas compared to the rest of the treatments.

Regarding the hybrid parameters (S_{dq}, S_{dr}), they demonstrated significant decreases for all surface treatments. However, they did not correlate with the modification degree. The MCN and SB+AE treatments presented the same variations although they underwent very different modification degrees.

Functional parameters separate peak (V_{mp}), core (V_{mc}) and valley (V_{vv}) features within the surface, allowing a more detailed analysis of the surfaces at different levels. As noted in the post inserted implants, the functional peak material volume (V_{mp}) was the most sensitive parameter presenting the most pronounced variations after modification. However, despite the different modification degrees observed in the SEM inspection for the AE and SB+AE surfaces, they presented similar V_{mp} variations.

Owing to the lack of correlations encountered, the field topographical parameter variation analysis appears to be unsuitable for ascertaining different modification behaviours. Due to the local nature of the modification, centred on the top site of the surface, it seems convenient to quantify the modified area separately in order to determine the percentage and distribution of the damaged area at each surface, which requires development of a modified surface separation technique (this issue will be addressed in the following chapter).

Concerning the in vitro results, the proliferation and attachment assays conducted at 72 hours and 4 hours respectively demonstrated that osteoblast-like cells were sensitive to variations in roughness. Regarding the influence of topographical modification generated during dental implant insertion, only a statistically significant decrease in cell proliferation on the machined surfaces could be detected. Hence, within the limits of the study, there was no consistent evidence of topographical modification effect on biological response in terms of proliferation and attachment.

The cell proliferation trend observed for the unmodified surfaces agrees with previously published results. To date, it can only be suggested that there is a decrease in proliferation as the roughness increases ([Ros03], [Ans00b]), which has been correlated with increased differentiation in osteoblast cultures ([Git11], [Ros03]). However, the decrease in proliferation encountered for the machined surface after modification is difficult to explain from the point of view of topographical variation. The general viewpoint says that the proliferation decreases when surface roughness is increased, but the modified surface (which was smoother than the unmodified one) presented a smaller amount of cells. This opens the possibility of other variables being introduced during the modification test affecting the cellular response, such for instance as changes in the oxide layer.

Regarding the cell attachment results, it was observed that the increase in roughness caused a decrease in the amount of cells attached to the surface, and non-statistically significant differences were observed for the modified surfaces when compared to their corresponding unmodified surface. A number of researchers have reported an enhancement in

the cell attachment as the roughness increases ([Dow10], [Nis07]]) while others have stated the opposite trend ([Git11], [Dav10]). Inconsistencies also emerge when speculating about reasonable explanations for roughness affecting cell attachment. Some authors hace suggested that the generation of multiple contacts is avoided due to the smaller area between cells and the rough area [Hor94]. Conversely, other authors [Die05] have suggested that the reduced number of focal adhesions does not alter the ability of cells to attach. There are many sources from where these contradictory results can originate. It is known that cell responses to titanium surface characteristics can vary with the origin of the cells (whether normal or transformed cell lines are used) as well as cell maturation states [Boy01]. There is little consistency in the published results and hence it is difficult to draw general conclusions from separate investigations about the role of the roughness on the cell attachment.

Despite the discrepancies encountered on in vitro studies, experimental studies on animal models have shown that implants with roughened surfaces had a better early anchorage in bone tissue and a higher percentage of BIC than implants with smooth machined surfaces ([AN08], [Yeo08], [Cho03], [Mar02], [Cor99], [Wen98], [Wen95b]). These results also have been demonstrated in human studies ([Gra07], [Sta03], [Iva01],[Kha01], [Coc99]), [Laz99]). Thus, as stated by Belem *et al.* [NJ10] it seems that more research is required in order to enhance understanding of how the surface treatments actually promotes fast osseointegration.

To the author's knowledge there has been no previous investigation into the influence of topographical modifications generated during dental implant insertion on cell behaviour. Fassina *et al.* [Fas07] investigated the effect of plastic deformation generated in a SB+AE surface through a punching process with biomimetic purposes. The resulting deformed holes had an upper diameter of 500 μm, lower diameter of 300 μm and depth of 170 μm. The in vitro test carried out using human SAOS-2 osteoblastic cells showed an increase in proliferation for the modified surface. However it must be taken into count that the modified surface used in the work concerned (generated for quite different purposes) is far from the modification analysed in the present work.

5.6. Conclusions

In this chapter the effect of dental implant modification on the cell response was analysed. To that end, a simple and scalable device was designed and fabricated to eject compressive forces reproducing the dental implant surface deformation generated during implant insertion on a disc surface. The main conclusions formed after the analysis and discussion of the results are:

- An experimental set-up was developed in order to reproduce the surface modification generated during implant insertion on a flat surface.

- Due to a curvature in the available samples, the modification experiments were carried out using compressive forces solely in order to obtain the required homogeneous

topographical alteration along the surface. However, the morphology of the plastic deformation generated during dental implant insertion was successfully reproduced.

- The damage generated when applying the same load varied from one treatment to another.
- The flattened areas encountered on AE and SB+AE surfaces were in close agreement with those observed in the post inserted implants.
- The MCN surface presented a non visually perceptible surface modification but the hybrid S_{dr} and S_{dq} parameters presented significant decreases after modification, which suggests that the surface had undergone a smoothing process without considerably affecting the height.
- The most affected parameters in decreasing order were: S_{sk}, V_{mp}, S_{dr} and S_{dq}, although the large dispersion of the first one should be emphasised.
- The field topographical parameter variations were unsuitable for ascertaining different modification behaviours.
- The proliferation and attachment assays conducted at 72 hours and 4 hours respectively demonstrated that MG-63 osteoblast-like cells were sensitive to variations in roughness.
- Cell proliferation and attachment decreased as the roughness increased.
- No statistically significant changes were encountered between the non-modified and modified surfaces, except for the proliferation of the machined surface.

The initial objectives of the chapter were to:

(I) To reproduce the modification generated during dental implant insertion homogeneously on the flat surface of a disc.

(II) To evaluate the in vitro response of modified and unmodified surfaces.

The first aim was partially satisfied, since only the plastic deformation could be reproduced on the disc samples due to a curvature existing in the available samples. As revealed in the last chapter, implant surface is damaged by wear and plastic deformation during surgical placement; therefore the surface damage was not fully represented, and this is the main limitation of the present study. The second aim (II) was fully satisfied through the proliferation and attachment study of modified and unmodified surfaces using MG-63 cell type. However, the assays were no sensitive to discern between surface treatments with markedly different topographies (AE, SB+AE) suggesting that the study was too limited. Therefore, more comprehensive in vitro studies analysing more biological markers and different cell types should be carried out in order to further analyse the effect of surface topography on cell response.

Within the limits of this study, the experimental data rejected the hypothesis that osteoblast attachment and proliferation could be significantly affected by the topographical modification generated during dental implant insertion.

CHAPTER 6

CORRELATION STUDY

"Nothing's random. Even if it looks that way, it's just because you don't know the causes."
Johnny Rich

The aim of this chapter is to find a correlation between the modification of dental implant surfaces (evaluated in the previous chapter) and 3D topographical parameters. To that end a method to separate the tested surfaces was first developed, which allowed quantification of the modified area percentages. Following this an analysis of wear predictive models and plasticity indexes was carried out, which detected the most relevant topographical characteristics for predicting wear and plastic deformation behaviour. Subsequently, the suitability of 3D topographical parameters to describe these characteristics was analysed. Because of the key role of some feature parameters, a deeper analysis was carried out, including a comparison between two commercial metrological software systems (SensoMap and SurfStand). Owing to the discrepancies encountered, and the lack of representativeness observed, a new parameter to characterize the relative surface mean peak curvature (named ΔS_{dq}) was developed. Finally, a correlation study between topography and surface modification was carried out, and a new integrated roughness parameter product was defined and successfully correlated with surface modification.

The work described in this chapter was carried out during a stay at the University of Huddersfield's Centre for Precision Technologies (CPT), under the supervision of Prof. Liam Blunt.

6.1. Introduction

The effect of surgical placement on dental implant surface topography was experimentally tested in Chapter 4, and modification in terms of wear and plastic deformation of surface peaks was demonstrated.

Due to the implications of the surface modification on implant performance and survival (discussed elsewhere, see section 2.5.3), the development of predictive models is of great importance, since such knowledge may well contribute to foster advancements in the design of better performing endosseous implants. However, owing to the variety and complexity of the degradation mechanisms, particularly in a biological environment, it may be unrealistic to search for an explicit and comprehensive wear and deformation model. A more profitable approach might be to select parameters whose correlation with surface modification may prove to be of more general applicability [LB03a].

In Chapter 5, the surface modification generated during surgical placement was reproduced on typical dental implant surface topographies by means of a controlled normal load, obtaining a plastic deformation similar to that observed on dental implant surfaces after insertion (analysed in Chapter 4). Taking into account that the only difference between the modified surfaces came from the variation in their surface treatment (all other variables were fixed: material, load and counterpart), it is reasonable to assume that there is a certain roughness characteristic capable of correlating with the observed changes in the surface. Thus, this study has attempted to relate the surface modification of dental implant surfaces to topographical properties.

To that end, a method to separate the tested surfaces into modified and non-modified regions was first developed. This was done in order to establish a quantitative ranking of surface modification in function of topography. Following this an analysis of wear predictive models and different plasticity indexes was carried out in order to detect those topographical characteristics pertinent for the prediction of wear and plastic deformation behaviour. Subsequently, the suitability of 3D topographical parameters to describe these characteristics was analysed. Due to the key role of some feature parameters, a deeper analysis was carried out, including a comparison between SensoMap and SurfStand commercial metrological software. Owing to the discrepancies encountered, and the lack of representativeness observed, a new parameter to characterize the relative surface mean peak curvature was developed (named ΔS_{dq}). Finally a correlation study was carried out, analysing topographical parameters individually, as well as the topographical combinations described in different plasticity indexes. In view of the lack of correlation encountered, a new integrated roughness parameter product was defined and successfully correlated with surface modification.

6.2. Objectives and hypothesis

The aim of this chapter was to find a correlation between the topographical modification of dental implant surfaces evaluated in the previous chapter and 3D topographical parameters. The specific aims of the chapter are listed below:

- To develop a method for separating the tested surfaces into modified and non-modified regions.
- To establish a correlation between the surface modification and 3D topographical parameters.

The following is the raised hypothesis:

- Topographic modification of dental implant surface generated during the insertion process can be correlated with 3D topographical parameters.

6.3. Samples

The analysed samples correspond to those tested in the previous chapter. In order to amplify the spectrum of roughness analysed, an additional acid etched treatment was added to the study. This treatment was tested following the same procedure as the rest of the samples, explained in section 5.3.2 of the previous chapter. The added etched surface (referred to as AE1) was less rough compared to the one analysed previously (so far referred to as AE, in this section named AE2). SEM images of the four surface treatments under study are depicted in Figure 6.1.

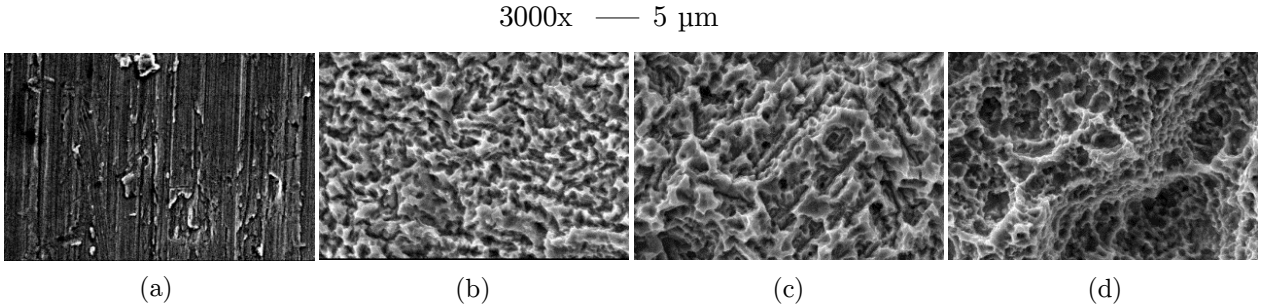

Figure 6.1: SEM images of the four surface treatments under study: (a) machined (MCN), (b) acid etched 1 (AE1), (c) acid etched 2 (AE2), and (d) sand blasted and acid etched (SB+AE).

The topographical analysis was based on five samples per treatment (four measurements each), analysed both before and after modification test (for more details, the reader is referred to section 5.3.3).

6.4. Quantification of modified area percentage

The objective was to quantify the percentage of the modified area in order to establish a quantitative ranking of the surface modification in function of the topography. This section describes the methodology developed for the data separation and presents the results obtained.

6.4.1. Development of data separation method

As can be seen in Figure 6.2, the modification of the surface turned the height distribution curve (histogram) to a negative skew (due to peak flattening), and this change was also reflected in the initial part of the Abbott-Firestone (or bearing area) curve. The modified regions could be easily approximated visually, but a routine for calculating the point of transition for data separation was required to ensure uniformity. Therefore, a method was sought to separate the surface data on modified and non-modified regions.

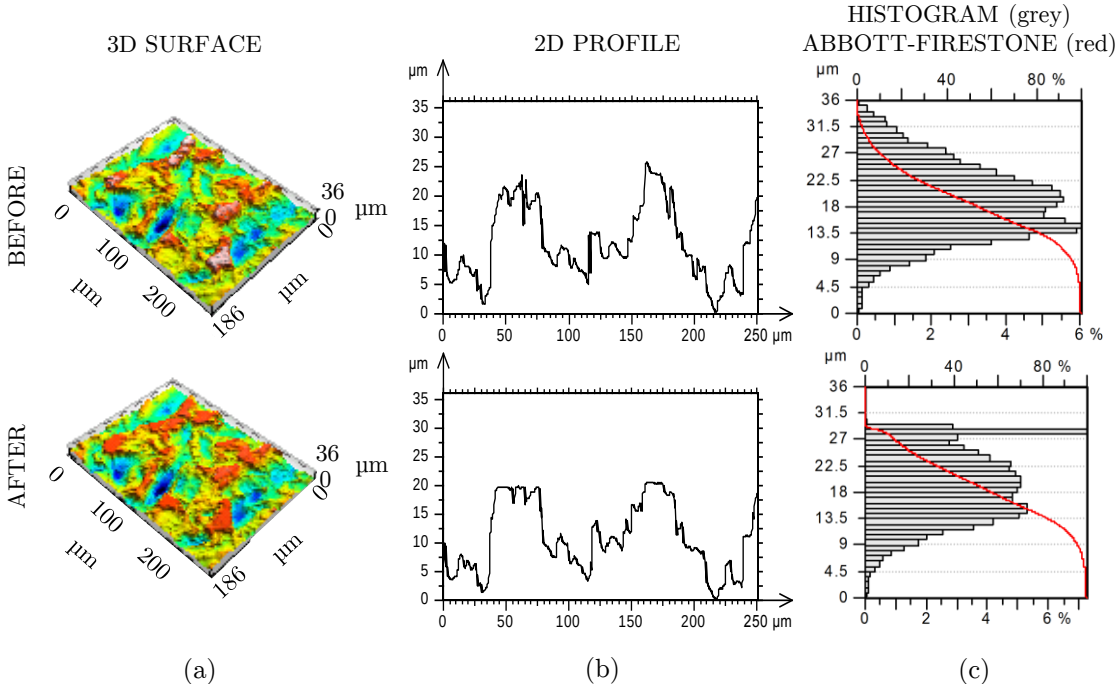

Figure 6.2: Comparative illustration of SB+AE surface both before and after modification. Smooth areas are observed after modification in 3D (a) and 2D (b) representations, which are reflected in the histogram and Abbot-Firestone curves (c).

The developed procedure is founded upon a standardized method for calculating the transition point between plateaus and valleys in stratified surfaces. This standard method, described in ISO 135651-3 [ISO98], is based on an analysis of the data from the Abbott-Firestone curve plotted on normal probability paper (the so called material probability curve). In this co-ordinate system the surface with Gaussian height distribution is described by a straight line, but the stratified surface resulting after two-process (*e.g.* plateau honed surface) is described by two straight lines of different slopes (see Figure 6.3 (a)). Similarly, the modified surfaces present different distributions (different slopes) corresponding to the modified and non-modified regions. As an example, Figure 6.3 (b) shows the material probability curves of the surfaces depicted in Figure 6.2 (a).

According to ISO 135651-3 standard [ISO98], the intersection between the two straight lines on the material probability curve corresponds to the threshold between the plateau and valley regions. Following the same rationale, this intersection corresponds to the sought-after transition point between the modified and non-modified regions of the tested surfaces.

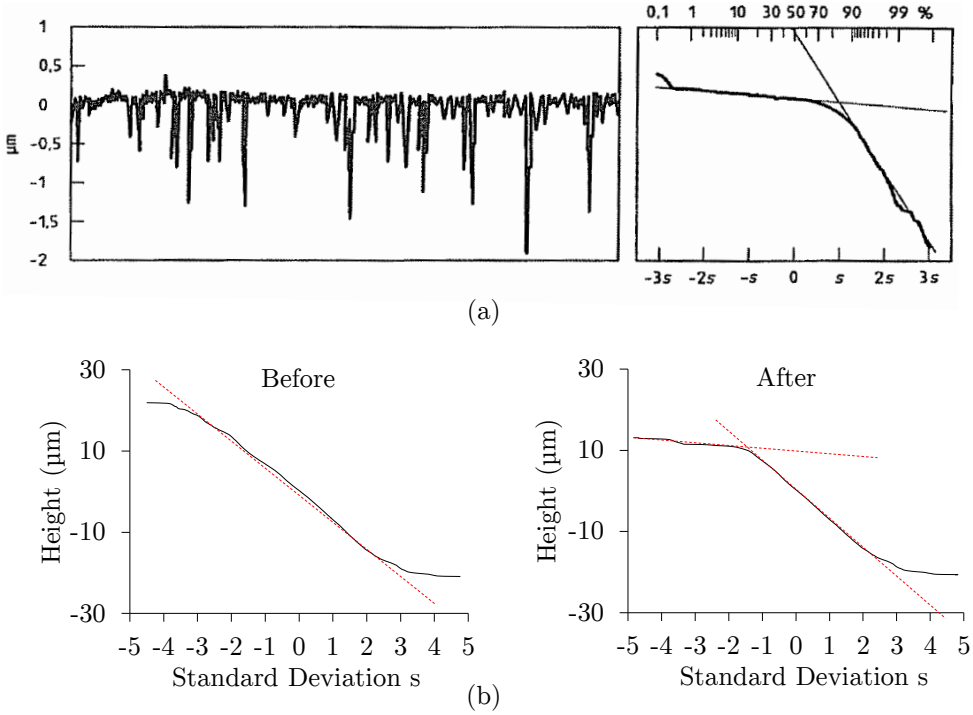

Figure 6.3: Examples of material probability curves. (a) illustration of 2D profile and material probability curve of a stratified surface [ISO98]; (b) material probability plots of the surfaces depicted in Figure 6.2 (a) both before and after modification test.

The previously mentioned standard specifies a method to obtain this transition point. However, imprecisions have been noticed by some authors ([Jak03] taken from [Gra11a]). Consequently Grabon *et al.* [Gra11b] proposed a different way of solving the problem, which has been adopted and adjusted for the present purpose due to its consistency.

According to the method proposed by Grabon *et al.*, the transition point is obtained by rotation of the material probability plot by α angle anticlockwise using the following equation:

$$\begin{aligned} x &= s \cdot \cos\alpha - height \cdot \sin\alpha \\ y &= s \cdot \sin\alpha - height \cdot \cos\alpha \end{aligned} \tag{6.1}$$

where α angle is the slope of the straight line passing by the first and the finishing point of the material probability curve (see Figure 6.4 (a)). The maximum point of the rotated diagram (C point, see Figure 6.4 (b)) corresponds to the intersection between the two straight lines of the material probability curve (see Figure 6.4 (a)), and is therefore treated as the transition point between the two regions (in this case, the modified and non-modified regions).

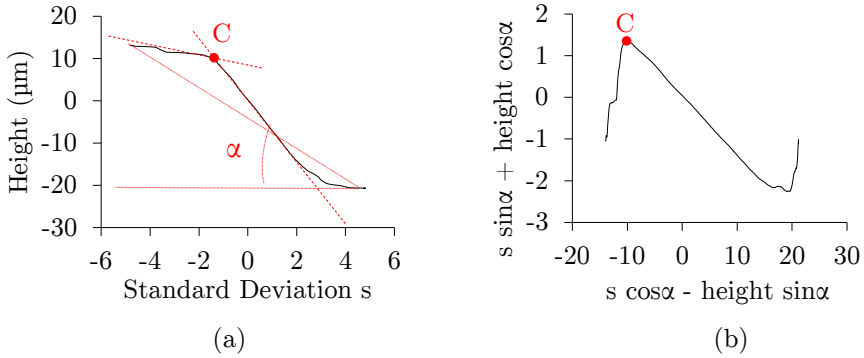

Figure 6.4: Determination of the transition point (C) through the rotation of the material probability curve. (a) calculation of the rotation angle (α); (b) material probability plot rotated by α angle (see Equation 6.1), where the maximum point (C) corresponds to the transition point between the modified and non-modified regions.

However, this method did not work properly for all the surface treatments under study, since the MCN and AE1 treatments presented non-Gaussian height distributions before the modification test. As an example, Figure 6.5 depicts the material probability curve and the rotated version of the AA1 treatment both before and after the modification test.

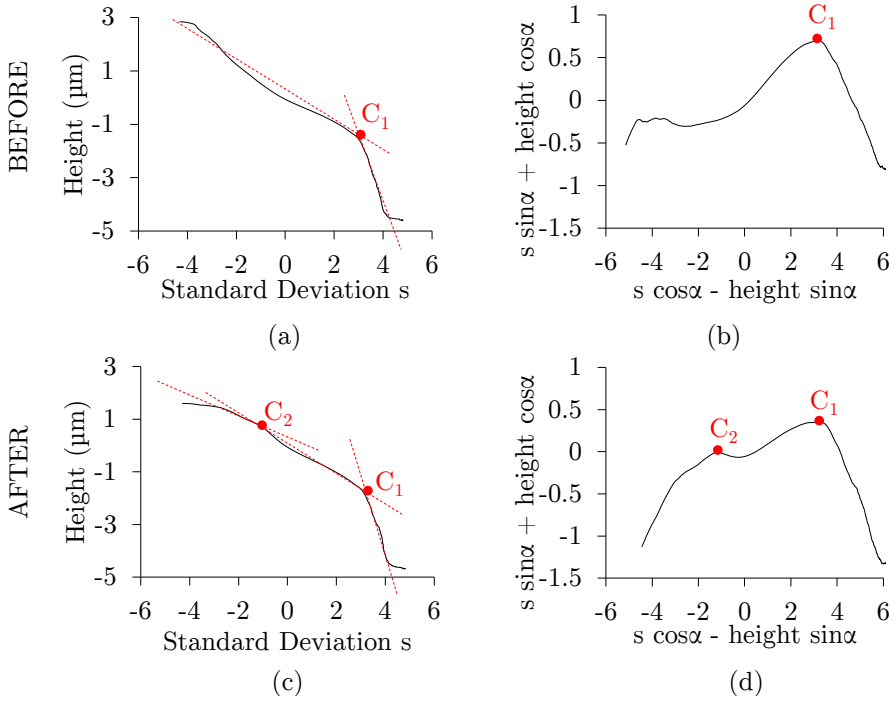

Figure 6.5: Material probability curve and its rotated version of AA1 treatment both before (a,b) and after (c,d) modification respectively.

As can be seen, the original surface is described by two straight lines of different slopes (see Figure 6.5 (a)), with the corresponding intersection (C1), which reflects the non-Gaussian nature of the surface height distribution. Consequently, the material probability curve of the surface after the modification test presents three straight lines (see Figure

6.5 (c)), with the corresponding intersections (C1, C2), which are reflected in the rotated curve (see Figure 6.5 (b)). In this case, the maximum point of the rotated curve (C1) does not correspond to the threshold between the modified and non-modified regions, but corresponds to the slope change of the original (non-modified) curve (see Figure 6.5 (a), (b)). As can be observed in Figure 6.5 (c), the C2 intersection, corresponding to the first peak of the rotated curve (Fig 6.5 (d)), would be the sought-after threshold.

In order to overcome this problem, the algorithm proposed by Grabon *et al.* was modified, and the maximum point of the rotated curve was determined considering only the first half of the rotated curve (which corresponds to 0-50 % of the material bearing percentage). This approach was successful for all cases, since all the modifications took place on the superior part of the surface (below 50 % of the bearing ratio).

Once the coordinates of the transition point in the rotated material probability curve were identified, the height was calculated through Equation 6.1, thus defining the height-axis transition point between the modified and non-modified regions. Further processing was carried out in the SensoMap software (previously used to calculate the 3D parameters). First of all the surface was cropped using the threshold already calculated, and thus separating the modified region (see Figure 6.6 (a)). Following this the cropped modified region was converted to binary data (see Figure 6.6 (b)), and finally the total modified area percentage and the quantity of modified regions (called islands) were calculated.

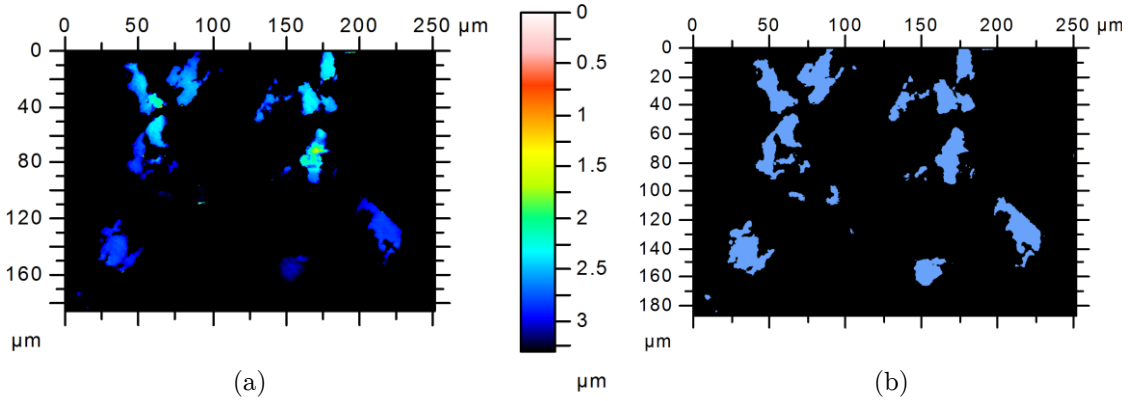

Figure 6.6: Steps for modified area percentage quantification: (a) crop the surface using the threshold calculated by the established method based on the material probability curve; (b) convert the cropped surface to binary data for modified area quantification.

The methodology described above is summarized in the following 5 points:

1. Plot the Abbott-Firestone (bearing area) curve (see Figure 6.2).

2. Plot the material probability curve (the Abbot-Firestone curve depicted in normal probabilistic axes), (see Figure 6.3 (b)).

3. Rotate the material probability curve by α angle, following Equation 6.1 (see Figure 6.4).

4. Find the maximum point of the rotated curve, considering only the first half of the data (corresponding to 0-50 % of the bearing ratio), and convert it into height following Equation 6.1.

5. Cut the surface (using the threshold calculated in the previous point), convert the modified region to binary data, and calculate the modified area percentage and quantity of islands (modified regions).

In order to analyse the sensitivity of the method, non-modified surfaces were introduced into the calculation. A maximum value of 1.5 % of modified area was obtained when analysing non-deformed surfaces. Consequently, a minimum threshold of 1.5 % of modified area was stabilised in order to ensure that a surface had been modified.

6.4.2. Results and discussion

Following the method described in the previous section, the modified area percentage and islands quantity of each treatment was quantified. The results depicted in Figure 6.7 (a) corresponds to the mean values and standard deviations calculated from five samples per treatment, with four measurements each (a total of 20 values per treatment).

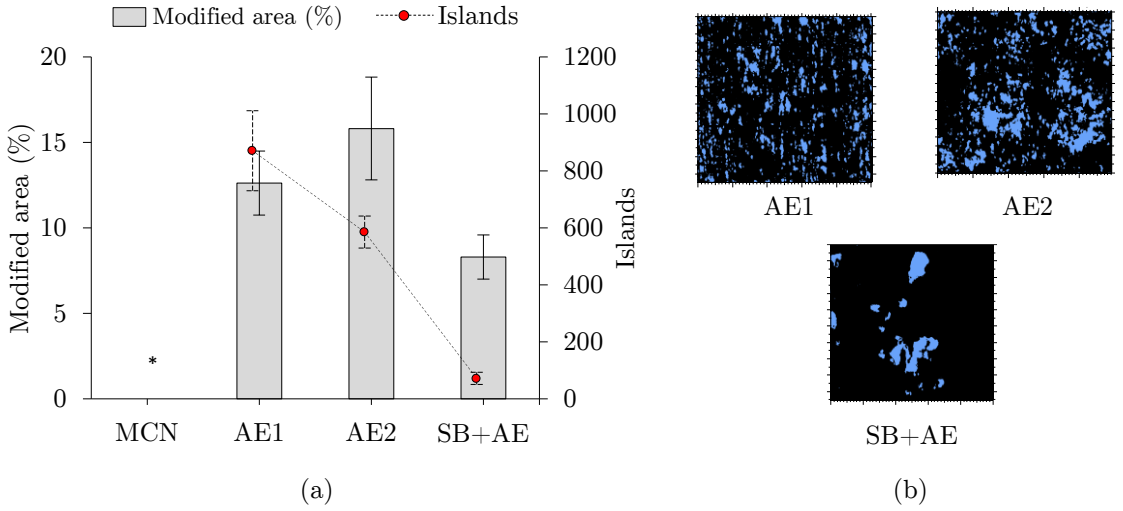

Figure 6.7: Characterization of the modified area. (a) mean values and standard deviations of the modified area percentages and islands quantities. *: Values below the established minimum threshold (1.5 %); (b) binary images of the modified regions.

The four treatments under study, although submitted to the same compressive load, presented differing modified area percentages (see Figure 6.7 (a)) and distributions (see Figure 6.7 (b)). The machined surface presented a mean modified value of 0.3 %, which fell well below the established minimum threshold (1.5 %). Therefore, it could be said that the MCN surface presented a modified area percentage of 0 %. This was expected

since the microscopic analysis carried out after the modification test revealed non visible changes in the surface (analysed in Chapter 5, see Figure 5.9). Furthermore, as can be seen in Figure 6.8, the Abbott Firestone curve (in red) of MCN treatment presented no perceptible changes after the test.

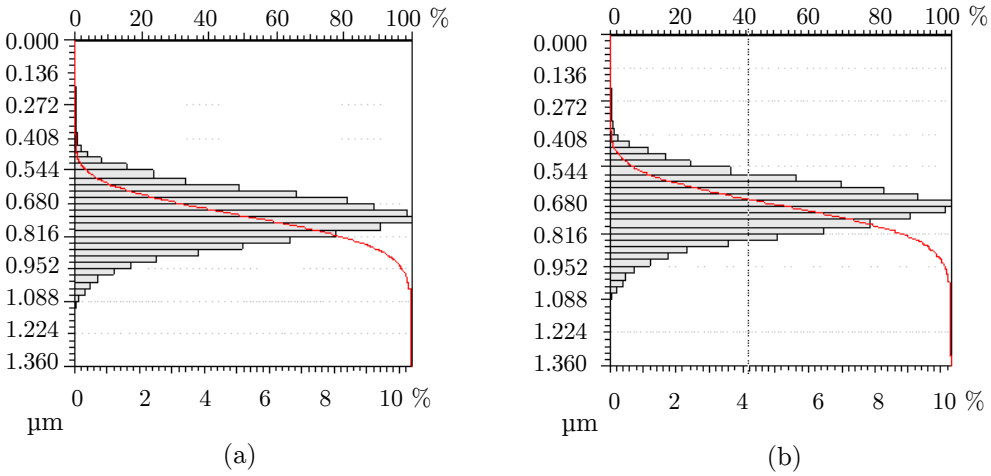

Figure 6.8: Height distribution histograms and Abbott-Firestone curves (in red) of the same MCN surface both before (a) and after (b) modification test.

Therefore the modified area percentage ranking from smaller to greater was: MCN, SB+AE, AE1, AE2. Moreover, the distribution of the modified areas differed considerably among different treatments (see Figure 6.7 (b)). The SB+AE surface presented few modified regions with a relatively large area, while the acid etched surfaces (AA1, AA2) presented smaller but more dispersed modified areas. This agrees with the observations on dental implant surfaces after the insertion test (analysed in Chapter 4). Regarding the MCN surface, the low roughness and the fact that no surface modification was detected suggest that the contact areas were numerous, distributing the force homogeneously, and avoiding perceptible surface modification. Although this is an hypothesis, it may be said that the ranking of the number of "islands" from smaller to greater was: SB+AE, AE2, AE1, MCN.

6.5. Wear predictive models and plasticity indexes

6.5.1. Wear models

Wear is a serious and costly problem for many areas in industry. Consequently, considerable efforts have been made to develop theories and deterministic models to describe and predict it.

However, as concluded by Sherringtong *et al.* [She00], the development of areal surface parameters for wear predictive roles appears to be limited. It is widely accepted that rough surfaces usually wear more quickly and have higher friction coefficients than smooth surfaces. However, the majority of models cannot account for differences in wear rates for

surfaces with differing topography operating in otherwise identical conditions. Meng and Ludema [Men95] identified nearly 200 "wear equations" involving an enormous spectrum of material properties and operating conditions. However, only 4 out of the 28 equations selected for further analysis considered topographically related parameters. In this respect, the mean peak curvature and the mean slope have been identified as wear-sensitive parameters [Tho72].

On the other hand, the plasticity index (a concept discussed in the following section) has been used by many workers to correlate wear behaviour. Greenwood and Williamson did not discuss the mechanism of wear particle generation, but they emphasised that wear is much more probable in touching plastic asperities than in elastic ones [Col07]. In line with this statement, a low plasticity index has been related to superior wear properties ([Tor10], [LB03a], [Ros01], [Che91]).

6.5.2. Plasticity index

Greenwood and Williamson [Gre66] defined a dimensionless parameter Ψ combining both material and topographical properties (the so called plasticity index), that could be used to determine whether contact would be elastic or plastic. In this model the rough surface is presumed to be covered with homogeneously distributed summits (density: η) spherical in shape (constant radius: β), presenting normal height distribution (standard deviation: σ). The plasticity index defined by Greenwood and Williamson is given by the following formula:

$$\Psi_{\mathrm{GW}} = \frac{E'}{H}\sqrt{\frac{\sigma}{\beta}} \tag{6.2}$$

where the E'/H ratio is known as material property ratio, E' corresponds to the so called reduced elastic modulus, derived from the material properties of the two contacting bodies as described in Equation 6.3 (where ν is the poisson coefficient and E is the elastic modulus) , and H is the hardness.

$$\frac{1}{E'} = \frac{1-\nu_1^2}{E_1} + \frac{1-\nu_2^2}{E_2} \tag{6.3}$$

Therefore, the approach developed above indicates that the contact behaviour of a surface can be described in terms of both material and topographical parameters. They were able to demonstrate that the highest percentiles of summits would deform at any load plastically for $\Psi_{\mathrm{GW}} > 1$, elastically when $\Psi_{\mathrm{GW}} < 0.6$, or would present different behaviours depending on the load in the following range $0.6 < \Psi_{\mathrm{GW}} < 1$.

A modified approach of the plasticity index was later suggested by Mikic [Mik74], which replaced peak parameters by the more readily obtainable mean profile slope (θ), see Equation 6.4.

$$\Psi_M = \frac{E'}{H}\theta \tag{6.4}$$

On the other hand, a rather different topographical parameter combination was introduced by Greenwood & Tripp [Gre70] (see Equation 6.5) to describe topographical characteristics on a formulation to calculate the contact pressure of two nominally flat rough surfaces. This dimensionless product of summit properties (η: density, β: curvature radius, and σ: deviation of the height distribution), has been successfully correlated with wear [LB03b].

$$\eta \cdot \beta \cdot \sigma \tag{6.5}$$

6.5.3. Characterization of the necessary input data

The above mentioned plasticity indexes and topographic parameter combination will be analysed as potential candidates to correlate with surface modification. However, the characterization of the necessary topographical input data is not straightforward and has been controversial. This section therefore discusses the different calculating and approximating methods to describe the surface characteristics considered important for plasticity behaviour prediction, namely: the surface asperity radius (β), density (η), and height distribution (σ) (see Equation 6.2 and 6.5), and the surface mean slope θ (see Equation 6.4).

The mean surface slope required for Mikic's plasticity index (Equation 6.4) is usually represented by the 3D topographical parameter S_{dq} (root mean square slope) [LB03b]. However, there is no standard method to characterize the remaining characteristics (σ, β, η), and huge differences are encountered in the published data.

Tomanik *et al.* [Tom03] analysed different reports on piston rings analysis, in which large variations were observed. The deviation of asperity heights (σ) ranged from 0.12-1 µm, the curvature radius (β) varied considerably (66-5000 µm), and the characterized asperity density (η) also differed significantly ($1{\cdot}10^9$-$3.9{\cdot}10^9$ $\frac{1}{m^2}$). It is to be presumed that the surfaces analysed on those works may be different, although those differences appear to be too large taking into account that they are surfaces with the same functionality.

Regarding the possible reasons for those discrepancies, it should be remembered that different methods are available to evaluate the mentioned asperity properties (σ, β, η). The discussion here is limited to the three most common methods.

The first method relies on determining the spectral moments (m0, m2, m4, see Equations 6.6, 6.7, 6.8) from a single arbitrary cross-section [Gre13]:

$$m_0 = \mathrm{AVG}\left[(z(x))^2\right] \tag{6.6}$$

$$m_2 = \mathrm{AVG}\left[\left(\frac{\mathrm{d}z(x)}{\mathrm{d}x}\right)^2\right] \tag{6.7}$$

$$m_4 = \mathrm{AVG}\left[\left(\frac{\mathrm{d}^2 z(x)}{\mathrm{d}x^2}\right)^2\right] \tag{6.8}$$

where AVG represents the average value, and z(x) is the surface profile of an arbitrary cross section (trace).

Nayak and McCool [McC87] demonstrated that topographical parameters describing surface asperities (σ, β, η) may be computed or approximated in terms of these quantities (see Equations 6.9, 6.10 and 6.11):

$$\sigma = \left(1 - \frac{0.8968}{\alpha}\right)^{\frac{1}{2}} m_0^{\frac{1}{2}} \tag{6.9}$$

$$\beta = 0.375 \left(\frac{\pi}{m_4}\right)^{\frac{1}{2}} \tag{6.10}$$

$$\eta = \frac{\left(\frac{m_4}{m_2}\right)}{6\pi\sqrt{3}} \tag{6.11}$$

where α is the so-called bandwidth parameter:

$$\alpha = \frac{(m_0)(m_4)}{(m_2^2)} \tag{6.12}$$

Although this approach is extensively used (see for instance [Pag10], [Lee10], [Lee07]), the values of σ, β and η for different arbitrary cross-sections may vary considerably [McC86]. That is why the second approach relies on the use of average values of the spectral moments (obtained from a finite number of cross sections of the 3D surface) to calculate the topographical parameters, obtaining more reliable parameters (some examples in [Dic11], [Jac11], [Rae07]). On the other hand, the third method of finding the topographical parameters mentioned is based on determining the asperities of the surface through the summit identification scheme. This approach (discussed in the following section) identifies the summits as local maxima, and parameters are calculated directly from these summits, thus not relying upon statistical methods.

Regarding the suitability of each method mentioned, different comparative studies have been carried out. The two methods based on the spectral moments have some practical difficulties, since the calculation of m2 and m4 involves the approximation of derivatives. Tomanik *et al.* [Tom03] analysed three different methods for calculating the first and second derivative, namely: (i) simple derivation, (ii) three point derivation and (iii) finite central differences. The results showed great variation between one method and another, and it was concluded that it would be unreliable to estimate the summits radius (β) and density (η) with the spectral moments. Similarly, Pawar *et al.* [Paw13] analysed the differences obtained when using approaches based on spectral moments and the summit identification scheme. They found that parameters vary significantly based on the method used and concluded that the summit identification scheme is perhaps the most reliable approach.

It can therefore be seen that the determination of the necessary input parameters for the analysed plasticity indexes and parameter combination is not straightforward. As mentioned at the beginning of this section, the surface slope (θ) defined in Mikic's formulation (Equation 6.4) will be described through the root mean square slope of the surface (S_{dq}). Regarding the height distribution of asperity heights (σ), this parameter is currently not provided by commercial metrological software. However, the parameter is usually replaced by the more readily obtainable height distribution of the whole surface (S_{q}), or profile (R_{q}) ([LB03b], [Ros01], [Arc97]). The assumption that asperity height deviation is equal to the surface deviation (σ=S_{q}) was analysed by Tomanik *et al.* [Tom03], and they found a reasonably good correlation (0.88) between the two parameters in a relatively large range of roughness values. Therefore, in this work the surface deviation S_{q} will be used to describe the asperity height distribution (σ). As far as the asperity density (η) and radius (β) calculation are concerned, the summit identification scheme has been pointed out as the most reliable approach. Thus, the following section will analyse the suitability of currently available 3D feature parameters (which are based on the summit identification approach) to describe these characteristics.

6.6. Feature parameters

Unlike field parameters, in which all the points on the surface are considered in the calculation, feature parameters take into account only identified features on the surface.

Feature characterization is defined in ISO 25178-2 [ISO12] through a toolbox of pattern recognition techniques that can be used to characterize specific features on a scaled-limited surface in five steps: (i) selection of the type of texture feature, (ii) segmentation, (iii) determination of the significant features, (iv) selection of feature attributes, and (v) quantification of feature attribute statistics.

Feature parameters have the added advantage that only the significant features are considered, since the tiny and insignificant motifs are eliminated based on the Wolf Pruning principle. Wolf's pruning method consists of finding the peak or pit with the smallest height difference and combining it with the adjacent saddle point in the change tree until a previously defined threshold[1] is reached ([ISO12], [Sco04]). Figure 6.9 shows two of the surfaces under analysis both before and after the pruning process. It can be seen that before pruning the surface is over-segmented into a large number of insignificant tiny features. By analysing surface peaks by eye it can be determined that after pruning only the significant peaks are considered.

[1]Standardized value: 5 % of S_{z}, *i.e.*: 5 % of the peak-to valley distance [ISO12].

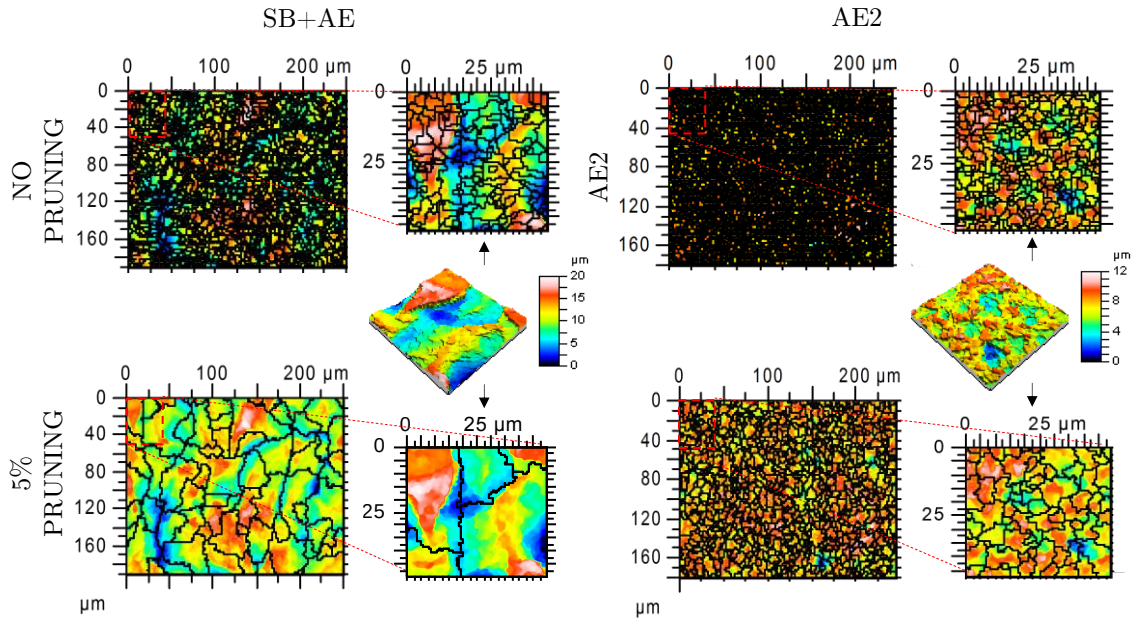

Figure 6.9: Analysis of the pruning effect (5 % of S_z) on two of the surface treatments under study: SB+AE, AE2.

A full description of the feature determination process can be found in the literature ([Bla13], [Sco03], [ISO12]). The following is an analysis of the feature parameters (S_{pd}, S_{pc}) and their respective ancestors (S_{ds}, S_{sc}) as potential candidates to describe the asperity density η and radius β.

The peak density feature parameter (S_{pd}) is calculated by dividing the number of peaks by the unit area, and is given in units of [1/mm^2]. On the other hand, the S_{pc} parameter corresponds to the arithmetic mean curvature of significant peaks (which is the reciprocal of the peak radius, *i.e.*, $S_{pc} = 1/\beta$) and is given in [1/µm]. These two parameters evolved from two ancestors defined in Birmingham 14 parameters [Sto93c], the summit density (S_{ds}) and summit curvature (S_{sc}) respectively, which are calculated based on the 8-nearest neighbour method [Sto00d]. The main difference between the old and new parameters is that for feature parameters (S_{pd}, S_{pc}) only significant peaks are taken into account, due to the pruning of the change tree [Bla13].

Feature parameters (S_{pd}, S_{pc}) and their corresponding conventional versions (S_{ds}, S_{sc}) were calculated through two different commercial metrological software systems for their analysis and comparison:

- SensoMap Turbo 5.0, developed by Digital Surf (software used for the rest of analysis in the present study).
- SurfStand, developed by the University of Huddersfield (pioneering the use of pattern analysis to define surface features).

6.6.1. Results and discussion

The results of the peak density and curvature parameters calculated with both software systems are shown in Table 6.1 and Figure 6.10.

Table 6.1: Results of the peak density (S_{pd}, S_{ds}) and curvature (S_{pc}, S_{sc}) parameters calculated through SensoMap (SM) and SurfStand (SS) software presented as mean value and covariance (in brackets). Differences between the two software systems (Δ) are presented as percentage change with respect to SensoMap results.

		MCN		AE1		AE2		SB+AE	
		Value (CV)	Δ	Value (CV)	Δ	Value (CV)	Δ	Value (CV)	Δ
S_{pd}	SM	3692 (11 %)	6 %	34805 (13 %)	-28 %	20748 (14 %)	-31 %	2369 (13 %)	-27 %
($1/mm^2$)	SS	3906 (26 %)		25213 (17 %)		14349 (14 %)		1862 (21 %)	
S_{ds}	SM	116296 (12 %)	-34 %	192145 (8 %)	-24 %	238575 (5 %)	-30 %	162216 (14 %)	-31 %
($1/mm^2$)	SS	76549 (13 %)		146100 (11 %)		167065 (6 %)		111685 (15 %)	
S_{pc}	SM	0.34 (41 %)	-33 %	4.82 (23 %)	-86 %	19.60 (24 %)	-95 %	28.85 (39 %)	-97 %
($1/\mu m$)	SS	0.22 (16 %)		0.69 (37 %)		0.93 (11 %)		0.93 (77 %)	
S_{sc}	SM	0.12 (17 %)	5 %	2.95 (21 %)	15 %	8.87 (20 %)	16 %	9.91 (18 %)	23 %
($1/\mu m$)	SS	0.13 (18 %)		3.43 (22 %)		10.3 (20 %)		12.17 (17 %)	

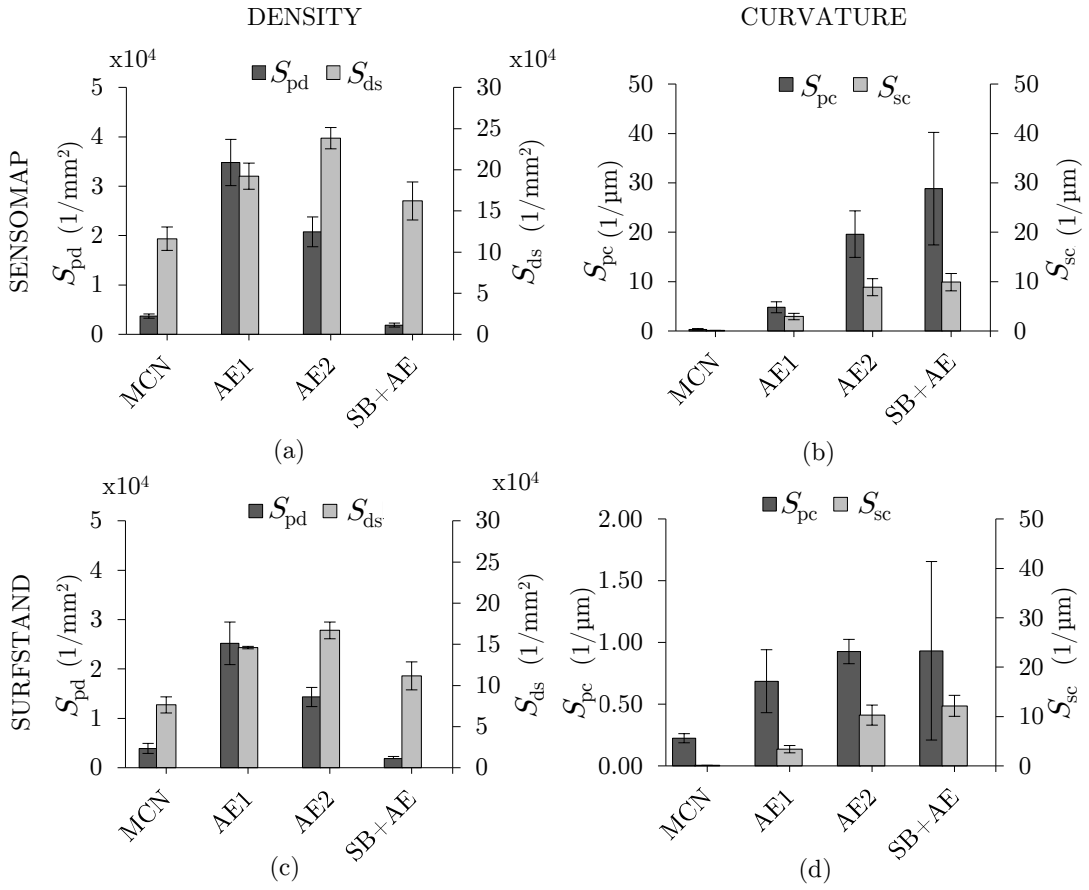

Figure 6.10: Comparison between parameters describing the peak density (S_{ds}, S_{pd}) and curvature (S_{sc}, S_{pc}) calculated through SensoMap and SurfStand software systems for the four surface treatments under study. The error bars represent the standard deviation of the mean.

Both software systems presented the same trends for the peak density parameters (S_{pd} and S_{ds}, see Figure 6.10 (a)-(c)), but the SurfStand values were in general around 30 % smaller than those obtained by SensoMap. However, the following applies to the results obtained by both software. As expected, the feature parameter S_{pd} presented markedly smaller values compared to its old version S_{ds}, due to the discrimination through Wolf's pruning method. In addition, it should be noted that the rankings of summit density values in decreasing order varied: AE2, AE1, SB+AE, MCN (for S_{ds}), and AE1, AE2, MCN, SB+AE (for S_{pd}).

As far as curvature S_{pc} parameter is concerned, major discrepancies were observed between the software systems. The results obtained by SurfStand software overall were two orders of magnitude smaller, and the trends between software also differed. Conversely, S_{sc} parameter presented similar trends, although SurfStand values were in general around 20 % higher compared to the SensoMap results (see Figure 6.10 (b)-(d)).

Due to the over-segmentation in which the S_{sc} calculus is based (8-nearest neighbour method without further discrimination), this parameter was expected to lead to greater curvature values (sharper peaks) when compared to its analogous S_{pc} (which considers only significant peaks, see Figure 6.11). Unlike the SensoMap results, the SurfStand values were consistent with the expected trend ($S_{sc} > S_{pc}$).

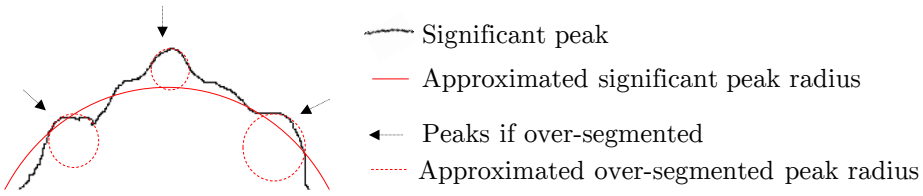

Figure 6.11: Illustrative representation of the different peak radius of significant and over-segmented peaks.

As mentioned previously, S_{pc} parameter trends differed from one software system to another. The SensoMap results presented a clearly increasing trend, while the trend was not that clear for the SurfStand results (see Figure 6.10 (b)-(d)), since AE2 and SB+AE treatments presented identical mean values (although the high deviation of the last one should be remarked upon). Based on a visual inspection of the surfaces (see Figure 6.12), it can be clearly seen that the SB+AE treatment generates less sharp peaks compared to etched surfaces, and should therefore present a smaller curvature value.

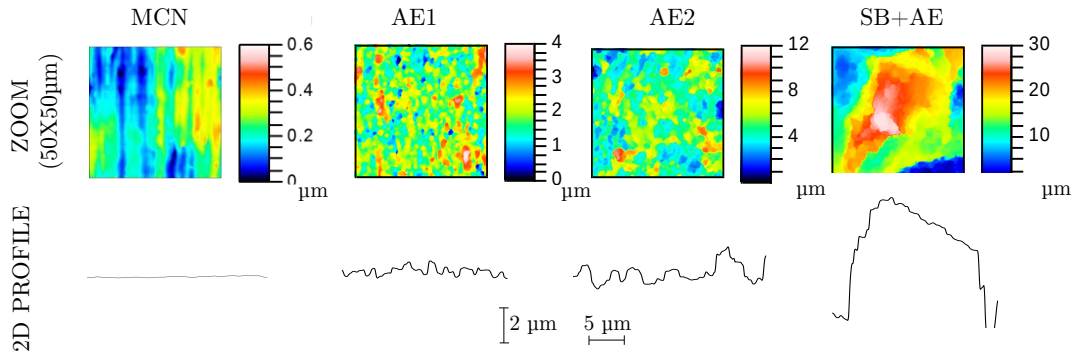

Figure 6.12: Representative zoom images of the four surface treatments under study and corresponding 2D profiles. NOTE: profiles are depicted at the same scale for comparison purposes.

It follows from these considerations that the peak curvature parameter S_{pc} calculated through the SensoMap software was not representative of the visually observed surface characteristics (since the SB+AE treatment presented the greatest S_{pc} value). On the other hand, the results obtained by SurfStand were more consistent. However, the deviation obtained for the SB+AE surface was extremely high (covariance value of 97 %), and the curvature between AE2 and SB+AE could not be discerned. In accordance with the present results, the instability of the S_{pc} parameter had been previously reported by Wang *et al.* [Wan11], and was attributed to the overestimation of the noise peak points.

Regarding the source of the high discrepancy concerning S_{pc} parameter values obtained by different software, it should be emphasised that the method by which the curvature should be calculated (once the surface is segmented) is not specified in the ISO 25178 standard [ISO12]. Its ancestor (S_{sc}) is not strictly defined in the standard, although it was established earlier in the research which contributed to ISO 25178-2 [Sto93d] as follows (Equation 6.13):

$$S_{sc} = -\frac{1}{2}\frac{1}{n}\left(\sum_{k=1}^{n}\frac{\partial\eta^2(x,y)}{\partial x^2} + \frac{\partial\eta^2(x,y)}{\partial y^2}\right) \tag{6.13}$$

There are however different ways to calculate the numerical form of the arithmetic peak curvature. The simplest way is to calculate the arithmetic mean summit curvature with three data points in each direction while other approaches take into account up to seven data points in each direction [Don94]. In this respect, SensoMap software does not provide information regarding the curvature determination method, while the SurfStand software carries out an individual fitting of each significant peak before curvature calculation. It is to be presumed that the method used to estimate the curvature may affect considerably the obtained value, since actual surfaces are not perfect spheres, and this was likely to have been the source of the discrepancies encountered (see Figure 6.13).

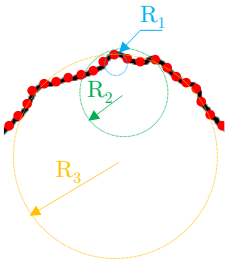

Curvature calculating method based on	Normalised radius	Normalised curvature
Three data points	R_1=1	S_{pc}=1
Seven data points	R_2=6	S_{pc}=0.16
Whole peak	R_3=13	S_{pc}=0.076

Figure 6.13: Illustrative representation of the effect of the curvature calculating method on the peak radius and curvature estimation.

6.6.2. Conclusion

To summarize, some differences between SensoMap and SurfStand software results were encountered. For the density parameters (S_{ds}, S_{pd}), the SurfStand values were in general around 30 % larger, though the trends were consistent. Regarding the suitability for surface peak density description, it was observed that the feature parameter S_{pd} represents only the significant peaks and therefore will be used for subsequent analysis. As far as parameters describing the mean peak curvature are concerned, the S_{sc} parameter presented consistent trends between software, but SurfStand values were in general around 20 % larger. Conversely, large discrepancies were observed for the curvature S_{pc} parameter, where the SurfStand results were in general two orders of magnitude smaller compared to those obtained by SensoMap. Visual inspection demonstrated that the curvature parameter provided by the SensoMap software did not represent the surface properties. On the other hand, the results obtained by SurfStand, although more consistent, presented high variability for the SB+AE surface, and was therefore not useful for the present study.

In the light of this situation, and due to the important role of the curvature on the contact phenomena, an alternative novel method to characterize mean surface peak curvature was developed, and is presented in the next section.

6.7. Curvature determination

A novel method has been developed to yield a representative parameter of mean peak curvature based on the root mean square slope (S_{dq}). The rationale behind the approach is based on the fact that the mean slope of the surface in function of height changes more rapidly in surfaces with sharp peaks compared to those with rounded peaks (see Figure 6.14).

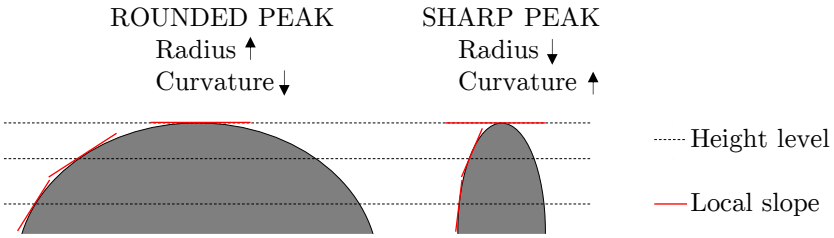

Figure 6.14: Illustrative representation of the evolution of the local slope in function of height for a rounded and a sharp peak.

6.7.1. S_{dq} evolution in function of truncation height

In order to obtain the evolution of the root mean square slope of the surface (S_{dq}) in function of height, an iterative process was programmed in Matlab® R2013a, where the primary surface was truncated at different heights and the S_{dq} value of the remaining surface was calculated for each truncation level. As shown in Figure 6.15 the process starts from the highest point on the surface (h_{tr}=0) and the truncation height is augmented progressively by a constant step size ($step_{tr}$) until completion of the total surface height (h_{tr}=S_z), (the effect and selection of the truncation step size ($step_{tr}$) is discussed further on). This way, an evolution curve of the S_{dq} in function of truncation height (h_{tr}) is obtained, which presents an "S" shape.

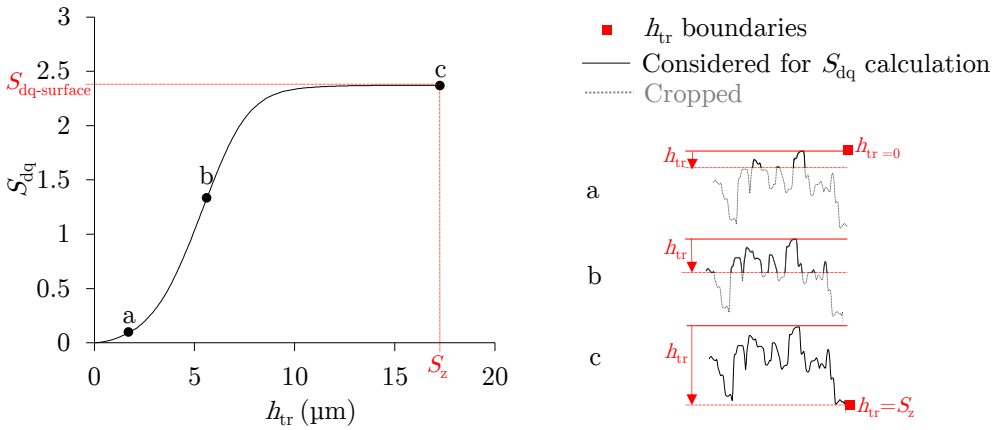

Figure 6.15: Calculation of the evolution of S_{dq} in function of the truncation height (h_{tr}). Increasing truncation levels are applied and the S_{dq} value is calculated at each remaining upper surface.

To demonstrate the relationship between the evolution of the surface mean slope (S_{dq}) in function of truncation height (h_{tr}) and the mean peak curvature, a series of surfaces of decreasing peak curvatures were generated through filtering. Figure 6.16 shows the S_{dq} evolution curve of an acid etched (AE1) primary (SF) and waviness (LF) surface of two different cut-off values (which possess lower mean curvatures respectively to the primary surface). It can be clearly seen that the growing rate of the curve (the slope of the lineal part, named ΔS_{dq}) decreases as the curvature decreases. Therefore, the ΔS_{dq} parameter can be used to characterize the mean peak curvature of a surface in relative terms (the larger the slope, the greater the curvature). The following section describes the methodology used to calculate this slope (ΔS_{dq}) in a reproducible way.

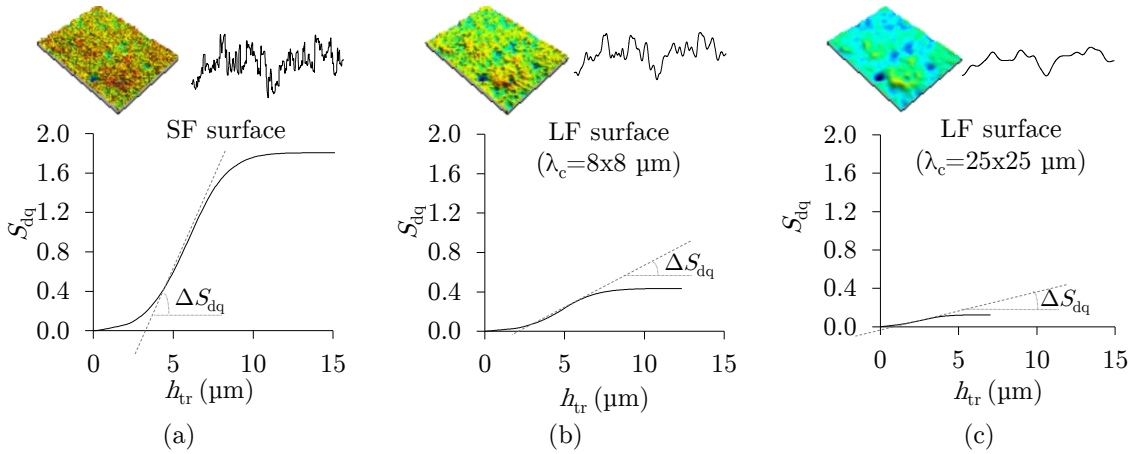

Figure 6.16: Demonstration of the relationship between the evolution of the S_{dq} in function of truncation height (h_{tr}) and the surface mean curvature, where the growing rate is called ΔS_{dq}. Different mean curvatures were simulated through filtering, in decreasing order: (a) AE1 primary (SF) surface; (b) AE1 waviness (LF) surface (λ_c=8x8 µm), (c) AE1 waviness (LF) surface (λ_c=25x25 µm).

6.7.2. Growing rate of the S_{dq} evolution curve (ΔS_{dq} parameter)

As discussed in the previous section, the growing rate of the S_{dq} evolution curve (ΔS_{dq}, see Figure 6.16) is representative of the relative mean surface curvature (the greater the slope the greater the curvature).

In order to calculate the ΔS_{dq} parameter in a reproducible way, firstly the numerical approximation of the first derivative of the curve was calculated through the *diff* function in Matlab, applying the resolution of the curve ($step_{tr}$) as step size (see Figure 6.17). Due to the "S" shape of the curve, the derivative curve presents a bell shape, since the trend changes from upward to downward when the original turns from convex to concave. Therefore the abscissa of the maximum point at the derivative graph (p) corresponds to the position of the inflection point of the original curve. Additionally, by definition, the value of the first derivative at p point corresponds to the slope of the tangent line to the original graph at the inflexion point. Thus, the ΔS_{dq} was obtained by calculating the first derivative of the S_{dq} evolution graph and finding the maximum value of it.

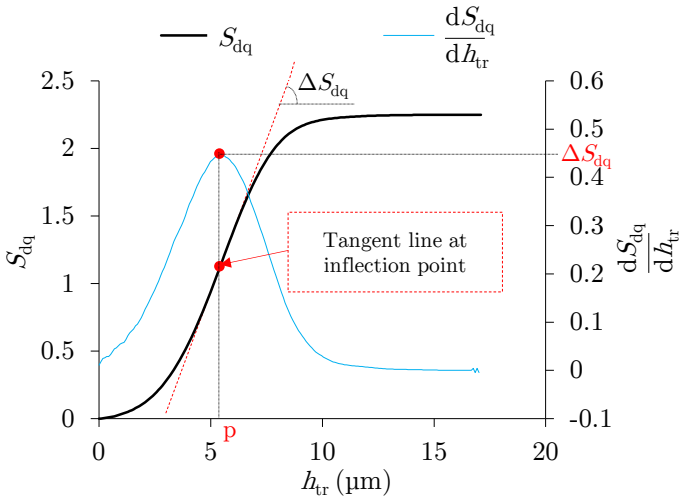

Figure 6.17: Calculation of the slope (ΔS_{dq}) of the lineal part of the "S" shaped S_{dq} evolution curve through its first derivative. h_{tr}= truncation height.

6.7.3. Selection of optimum truncation step size

It should be taken into account that the S_{dq} evolution curve will be sensitive to the truncation step size ($step_{tr}$), and therefore the slope value (ΔS_{dq}) may vary. Figure 6.18 displays the slope value (ΔS_{dq}) and calculation time obtained for different truncation step sizes ($step_{tr}$).

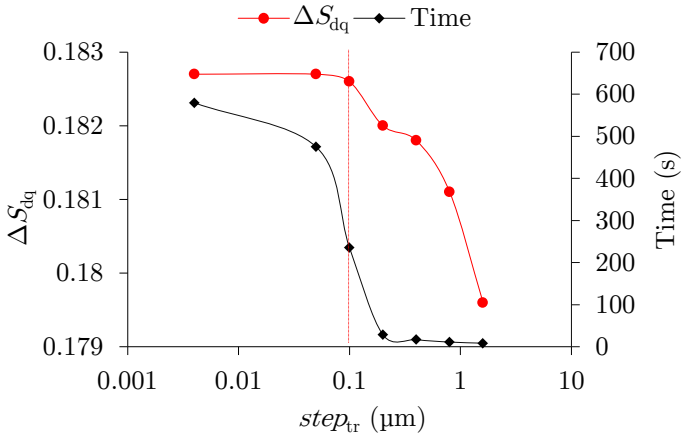

Figure 6.18: Effect of the step size on the ΔS_{dq} value and calculation time. $step_{tr}$=truncation step size.

It was observed that the calculation time decreased exponentially when the step size was increased until reaching an stable trend (for $step_{tr}$ values greater than 0.2 µm). This had been anticipated, since the $step_{tr}$ value determines the resolution of the curve, and will therefore be directly related to the calculation time. Regarding the slope (ΔS_{dq}) value, it remained fairly stable until a $step_{tr}$ size of 0.1 µm and from there it decreased considerably. Considering that the most reliable value is at the smallest $step_{tr}$, the relative errors were calculated (see Table 6.2). A compromise between reliability and calculation time was

sought through selecting a $step_{tr}$ of 0.1 µm (corresponding to 367 steps) as optimum value. The step size of each surface was therefore calculated following Equation 6.14:

$$h_{tr} = \frac{S_z}{367} \tag{6.14}$$

Table 6.2: Results of the $step_{tr}$ sensitivity study.

$step_{tr}$ (µm)	ΔS_{dq}	Time (s)	N_{step} (S_z =36.7 µm)	Relative error (%)
0.004	0.1827	579	9175	0.00
0.05	0.1827	475	734	0.00
0.1	0.1826	235	367	-0.05
0.2	0.1820	29	183	-0.38
0.4	0.1818	17	92	-0.49
0.8	0.1811	11	46	-0.88
1.6	0.1796	8	23	-1.70

6.7.4. Results and discussion

By means of the method explained in previous sections, the ΔS_{dq} parameter that describes the relative surface peak curvature was calculated for all surface treatments under study. Figure 6.19 depicts representative S_{dq} evolution curves and the results of ΔS_{dq} values calculated from five samples (four measurements each) of the four surface treatments under study.

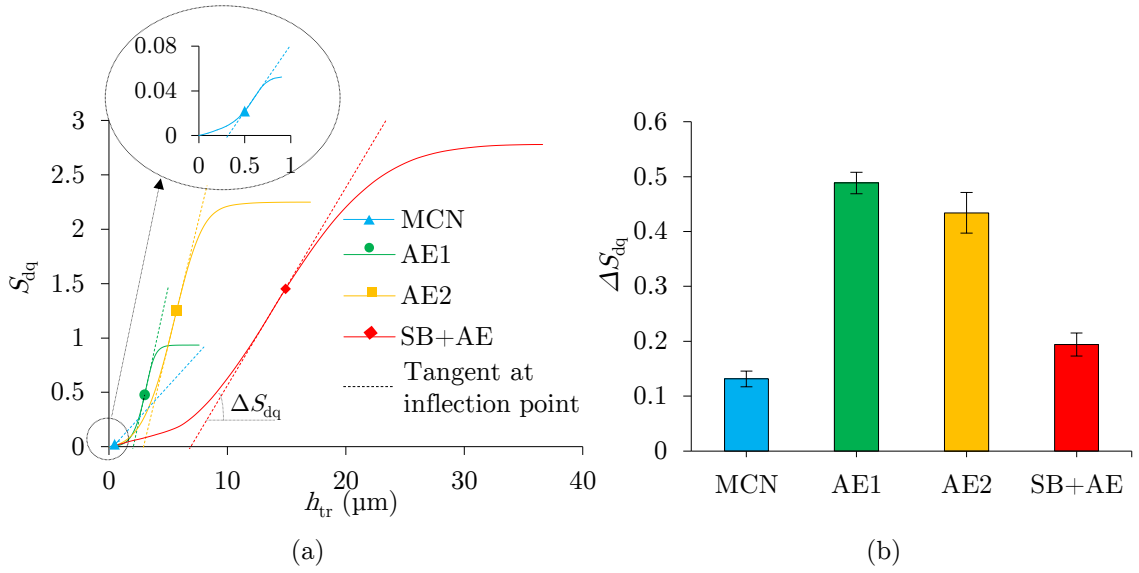

Figure 6.19: Results of the ΔS_{dq} parameter. (a) representative curves of the S_{dq} evolution in function of truncation height (h_{tr}) from which the ΔS_{dq} value is calculated; (b) results of the ΔS_{dq} value for the four surfaces under analysis.

The ΔS_{dq} parameter presented stable values (covariances lower than 11 %). Based on visual inspection of the surfaces (see Figure 6.12), it could be observed that unlike S_{pc} and S_{sc} parameters (analysed in section 6.6), the ΔS_{dq} parameter represented the relative surface curvature properties. The curvature ranking from smaller to greater was as follows: MCN, SB+AE, AE2 and AE1.

6.8. Correlation between topography and surface modification

6.8.1. Individual topographical parameters

In order to better understand the relationship between surface texture and modification, the results of the modified surface area percentages determined in section 6.4 were analysed as a function of various roughness parameters in order to look for a possible correlation.

For each parameter a graph was generated in wich the modified surface percentage was plotted against the mean value of each topographical parameter for the four surface treatments under study. A trend was calculated for each scatter graph, and the R-squared value was calculated.

Figure 6.20 presents the modified area percentages as a function of the parameters representing the surface characteristics considered to have an important role in wear and plastic deformation (discussed in previous sections): (i) the height dispersion of surface asperities ($\sigma = S_q$), (ii) the curvature of asperities ($\frac{1}{\beta} = \Delta S_{dq}$), (iii) the density of asperities ($\eta = S_{pd}$) and (iv) the main slope of the surface ($\theta = S_{dq}$). The correlation obtained in this way for each of the 3D parameters analysed in previous sections is shown in Figure 6.21.

The R-squared value, also known as the coefficient of determination, is an indicator that ranges in value from 0 to 1 and reveals how closely the estimated values from the trend-line correspond to the reality. A trend-line is more reliable when the R-squared value is close to 1 and should preferably exceed 0.9 in order to assume a good correlation [Ohl03]. The best correlation obtained for all 3D parameters was for the newly developed parameter ΔS_{dq} describing relative mean peak curvature. However, its value was far from 1 (0.79), and therefore no strong correlation could be assumed.

Thus, analysing the effects of the roughness, it was shown that 3D surface topographical parameters in isolation cannot be used to explain topographically-related variation in surface modification.

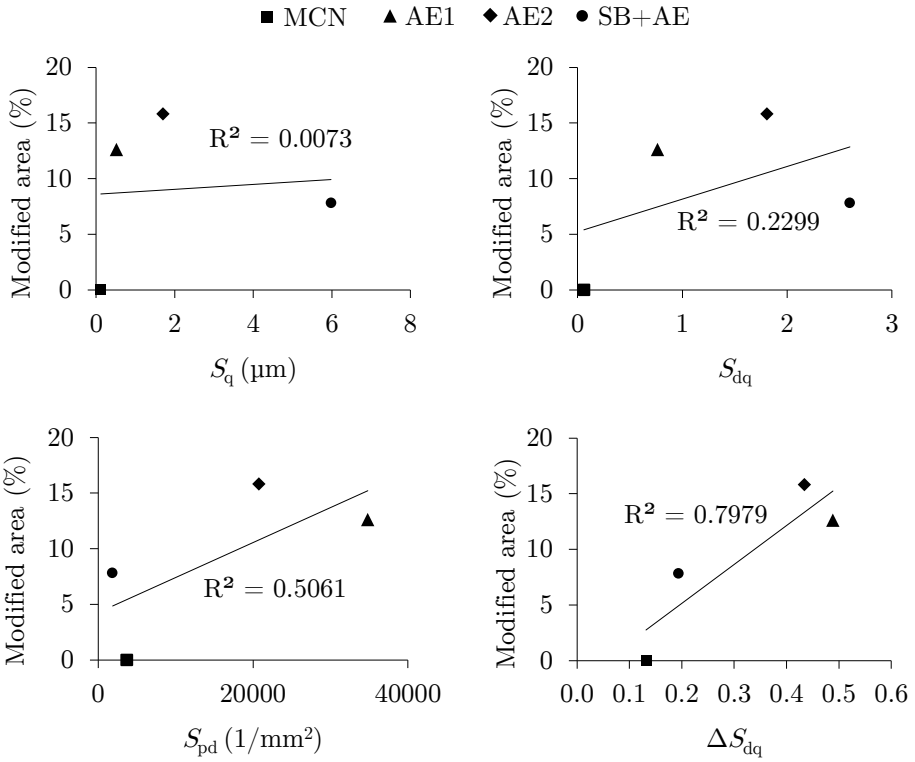

Figure 6.20: The mean modified area percentage presented as a function of the height parameter S_q, the hybrid parameter S_{dq}, the feature parameter S_{pd}, and the newly developed ΔS_{dq} parameter (representing the relative peak curvature).

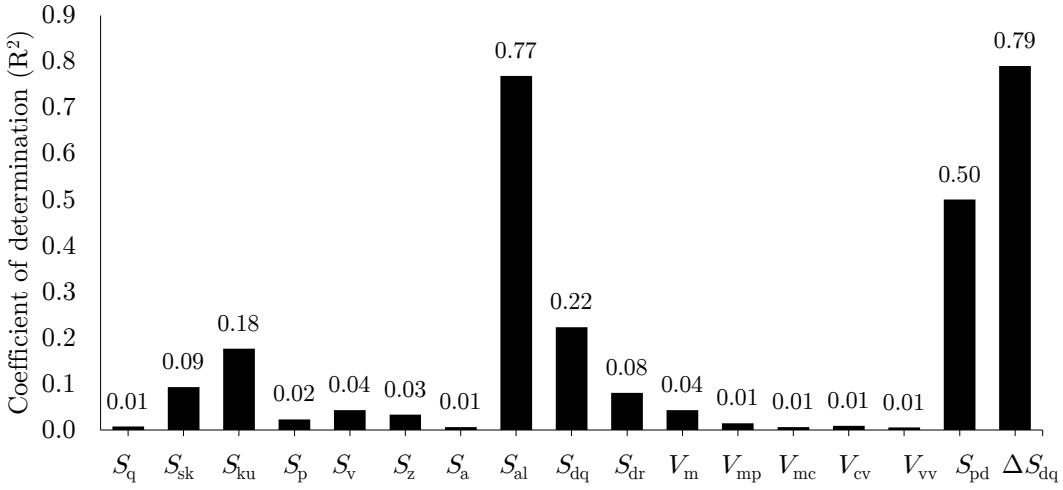

Figure 6.21: The correlation for each 3D parameter and the modified surface percentage.

6.8.2. Plasticity indexes and topographical relations

In this section, different plasticity indexes and topographical relations described and discussed in section 6.5 will be analysed as potential parameter combinations to correlate with surface modification. The plasticity indexes contain both surface and material properties in order to define the contact behaviour of the surface. However, taking into account the fact that the only difference between the modification of tested surfaces came from the variation in their roughness (all other parameters were kept constant), only the parameters describing topography were considered for the study.

Table 6.3 summarizes the models under analysis, the topographical relationship defined in its formulations, and the 3D topographical parameters selected to describe the required surface properties (extensively discussed in previous sections of this chapter), where: σ: height deviation of surface asperities (described by S_{q}), β: peak radius of surface asperities (described by the reciprocal of the newly developed parameter describing relative peak curvature ΔS_{dq}), η: density of surface asperities (described by S_{pd}) and θ: mean slope of the surface (described by S_{dq}).

Table 6.3: Summary of the plasticity indexes (described by Greenwood&Williamson and Mikic) and topographycal association (described by Greenwood&Tripp) under analysis. *Only parameters related to surface topography are considered.

Source	Model	Described formulation *	Used formulation
[Gre66]	Greenwood&Williamson	$\left(\frac{\sigma}{\beta}\right)^{\frac{1}{2}}$	$(S_{\mathrm{q}} \cdot \Delta S_{\mathrm{dq}})^{\frac{1}{2}}$
[Mik74]	Mikic	θ	S_{dq}
[Gre70]	Greenwood&Tripp	$\sigma \cdot \beta \cdot \eta$	$S_{\mathrm{q}} \cdot \frac{1}{\Delta S_{\mathrm{dq}}} \cdot S_{\mathrm{pd}}$

The topographical relationships were computed using the mean value of each parameter (calculated from five samples and four repetitions each) for the four surface treatments under study. Afterwards, following the methodology used for analysing the correlation of individual parameters (see previous section 6.8.1) each relationship was plotted against the modified surface percentage, and the coefficient of determination (R-squared value) was determined (see Figure 6.22).

Both plasticity index formulations (described by Greenwood&Williamson and Mikic) gave the same rankings, neither of which in accordance with the modified area percentage results. In agreement with previous works [LB03b] the best correlation was realized for the topographical association described by Greenwood&Tripp. However, the coefficient of determination was only 0.7, and therefore no strong correlation could be assumed.

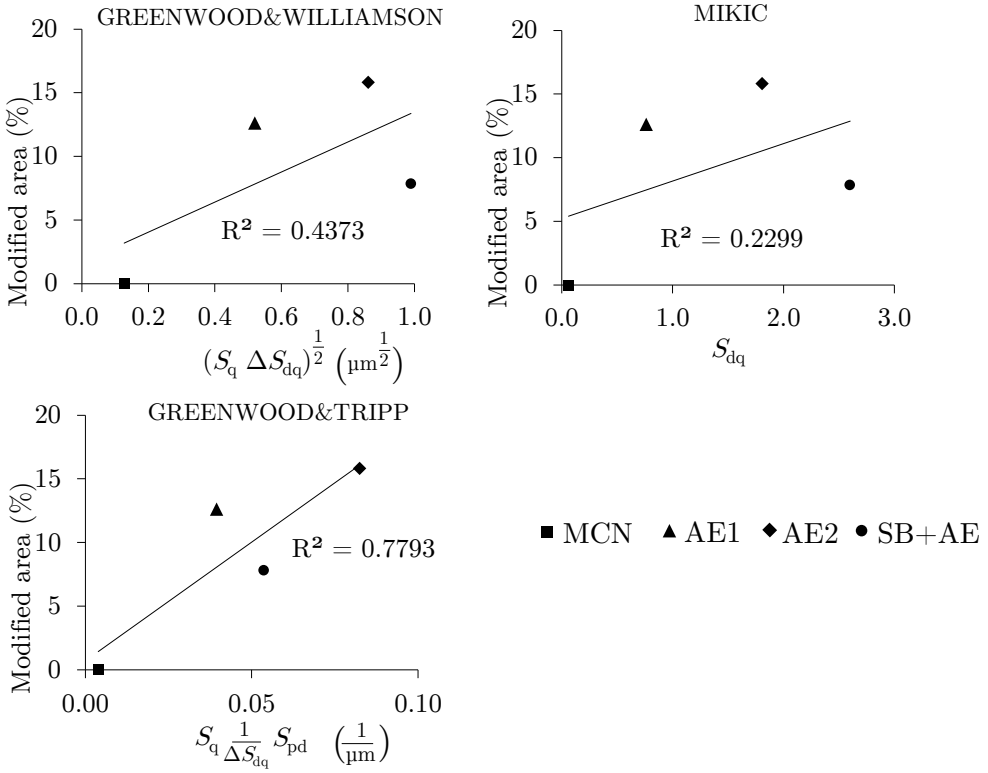

Figure 6.22: The mean modified area percentage presented as a function of the topographical combinations described in the plasticity indexes defined by Greenwood&Williamson and Mikic, and for the topographical parameter association described by Greenwood&Tipp.

6.8.3. Definition of an integrated topographical parameter product

Due to the lack of any strong correlation encountered when analysing topographical parameters individually and different plasticity index formulations and topographical associations, a new integrated topographic parameter was established, based on empirical results.

It results intuitive that the more asperities (contact points) the surface have, the more potential wear sites will be present [LB03b]. Similarly, the asperity height distribution largely influences the wear rate, since it is the asperities with larger heights that bring about the maximum amount of wear debris [Mar13]. As far as peak radius is concerned, a sharp peak (large curvature) is more likely to be worn away during sliding contact or be plastically deformed during a static contact compared to a more rounded peak [Bla13].

Thus, based on these tendencies, and using the surface density of asperities (S_{pd}), the relative mean curvature of asperity summits (ΔS_{dq}) and the standard deviation of surface height distribution (S_q), a new integrated topographical parameter product called S_i was defined (see Equation 6.15) as potential parameter combination to correlate with surface modification.

$$S_i = S_q \cdot \Delta S_{dq} \cdot S_{pd} \tag{6.15}$$

Figure 6.23 depicts the modified surface area percentage as a function of the defined integrated parameter S_{i}. This chart shows a clear correlation with an acceptable coefficient of determination of 0.9. Therefore the new S_{i} parameter presents a good agreement with the surface modification and could be used to predict whether a surface is more prone to suffer topographical alterations during insertion.

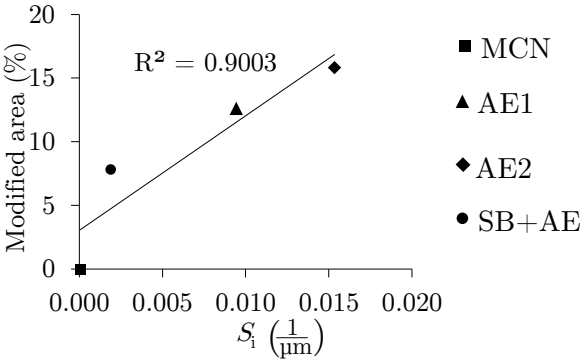

Figure 6.23: The mean modified area percentage presented as a function of the integrated topographical parameter S_{i}.

6.9. Conclusions

The aim of this chapter was to correlate the modification of dental implant surfaces generated during surgical placement (simulated in previous Chapter 5) with 3D topographical parameters. The following points can be concluded from the various components of this study, divided into three blocks:

Surface data separation

- A method for data separation has been developed that provides a tool for the assessment of surface modification percentage.
- The calculated modified area percentage of the MCN treatment was well below the established minimum threshold, and therefore, 0 % modification was assumed.
- The modified area percentage ranking from smaller to greater was: MCN (0 %), SB+AE (8 %), AE1 (13 %), AE2 (16 %).
- The modified area distributions differed from one treatment to another, and were similar to those observed in the insertion tests: the acid etched surfaces (AE1, AE2) presented widespread small flattened areas while for the sand blasted treatment (SB+AE) the modified regions were fewer but larger.

Wear predictive models and plasticity indexes analysis

- The most relevant topographical characteristics for predicting wear and plastic deformation behaviour relies on surface mean slope (θ) and surface asperity's density (η), height distribution (σ) and radius (β).
- The surface asperity's height distribution (σ) can be approximated by the more readily obtainable surface height deviation parameter S_{q}.
- The surface mean slope defined by Mikic (θ) can be approximated by S_{dq}.
- Feature parameters are potential parameters used to calculate the density of the surface asperity (η) and radius (β).
- Discrepancies between SensoMap and SurfStand software were observed regarding feature parameter calculation.
- Although differences were encountered between software systems when calculating S_{pd} and S_{ds} parameters, the trends were consistent. The feature parameter S_{pd} represents only the significant peaks and is therefore considered more suitable than its older version S_{ds} for asperity density (η) description.
- The summit curvature S_{sc} parameter presented discrepancies between software systems but the trends were consistent. However, the trend was not representative of the analysed surface's curvature.
- Big discrepancies (up to two orders of magnitude) were observed for the curvature S_{pc} parameter when comparing SensoMap and SurfStand results.
- The S_{pc} parameter provided by the SensoMap software did not represent surface properties. Although the results obtained by SurfStand were more consistent, high variability was observed and therefore was not useful.
- A new parameter based on surface mean slope (S_{dq}) variation in function of truncation height was developed (named ΔS_{dq}) which described the relative mean curvature of the surface successfully, and was used to describe the asperity's radius ($\beta \propto \frac{1}{\Delta S_{\mathrm{dq}}}$).

Correlation between topography and surface modification

- 3D topographical parameters in isolation did not correlate with surface modification.
- Neither the topographical relations of the plasticity indexes described by Greenwood & Williamson, nor the combination of topographycal parameters described by Greenwood& Tripp correlated with the surface modification percentage.
- A new integrated topographic parameter combination based on empirical data was defined (S_{i}) and successfully correlated with surface modification.

The initial objectives of the Chapter were to:

(I) To develop a method for separating the tested surfaces into modified and non-modified regions.

(II) To establish a correlation between the surface modification and 3D topographical parameters.

Both aims were fully satisfied. A data separation method based on the material probability curve was developed, which allowed quantifying of the modified area percentage and determination of a quantitative ranking of the surface modification in function of the topography. This quantitative characterization of the modification made the correlation study possible.

To sum up, the correlation between the surface modification and some physically meaningful properties of surface topography was successfully established through the integrative parameter S_{i}. This newly developed parameter could be used to predict whether a surface is more prone to suffer alterations during insertion, and may therefore contribute to foster advancements in the design of better performing endosseous implants and improved surgical procedures. However, the modified surfaces used for the study were obtained through a simplified simulation (analysed in the previous chapter) and only represented the plastic deformation occurring during dental implant insertion. Considering that the surface properties affecting the wear and plastic behaviour are the same, it is hypothesized that this parameter will also correlate to surfaces subjected to both wear and deformation. The question of whether this assumption is true, however, remains open and calls for further research.

CHAPTER 7

CONCLUSIONS AND FUTURE WORK

"When you have a great and difficult task, something perhaps almost impossible, if you only work a little at a time, every day a little, suddenly the work will finish itself"
Karen Blixen

"What we know is a drop, what we don't know is an ocean"
Isaac Newton

In this chapter the outcomes of the project are summarized and proposals for further work are given.

7.1. Conclussions

The main goal of the present dissertation has been to analyse and predict the topographical alteration of endosseous dental implants generated during the surgical insertion.

The following objectives were set out in order to achieve this goal:

(I) Using the 3D techniques available, to define a topographical characterization strategy to effectively and robustly characterize the topography of endosseous dental implants.

(II) To evaluate the modification of dental implants surface topography generated during standard surgical insertion.

(III) To characterize the influence of surface modification generated during surgical insertion on cell response.

(IV) To establish a correlation between the surface modification generated during surgical insertion and 3D topographical parameters.

A number of studies were conducted in order to fulfil these aims. First of all, implant positioning devices were developed and the effect of the data acquisition and treatment variables on the 3D topographical parameters was analysed and evaluated. This led to the definition of a generalized topographical characterization strategy for dental implants (objective I, dealt with in Chapter 3). Following this, the effect of the surgical insertion on dental implant surface topography was analysed by means of qualitative and quantitative evaluation of commercially available dental implants both before and after standard surgical insertion in cow rib bone (objective II, dealt with in Chapter 4). This study revealed that the surface was altered in terms of wear and plastic deformation during the surgical insertion. The next step was to evaluate whether the topographic alterations observed in the post-inserted implants affects the cellular response. To that end a device was developed for reproducing the modification generated during implant insertion on disc samples and In Vitro evaluation of human osteoblast-like cell (MG-63) proliferation and attachment was conducted on modified and non-modified surfaces (objective III, dealt with in Chapter 5). Within the limits of the study, the experimental data did not support the hypothesis that osteoblast attachment and proliferation could be significantly affected by the topographical modification generated during dental implant insertion. Finally, a correlation study between the modified surfaces and 3D topographical parameters was carried out and a new integrated topographical parameter was developed and successfully correlated with surface modification (objective IV, dealt with in Chapter 6). Following the main conclusions of each objective are outlined and the importance and implications of the work are highlighted.

The main conclusions concerning objective (I), dealt with in Chapter 3, are:

- Using the correct measurement strategy is imperative to avoid misleading data. Dental implant handling and positioning devices were developed in order to aid in the

quality, repeatability and time optimization of the measurement, and a generalized data acquisition strategy for endosseous dental implants was defined.

- 3D topographical parameters are strongly influenced by the data processing variables, in which the most influential are the L filter type and size. Due to the lack of awareness of the functional scale of the surface, 3D topographical parameters should be calculated both in the primary (SF) and roughness (SL) surfaces for a proper description of surface topography of an endosseous dental implant.

- All data acquisition and processing variables must be clearly specified in order to report a meaningful topographical characterization.

- The topography of commercial dental implants can vary significantly according to the evaluation site. Therefore four evaluation sites are suggested for a complete description of the surface: neck, top, valley and flank.

Although the importance of the surface topography on the functional response of dental implants is widely accepted there is a lack of standards and consensus regarding the topographical characterization of dental implants. This leads to ambiguous topographical analysis reports and difficulties in sorting and interpreting the published findings. This study has presented a generalized topographical characterization strategy in order to advance standards for dental implant topographical characterization.

The main conclusions concerning objective (II), dealt with in Chapter 4, are:

- This investigation has demonstrated that changes in the surface topography of commercial endosseous implants occurred during standard insertion procedures. Specifically, two degradation mechanisms were detected: wear phenomena (with the resulting particle removal), and plastic deformation (with the corresponding morphological variation).

- 3D surface topographical assessment can be a useful tool in the investigation of the surface modification generated during the surgical insertion. This study has demonstrated that the surface damage varied along different regions of the implants (neck, top, valley and flank) as well as along the implant for each region.

- The mass loss was approximated based on the functional material volume (V_{m} calculated at 100 % rate) variation analysis, which allowed for quantification of the material loss for each implant system at different regions of the implant.

- The morphological analysis of detached titanium particles through SEM analysis of the bone underlying the implants revealed that the size and quantity of particles depends on the surface treatment.

- The developed interfacial ratio (S_{dr}) was one of the most sensitive parameters and correlated positively with material loss and is considered to be the best damage

indicator. It is suggested to use the functional volume parameters from the ISO 25178 standard rather than the R_k family parameters defined in the European report EUR 15178N due to the higher sensitivity encountered.

The study of the modification generated during dental implant insertion is of great importance due to the implications of the degradation mechanisms encountered. These include the detachment of particles and the alteration of the surface topography.

To the author's knowledge, this is the first study dealing with the qualitative and quantitative study of surface modification generated during surgical insertion analysing different regions of the implant. This approach allowed for a better understanding of the phenomena.

The results obtained suggest that the modification generated during surgical insertion is a multivariable interaction, influenced by the implant macro geometry, surgical procedure and surface treatment.

The main conclusions towards objective (III), dealt with in Chapter 5, are:

- An experimental set-up was developed in order to reproduce the surface modification generated during implant insertion on a flat surface, required for an In Vitro study. Although two mechanisms were detected in the post-inserted dental implant surfaces, namely wear and plastic deformation, only plastic deformation could be successfully reproduced. .
- The damage generated when applying the same load varied from one treatment to another.
- The field topographical parameter variations were unsuitable for ascertaining different modification behaviours. However, the most suitable parameters for describing the surface modification were the V_{mp} and S_{dr}.
- The proliferation and attachment assays conducted at 72 hours and 4 hours respectively demonstrated that MG-63 osteoblast-like cells were sensitive to variations in roughness. Cell proliferation and attachment decreased as the roughness increased.
- No statistically significant changes were encountered between the non-modified and modified surfaces, except for the proliferation of the machined surface.

The topographical alterations observed in the post-inserted implants have two main implications. Firstly, the effect of the released particles, and secondly the possibility of a different cell response of the modified surfaces compared to the original ones, which could lead to unexpected results. To the author's knowledge this is the first attempt to evaluate the effect of surface modification generated during dental implant insertion on the cell response. The surface damage of post-inserted dental implants was only partially reproduced, and this was the main limitation of present study. However, the device developed

allowed to set a test method to compare different surface treatments under the same load conditions. This represents an advance towards better understanding of the behaviour of different surface treatments, since the stresses generated during dental implant insertion are difficult to measure and control, which prevents the direct comparison between the surface damage generated at different implant systems.

Within the limits of the study, the experimental data rejected the hypothesis that osteoblast attachment and proliferation could be significantly affected by the topographical modification generated during dental implant insertion.

The main conclusions concerning objective (VI), dealt with in Chapter 6, are:

- A method for data separation has been developed that provides a tool for assessing surface modification percentage. The modified area percentages and distributions differed from one treatment to another.
- 3D topographical parameters are suitable for describing three of the four topographical properties identified in the literature as important for wear and plastic behaviour prediction: (i) the high dispersion of the surface asperities (σ-S_{q}), (ii) the density of asperities (η-S_{pd}) and (iii) the main slope of te surface (θ-S_{dq}). The asperity radius (β) was not properly defined by the feature parameters (S_{pc}, S_{sc}), and large discrepancies (up to two orders of magnitude) were observed for the S_{pc} parameter when comparing SensoMap and SurfStand software.
- A new parameter was developed in order to describe the relative mean curvature of the surface successfully, and was used to describe the asperity's radius ($\beta \propto \frac{1}{\Delta S_{\mathrm{dq}}}$).
- Neither the 3D topographical parameters in isolation nor the plasticity indexes that were analysed correlated with the surface modification.
- A new integrated topographical parameter combination based on empirical data was defined and successfully correlated with surface modification ($S_{\mathrm{i}} = S_{\mathrm{q}} \cdot \Delta S_{\mathrm{dq}} \cdot S_{\mathrm{pd}}$).

Due to the implications of the surface modification on implant performance and survival, the development of predictive models are of great importance. However, owing to the variety and complexity of the degradation mechanisms, particularly in a biological environment, it may be unrealistic to search for an explicit and comprehensive wear and deformation model. As stated by some authors [LB03b], a more profitable approach might be to select parameters whose correlation with surface modification might prove to be of more general applicability.

In the present work the correlation between surface modification in terms of plastic deformation and some physically meaningful properties of surface topography was successfully established thorough a newly developed integrative parameter (S_{i}). Considering that the surface properties affecting wear and plastic behaviour are the same, it is hypothesized that this parameter will also correlate to surface subjected to both wear and deformation.

The developed parameter is presented as a useful to predict whether a surface is more prone to suffer alterations during dental implant insertion

7.2. Future work

The work developed in this thesis concerning the analysis and prediction of the surface modification of dental implants during surgical insertion has raised new interesting issues and starting points for new research paths. These have not been addressed, however, due either to the finite nature of this work, or because they deviated from the main targets defined in this thesis, and are mentioned below as suggestions for future work.

- In the present work the analysis of the surface modification generated during dental implant insertion was centred in the evaluation of the titanium dental implant surface both prior and after insertion. In practice, two contacting surfaces are involved and the surface features on each may have a part to play in causing wear and plastic deformation. It would therefore be of great interest to analyse the effect of the surgical procedure in the bone surface finish, since the roughness of the bone at the implant bed will affect the bone-implant interplay. Such a study could lead to a greater understanding of the phenomena and shed insights onto the establishment of optimized surgical procedure settings.

- The release of titanium particles into the surrounding bone is a major concern due to the implications this could have in the functionality of the implant as well as a potential health hazard. Therefore the quantification of material loss is of significant importance. The approach used in the present study is based on the variation analysis of the functional V_{m} parameter, which was useful in approximating the material loss at different regions of the implants. However, further work is required in order to analyse the accuracy of this method. On the other hand, it should be emphasized that the topographical parameter analysis for material loss approximation is a very time-consuming process and may therefore become impractical as a screening test for studies using a large number of samples. Thus, further studies should evaluate alternative methods for material loss quantification, in order to evaluate the accuracy of this selected approach and to determine a material loss screening test for larger studies. Gravimetric studies using high resolution micro-balances or methods based on the titanium concentration analysis after dissolving the bone, such as the induction-coupled plasma [Kra94], should be evaluated.

- The stresses to which implant surfaces are subjected during dental implant insertion depends on a number of variables, such as the macro geometry and the surgical procedure, and are difficult to measure and control. It is therefore be interesting to develop a methodology to simulate the surface modification generated during dental implant insertion in order to establish a test method to compare different surface

treatments under the same load conditions. In the present study a simplified reproduction of the surface modification was carried out, representing only the plastic deformation. Further research is therefore required in order to simulate both wear and plastic deformation.

- The in vitro test carried out in Chapter 5 did not disclose any differences between the acid etching and sand blasting followed by acid etching surfaces, although the topography of these treatments varies significantly. This suggests that the in vitro experiment was too limited and further studies should be carried out, using different cell types and additional biological markers. The fundamental understanding of key biological interactions with surface topography would enable the establishment of a functional filtering of surface topography and ultimately yield criteria for the systematic refinement of implant surface designs.

  Likewise, the comparison between the modified and non-modified surfaces did not reveal statistically significant differences, and therefore further in vitro studies should be carried out in order to bring greater understanding to this interaction. Due to the local nature of the surface modification, the use of averaged values for the whole surface may mask the effects of the modification on the cell response. Therefore, more local cell behaviour analysis methods should be explored.

- A new integrated topographical parameter was developed for predicting whether a surface topography is more prone to suffer alterations during dental implant insertion in terms of plastic deformation. Considering that surface properties affecting the wear and plastic behaviour are the same, it was hypothesized that this parameter would also correlate to surfaces subjected to both wear and deformation. Therefore, tribological studies on dental implant surface treatments should be carried out in order to test the established hypothesis.

APPENDIX A

3D Topographic parameters

Introduction

The most used topographic 3D parameters are described in this appendix. The discrete approximations of the formulas are given since surfaces are always sampled and digitised. For continuous descriptions of the formulas (i.e expressed with integrals) the reader is referred to [ISO 25178-2].

Coordinate system

Figure A.1 shows the coordinate system used to define 3D topographic parameters, where η is the mean value surface (the reference datum).

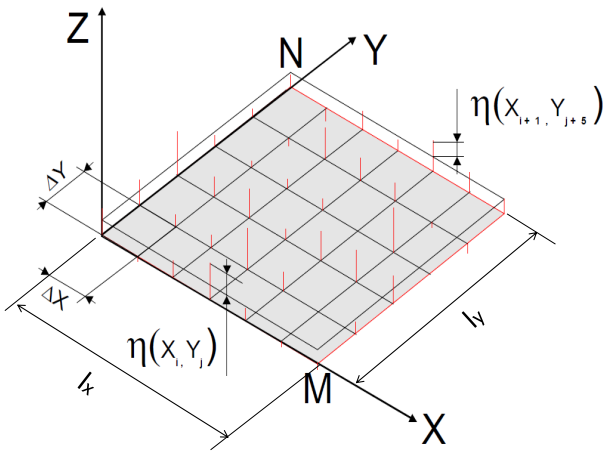

Figure A.1: Coordinate system for 3D topographical parameter definition.

Amplitude parameters

The amplitude parameters can be divided into three categories depending on the properties they are describing:

- Statistical characteristics of surface height (S_a, S_q).
- The shape of surface height distributions (S_{sk}, S_{ku}).
- Extreme characteristics of surface height (S_p, S_v, S_z).

The statistical parameters S_a and S_q are the Average Roughness and Root mean Square Roughness. They are evaluated over the complete 3D surface; the formulation of each parameter is shown in the equations (A.1) and (A.2) respectively.

$$S_a = \frac{1}{MN} \sum_{j=1}^{N} \sum_{i=1}^{M} |\eta(x_i, y_j)| \tag{A.1}$$

$$S_q = \sqrt{\frac{1}{MN} \sum_{j=1}^{N} \sum_{i=1}^{M} \eta^2(x_i, y_j)} \tag{A.2}$$

These parameters represent an overall measure and are insensitive in differentiating peaks, valleys, and the spacing of the various texture features. Nonetheless, once a surface type has been established, the S_a and S_q parameters may be used to indicate significant deviations in the texture characteristics. In statistics, S_a is the arithmetic mean and S_q is the sample standard deviation. S_a and S_q are a very general and widely used parameters [Met11].

The parameters S_{sk} (Skewness) and S_{ku} (Kurtosis) are defined from the height distribution curve of the surface (see Figure A.2) .

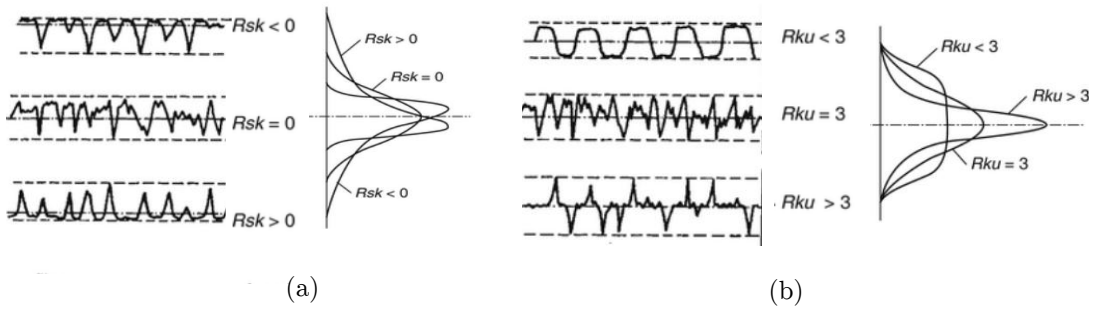

Figure A.2: Illustrative representations of the amplitude parameters (a) skewness (S_{sk}) and (b) kurtosis (S_{ku}) [Kaj90].

The Skewness of the heigh distribution is the third statistical moment, qualifying the symmetry of the height distribution and mathematically is evaluated as shown in the equation (A.3).

$$S_{sk} = \frac{1}{MNS_q^3} \sum_{j=1}^{N} \sum_{i=1}^{M} \eta^3(x_i, y_j) \tag{A.3}$$

This parameter can be used to describe the shape of the height distribution. For a Gaussian surface (which has a symmetrical shape for the surface height distribution), the skewness is zero. A negative S_{sk} indicates a predominance of valleys, whereas a positive S_{sk} indicates a predominance of peaks. Due to the big exponent used, this parameter is very sensitive to the sampling and to the noise of the measurement.

The kurtosis is the fourth statistical moment, qualifying the peakedness or sharpness of the surface height distribution and is calculates as follows (see equation (A.4)).

$$S_{\mathrm{ku}} = \frac{1}{MNS_{\mathrm{q}}^4} \sum_{j=1}^{N} \sum_{i=1}^{M} \eta^4(x_i, y_j) \tag{A.4}$$

This parameter characterizes the spread of the height distribution. A surface distribution with sharp shape will have a kurtosis value larger than 3 whereas the kurtosis of a well spread distribution is smaller than 3 (a Gaussian surface has a kurtosis value of 3).

The parameters S_{p}, S_{v} and S_{z} describe the extreme characteristics of surface height. The highest peak of the surface S_{p} is defined as the height of the highest peak from the mean surface plane within the sampling area, and is defined mathematically as follows (see equation (A.5)).

$$S_{\mathrm{p}} = \mathrm{MAX}(\eta_{\mathrm{p}}) \qquad with \qquad \eta_{\mathrm{p}} > 0 \tag{A.5}$$

Where η_{p} are the highest summits on the surface, which are calculated by means of the eight nearest neighbour summit definition: a peak is defined if it is higher than its 8 nearest neighbours. The lowest valley of the surface, S_{v}, is defined as the height of the lowest valley from the mean surface plane within the sampling area (see equation (A.6)):

$$S_{\mathrm{v}} = \mathrm{MIN}(\eta_{\mathrm{v}}) \qquad with \qquad \eta_{\mathrm{n}} > 0 \tag{A.6}$$

Where η_{v} are the lowest valleys on the surface, which relies on the eight nearest neighbour definition.

S_{z} expresses the sum of the maximum value of surface peak height and the maximum value of surface valley in a sampling area (see equation (A.7)):

$$S_{\mathrm{z}} = (|S_{\mathrm{p}}| + |S_{\mathrm{v}}|) \tag{A.7}$$

Spatial parameters

Spatial parameters describe the texture of the surface such as randomness and periodicity. In order to understand spatial parameters some basic concepts about the auto correlation function (ACF) and the Angular Power Spectral Density Function (APSDF) are given.

Autocorrelation is a correlation coefficient. However, instead of correlation between two different variables, the correlation is between two values of the same variable with a relative lateral displacement X_i and $X_i + \tau_x$. The ACF is determined by taking a duplicate surface ($Z(x - \tau_x, y - \tau_y)$) of the measured surface ($Z(x, y)$) and mathematically multiplying the two surfaces together, with a relative lateral displacement (τ_x, τ_y) between the two surfaces (see the equation (A.8)).

$$\mathrm{ACF}(\tau_x, \tau_y) = \frac{\iint_A z(x, y) \cdot z(x - \tau_x, y - \tau_y) \mathrm{d}x\mathrm{d}y}{\iint_A z^2(x, y) \mathrm{d}x\mathrm{d}y} \tag{A.8}$$

If the shifted version of the surface is identical to the original surface then the ACF is 1.00. If the shifted surface is such that all peaks align with corresponding valleys then the ACF will approach -1.00 ([Met11], [Bla06]). Thus the ACF is a measure of how similar the texture is at a given distance from the original location. If the ACF stays near 1.00 for a given amount of shift, then the texture is similar along that direction. If the ACF falls rapidly to zero along a given direction, then the surface is different and thus "uncorrelated" with the original measurement location. Applying this equation along the surface, an image could be generated on which it is possible to measure characteristic quantities. Figure A.3 shows an example of autorrorrelation image of isotropic and anisotropic surfaces.

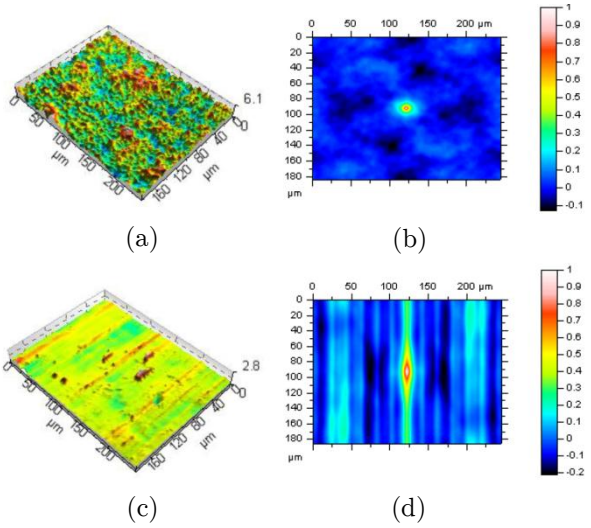

Figure A.3: Measured surface and autocorrelation image. (a)-(b): Acid etched (isotropic) surface. (c)-(d): Machined (anisotropic) surface.

The autocorrelation image always shows a central peak with a standard value of 1 (which belongs to the $\tau_x = 0$, $\tau_y = 0$ shift position). The form of the central peak is an indicator of the isotropy of the surface. The isotropic surface (Figure A.5 (b)) shows a symmetric peak whereas the anisotropic surface (Figure A.5 (d)) posses an elongated peak. In order to characterise the form of the central peak, a thresholding s of 0.2 is carried out. Then, the central zone of the image corresponding to the portion of the peak that remains after thresholding is quantified. Finally, the minimum and maximum radius of the central

zone are calculated (see Figure A.4) and used to calculate the S_{al} and S_{tr} parameters as explained later on.

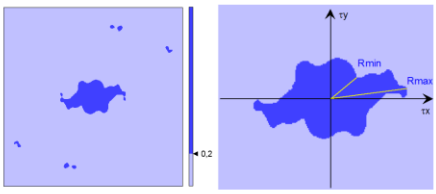

(a) (b)

Figure A.4: Characterization of the ACF central peak. (a): Thresholding of 0.2. (b): Calculation of the maximum and minimum distances Rmax, Rmin [Sur15].

On the other hand, from Fourier analysis, the surface texture is composed of a series of sine waves in all directions with different spatial frequencies and amplitudes. The power spectral density of the signal is the square of the magnitude of the continuous Fourier transform of the signal. Thus it is a real and positive function. The power spectrum is a measure of the amplitude of each sine wave for a particular spatial frequency, along a given direction. Therefore, for a 3D surface, the power spectrum would be displayed as a 3D function in which the x and y axes represent the various spatial frequencies for a given direction. The z direction represents the amplitude of the sine wave at a particular spatial frequency direction given in dB. Figure A.5 shows the power spectral density function and angular power spectral density function (explained below) of the surfaces seen in Figure A.3.

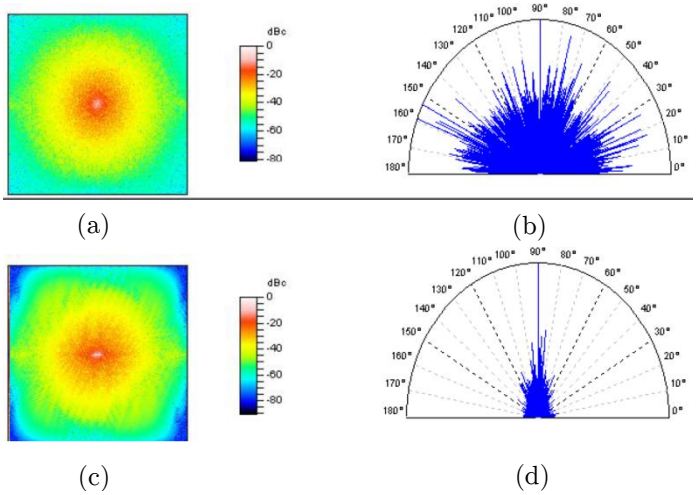

(a) (b)

(c) (d)

Figure A.5: Power spectral density function and angular power spectrum. (a)-(b): Acid etched (isotropic) surface. (c)-(d): Machined (anisotropic) surface.

The centre of the image represents the 0 frequency. The top left quadrant is the same as the bottom right quadrant, and the bottom left quadrant is the same as the top right quadrant. Each point represents a frequency and all points that lie on a circle with a given

radius represent the same wavelength. As can be seen in Figure A.5, the dominant frequency of the anisotropic surface is highlighted (see Figure A.5 (c)), whereas in the isotropic surface there is not a dominant direction (see Figure A.5 (a)). It should be noted that the direction of the distribution in the frequency plane (Figure A.5 (c)) is perpendicular to the lay orientation of the real surface (Figure A.3 (c)).

The angular power spectral density function (APSDF) is used to determine the angle of the dominant direction. The angular power spectrum is found by integrating the amplitudes of each component sine wave as a function of angle [Met11]. An example can be seen in Figure A.5 (b) and (d), where the angle is given counterclockwise. Obviously, in the case of the isotropic surface (Figure A.5 (b)) there is not any preferential angle.

After reviewing the basic concepts, the spacial parameters S_{al}, S_{tr}, and S_{td} are defined.

The spatial parameter $\boldsymbol{S_{\mathrm{al}}}$, *i.e.*, the autocorrelation length, is the horizontal distance of the autocorrelation function (equation A.8) which has the fastest decay to a specified values at any direction, being $0 < s < 1$[1](*i.e.* S_{al} =Rmin, see Figure A.4). This parameter express the content in wavelength of the surface. A high value indicates low frequency surface features and vice versa.

The texture aspect ratio of the surface, $\boldsymbol{S_{\mathrm{tr}}}$, is used to identify texture pattern. A surface with a oriented texture has the fastest decay along the perpendicular lay direction, and the slowest decay along the lay direction.

Therefore the texture aspect ratio is defined as it can be seen in the equation (A.9) (Rmin and Rmax described in Figure A.4) and has a value between 0 and 1. If the value is near 1 indicates that the surface is isotropic, *i.e.*, it has the same characteristics in all directions. If the value is near 0, the surface is anisotropic, *i.e.*, it has an oriented and/or periodic structure.

$$0 < S_{\mathrm{tr}} = \frac{\textit{shortest ACF decrease length to } 0.2 \textit{ at any direction } (Rmin)}{\textit{largest ACF decrease length to } 0.2 \textit{ at any direction } (Rmax)} < 1 \tag{A.9}$$

The texture direction of the surface $\boldsymbol{S_{\mathrm{td}}}$, gives the lay direction of the surface. Therefore this parameter is meaningful if S_{tr} <0.5, *i.e.*, if the surface is anisotropic. The parameter is calculated form the Angular Power Spectral Density Function (APSDF), where the angle with the largest power spectrum belongs to the privileged surface direction.

Hybrid parameters

Hybrid parameters describe a combination of spatial and amplitude characteristics, thus any changes which occur either amplitude or spacing may have an effect on the hybrid property.

[1]The default value of s defined in ISO 25178 is 0.2.

The $S_{\Delta \mathbf{q}}$, also called $S_{\mathbf{dq}}$, is the root mean square slope of the surface. This parameter is a general measurement of the slopes which comprise the surface and is given by the equation (A.10).

$$S_{\mathrm{dq}} = \sqrt{\frac{1}{(M-1)(N-1)} \sum_{j=2}^{N} \sum_{i=2}^{M} \left[\left(\frac{\eta(x_i, y_i) - \eta(x_{i-1}, y_j)}{\Delta x} \right)^2 + \left(\frac{\eta(x_i, y_i) - \eta(x_i, y_{j-1})}{\Delta y} \right)^2 \right]} \tag{A.10}$$

The Developed Interfacial Area Ratio, $S_{\mathbf{dr}}$, is expressed as the percentage of additional surface area contributed by the texture as compared to an ideal plane. The surface area is the total area of all triangles formed over the texture (see Figure A.6) whereas the ideal plane is the projection of the surface.

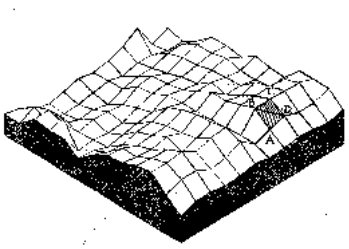

Figure A.6: Schematic diagram of the developed area [Sto00c].

The parameter is calculated by equation (A.11), and detailed formulation can be found in [Sto00d].

$$S_{\mathrm{dr}} = \frac{(Texture\ surface\ area) - (Cross\ sectional\ area)}{(Cross\ sectional\ area)} \tag{A.11}$$

A completely flat surface will have a S_{dr} near 0 %, and a complex surface will have a S_{dr} of some percents.

Functional parameters

Functional parameters are calculated from the Abbott-Firestone curve (also called the areal material ratio curve) obtained by the integration of height distribution on the whole surface. It presents the percentage of material traversed (in relation to the area covered) for a given depth, being useful for understanding the properties of sealing and bearing surfaces. Functional volume parameters are shown in Figure A.7 and explained below.

The peak material volume of the scale limited surfaceV_{mp} is defined as the material volume enclosed in the 5 % [2] material ratio and normalised to unit sampling area.

[2]Default value in ISO 25178-2 standard is 10 %.

The core material volume of the scale limited surface V_{mc} is the material volume enclosed from 5 % [2] to 80 % of surface material ratio and normalised to the unit sampling area.
The core void volume of the scale limited surface V_{vc} is the void volume enclosed from 5 % [2] to 80 % of surface material ratio and normalised to the unit sampling area.

The pit void volume of the scale limited surface V_{vv} of the unit sampling area is defined as a void volume in the valley zone from 80 % to 100 % surface material ratio and normalised to the unit sampling area.

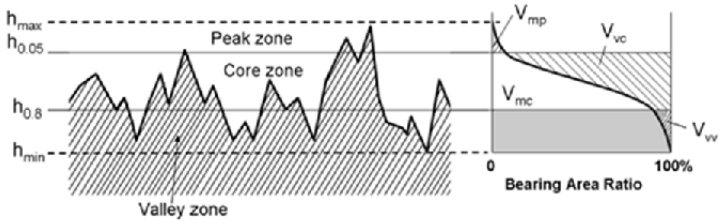

Figure A.7: Schematic description of the volume parameters defined from the bearing area ratio [Löb10].

Feature parameters

Feature parameters are defined using subsets of pre-defined features using segmentation based on pattern recognition (further information can be found in [Sco09]).

Density of Summits of the Surface, S_{pd} is the number of peaks of a unit sampling area, and is given in units of [1/mm^2] or [peaks/mm^2].

This parameter evolved form the S_{ds} (density of summits) described at the Birmingham 14 parameters. The main difference between the old and new parameters is the watershed segmentation of the surface and the pruning of the change tree by an specified pruning factor introduced in S_{pd}. In this way only significant peaks are taken into account in the new S_{pd} parameter.

Arithmetic mean peak curvature of the surface S_{pc} is defined as the arithmetic mean of the principal curvatures of significant peaks within the sampling area, and is given in [1/mm]. As S_{pd}, this parameter derives from the S_{sc} parameter described at Birmingham 14 parameters and takes into account only significant peaks.

APPENDIX B

Results of the data acquisition variable analysis

Table B.1: Topographical parameters of the same surface area acquired at varying microscopic objectives.

	Microscopic objective			
	10x	20x	50x	100x
S_q (µm)	0.735	0.714	0.851	0.886
S_{sk}	1.262	0.852	0.517	0.267
S_{ku}	8.876	4.779	2.926	2.618
S_{al} (µm)	3.570	3.505	2.925	2.810
S_{dq}	0.258	0.382	0.859	1.586
S_{dr} (%)	3.108	6.852	30.021	82.247
V_{mp} ($\mu m^3/\mu m^2$)	0.034	0.027	0.018	0.015
V_{mc} ($\mu m^3/\mu m^2$)	0.605	0.601	0.770	0.836
V_{vc} ($\mu m^3/\mu m^2$)	1.149	1.246	1.534	1.501
V_{vv} ($\mu m^3/\mu m^2$)	0.064	0.060	0.067	0.078

Table B.2: Topographical parameters of the same surface area acquired at varying z_{scan} values.

	z_{scan}		
	14 µm	50 µm	100 µm
S_q (µm)	0.923	0.924	0.925
S_{sk}	0.339	0.336	0.331
S_{ku}	2.700	2.710	2.700
S_{al} (µm)	2.540	2.540	2.540
S_{dq}	1.740	1.740	1.750
S_{dr} (%)	96.000	96.000	96.400
V_{mp} ($\mu m^3/\mu m^2$)	0.016	0.016	0.016
V_{mc} ($\mu m^3/\mu m^2$)	0.857	0.857	0.859
V_{vc} ($\mu m^3/\mu m^2$)	1.580	1.580	1.580
V_{vv} ($\mu m^3/\mu m^2$)	0.080	0.080	0.081

Table B.3: Topographical parameters of the same surface area acquired at varying step size values.

	step size				
	0.2 µm	0.4 µm	0.8 µm	1.6 µm	2.4 µm
S_q (µm)	0.881	0.878	0.857	0.846	0.865
S_{sk}	0.254	0.309	0.382	0.450	0.617
S_{ku}	2.574	2.601	2.676	2.843	3.022
S_{al} (µm)	2.895	2.948	3.026	3.082	2.948
S_{dq}	1.557	1.420	1.188	1.084	1.099
S_{dr} (%)	79.977	69.755	53.950	46.944	47.374
V_{mp} ($\mu m^3/\mu m^2$)	0.014	0.015	0.016	0.020	0.012
V_{mc} ($\mu m^3/\mu m^2$)	0.835	0.827	0.804	0.773	0.688
V_{vc} ($\mu m^3/\mu m^2$)	1.499	1.514	1.503	1.466	1.637
V_{vv} ($\mu m^3/\mu m^2$)	0.078	0.075	0.070	0.069	0.074

APPENDIX C

Results of the data processing variable analysis

Table C.1: Experimental matrix for two-level full factorial design with 5 variables.

Exp. No	$\boldsymbol{\lambda}_s$	F	L	$\boldsymbol{\lambda}_c$	S	Exp. No	$\boldsymbol{\lambda}_s$	F	L	$\boldsymbol{\lambda}_c$	S
1	-	-	-	-	-	17	-	-	-	-	+
2	+	-	-	-	-	18	+	-	-	-	+
3	-	+	-	-	-	19	-	+	-	-	+
4	+	+	-	-	-	20	+	+	-	-	+
5	-	-	+	-	-	21	-	-	+	-	+
6	+	-	+	-	-	22	+	-	+	-	+
7	-	+	+	-	-	23	-	+	+	-	+
8	+	+	+	-	-	24	+	+	+	-	+
9	-	-	-	+	-	25	-	-	-	+	+
10	+	-	-	+	-	26	+	-	-	+	+
11	-	+	-	+	-	27	-	+	-	+	+
12	+	+	-	+	-	28	+	+	-	+	+
13	-	-	+	+	-	29	-	-	+	+	+
14	+	-	+	+	-	30	+	-	+	+	+
15	-	+	+	+	-	31	-	+	+	+	+
16	+	+	+	+	-	32	+	+	+	+	+

Table C.2: Results of the tests defined through design of experiments expressed as mean ± standard deviation.

	ROUGHNESS			WAVINESS		
No	$\boldsymbol{S}_{\mathrm{q}}$	$\boldsymbol{S}_{\mathrm{dq}}$	$\boldsymbol{V}_{\mathrm{vc}}$	$\boldsymbol{S}_{\mathrm{q}}$	$\boldsymbol{S}_{\mathrm{dq}}$	$\boldsymbol{V}_{\mathrm{vc}}$
1	0.72±0.05	1.10±0.14	1.19±0.11	0.80±0.06	0.10±0.00	1.18±0.11
2	0.63±0.05	0.67±0.07	1.06±0.10	0.80±0.06	0.10±0.00	1.16±0.11
3	0.72±0.05	1.10±0.14	1.19±0.11	0.56±0.08	0.10±0.00	1.04±0.14
4	0.63±0.05	0.67±0.07	1.06±0.10	0.56±0.08	0.10±0.00	0.95±0.14
5	0.77±0.06	1.18±0.17	1.29±0.13	0.80±0.08	0.09±0.01	1.06±0.14
6	0.69±0.05	0.69±0.07	1.20±0.12	0.79±0.08	0.09±0.01	1.12±0.14
7	0.77±0.06	1.18±0.17	1.29±0.13	0.55±0.10	0.09±0.01	0.99±0.19
8	0.69±0.05	0.69±0.07	1.20±0.12	0.53±0.11	0.08±0.01	0.87±0.20
9	0.89±0.04	1.11±0.13	1.53±0.10	0.52±0.07	0.04±0.00	0.77±0.15
10	0.82±0.04	0.69±0.06	1.43±0.09	0.52±0.07	0.04±0.00	0.71±0.15
11	0.89±0.04	1.11±0.13	1.53±0.10	0.34±0.09	0.03±0.01	0.61±0.26
12	0.82±0.04	0.69±0.06	1.43±0.09	0.34±0.09	0.03±0.01	0.51±0.26
13	0.95±0.03	1.19±0.15	1.64±0.06	0.45±0.04	0.03±0.00	0.52±0.07
14	0.89±0.03	0.70±0.06	1.57±0.04	0.44±0.03	0.03±0.00	0.58±0.05
15	0.95±0.03	1.18±0.15	1.64±0.06	0.24±0.04	0.02±0.00	0.46±0.12
16	0.88±0.03	0.70±0.06	1.57±0.04	0.23±0.03	0.02±0.00	0.35±0.10
17	1.69±0.31	1.90±0.38	2.03±0.24	3.78±0.48	0.47±0.07	3.63±1.14
18	1.56±.27	1.27±0.24	1.88±0.19	3.76±0.48	0.46±0.07	5.86±1.14
19	1.69±0.31	1.90±0.38	2.03±0.24	3.43±0.50	0.47±0.07	5.20±0.93
20	1.56±0.27	1.27±0.24	1.88±0.19	3.41±0.49	0.46±0.07	4.98±0.92
21	2.48±0.60	2.14±0.45	1.91±0.10	3.45±0.38	0.39±0.03	5.40±0.95
22	2.38±0.55	1.41±0.27	1.81±0.10	3.41±0.40	0.38±0.03	5.35±0.97
23	2.48±0.60	2.14±0.45	1.91±0.10	3.07±0.39	0.39±0.03	4.68±0.69
24	2.38±0.55	1.41±0.27	1.81±0.10	3.03±0.40	0.38±0.03	4.46±0.69
25	2.89±0.45	2.02±0.40	3.38±0.35	2.76±0.41	0.21±0.03	4.62±1.19
26	2.79±0.42	1.41±0.24	3.27±0.33	2.75±0.41	0.20±0.03	4.56±1.19
27	2.89±0.45	2.02±0.40	3.38±0.35	2.43±0.43	0.20±0.02	4.08±0.98
28	2.79±0.42	1.41±0.24	3.27±0.33	2.41±0.44	0.20±0.03	3.87±0.97
29	3.57±0.42	2.20±0.46	3.30±0.39	2.28±0.28	0.15±0.02	4.02±0.88
30	3.46±0.40	1.48±.25	3.24±0.37	2.28±0.28	0.15±0.02	3.99±0.89
31	3.57±0.42	2.20±0.46	3.30±0.38	1.90±0.23	0.14±0.02	3.45±0.62
32	3.46±0.40	1.48±0.25	3.24±0.36	1.89±0.23	0.14±0.02	3.30±0.62

References

[Abr09] I. Abrahamsson, E. Linder, and N.P. Lang. Implant stability in relation to osseointegration: an experimental study in the labrador dog. *Clinical Oral Implants Research*, vol. 20(3):pp. 313–318, 2009.

[Abu10] H. Abuhussein, G. Pagni, A. Rebaudi, and H.L. Wang. The effect of thread pattern upon implant osseointegration. *Clinical oral implants research*, vol. 21(2):pp. 129–136, 2010.

[AG09] R. Andrés-García, N. García Vives, F. Herrero Climent, A. Fernández Palacín, V. Ríos Santos, M. Herrero Climent, and P. Bullón. In vitro evaluation of the influence of the cortical bone on the primary stability of two implant systems. *Med Oral Patol Oral Cir Bucal*, vol. 14(2):pp. E93–97, 2009.

[AL08] M. Peuten A. Laseca, M. Pienkowski. Análisis comparativo de la rugosidad de la superficie de seis implantes dentales de diferentes sistemas (c.e.) antes de la inserción ósea y después del efecto de las fuerzas de inserción sobre la topografía de las superficies. *Revista Europea de Odontoestomatología*, 2008.

[Alb81] T. Albrektsson, P.I. Brånemark, H.A. Hansson, and J.T.Y. Lindström. Osseointegrated titanium implants: Requirements for ensuring a long-lasting, direct bone-to-implant anchorage in man. *Acta Orthopaedica*, vol. 52(2):pp. 155–170, 1981.

[Alb01] T. Albrektsson. Is surgical skill more important for clinical success than changes in implant hardware? *Clinical implant dentistry and related research*, vol. 3(4):pp. A6–A6, 2001.

[Alb04] T. Albrektsson and A. Wennerberg. Oral implant surfaces: Part 1–review focusing on topographic and chemical properties of different surfaces and in vivo responses to them. *The International journal of prosthodontics*, vol. 17(5):pp. 536–543, 2004.

[Ale13] A. Alenezi, Y. Naito, B. R Andersson, M.and Chrcanovic, A. Wennerberg, and R. Jimbo. Characteristics of 2 different commercially available implants with or without nanotopography. *International Journal of Dentistry*, vol. 2013:p. 8, 2013.

[AN08] B. Al-Nawas, KA. Groetz, H. Goetz, H. Duschner, and W. Wagner. Comparative histomorphometry and resonance frequency analysis of implants with modera-

tely rough surfaces in a loaded animal model. *Clinical oral implants research*, vol. 19(1):pp. 1–8, 2008.

[Ans00a] K. Anselme. Osteoblast adhesion on biomaterials. *Biomaterials*, vol. 21(7):pp. 667–681, 2000.

[Ans00b] K. Anselme, M. Bigerelle, B. Noel, E. Dufresne, D. Judas, A. Iost, and P. Hardouin. Qualitative and quantitative study of human osteoblast adhesion on materials with various surface roughnesses. *Journal of biomedical materials research*, vol. 49(2):pp. 155–166, 2000.

[Apa03] C. Aparicio, F.J. Gil, C. Fonsecab, M.Barbosab, and J. A. Planella. Corrosion behaviour of commercially pure titanium shot blasted with different materials and sizes of shot particles for dental implant applications. *Biomaterials*, vol. 24:pp. 263–273, 2003.

[Apa05] C. Aparicio. *Tratamientos de superficie sobre titanio comercialmente puro para la mejora de la osteointegración de los implantes dentales*. Ph.D. thesis, Universitat Politècnica de Catalunya, 2005.

[Arc97] C. Arcoumanis, P. Ostovar, and R. Mortier. Mixed lubrication modelling of newtonian and shear thinning liquids in a piston-ring configuration. Tech. rep., SAE, 1997.

[Arv06] A. Arvidsson, B.A. Sater, and A. Wennerberg. The role of functional parameters for topographical characterization of bone-anchored implants. *Clinical implant dentistry and related research*, vol. 8(2):pp. 70–76, 2006.

[ASTa] ASTM F1839 - 08(2012): Standard specification for rigid polyurethane foam for use as a standard material for testing orthopaedic devices and instruments.

[ASTb] ASTM F67 - 13 (2013): Standard specification for unalloyed titanium, for surgical implant applications (UNS R50250, UNS R50400, UNS R50550, UNS R50700).

[Ats07] M. Atsumi, S.H. Park, and H.L. Wang. Methods used to assess implant stability: current status. *The International journal of oral & maxillofacial implants*, vol. 22(5):pp. 743–754, 2007.

[Avi09] G. Avila, K. Misch, P. Galindo-Moreno, and H.L. Wang. Implant surface treatment using biomimetic agents. *Implant Dentistry*, vol. 18(1):pp. 17–26, 2009.

[Bag04] A. Bagno and C. Di Bello. Surface treatments and roughness properties of ti-based biomaterials. *Journal of Materials Science: Materials in Medicine*, vol. 15(9):pp. 935–949, 2004.

[Bai11] Y.J. Bai, Y.B. Wang, Y. Cheng, F. Deng, Y.F. Zheng, and S.C. Wei. Comparative study on the corrosion behavior of ti-nb and tma alloys for dental application

in various artificial solutions. *Materials Science and Engineering C*, vol. 31:pp. 702–711, 2011.

[Bal08] A. M. Ballo. *Fiber Reinforced Composite as Oral Implant Material*. Ph.D. thesis, Turun Yliopisto, 2008.

[Bar11] V. Barranco, M.L. Escudero, and M.C. García-Alonso. Influence of the microstructure and topography on the barrier properties of oxide scales generated on blasted Ti6Al4V surfaces. *Acta Biomaterialia*, vol. 7:pp. 2716–2725, 2011.

[Bat12] S. Battula, S. Papanicolaou, H.B. Wen, and M. Collins. Evaluation of a trabecular metal dental implant design for primary stability, structural integrity and abrasion. In *Academy of Osseointegration.* Phoenix; 2012.

[Bin00] P. P. Binon. Implants and components: entering the new millennium. *The International journal of oral & maxillofacial implants*, vol. 15(1):p. 76, 2000.

[BIO13] BIOMET 3i. *Surgical Manual Preservation By Design*, 2013.

[Bio14] Biotechnology Institute. *Guia rapida interna. Implante Tiny ®*, 2014.

[Bla06] F. Blateyron. New 3d parameters and filtration techniques for surface metrology. In *Proceeding of JSPE Annual Congress*, vol. White Paper. 2006.

[Bla13] F. Blateyron. *Characteriasation of Areal Surface Texture*, chap. 3 The Areal Feature Parameters. Springer, 2013.

[Blo00] T.J. Blokhuis, M.F. Termaat, F.C. den Boer, P. Patka, F.C. Bakker, and H.J.T.M. Haarman. Properties of calcium phosphate ceramics in relation to their in vivo behavior. *The Journal of trauma*, vol. 48(1):pp. 179–189, 2000.

[Blu03] L. Blunt and X. Jiang. *Advanced techniques for assessment surface topography: development of a basis for 3D surface texture standards "surfstand"*, chap. 8 Reference datum (software datum) for 3-D topography characterisation. Kogan Page Science, 2003.

[Böl13] N. Bölükbaşı, S. Mercan, M. S. Tekkesin, M. K. Bölükbaşı, and N. Bölükbaşı. Determination of titanium particles around a failed dental implant. *Int J Dent Case Reports March*, vol. 3(1):pp. 83–88, 2013.

[Boy00] B.D. Boyan and Z. Schwartz. Modulation of osteogenesis via implant surface design. In *International bone engineering workshop*, pp. 232–9. 2000.

[Boy01] B.D. Boyan, D.D. Dean, C.H. andCochran D.L. Lohmann, V.L. Sylvia, and S.Z. Schawartz. The titanium-bone cell interface in vitro: The role of the surface in promoting osteointegration. In D.M. Brunette, M.T. Tengvall, and P. Thomsen, editors, *Titanium in Medicine*. Springer, 2001.

[Brå83] P.I. Brånemark, R. Adell, T. Albrektsson, U. Lekholm, S. Lundkvist, and B. Rockler. Osseointegrated titanium fixtures in the treatment of edentulousness. *Biomaterials*, vol. 4(1):pp. 25–28, 1983.

[BRA12] Osseointegration pioneer per-ingvar brånemark receives lifetime achievement european inventor award. http:/ /medtechinsider.com/archives/23060, 2012.

[Bri03] S. Brinkman and H.Bodschwinna. *Advanced Techniques for Assessment Surface Topography*, chap. 4 Advanced Gaussian Filters. Kogan Page Science, 2003.

[Bro00] M. Browne and P.J. Gregson. Effect of mechanical surface pretreatment on metal ion release. *Biomaterials*, vol. 21(4):pp. 385–392, 2000.

[Bru01a] D.M. Brunette, P. Tengvall, M. Textor, and P. Thomsen. *Titanium in Medicine*, vol. 35, chap. V Medical Applications, pp. 875–889. Springer, 2001.

[Bru01b] D.M. Brunette, P. Tengvall, M. Textor, and P. Thomsen. *Titanium in medicine*, vol. 35, chap. IV Biological Performance, pp. 485–513. Springer, 2001.

[BS12] Bone BF Suma and Cartilage. http://www.bfsuma.com, September 2012.

[Bus04] D. Buser, N. Broggini, M. Wieland, R.K. Schenk, A.J. Denzer, D.L. Cochran, B. Hoffmann, A. Lussi, and S.G. Steinemann. Enhanced bone apposition to a chemically modified sla titanium surface. *Journal of dental research*, vol. 83(7):pp. 529–533, 2004.

[CA10] I. Cvijović-Alagić, Z. Cvijović, S. Mitrović, M. Rakin, Đ. Veljović, and M. Babić. Tribological Behaviour of Orthopaedic Ti-13Nb-13Zr and Ti-6Al-4V Alloys. *Tribology Letters*, vol. 40:pp. 1–12, 2010.

[CAR15] Scientific rationale for dental implant design. http://pocketdentistry.com/11-scientific-rationale-for-dental-implant-design/, January 2015.

[Che91] W. Chengwei and Z. Linqing. Effect of waviness and roughness on lubricated wear related to running-in. *Wear*, vol. 147(2):pp. 323–334, 1991.

[Che12] L. C. Chen, Y. W. Chang, and H. W. Li. Full-field chromatic confocal surface profilometry employing digital micromirror device correspondence for minimizing lateral cross talks. *Optical Engineering*, vol. 51(8):pp. 081507–1, 2012.

[Cho03] S. A. Cho and K. T. Park. The removal torque of titanium screw inserted in rabbit tibia treated by dual acid etching. *Biomaterials*, vol. 24(20):pp. 3611–3617, 2003.

[Cho11] R. Chowdhary, R. Jimbo, C. Thomsen, L. Carlsson, and A. Wennerberg. Biomechanical evaluation of macro and micro designed screw-type implants: an insertion torque and removal torque study in rabbits. *Clinical Oral Implants Research*, pp. 1–5, 2011.

[Cho14] Y. D. Cho, J. C. Shin, H. L. Kim, M. Gerelmaa, H. I. Yoon, H. M. Ryoo, D. J. Kim, and J. S. Han. Comparison of the osteogenic potential of titanium-and modified zirconia-based bioceramics. *International journal of molecular sciences*, vol. 15(3):pp. 4442–4452, 2014.

[Chr12] B. R. Chrcanovic, A. R. Pedrosa, and M. D. Martins. Chemical and topographic analysis of treated surfaces of five different commercial dental titanium implants. *Materials Research*, vol. 15(3):pp. 372–382, 2012.

[Cla08] B. Clarke. Normal bone anatomy and physiology. *Clinical Journal of the American Society of Nephrology*, vol. 3(Supplement 3):pp. S131–S139, 2008.

[Coc99] D. L Cochran. A comparison of endosseous dental implant surfaces. *Journal of Periodontology*, vol. 70(12):pp. 1523–1539, 1999.

[Coe11] P.G. Coelho, R. Granato, C. Marin, H.S. Teixeira, M. Suzuki, G.B. Valverde, M.N. Janal, T. Lilin, and E.A. Bonfante. The effect of different implant macrogeometries and surface treatment in early biomechanical fixation: An experimental study in dogs. *Journal of the Mechanical Behavior of Biomedical Materials*, vol. 4:pp. 1974–1981, 2011.

[Col07] R. Colaco. *Fundamentals of Friction and Wear on the Nanoscale*, chap. 21 Surface-Damage Mechanisms: from Nano- and Microcontacts to Wear of Materials. Springer, 2007.

[Coo00] L.F. Cooper. A role for surface topography in creating and maintaining bone at titanium endosseous implants. *The Journal of prosthetic dentistry*, vol. 84(5):pp. 522–534, 2000.

[Coo06] L.F. Cooper, Y. Zhou, J. Takebe, J. Guo, A. Abron, A. Holmén, and J.E. Ellingsen. Fluoride modification effects on osteoblast behavior and bone formation at tio2 grit-blasted cp titanium endosseous implants. *Biomaterials*, vol. 27(6):pp. 926–936, 2006.

[Cor99] G. Cordioli, Z. Majzoub, A. Piattelli, and A. Scarano. Removal torque and histomorphometric investigation of 4 different titanium surfaces: an experimental study in the rabbit tibia. *The International journal of oral & maxillofacial implants*, vol. 15(5):pp. 668–674, 1999.

[CV14] M. L. da Costa Valente, A. C. Shimano, C. R. Mazzo, C. P. Lepri, A. C. dos Reis, et al. Analysis of the surface deformation of dental implants submitted to pullout and insertion test. *Indian Journal of Dental Research*, vol. 25(1):p. 32, 2014.

[Dag80] H. Dagnall. *Exploring surface texture*. Rank Taylor Hobson, 1980.

[Dan11] R. Danzl, F. Helmli, and S. Scherer. Focus variation–a robust technology for high resolution optical 3d surface metrology. *Strojniški vestnik-Journal of mechanical engineering*, vol. 57(3):pp. 245–256, 2011.

[Dav10] J.T. Davies, J. Lam, P.E. Tomlins, and D. Marshall. An in vitro multi-parametric approach to measuring the effect of implant surface characteristics on cell behaviour. *Biomedical Materials*, vol. 5:p. 015002, 2010.

[Dav14] J. P. Davidas. Looking for a new international standard for characterization, classification and identification of surfaces in implantable materials: the long march for the evaluation of dental implant surfaces has just begun. *Periodontology, Oral Surgery, Esthetic and Implant Dentistry Open Journal*, vol. 2(1):pp. 1–5, 2014.

[DE11] D. M. Dohan Ehrenfest, L. Vazquez, Y. J. Park, G. Sammartino, and J. P. Bernard. Identification card and codification of the chemical and morphological characteristics of 14 dental implant surfaces. *Journal of Oral Implantology*, vol. 37(5):pp. 525–542, 2011.

[Den10] I. Denry and J.A. Holloway. Ceramics for dental applications: A review. *Materials*, vol. 3(1):pp. 351–368, 2010.

[Dic11] R. D. Ibrahim Dickey, R. L. Jackson, and G. T. Flowers. Measurements of the static friction coefficient between tin surfaces and comparison to a theoretical model. *Journal of Tribology*, vol. 133(3):p. 031408, 2011.

[Die05] A. Diener, B. Nebe, F. Lüthen, P. Becker, U. Beck, and J. Neumann, H. G.and Rychly. Control of focal adhesion dynamics by material surface characteristics. *Biomaterials*, vol. 26(4):pp. 383–392, 2005.

[Dig08] Digital Surf. *SensoMap Turbo 5.1*, 2008.

[Dob11] P. Dobrzański and P. Pawlus. A study of filtering techniques for areal surface topography assessment. *Proceedings of the Institution of Mechanical Engineers, Part B: Journal of Engineering Manufacture*, vol. 225(11):pp. 2096–2107, 2011.

[Don94] W.P. Dong, P.J. Sullivan, and K.J. Stout. Comprehensive study of parameters for characterising three-dimensional surface topography: Iv: parameters for characterising spatial and hybrid properties. *Wear*, vol. 178(1):pp. 45–60, 1994.

[Dow10] D. P. Dowling, I. S. Miller, M. Ardhaoui, and W. M. Gallagher. Effect of surface wettability and topography on the adhesion of osteosarcoma cells on plasma-modified polystyrene. *Journal of biomaterials applications*, 2010.

[Dow11] S. Dowdy and D. Wearden, S.and Chilko. *Statistics for research*. Wiley-Interscience, 2011.

[Edm96] R.M. Edmonds, R. A. Yukna, and R. L. Moses. Evaluation of the surface integrity of hydroxyapatite-coated threaded dental implants after insertion. *Implant dentistry*, vol. 5(4):pp. 273–278, 1996.

[Ehr10] D.M.D. Ehrenfest, P.G. Coelho, B.S. Kang, Y.T. Sul, and T. Albrektsson. Classification of osseointegrated implant surfaces: materials, chemistry and topography. *Trends in Biotechnology*, vol. 28(4):pp. 198–206, 2010.

[Ehr13] D. M. D. Ehrenfest, B. S. Kang, G. Sammartino, H. L. Shibli, J. A.and Wang, D. R. Zou, and J. P. Bernard. Guidelines for the publication of articles related to implant surfaces and design from the poseido: a standard for surface characterization. *POSEIDO Journal*, vol. 1:pp. 7–15, 2013.

[Eli06] L.M. Elias, S.G. Schneider, S. Schneider, H.M. Silva, and F. Malvisi. Microstructural and mechanical characterization of biomedical Ti-Nb-Zr (-Ta) alloys. *Materials Science and Engineering: A*, vol. 432(1-2):pp. 108–112, 2006.

[Eli08] C.N. Elias, Y. Oshida, J.H.C. Lima, and C.A. Muller. Relationship between surface properties (roughness, wettability and morphology) of titanium and dental implant removal torque. *Journal of the mechanical behavior of biomedical materials*, vol. 1(3):pp. 234–242, 2008.

[Eli10] C.N. Elias and L. Meirelles. Improving osseointegration of dental implants. *Expert Review of Medical Devices*, vol. 7(2):pp. 241–256, 2010.

[Eli11] C. N. Elias. *Implant Dentistry - A Rapidly Evolving Practice*, chap. 14 Factors affecting the success of dental implants. INTECH Open Access Publisher, 2011.

[Eri84a] A.R. Eriksson. *Heat-induced bone tissue injury: an in vivo investigation of heat tolerance of bone tissue and temperature rise in the drilling of cortical bone.* Ph.D. thesis, University of Foteborg, 1984.

[Eri84b] R.A. Eriksson and T. Albrektsson. The effect of heat on bone regeneration: an experimental study in the rabbit using the bone growth chamber. *Journal of oral and maxillofacial surgery*, vol. 42(11):pp. 705–711, 1984.

[Eri04] C. Eriksson, H. Nygren, and K. Ohlson. Implantation of hydrophilic and hydrophobic titanium discs in rat tibia: cellular reactions on the surfaces during the first 3 weeks in bone. *Biomaterials*, vol. 25(19):pp. 4759–4766, 2004.

[Esp98] M. Esposito, J.M. Hirsch, U. Lekholm, and P. Thomsen. Biological factors contributing. *Eur J Oral Sci*, vol. 106:pp. 527–551, 1998.

[Esp99] M. Esposito. *On Biological Failures of Osseointegrated Oral Implants.* Ph.D. thesis, Goteborg University, 1999.

[Fas07] L. Fassina, E. Saino, L. Visai, M. G. C. De Angelis, F. Benazzo, and G. Magenes. Enhanced in vitro culture of human saos-2 osteoblasts on a sand-blasted titanium surface modified with plastic deformation. In *Engineering in Medicine and Biology Society, 2007. EMBS 2007. 29th Annual International Conference of the IEEE*, pp. 6410–6413. IEEE, 2007.

[FM08] J. Faig-Martí and F.J. Gil-Mur. Los recubrimientos de hidroxiapatita en las prótesis articulares. *Revista Española de Cirugía Ortopédica y Traumatología*, vol. 52(2):pp. 113–120, 2008.

[For10] A. Forbes, P. Tomlins, E. Gurdak, M. Illsely, S. James, and E. James. Methodologies for assessing local surface texture features that are relevant to cell attachment. vol. 21, pp. 2463–2477. Springer, 2010.

[Fra04] M. Franchi, B. Bacchelli, D. Martini, V. De Pasquale, E. Orsini, V. Ottani, M. Fini, G. Giavaresi, R. Giardino, and A. Ruggeri. Early detachment of titanium particles from various different surfaces of endosseous dental implants. *Biomaterials*, vol. 25(12):pp. 2239–2246, 2004.

[Fri02] B. Friberg, A. Ekestubbe, L. Sennerby, et al. Clinical outcome of branemark system implants of various diameters: a retrospective study. *The International journal of oral & maxillofacial implants*, vol. 17(5):pp. 671–677, 2002.

[Fro90a] H.M. Frost. Skeletal structural adaptations to mechanical usage (satmu): 1. redefining wolff's law: the bone modeling problem. *The Anatomical Record*, vol. 226(4):pp. 403–413, 1990.

[Fro90b] H.M. Frost. Skeletal structural adaptations to mechanical usage (satmu): 2. redefining wolff's law: the remodeling problem. *The Anatomical Record*, vol. 226(4):pp. 414–422, 1990.

[Gap03] R. Gapski, H.L. Wang, P. Mascarenhas, and N.P. Lang. Critical review of immediate implant loading. *Clinical Oral Implants Research*, vol. 14(5):pp. 515–527, 2003.

[Gee09] M. Geetha, A.K. Singh, R. Asokamani, and A.K. Gogia. Ti based biomaterials, the ultimate choice for orthopaedic implants-A review. *Progress in Materials Science*, vol. 54(3):pp. 397–425, 2009.

[Gen04a] J.P. Geng, Q.S. Ma, W. Xu, K.B.C. Tan, and G.R. Liu. Finite element analysis of four thread-form configurations in a stepped screw implant. *Journal of oral rehabilitation*, vol. 31(3):pp. 233–239, 2004.

[Gen04b] J.P. Geng, W. Xu, K.B.C. Tan, and G.R. Liu. Finite element analysis of an osseointegrated stepped screw dental implant. *Journal of Oral Implantology*, vol. 30(4):pp. 223–233, 2004.

[Git11] R.A. Gittens, T. McLachlan, R. Olivares-Navarrete, Y. Cai, S. Berner, R. Tannenbaum, Z. Schwartz, K.H. Sandhage, and B.D. Boyan. The effects of combined micron-/submicron-scale surface roughness and nanoscale features on cell proliferation and differentiation. *Biomaterials*, vol. 32:pp. 3395–3403, 2011.

[Gol03] J. Goldstein. *Scanning electron microscopy and X ray microanalysis*, vol. 1. Springer Us, 2003.

[Gol15] I. Golvano, I. Garcia, A. Conde, W. Tato, and A. Aginagalde. Influence of fluoride content and ph on corrosion and tribocorrosion behaviour of ti13nb13zr alloy in oral environment. *Journal of the Mechanical Behavior of Biomedical Materials*, vol. 49:pp. 186–196, 2015.

[Gra07] S. Grassi, A. Piattelli, D. S Ferrari, L. C. Figueiredo, M. Feres, G. Iezzi, and J. A. Shibli. Histologic evaluation of human bone integration on machined and sandblasted acid-etched titanium surfaces in type iv bone. *Journal of Oral Implantology*, vol. 33(1):pp. 8–12, 2007.

[Gra11a] W. Graboń. Description of surfaces having stratified functional properties. *Business and Engineering Applications of Intelligent and Information Systems*, pp. 255–266, 2011.

[Gra11b] W. Grabon, P. Pawlus, L. Galda, A. Dzierwa, and P. Podulka. Problems of surface topography with oil pockets analysis. In *Journal of Physics: Conference Series*, vol. 311, p. 012023. IOP Publishing, 2011.

[Gre66] J.A. Greenwood and J.B.P. Williamson. Contact of nominally flat surfaces. In *Proceedings of the Royal Society of London A: Mathematical, Physical and Engineering Sciences*, vol. 295, pp. 300–319. The Royal Society, 1966.

[Gre70] J.A. Greenwood and J.H. Tripp. The contact of two nominally flat rough surfaces. *Proceedings of the institution of mechanical engineers*, vol. 185(1):pp. 625–633, 1970.

[Gre13] J.A. Greenwood. *Encyclopedia of tribology*, chap. Contact of Rough Surfaces: The Greenwood and Williamson/Tripp, Fuller and Tabor Theories. Springer New York, 2013.

[Gua11] H. Guan, R.C. Van Staden, N.W. Johnson, and Y.C. Loo. Dynamic modelling and simulation of dental implant insertion process–a finite element study. *Finite Elements in Analysis and Design*, vol. 47:pp. 886–897, 2011.

[Guo10] Q.H. Guo, Y.Z. Zhan, X.J. Zhang, Y. Du, M.N. Lin, and G.R. Huang, Z.Z.and Huang. Effects of fe and nb content on microstructure and mechanical characteristics of biomedical ti based alloys. *Materials Science and Technology,*, vol. 26:pp. 1448–1452, 2010.

[Gup09] A. Gupta, M. Dhanraj, and G. Sivagami. Implant surface modification reviwe of literature. *The Internet Journal of Dental Science*, vol. 7(1):p. 7, 2009.

[Han99] S. Hansson and M. Norton. The relation between surface roughness and interfacial shear strength for bone-anchored implants. a mathematical model* 1. *Journal of biomechanics*, vol. 32(8):pp. 829–836, 1999.

[Han00] S. Hansson. Surface roughness parameters as predictors of anchorage strength in bone: a critical analysis. *Journal of Biomechanics*, vol. 33(10):pp. 1297–1303, 2000.

[Han10] S. Hansson, J.Löberg, I. Mattisson, and E. Alhlberg. Characterisation of titanium dental implants. ii: Local biomechanical model. *The Open Biomaterials JOurnal*, vol. 2:pp. 36–52, 2010.

[Hen98] L.L. Hench. Bioactive glasses and glass-ceramics. In *Materials Science Forum*, vol. 293, pp. 37–64. Trans Tech Publ, 1998.

[Hen04] G. Heness and B. Ben-Nissan. Innovative bioceramics. In *Materials Forum*, vol. 27, pp. 104–114. 2004.

[Hen05] L.L. Hench and J.R. Jones. *Biomaterials, artificial organs and tissue engineering*. Woodhead, 2005.

[Hor94] M. Hormia and M. Könönen. Immunolocalization of fibronectin and vitronectin receptors in human gingival fibroblasts spreading on titanium surfaces. *Journal of periodontal research*, vol. 29(2):pp. 146–152, 1994.

[Hua04] H. H. Huang, C. T. Ho, T. H. Lee, T. L. Lee, K. K. Liao, and F. L. Chen. Effect of surface roughness of ground titanium on initial cell adhesion. *Biomolecular engineering*, vol. 21(3):pp. 93–97, 2004.

[ISO96a] ISO 3274:1996 Geometrical product specifications (GPS) – Surface texture: Profile method – Nominal characteristics of contact (stylus) instruments, 1996.

[ISO96b] ISO 4288:1996 Geometrical product specifications (GPS) – Surface texture: Profile method – Rules and procedures for the assessment of surface texture, 1996.

[ISO97] ISO 4287:1997 Geometrical product specifications (GPS) – Surface texture: Profile method – Terms, definitions and surface texture parameters, 1997.

[ISO98] ISO 13565-3:1998 Geometrical product specifications (GPS) – Surface texture: Profile method; surfaces having stratified functional properties – Part 1: Height characterization using the material probability curve, 1998.

[ISO06] ISO/TS 16610-1:2006 Geometrical product specifications (GPS) – Filtration – Part 1: Overview and basic concepts, 2006.

[ISO10] ISO/TS 16610-31:2010 Geometrical product specifications (GPS) – Filtration – Part 31: Robust profile filters: Gaussian regression filters, 2010.

[ISO11] ISO/TS 16610-21:2011 Geometrical product specifications (GPS) – Filtration – Part 22: Linear profile filters: Gaussian filters, 2011.

[ISO12] ISO 25178-2:2012 Geometrical product specifications (GPS) – Surface texture: Areal – Part 2: Terms, definitions and surface texture parameters, 2012.

[ISO15] ISO 25178-606:2015. Geometrical product specification (GPS) – Surface texture: Areal – Part 606: Nominal characteristics of non-contact (focus variation) instruments, 2015.

[Ito13] H. Ito, H. Sasaki, K. SAITO, S. HONMA, Y. YAJIMA, M. YOSHINARI, et al. Response of osteoblast-like cells to zirconia with different surface topography. *Dental materials journal*, vol. 32(1):pp. 122–129, 2013.

[Iva01] C. J. Ivanoff, G. Widmark, L. Hallgren, C.and Sennerby, and A. Wennerberg. Histologic evaluation of the bone integration of tio2 blasted and turned titanium microimplants in humans. *Clinical oral implants research*, vol. 12(2):pp. 128–134, 2001.

[Jac11] R. L. Jackson and I. Green. On the modeling of elastic contact between rough surfaces. *Tribology Transactions*, vol. 54(2):pp. 300–314, 2011.

[Jak03] W. Jakubiec and M. Brylski. Validation of software for calculating surface roughness parameters according to iso 13565-3. In *Proceedings of the 9th International Conference on Metrology and Properties of Engineering Surfaces, Halmstad University, Sweden.* 2003.

[Jay07] A. Jayagopal and V.P. Shastri. Nanoengineering of biomaterial surfaces. *Nanotechnologies for the Life Sciences*, vol. V. P., 2007.

[Jia07a] X. Jiang, P.J. Scott, DJ Whitehouse, and L. Blunt. Paradigm shifts in surface metrology. part i. historical philosophy. *Proceedings of the Royal Society A: Mathematical, Physical and Engineering Science*, vol. 463(2085):p. 2049, 2007.

[Jia07b] X. Jiang, P.J. Scott, DJ Whitehouse, and L. Blunt. Paradigm shifts in surface metrology. part ii. the current shift. *Proceedings of the Royal Society A: Mathematical, Physical and Engineering Science*, vol. 463(2085):pp. 2071–2099, 2007.

[Jia11] X. Jiang. Surface filtration, 2011. The 13th International Conference on Metrology and Properties of Engineering, 12-15 April 2011, Teddington.

[Juo03] G. Juodzbalys, M. Sapragoniene, and A. Wennerberg. New acid-etched titanium dental implant surface. *Stomatol Balt Dent Maxillofac J*, vol. 5:pp. 101–105, 2003.

[Kaj90] C. Kajdas, E. Wilusz, and S. Harvey. *Encyclopedia of tribology*, vol. 15. Elsevier, 1990.

[Kat07] A. Katranji, K. Misch, and H. L. Wang. Cortical bone thickness in dentate and edentulous human cadavers. *Journal of periodontology*, vol. 78(5):pp. 874–878, 2007.

[Kha01] W. Khang, S. Feldman, C.E. Hawley, and J. Gunsolley. A multi-center study comparing dual acid-etched and machined-surfaced implants in various bone qualities. *Journal of Periodontology*, vol. 72(10):pp. 1384–1390, 2001.

[Kin94] R.G. King and PM) Delaney, P.M. (DELANEY. Confocal microscopy. *Materials forum*, vol. 18:pp. 21–29, 1994.

[Koh13] R. J. Kohal, M. Bächle, W.l Att, S. Chaar, B. Altmann, A. Renz, and F. Butz. Osteoblast and bone tissue response to surface modified zirconia and titanium implant materials. *Dental Materials*, vol. 29(7):pp. 763–776, 2013.

[Kok04] T. Kokubo, H.M. Kim, M. Kawashita, and T. Nakamura. Review bioactive metals: preparation and properties. *Journal of Materials Science: materials in medicine*, vol. 15(2):pp. 99–107, 2004.

[Kra94] T. Krafft and M. Peschla. Abrasion of surface components in endosseous implants depending on their shape and coating. *International journal of oral and maxillofacial surgery*, vol. 23(6):pp. 418–419, 1994.

[Kry08] M. P. Krystek. Filtration of data according to the new ISO 16610 series. 5th Meeting CMU-CMM, Querétaro, Mexico, 2008.

[Kum10] S. Kumar, T.S.N. Sankara Narayanan, and S. Saravana Kumar. Influence of fluoride ion on the electrochemical behaviour of [beta]-ti alloy for dental implant application. *Corrosion Science*, vol. 52(5):pp. 1721–1727, 2010.

[Lab12] Glidewell Laboratories. http://www.glidewelldental.com/dentist/inclusive/volume3-2/small-diameter.aspx, Agoust 2012.

[Laz99] R. J. Lazzara, T. Testori, P. Trisi, S. S. Porter, and R. L. Weinstein. A human histologic analysis of osseotite and machined surfaces using implants with 2 opposing surfaces. *The International journal of periodontics & restorative dentistry*, vol. 19(2):pp. 117–129, 1999.

[LB03a] X. Jiang L. Blunt. *Advanced Techniques for Assessment Surface Topography*, chap. 9. Applications of Numerical Parameters and Filtration. Kogan Page Science, 2003.

[LB03b] X. Jiang L. Blunt, editor. *Advanced Techniques for Assessment Surface Topography*, chap. 9.3 Caste study: wear ranking of hard on hard bearings for prosthetic hip joints. 2003.

[L.B03c] L.Blunt and X. Jiang. 2. numerical parameters for characterisation of topography. In X. Jiang L.Blunt, editor, *Advanced Techniques for Assessment Surface Topography*. Kogan Page Science, 2003.

[Löb10] J. Löberg, I. Mattisson, S. Hansson, and E. Ahlberg. Characterisation of dental implants. i: Critical assessment of surface roughness parameters. *The Open Biomaterials Journal*, vol. 2:pp. 18–35, 2010.

[Lea13] R. K. Leach. *Characterisation of areal surface texture*. Springer, 2013.

[Lee00] J.J. Lee, L. Rouhfar, and O.R. Beirne. Survival of hydroxyapatite-coated implants: a meta-analytic review. *Journal of oral and maxillofacial surgery*, vol. 58(12):pp. 1372–1379, 2000.

[Lee07] C.H. Lee and A. A. Polycarpou. Static friction experiments and verification of an improved elastic-plastic model including roughness effects. *Journal of Tribology*, vol. 129(4):pp. 754–760, 2007.

[Lee10] C.H Lee, M. Eriten, and A. A. Polycarpou. Application of elastic-plastic static friction models to rough surfaces with asymmetric asperity distribution. *Journal of Tribology*, vol. 132(3):p. 031602, 2010.

[Lek85] U. Lekholm. Patient selection and preparation. *Tissue integrated prostheses*, 1985.

[LG07] L. Le Guehennec, A. Soueidan, P. Layrolle, and Y. Amouriq. Surface treatments of titanium dental implants for rapid osseointegration. *Dental materials*, vol. 23(7):pp. 844–854, 2007.

[Li02] D. Li, S.J. Ferguson, T. Beutler, D.L. Cochran, C. Sittig, H.P. Hirt, and D. Buser. Biomechanical comparison of the sandblasted and acid-etched and the machined and acid-etched titanium surface for dental implants. *Journal of biomedical materials research*, vol. 60(2):pp. 325–332, 2002.

[Li04] S.J. Li, R. Yang, S. Li, Y.L. Hao, Y.Y. Cui, M. Niinomi, and Z.X. Guo. Wear characteristics of Ti-Nb-Ta-Zr and Ti-6Al-4V alloys for biomedical applications. *Wear*, vol. 257(9-10):pp. 869–876, 2004.

[Lim07] J.Y. Lim and H.J. Donahue. Cell sensing and response to micro-and nanostructured surfaces produced by chemical and topographic patterning. *Tissue Engineering*, vol. 13(8):pp. 1879–1891, 2007.

[Liu99] X. Liu. *Advanced techniques for separation of roughness, waviness and form.* Ph.D. thesis, University of North Carolina at Charlotte, 1999.

[Liu10] X. Liu, P.K. Chu, and C. Ding. Surface nano-functionalization of biomaterials. *Materials Science and Engineering: R: Reports*, vol. 70:pp. 275–302, 2010.

[Mac04] W. Macdonald, P. Campbell, J. Fisher, and A. Wennerberg. Variation in surface texture measurements. *Journal of Biomedical Materials Research Part B: Applied Biomaterials*, vol. 70(2):pp. 262–269, 2004.

[Mac07] J.M. Macak, H. Tsuchiya, A. Ghicov, K. Yasuda, R. Hahn, S. Bauer, and P. Schmuki. Tio2 nanotubes: Self-organized electrochemical formation, properties and applications. *Current Opinion in Solid State and Materials Science*, vol. 11(1-2):pp. 3–18, 2007.

[Maj08] P. Majumdar, SB Singh, and M. Chakraborty. Wear response of heat-treated Ti-13Zr-13Nb alloy in dry condition and simulated body fluid. *Wear*, vol. 264(11-12):pp. 1015–1025, 2008.

[Mar02] V. C. Marinho, R. Celletti, G. Bracchetti, G. Petrone, C. Minkin, and A. Piattelli. Sandblasted and acid-etched dental implants: a histologic study in rats. *The International journal of oral & maxillofacial implants*, vol. 18(1):pp. 75–81, 2002.

[Mar03] D. Martini, M. Fini, M. Franchi, V.D. Pasquale, B. Bacchelli, M. Gamberini, A. Tinti, P. Taddei, G. Giavaresi, V. Ottani, et al. Detachment of titanium and fluorohydroxyapatite particles in unloaded endosseous implants. *Biomaterials*, vol. 24(7):pp. 1309–1316, 2003.

[Mar04] J.Y. Martin, Z. Schwartz, T.W. Hummert, D.M. Schraub, J. Simpson, J. Lankford, D.D. Dean, D.L. Cochran, and B.D. Boyan. Effect of titanium surface roughness on proliferation, differentiation, and protein synthesis of human osteoblast-like cells (mg63). *Journal of Biomedical Materials Research*, vol. 29(3):pp. 389–401, 2004.

[Mar13] H. F. Mark. *Encyclopedia of polymer science and technology, concise.* John Wiley & Sons, 2013.

[Mas02] C. Massaro, P. Rotolo, F. De Riccardis, E. Milella, A. Napoli, M. Wieland, M. Textor, ND Spencer, and D.M. Brunette. Comparative investigation of the surface properties of commercial titanium dental implants. part i: chemical composition. *Journal of Materials Science: Materials in Medicine*, vol. 13(6):pp. 535–548, 2002.

[Mat10] T.G. Mathia, P. Pawlus, and M. Wieczorowski. Recent trends in surface metrology. *Wear*, vol. 271:pp. 494–508, 2010.

[MB06] P. Miranda-Burgos. *On the influence of micro-and macroscopic surface modifications on bone integration of titanium implants.* Ph.D. thesis, Göteborg University, 2006.

[McC86] J.I. McCool. Predicting microfracture in ceramics via a microcontact model. *Journal of tribology*, vol. 108(3):pp. 380–385, 1986.

[McC87] J.I. McCool. Relating profile instrument measurements to the functional performance of rough surfaces. *Journal of tribology*, vol. 109(2):pp. 264–270, 1987.

[Mel09] A. Meltzer, H. Baumgarten, T. Testori, and P. Trisi. Pressure necrosis and osseointegration. *restoration*, vol. 4:p. 7, 2009.

[Men95] H.C. Meng and K.C. Ludema. Wear models and predictive equations: their form and content. *Wear*, vol. 181:pp. 443–457, 1995.

[Men08] G. Mendonca, D. Mendonca, F.J.L. Aragao, and L.F. Cooper. Advancing dental implant surface technology-from micron-to nanotopography. *Biomaterials*, vol. 29(28):pp. 3822–3835, 2008.

[Men13a] D. B. S. Mendonça, L. Cooper, G. Mendonça, and P. Dechichi. Effects of titanium surface anodization with cap incorporation on human osteoblastic response. *Materials Science and Engineering: C*, vol. 33(4):pp. 1958–1962, 2013.

[Men13b] B. Meng and X. Yang. Titanium particles enhanced osteoclast differentiation and osteoclast bone resorption activity in vitro. *Journal of Dentistry and Oral Hygiene*, vol. 5(2):pp. 7–12, 2013.

[Met11] Michigan Metrology. http://www.michmet.com/3d_s_parameters.htm, 2011.

[Mey05] U. Meyer, A. Büchter, H.P. Wiesmann, U. Joos, and D.B. Jones. Basic reactions of osteoblasts on structured material surfaces. *Eur Cell Mater*, vol. 9:pp. 39–49, 2005.

[Mic05] A. Michiardi. *Nuevo tratamiento de oxidación en aleaciones de NiTi para aplicaciones biomédicas. Caracterización superficial y respuesta biológica in vitro*. Ph.D. thesis, E.T.S Énginyeria Industrial de Barcelona Universitat Politècnica de Catalunya, 2005.

[Mik74] B.B. Mikić. Thermal contact conductance; theoretical considerations. *International Journal of Heat and Mass Transfer*, vol. 17(2):pp. 205–214, 1974.

[Min14] D. Mints, C. Elias, P. Funkenbusch, and L. Meirelles. Integrity of implant surface modifications after insertion. *International Journal of Oral & Maxillofacial Implants*, vol. 29(1):pp. 97–104, 2014.

[Mis09] C.E. Misch. *Implantología contemporánea*, vol. 209. Elsevier, 2009.

[Miy05] I. Miyamoto, Y. Tsuboi, E. Wada, H. Suwa, and T. Iizuka. Influence of cortical bone thickness and implant length on implant stability at the time of surgery–clinical, prospective, biomechanical, and imaging study. *Bone*, vol. 37(6):pp. 776–780, 2005.

[Mon12] M. Monjo, C. Petzold, J. M. Ramis, S. P. Lyngstadaas, and J. E. Ellingsen. In vitro osteogenic properties of two dental implant surfaces. *International journal of biomaterials*, vol. 2012:p. 14, 2012.

[Müe03] W.D. Müeller, U. Gross, T. Fritz, C. Voigt, P. Fischer, G. Berger, S. Rogaschewski, and K.P. Lange. Evaluation of the interface between bone and titanium surfaces being blasted by aluminium oxide or bioceramic particles. *Clinical Oral Implants Research*, vol. 14(3):pp. 349–356, 2003.

[Nay92] S. K. Nayar. Shape from focus system. In *Computer Vision and Pattern Recognition, 1992. Proceedings CVPR'92., 1992 IEEE Computer Society Conference on*, pp. 302–308. IEEE, 1992.

[Ned04] R. Nedir, M. Bischof, S. Szmukler-Moncler, J.P. Bernard, and J. Samson. Predicting osseointegration by means of implant primary stability. *Clinical Oral Implants Research*, vol. 15(5):pp. 520–528, 2004.

[Neo09] Neoss. *Implant System Guidelines*, 2009.

[NEO15] NEOX. Non contact 3D optical profiler, 2015.

[Nik12] M. Nikkhah, F. Edalat, S. Manoucheri, and A. Khademhosseini. Engineering microscale topographies to control the cell–substrate interface. *Biomaterials*, vol. 33(21):pp. 1–17, 2012.

[Nis07] S. K. Nishimoto, M. Nishimoto, S.W. Park, K.M. Lee, H.S. Kim, J.T. Koh, J.L. Ong, Y. Liu, and Y. Yang. The effect of titanium surface roughening on protein absorption, cell attachment, and cell spreading. *The International journal of oral & maxillofacial implants*, vol. 23(4):pp. 675–680, 2007.

[NJ10] A. B. Novaes Jr, S. L. Souza, R. R. Barros, K. K. Pereira, G. Iezzi, and A. Piattelli. Influence of implant surfaces on osseointegration. *Brazilian dental journal*, vol. 21(6):pp. 471–481, 2010.

[Nor01] M.R. Norton and C. Gamble. Bone classification: an objective scale of bone density using the computerized tomography scan. *Clinical oral implants research*, vol. 12(1):pp. 79–84, 2001.

[O'B97a] W.J. O'Brien. *Dental materials and their selection*, chap. 23- Implant and Bone Augmentation Materials. Quintessence publishing Chicago, 1997.

[O'B97b] W.J. O'Brien. *Dental materials and their selection.* Quintessence publishing Chicago, 1997.

[OH15] Eastman Institute for Oral Health. https://www.urmc.rochester.edu/dentistry/research/current-research.aspx, July 2015.

[Ohl03] R. Ohlsson, Goran G., and Westberg J. *Advanced Techniques for Assessment Surface Topography*, chap. 8. The Interrelationship of 3D Surface Characterisation Techniques with Standarised 2D Techniques. Kogan Page Science, 2003.

[Olm13] D. G. Olmedo, G. Nalli, S. Verdú, M. L. Paparella, and R. L. Cabrini. Exfoliative cytology and titanium dental implants: A pilot study. *Journal of periodontology*, vol. 84(1):pp. 78–83, 2013.

[Ong04] J.L. Ong, D.L. Carnes, and K. Bessho. Evaluation of titanium plasma-sprayed and plasma-sprayed hydroxyapatite implants in vivo. *Biomaterials*, vol. 25(19):pp. 4601–4606, 2004.

[O'S00] D. O'Sullivan and N. Sennerby, L.and Meredith. Measurements comparing the initial stability of five designs of dental implants: a human cadaver study. *Clinical implant dentistry and related research*, vol. 2(2):pp. 85–92, 2000.

[Osh07a] Y. Oshida. *Bioscience and bioengineering of titanium materials.* Elsevier, 2007.

[Osh07b] Y. Oshida. *Bioscience and bioengineering of titanium materials*, chap. 2- Maaterials Classification. Elsevier, 2007.

[Osh10] Y. Oshida, E.B. Tuna, O. Aktören, and K. Gençay. Dental Implant Systems. *International journal of molecular sciences*, vol. 11(4):pp. 1580–1678, 2010.

[Pag10] M. Paggi and M. Ciavarella. The coefficient of proportionality $\boldsymbol{\kappa}$ between real contact area and load, with new asperity models. *Wear*, vol. 268(7):pp. 1020–1029, 2010.

[Pas10] G. Passeri, A. Cacchioli, C.and Elezi E. Ravanetti, F.and Galli, and G. M. Macaluso. Adhesion pattern and growth of primary human osteoblastic cells on five commercially available titanium surfaces. *Clinical Oral Implants Research*, vol. 21(7):pp. 756–765, 2010.

[Paw13] G. Pawar, P. Pawlus, I. Etsion, and B. Raeymaekers. The effect of determining topography parameters on analyzing elastic contact between isotropic rough surfaces. *Journal of Tribology*, vol. 135(1):p. 011401, 2013.

[Pet03] M. Peters, J. Hemptenmacher, J. Kumpfert, and C. Leyens. 1. structure and properties of titanium and titanium alloys. In C.Leyens and M. Peters, editors, *Titanium and titanium alloys*, pp. 1–36. Wiley-VCH, 2003.

[Pri11] D.R. Prithviraj, K.M. Regish, S. Deeksha, and D.P. Shruthi. Extraction and immediate placement of root analogue zirconia implants: an overview. *Clinical and Experimental Dentistry*, vol. 3:pp. 240–245, 2011.

[Rae07] I. Raeymaekers, B.and Etsion and F.E. Talke. Enhancing tribological performance of the magnetic tape/guide interface by laser surface texturing. *Tribology Letters*, vol. 27(1):pp. 89–95, 2007.

[Raj02] J. Raja, B. Muralikrishnan, and S. Fu. Recent advances in separation of roughness, waviness and form. *Precision engineering*, vol. 26(2):pp. 222–235, 2002.

[Ram07] J.J. Ramsden, D.M. Allen, D.J. Stephenson, J.R. Alcock, G.N. Peggs, G. Fuller, and G. Goch. The design and manufacture of biomedical surfaces. *CIRP Annals-Manufacturing Technology*, vol. 56(2):pp. 687–711, 2007.

[Rao96] S. Rao, T. Ushida, T. Tateishi, Y. Okazaki, and S. Asao. Effect of Ti, Al, and V ions on the relative growth rate of fibroblasts (L929) and osteoblasts (MC3T3-E1) cells. *Bio-medical materials and engineering*, vol. 6(2):pp. 79–86, 1996.

[Rea44] R.E. Reason. Surface finish and its measurement. *Journal of the Institute of Production Engineers*, vol. 23:pp. 347–372, 1944.

[Rec98] A.F. von Recum. *Handbook of biomaterials evaluation: scientific, technical and clinical testing of implant materials.* CRC, 1998.

[Rho98] J.Y. Rho, L. Kuhn-Spearing, and P. Zioupos. Mechanical properties and the hierarchical structure of bone. *Medical engineering & physics*, vol. 20(2):pp. 92–102, 1998.

[Ros01] B.G. Rosén and T.R. Thomas. Relationship of the plasticity index to machining parameters. *International Journal of Machine Tools and Manufacture*, vol. 41(13):pp. 2061–2069, 2001.

[Ros03] M. M. Rosa, A. L.and Beloti. Effect of cpti surface roughness on human bone marrow cell attachment, proliferation, and differentiation. *Brazilian dental journal*, vol. 14(1):pp. 16–21, 2003.

[Ros13] M.B. Rosa, T. Albrektsson, C.E. Francischone, A. Wennerberg, et al. Micrometric characterization of the implant surfaces from the five largest companies in brazil, the second largest worldwide implant market. *The International journal of oral & maxillofacial implants*, vol. 28(2):p. 358, 2013.

[RR05] D. Rodríguez Rius and F. García Sabán. Caracterización físico-química de la superficie de 9 implantes dentales con 3 distintos tratamientos de superficie. *Medicina oral, patología oral y cirugía bucal*, vol. 10(1):pp. 58–65, 2005.

[Rui05] R. Ruimerman. *Modeling and remodeling in bone tissue*. Ph.D. thesis, Technische Universiteit Eindhoven, 2005.

[Sam05] R.L. Sammons, N. Lumbikanonda, M. Gross, and P. Cantzler. Comparison of osteoblast spreading on microstructured dental implant surfaces and cell behaviour in an explant model of osseointegration. *Clinical oral implants research*, vol. 16(6):pp. 657–666, 2005.

[Sam08] S. Samuel, S. Nag, T.W. Scharf, and R. Banerjee. Wear resistance of laser-deposited boride reinforced Ti-Nb-Zr-Ta alloy composites for orthopedic implants. *Materials Science and Engineering: C*, vol. 28(3):pp. 414–420, 2008.

[Sch84] W. Schulte. The intra-osseous al2o3 (frialit) tuebingen implant. developmental status after eight years (i-iii). *Quintessence Int*, vol. 15(2):pp. 147–163, 1984.

[Sch91] H. Schliephake, J. Reiss, R. Urban, F.W. Neukam, and H. Günay. Freisetzung von titan aus schraubenimplantaten. *Z Zahnärztl Implantol*, vol. 7:pp. 6–10, 1991.

[Sch92] H. Schliephake, G. Reiss, F.W. Urban, R.and Neukam, and S. Guckel. Metal release from titanium fixtures during placement in the mandible: an experimental study. *The International journal of oral & maxillofacial implants*, vol. 8(5):pp. 502–511, 1992.

[Sch98] R.K. Schenk and D. Buser. Osseointegration: a reality. *Periodontology 2000*, vol. 17(1):pp. 22–35, 1998.

[Sco03] P.J. Scott. *Advanced Techniques for Assessment Surface Topography*, chap. 3 Novel Areal Characterisation Techniques. Kogan Page Science, 2003.

[Sco04] P.J. Scott. Pattern analysis and metrology: the extraction of stable features from observable measurements. *Proceedings of the Royal Society of London Series A: Mathematical, Physical and Engineering Sciences*, vol. 460(2050):pp. 2845–2864, 2004.

[Sco09] P. J. Scott. Feature parameters. *Wear*, vol. 266(5):pp. 548–551, 2009.

[SEM] The application of VSI (Vertical scanning interferometry) to the study of crystal surface processes. http://cnx.org/content/m22326/latest/.

[Sem05] D. Semwogerere and E.R. Weeks. *Encyclopedia of biomaterials and biomedical engineering*. 2005.

[Sen13] P. Senna, A. Antoninha Del Bel Cury, S. Kates, and L. Meirelles. Surface damage on dental implants with release of loose particles after insertion into bone. *Clinical implant dentistry and related research*, vol. 14(4):pp. 681–692, 2013.

[Sha06] M.M. Shalabi, A. Gortemaker, M.A. Vant Hof, J.A. Jansen, and N.H.J. Creugers. Implant surface roughness and bone healing: a systematic review. *Journal of dental research*, vol. 85(6):pp. 496–500, 2006.

[She00] I. Sherrington and S. Mercer. The use of topography-based parameters for the assessment and prediction of surface wear. *TriboTest*, vol. 7(1):pp. 1–11, 2000.

[Shi06] Y.K. Shin, C.H. Han, S.J. Heo, S. Kim, and H.J. Chun. Radiographic evaluation of marginal bone level around implants with different neck designs after 1 year. *The International journal of oral & maxillofacial implants*, vol. 21(5):pp. 789–794, 2006.

[Sim05] A. Simunek, D. Kopecka, M. Cierny, and I. Krulichova. A six-year study of hydroxyapatite-coated root-form dental implants. *West indian medical journal*, vol. 54(6):pp. 393–397, 2005.

[Ska00] R. Skalak and Y. Zhao. Interaction of force-fitting and surface roughness of implants. *Clinical implant dentistry and related research*, vol. 2(4):pp. 219–224, 2000.

[SM98] S. Szmukler-Moncler, H. Salama, Y. Reingewirtz, and JH Dubruille. Timing of loading and effect of micromotion on bone–dental implant interface: review of experimental literature. *Journal of Biomedical Materials Research*, vol. 43(2):pp. 192–203, 1998.

[SM10] B.S. Sotto-Maior, E.P. Rocha, E.O. Almeida, A.C. Freitas-Júnior, R.B. Anchieta, and AA Cury. Influence of high insertion torque on implant placement: an anisotropic bone stress analysis. *Braz Dent J*, vol. 21:pp. 508–514, 2010.

[Sos08] G. Sosale, S.A. Hacking, and S. Vengallatore. Topography analysis of grit-blasted and grit-blasted-acid-etched titanium implant surfaces using multi-scale measurements and multi-parameter statistics. *J Mater Res*, vol. 23(10):pp. 2704–2713, 2008.

[Sri15] S. Sridhar, T. G. Wilson Jr, P. Valderrama, P. Watkins-Curry, J. Y. Chan, and D. C. Rodrigues. In-vitro evaluation of titanium exfoliation during simulated surgical insertion of dental implants. *Journal of Oral Implantology*, 2015.

[Sta03] R-M Stach and S.S. Kohles. A meta-analysis examining the clinical survivability of machined-surfaced and osseotite implants in poor-quality bone. *Implant Dentistry*, vol. 12(1):pp. 87–96, 2003.

[Ste87] M. Stedman. Basis for comparing the performance of surface-measuring machines. *Precision engineering*, vol. 9(3):pp. 149–152, 1987.

[Sto93a] K.J. Stout, P.J. Sullivan, W. Dong, E. Mainsah, N. Luo, T. Mathia, and H. Zahouani. *The development of methods for the characterisation of roughness in three dimensions*, chap. 3- Techniques and Fidelity of Data Collection. Butterworth-Heinemann, 1993.

[Sto93b] K.J. Stout, P.J. Sullivan, W. Dong, E. Mainsah, N. Luo, T. Mathia, and H. Zahouani. *The development of methods for the characterisation of roughness in three dimensions*, chap. 10- Digital Filtering of 3-D Surface Topography. Butterworth-Heinemann, 1993.

[Sto93c] K.J. Stout, P.J. Sullivan, W. Dong, E. Mainsah, N. Luo, T. Mathia, and H. Zahouani. *The development of methods for the characterisation of roughness in three dimensions*. ISBN 0704413132, 1993.

[Sto93d] K.J. Stout, P.J. Sullivan, W. Dong, E. Mainsah, N. Luo, T. Mathia, and H. Zahouani. *The development of methods for the characterisation of roughness in three dimensions*. Butterworth Heinemann, 1993.

[Sto93e] K.J. Stout, P.J. Sullivan, W. Dong, E. Mainsah, N. Luo, T. Mathia, and H. Zahouani. The development of methods for the characterization of roughness in theree dimensions. Tech. rep., Commission of the European Communities, Brussels, 1993.

[Sto93f] K.J. Stout, P.J. Sullivan, W. Dong, E. Mainsah, N. Luo, T. Mathia, and H. Zahouani. *The Development of Methods for the Characterization of Roughness on Three Dimensions*, chap. 10- Digital filtering of 3-D surface topography, pp. 130–174. Butterworth-Heinemann, 1993.

[Sto00a] K.J. Stout and L. Blunt. *Three-dimensional surface topography*, chap. II- Instruments and Measurement Techniques of Three-Dimensional Surface Topography. Butterworth-Heinemann, 2000.

[Sto00b] K.J. Stout and L. Blunt. *Three Dimensional Surface Topography*, chap. III-Filtering Technology for Three-Dimensional Surface TOpography Analysis. Butterworth-Heinemann, 2000.

[Sto00c] K.J. Stout, P.J. Sullivan, W. Dong, E. Mainsah, N. Luo, T. Mathia, and H. Zahouani. *The development of methods for the characterisation of roughness in three dimensions*, chap. 12 Parameters for characterising 3-D surfaces, p. 228. Butterworth-Heinemann, 2000.

[Sto00d] K. J. Stout and L. Blunt. *Three Dimensional Surface Topography.*, chap. IV-Visualization Techniques and Parameters for Characterizing Three-Dimensional Surface Topography. Penton Press, 2000.

[Sub10] K. Subramani. Titanium surface modification techniques for implant fabrication-from microscale to the nanoscale. *Journal of Biomimetics, Biomaterials and Tissue Engineering*, vol. 5:pp. 39–56, 2010.

[Sul09] Y.T. Sul, B.S. Kang, C. Johansson, H.S. Um, C.J. Park, and T. Albrektsson. The roles of surface chemistry and topography in the strength and rate of osseointegration of titanium implants in bone. *Journal of Biomedical Materials Research Part A*, vol. 89(4):pp. 942–950, 2009.

[Sum94] R.B. Summers. A new concept in maxillary implant surgery: the osteotome technique. *Compendium (Newtown, Pa)*, vol. 15(2):pp. 152–154, 1994.

[Sur15] Digital Surf. http://www.digitalsurf.com/en/guidearealfieldparameters.html, 2015.

[Sva09] L. M. Svanborg, M. Andersson, and A. Wennerberg. Surface characterization of commercial oral implants on the nanometer level. *Biomed Mater Res B Appl Biomater*, vol. 92B,:pp. 462–469, 2009.

[Swa91] M. Swann. Black staining around titanium alloy prostheses. *J Bone Joint Surg [Br]*, vol. 1991(73-B):pp. 534–6, 1991.

[Tab09] A. Tabassum, F. Walboomers, J.G.C. Wolke, G.J. Meijer, and J.A. Jansen. The Influence of Surface Roughness on the Displacement of Osteogenic Bone Particles during Placement of Titanium Screw-Type Implants. *Clinical implant dentistry and related research*, vol. 13:pp. 269–278, 2009.

[Tab10a] A. Tabassum, G.J. Meijer, X. Frank Walboomers, and J.A. Jansen. Biological limits of the undersized surgical technique: a study in goats. *Clinical Oral Implants Research*, vol. 22(2):pp. 129–134, 2010.

[Tab10b] A. Tabassum, G.J. Meijer, J.G.C. Wolke, and J.A. Jansen. Influence of surgical technique and surface roughness on the primary stability of an implant in artificial bone with different cortical thickness: a laboratory study. *Clinical Oral Implants Research*, vol. 21(2):pp. 213–220, 2010.

[Tan03] L. Tana, R.A. Doddb, and W.C. Cronec. Corrosion and wear-corrosion behavior of niti modified by plasma source ion implantation. *Biomaterials*, vol. 24:pp. 3931–3939, 2003.

[Tay90] T.D. Taylor and W.R. Laney. *Dental implants: Are they for me?* Quintessence Publishing Company, 1990.

[Tho72] T.R. Thomas. Computer simulation of wear. *Wear*, vol. 22(1):pp. 83–90, 1972.

[Tom03] E. Tomanik, H. Chacon, and G. Teixeira. A simple numerical procedure to calculate the input data of greenwood-williamson model of asperity contact for actual engineering surfaces. *Tribology Series*, vol. 41:pp. 205–215, 2003.

[too12] Chiropractic tools. http://www.chiropractictools.com /dental_model.php, 2012.

[Tor10] B. Torres, M.A. Garrido, A. Rico, P. Rodrigo, M. Campo, and J. Rams. Wear behaviour of thermal spray al/sicp coatings. *Wear*, vol. 268(5):pp. 828–836, 2010.

[Tri09] P. Trisi, G. Perfetti, E. Baldoni, D. Berardi, M. Colagiovanni, and G. Scogna. Implant micromotion is related to peak insertion torque and bone density. *Clinical oral implants research*, vol. 20(5):pp. 467–471, 2009.

[TS14] A. Tawse-Smith, M. A Atieh, J. Leichter, L. Girvan, and A. M. Rich. Peri-implant bone loss and its uncommon causes: A case report. *Clinical Advances in Periodontics*, vol. 5(4):pp. 242–247, 2014.

[Tuk11] Li. Tukun. *Softgauges for surface texture.* Ph.D. thesis, University of Huddersfield, 2011.

[Uni15] Purdue University. How does a SEM work? https://www.purdue.edu/ehps/rem/rs/sem.htm, 2015.

[Van08] K. Vandamme, I. Naert, J. Vander Sloten, R. Puers, and J. Duyck. Effect of implant surface roughness and loading on peri-implant bone formation. *Journal of periodontology*, vol. 79(1):pp. 150–157, 2008.

[Vör01] J. Vörös, M. Wieland, L. Ruiz-Taylor, M. Textor, and D.M. Brunette. Characterization of titanium surfaces. *Titanium in Medicine*, pp. 87–144, 2001.

[Wan03] M. L Wang, R. Tuli, P.l A Manner, P.F. Sharkey, D. J. Hall, and R.S. Tuan. Direct and indirect induction of apoptosis in human mesenchymal stem cells in response to titanium particles. *Journal of orthopaedic research*, vol. 21(4):pp. 697–707, 2003.

[Wan11] J. Wang, X. Jiang, E. Gurdak, P.l Scott, R. Leach, P. Tomlins, and L. Blunt. Numerical characterisation of biomedical titanium surface texture using novel feature parameters. *Wear*, vol. 271(7):pp. 1059–1065, 2011.

[Wan15] J. Wang, R. K. Leach, and X. Jiang. Review of the mathematical foundations of data fusion techniques in surface metrology. *Surface Topography: Metrology and Properties*, vol. 3(2):p. 023001, 2015.

[Web99] R.H. Webb. Confocal optical microscopy. *Reports on Progress in Physics*, vol. 59(3):p. 427, 1999.

[Wei94] D. Weingart, S. Steinemann, W. Schilli, J.R. Strub, U. Hellerich, J. Assenmacher, and J. Simpson. Titanium deposition in regional lymph nodes after insertion of titanium screw implants in maxillofacial region. *International journal of oral and maxillofacial surgery*, vol. 23(6):pp. 450–452, 1994.

[Wen93] A. Wennerberg, T. Albrektsson, B. Andersson, et al. Design and surface characteristics of 13 commercially available oral implant systems. *International Journal of Oral and Maxillofacial Implants*, vol. 8(6):pp. 622–634, 1993.

[Wen95a] A. Wennerberg, T. Albrektsson, and B. Andersson. An animal study of cp titanium screws with different surface topographies. *Journal of Materials Science: Materials in Medicine*, vol. 6(5):pp. 302–309, 1995.

[Wen95b] A. Wennerberg, T. Albrektsson, B. Andersson, and J.J. Krol. A histomorghometric study of screw-shaped and removal torque titanium implants with three different surface topographies. *Clinical Oral Implants Research*, vol. 6(1):pp. 24–30, 1995.

[Wen96a] A. Wennerberg. *On surface roughness and inmplant incorporation.* Ph.D. thesis, Göteborgs university, 1996.

[Wen96b] A. Wennerberg, T. Albrektsson, B. Andersson, et al. Bone tissue response to commercially pure titanium implants blasted with fine and coarse particles of aluminum oxide. *International Journal of Oral and Maxillofacial Implants*, vol. 11(1):pp. 38–45, 1996.

[Wen98] A. Wennerberg, C. Hallgren, C. Johansson, and S. Danelli. A histomorphometric evaluation of screw-shaped implants each prepared with two surface roughnesses. *Clinical Oral Implants Research*, vol. 9(1):pp. 11–19, 1998.

[Wen00] A. Wennerberg and T. Albrektsson. Suggested guidelines for the topographic evaluation of implant surfaces. *The International journal of oral & maxillofacial implants*, vol. 15(3):pp. 331–344, 2000.

[Wen08] H.J. Wenz, J. Bartsch, S. Wolfart, and M. Kern. Osseointegration and clinical success of zirconia dental implants: a systematic review. *The International journal of prosthodontics*, vol. 21(1):pp. 27–36, 2008.

[Wen09] A. Wennerberg and T. Albrektsson. Effects of titanium surface topography on bone integration: a systematic review. *Clinical Oral Implants Research*, vol. 20:pp. 172–184, 2009.

[Whi82] D.J. Whitehouse. The parameter rash – is there a cure? *Wear*, vol. 83(1):pp. 75–78, 1982.

[Wil96] L. J. William and F.S. David. Current concepts review-total hip arthroplasty with hydroxyapatite-coated prostheses*. *The Journal of Bone and Joint Surgery (American)*, vol. 78(12):pp. 1918–34, 1996.

[Wil08] D.F. Williams. On the mechanisms of biocompatibility. *Biomaterials*, vol. 29(20):pp. 2941–2953, 2008.

[WJ15] T. G. Wilson Jr, P. Valderrama, M. Burbano, J. Blansett, R. Levine, H. Kessler, and D.C. Rodrigues. Foreign bodies associated with peri-implantitis human biopsies. *Journal of periodontology*, vol. 86(1):pp. 9–15, 2015.

[Yao05] C. Yao, V. Perla, J.L. McKenzie, E.B. Slamovich, and T.J. Webster. Anodized ti and ti6al4v possessing nanometer surface features enhances osteoblast adhesion. *Journal of Biomedical Nanotechnology*, vol. 1(1):pp. 68–73, 2005.

[Yeo08] I.S. Yeo and J.H. Han, J.S.and Yang. Biomechanical and histomorphometric study of dental implants with different surface characteristics. *Journal of Biomedical Materials Research Part B: Applied Biomaterials*, vol. 87(2):pp. 303–311, 2008.

[Yok02] K. Yokoyama, T. Ichikawa, H. Murakami, Y. Miyamoto, and K. Asaoka. Fracture mechanisms of retrieved titanium screw thread in dental implant. *Biomaterials*, vol. 23(12):pp. 2459–2465, 2002.

[Zab12] A. Zabala, N. Ibarguren, G. Arruebarrena, R. Tejero, A. Aginagalde, and W. Tato. Estudio topográfico 3D de implantes dentales: Influencia de la zona de medida y del tratamiento superficial. *XII COngreso Nacional de Materiales*, 2012.

[Zaf03] D. Zaffe, C. Bertoldi, and U. Consolo. Element release from titanium devices used in oral and maxillofacial surgery. *Biomaterials*, vol. 24(6):pp. 1093–1099, 2003.

[Zar85] G.A. Zarb, T. Albrektsson, and P.I. Branemark. *Tissue-integrated prostheses: osseointegration in clinical dentistry*. Quintessence, 1985.